FRICTIONAL HEATING IN SHEAR FLOWS

By

NARAYANAN SUBRAHMANIAM

A DISSERTATION PRESENTED TO THE GRADUATE SCHOOL
OF THE UNIVERSITY OF FLORIDA IN PARTIAL FULFILLMENT
OF THE REQUIREMENTS FOR THE DEGREE OF
DOCTOR OF PHILOSOPHY

UNIVERSITY OF FLORIDA

2000

Copyright 2000

by

NARAYANAN SUBRAHMANIAM

ACKNOWLEDGMENTS

I am grateful to my advisors, Dr. Narayanan and Dr. Johns. At every stage of this work, their input was invaluable.

My sincere thanks to the other committee members, Dr. Sukanek, Dr. Park, Dr. Rajagopalan and Dr. DeHoff for their suggestions.

It was a pleasure interacting with the graduate and undergraduate students who worked in the Bifurcation and Nonlinear Instability Laboratory over the years.

Thanks to all my friends who made my stay at Gainesville memorable.

Finally, my heartfelt gratitude to my parents, brother and sisters for being supportive over the years.

TABLE OF CONTENTS

ACKNOWLEDGMENTS iii

LIST OF TABLES vii

LIST OF FIGURES ix

ABSTRACT xiii

CHAPTERS

1 THE PROBLEM AND AN EXPLANATION OF ITS PHYSICS . . . 1

2 THE BASE STATE 10

- 2.1 The Model 11
- 2.2 The Base Equations 12
- 2.3 Thin Gapping the Circular Couette Flow Equations 17
- 2.4 Scaling 21
- 2.5 The Base Solution for the Case of Linear Fluidity 23
- 2.6 Prediction of the Nose on the Base Curve 25
- 2.7 Predictions about the Stability of the Base State 36
- 2.8 Endnotes 39
  - 2.8.1 Comparison of the Couette Flow problem to the Ignition problem 39
  - 2.8.2 Other Scaling Options 42
  - 2.8.3 Summary of the method that predicts a Nose 44
  - 2.8.4 The prediction of nose for general Fluidities based on a Slope-Chord Formula 46
  - 2.8.5 A note on the Base Curve of Fluids with $f_0' < 0$ 49
  - 2.8.6 The variation of $\tau_0\Delta/r_1^2$ with respect to Δ in the limit of $\Delta \to 0$ 51
  - 2.8.7 A Heuristic Model for the Plane Couette Flow problem . 55
  - 2.8.8 $V_0 - \tau_0 - \theta_{0_m}$ relationship in Circular Couette Flow 60
  - 2.8.9 Prediction of the nose in Circular Couette Flow 62
  - 2.8.10 Calculation of $V_0, \tau_0, \theta_{0_m}$ using the Base Solutions in Circular Couette Flow 67

3 THE PERTURBED EQUATIONS 75

4 THE STABILITY FOR A ZERO WAVE NUMBER DISTURBANCE 78

4.1 Stability to a Zero Wave Number Disturbance 83
4.1.1 Stability Results at Constant Wall Stress 85
4.1.2 The Stability Results at Constant Wall Speed 86
4.2 The rate of change of Eigenvalues with a change in the Input Variables 89
4.3 Endnotes 94
4.3.1 Proof of the Self-Adjointness of the Operator A 94
4.3.2 The Equations at Zero Wave Number for Circular Couette Flow 97
4.3.3 The plane Couette Flow Equations in the 2×2 formulation in $\hat{v}_{z_1}$ and $\hat{\theta}_1$ 97
4.3.4 Can the sign of σ be obtained from an Energy Argument ? 98
4.3.5 Neutral points for the case $f_0' < 0$ 99

5 THE ROLE OF PRANDTL NUMBER 101

5.1 Endnotes 108
5.1.1 The purely Thermal and Mechanical Limit from a Scaling Argument 108
5.1.2 Rate of decay of Perturbations for various combinations of Boundary Conditions 113
5.1.3 The Perturbed Equation in the Thermal Ignition problem 118
5.1.4 Comparison of the Perturbed Temperature Equations: Ignition vs. Couette 119

6 THE STABILITY FOR NON-ZERO WAVE NUMBER DISTURBANCES 121

6.1 Endnotes 138
6.1.1 The Thin Gapping of Perturbed Equations in Circular Couette flow 138
6.1.2 The Boundary Condition at Constant Wall Stress 143
6.1.3 The Stability of the Perturbed Equations when the Wave Number, $\gamma = 0, \beta \neq 0$ 144
6.1.4 A comment on the Non-Zero Wave Number Equations in the Limit $\gamma \to 0$ 147
6.1.5 Is an Inflexion point necessary for an Instability in Viscous Shear Flows? 150
6.1.6 Comparison of our Stability Results with an earlier work 151
6.1.7 A note on the stability of Isoviscous Plane Couette Flow 154

7 OVERVIEW OF A TYPICAL EXPERIMENT 157

7.1 Endnotes 176
7.1.1 A note about the Boundary Condition at Constant Power 176
7.1.2 A Proof to show that Wall Speed increases with Power 177
7.1.3 A comment on Stability at Constant Input Power 179
7.1.4 A comment on the Taylor Instability Problem 181
7.1.5 Simulation of the dynamics of the Nonlinear Equations 188

8 EXPERIMENTAL DESIGN AND RESULTS 195

- 8.1 Endnotes 204
  - 8.1.1 Check to see whether the Experimental Liquid is Newtonian 204
  - 8.1.2 The choice of a Radius Ratio 204
  - 8.1.3 Other Design Improvements 206
  - 8.1.4 Effect of Convection 209
  - 8.1.5 Details of the calculation of the Base Curve 210
  - 8.1.6 Sensitivity of the Base Curve to a change in the Physical Properties 211
  - 8.1.7 The Effect of Eccentricity of the cylinders on the Calculated Torque 212

9 CONCLUSIONS 213

REFERENCES 220

BIOGRAPHICAL SKETCH 221

LIST OF TABLES

2.1 $\lambda_1(\tau_{xz0}), \lambda_2(\tau_{xz0})$ vs. τ_{xz0} for an exponential fluidity: * indicates the value of τ_{xz0} at the nose. All values above this on the table are on the lower branch and below this are on the upper branch. 37

2.2 $\lambda_1(\tau_0), \lambda_2(\tau_0)$ vs. τ_0 for an exponential fluidity for $\eta = 0.5$ 66
2.3 Torque at the nose for linear fluidity 68

2.4 Torque, Wall speed and the maximum temperature at the nose for exponential fluidity 70

2.5 Conditions at the nose for an adiabatic inner wall and conducting outer wall 73

2.6 Conditions at the nose for an adiabatic inner wall and Newton's law at the outer wall 73

2.7 An estimate of actual parameter values at the nose for an experiment 74

4.1 The rate of decay of perturbations as a function of wall speed. 92

5.1 The rate of change of the largest eigenvalue with respect to the Prandtl number for $\tau_{xz0} = 0.5$ along the lower branch. 106

5.2 The rate of change of the largest eigenvalue with respect to the Prandtl number for $\tau_{xz0} = 0.5$ along the upper branch. 106

5.3 The largest eigenvalues as a function of the Prandtl number on the lower branch. 116

5.4 The largest eigenvalues as a function of the Prandtl number on the upper branch 117

6.1 Stability at constant wall stress: The real part of the largest eigenvalue vs. the wave number for a point on the lower branch for the chosen experimental conditions. 137

6.2 The stability at constant wall speed: The plot of the largest eigenvalue vs. the wave number for a point on the upper branch and for properties based on our experimental liquid. 137

6.3 Correspondence between circular Couette flow and the plane Couette flow 143

6.4 The comparison of the first few eigenvalues from a zero wave number calculation with those arising from setting $\gamma = 0.01$ in the non-zero wave number equations. The chosen parameter values are $\tau_{xz_0} = 0.5, V_0 = 1.09$, Re=1, Pr=1. 149

6.5 Comparison of the result of Yueh and Weng with our calculations: The critical Reynold's number vs. the wave number for $\mathrm{Br} = 20, \mathrm{Pr} = 50$. 154

7.1 Comparison of the critical value of K, $K_c = \mathrm{d}V_0/\mathrm{d}\tau_{xz_0}$ with V_0/τ_{xz_0} on the upper branch for a mixed boundary condition 181

7.2 The critical Taylor number for various radius ratios at constant rpm and at constant power 186

7.3 The critical parameters for various radius ratios at constant rpm . . . 188

8.1 The viscosity-temperature data for the experimental liquid. 198

8.2 The comparison of the viscosity data with the fit. 198

8.3 The torque and the ambient temperature at various rpms in an experiment with r_2=1 inch, $\eta = 0.75$, L=0.34m. 201

8.4 The details of the calculation that generated the base curve. 210

8.5 The effect of a change in the thermal conductivity on the calculated base curve 211

8.6 The effect of a change in the viscosity on the calculated base curve . . 212

LIST OF FIGURES

1.1 Illustration of plane Couette flow 2

1.2 Wall speed vs. the Wall shear stress curve for various fluidities 4

1.3 Schematic of Couette flow with arbitrary perturbations on the base velocity 5

1.4 Illustration of Poiseulle flow in a pipe 9

2.1 Schematic of Plane Couette flow 12

2.2 Schematic of Circular Couette flow 13

2.3 V_0 vs.τ_{xz_0} for linear fluidity 24

2.4 The base temperature profile with a zero in the interior. 26

2.5 A hypothetical θ_{0_m} vs. τ_{xz_0} curve with $\dot{\theta}_0 > 0$ on the upper branch . . 30

2.6 The prediction of the nose based on the second eigenvalue problem . 30

2.7 The $\lambda_1(\tau_{xz_0})$ vs. τ_{xz_0} curve for a case with multiple noses 31

2.8 V_0 vs.τ_{xz_0} for exponential fluidity 35

2.9 The $\lambda_1(\tau_{xz_0})$ vs. τ_{xz_0} curve for a case with $f_0^{''} < 0$ 36

2.10 Prediction of the nose based on the Slope-Chord relationship. a)$f_0^{''} > 0$, b)$f_0^{''} < 0$, c) Arrhenius fluidity 48

2.11 A $\dot{\theta}_0$ profile with a zero in the interior. 51

2.12 Schematic of the variation of scaled torque with gap width in the limit of zero gap width 55

2.13 Heuristic Model: Plot of Wall speed vs. wall stress 59

2.14 The base temperature profile with a zero in the interior 63

2.15 The prediction of the nose based on the eigenvalue problem: $\lambda_1(\tau_0), \lambda_2(\tau_0)$ vs. τ_0 behavior. 65

2.16 Schematic of Circular Couette flow 70

4.1 Depiction of plane Couette flow 79

4.2 Schematic of the Couette flow with arbitrary perturbations on the base state. 82

5.1 The wall speed vs. the wall stress curve as a function of the Prandtl number. 110

5.2 Schematic of plane Couette flow: Constant wall stress on the bottom plate and a constant wall speed on the top plate. 114

5.3 Schematic of plane Couette flow: Constant wall speed on the bottom plate and a constant wall stress on the top plate. 115

6.1 Schematic of plane Couette flow with an adiabatic top wall and a conducting bottom wall 151

6.2 Isoviscous plane Couette flow: The plot of the largest eigenvalue vs. the wavenumber for a range of Reynolds numbers for conditions of constant wall speed. 156

6.3 Isoviscous plane Couette flow: The plot of the largest eigenvalue vs. the wavenumber for a range of Reynolds numbers for conditions of constant wall stress. 156

7.1 Experimental setup 158

7.2 A schematic of the constant power input for plane Couette flow . . . 159

7.3 Illustration of Couette flow with a braking mechanism to control the wall stress 167

7.4 The Base curve drawn along with a series of constant power curves . 169

7.5 Two possible kinds of perturbation at constant power 170

7.6 A perturbation that decreases the wall stress at constant power and a control action to bring the wall stress back. 171

7.7 Dynamic behavior when wall stress is controlled after imposing a perturbation that decreases the wall stress from the set point: The case where the initial response of the flow at constant power is away from its steady state 172

7.8 Dynamic behavior when wall stress is controlled after imposing a perturbation that decreases the wall stress from the set point: The case where the initial response of the flow at constant power is towards its steady state 173

7.9 A perturbation that increases the wall stress and a control action to bring the wall stress back to the set point. 173

7.10 Dynamic behavior when wall stress is controlled after imposing a perturbation that increases the wall stress: The case where the wall stress starts to move away from the set point at constant power 174

7.11 Dynamic behavior when wall stress is controlled after imposing a perturbation that increases the wall stress: The case where the wall stress starts to move towards the set point at constant power . 175

7.12 Step change in power: The initial and the final steady state points . . 189

7.13 Step increase in power: The response of wall speed. 190

7.14 Step increase in power: The response of wall stress. 190

7.15 Step decrease in power: The response of wall speed. 191

7.16 Step decrease in power: The response of wall stress. 191

7.17 The dynamics of the wall stress when a perturbation that decreases the wall stress is imposed and a control action is then instituted to keep the wall stress close to the set point 192

7.18 The dynamics of the wall speed when a perturbation that decreases the wall stress is imposed and a control action is then instituted to keep the wall stress close to the set point. 193

7.19 The dynamics of the wall stress when a perturbation that increases the wall stress is imposed and a control action is then instituted to keep the wall stress close to the set point. 193

7.20 The dynamics of the wall speed when a perturbation that increases the wall stress is imposed and a control action is then instituted to keep the wall stress close to the set point. 194

8.1 Experimental Setup 196

8.2 Viscosity-temperature data for the experimental liquid plotted along with an exponential fit. 199

8.3 Comparison of the experimental base curve of torque vs. rpm with the theoretical predictions 203

8.4 Shear viscosity vs. shear rate at various temperatures. 205

8.5 Couette Cylinder assembled in a split-house bearing 207

8.6 Couette Cylinder disassembled from a split-house bearing 208

8.7 Illustration of a convective flow between a hot plate and a cold plate. 209

Abstract of Dissertation Presented to the Graduate School
of the University of Florida in Partial Fulfillment of the
Requirements for the Degree of Doctor of Philosophy

FRICTIONAL HEATING IN SHEAR FLOWS

By

Narayanan Subrahmaniam

May 2000

Chairman: Dr. Ranganathan Narayanan
Major Department: Chemical Engineering

A curve of wall speed vs. wall stress for a strongly temperature thinning liquid turns out to be double-valued. The stability of this curve turns out to be surprising. At constant wall speed, the curve is completely stable while at constant wall stress, it is partly stable. This result is independent of the Prandtl number of the fluid in the gap. Yet the Prandtl number can be used to decide whether it is the velocity perturbations or the temperature perturbations that predict the fate of the disturbances. Experiments confirmed the predictions at constant wall speed but not the predictions at constant wall stress. This was puzzling. However it seems that it is the power to the fluid that is the real input to the flow, not the wall speed nor the wall stress. The stability results at constant power then explain the complete stability seen in the experiments. Then it was proved that power, the input, cannot be used to run experiments at constant wall stress. These conclusions bear on the problem of Taylor-Couette instability. The calculations in this case match the experimental results. However the calculations are performed at constant wall speed

whereas the experiments must be done at constant power. This is surprising but what we have shown is that these two conditions become identical when the mass of the wall becomes large. And this is what we think happens in experiments.

CHAPTER 1
THE PROBLEM AND AN EXPLANATION OF ITS PHYSICS

The aim of this thesis is to understand some of the interesting phenomena that occur when a viscous liquid with a temperature dependent viscosity is made to undergo a shearing flow. We will begin this by first describing the problem and explaining its physics. To do this, we will consider plane Couette flow, the simplest of shearing flows.

Consider a viscous liquid in plane Couette flow with a fixed bottom wall and a moving top wall illustrated in figure 1.1. One way of realizing this flow in an experiment is to set the speed of the moving wall while measuring the shearing stress that the fluid exerts on this wall. This is obtained by measuring the force on the wall required to obtain the desired speed. A curve of the wall speed vs. the shear stress exerted by the fluid on the wall could then be drawn to characterize the experiment and we call this the base curve. The shape of this base curve turns out to be dependent on the strength of the viscosity-temperature relationship. To get a feel for this, first observe that as the top wall moves, frictional heat is produced due to shear between adjacent fluid layers and a temperature rise is required to dissipate the frictional heat produced. Assuming that the walls are held at constant temperature, a temperature profile is set up in the gap with the temperature rise being greater at points farther from the boundary. Now, the viscosity of the liquid is dependent on its temperature. The question then is what happens to the wall shear stress as the wall speed is increased. In trying to answer this question, we will first assert that the shear stress across the gap is a constant.[1] Therefore, we can replace the

---

[1] If a model is written for the base flow, then it becomes obvious that the shear stress across the gap is indeed a constant. However, at this stage we will just pretend this is true.

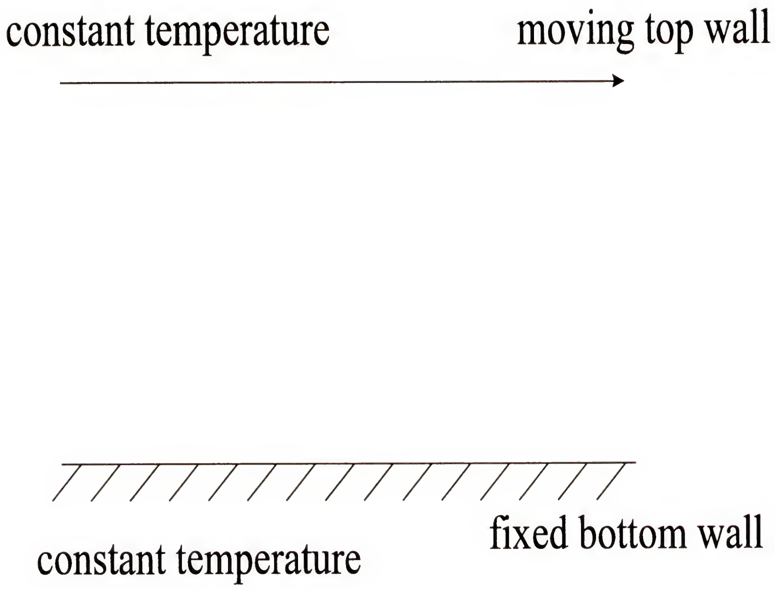

Figure 1.1: Illustration of plane Couette flow

stress at any position in the gap. Now, the shear stress at any position is equal to the product of the viscosity and the velocity gradient at that position. We will pretend that the velocity gradient is the velocity of the wall divided by the gap width and the viscosity is the lumped average viscosity of the liquid in the gap. This simplified picture of the problem in fact turns out to be sufficient to capture the essence of the physics of the base curve at this stage wherein only rough arguments are being advanced. We will later on find in an endnote of chapter 2 that a heuristic model of this flow based on this simplified picture captures all of the essential qualitative features of this problem. Now, typically, viscosity of liquids decrease with an increase in temperature. Therefore, we find that with an increase in the speed of the wall, the viscosity of the liquid in the gap falls while the velocity gradient increases. Hence, an estimate of how the wall shear stress behaves as the speed of the wall increases, turns out to be dependent on the strength of the viscosity-temperature relationship.

At low wall speeds, the frictional heat generated is small. Consequently, the temperature rise is small and so too is the decrease in the viscosity of the liquid. Therefore, one can imagine that the increase in velocity gradient is stronger than the decrease in viscosity and that the wall stress increases with an increase in wall speed. However, with a high enough increase in the wall speed, the temperature rise may be strong enough to cause an appreciable decrease in the viscosity. Therefore, the wall stress can either increase or decrease depending on whether the product of the viscosity and the velocity gradient increases or decreases. If the increase in velocity gradient is greater than the decrease in viscosity, the product, the wall stress, increases with an increase in wall speed. However, if the increase in velocity gradient is weaker than the decrease in viscosity, the wall stress decreases with an increase in wall speed. Thus the relationship between the viscosity of the liquid and its temperature determines the shape of the base curve, i.e., the wall speed vs. the wall stress curve. If the fluidity, which is the reciprocal of viscosity, increases weakly with temperature such that the increase is less than proportional to the increase in temperature, then it turns out that the wall stress continuously increases with an increase in wall speed but the rate of increase in the wall stress becomes progressively weaker. If the fluidity-temperature relationship is exactly linear, then it turns out there is an upper bound on the wall stress and for every possible wall speed there corresponds a wall stress lower than this upper bound. The curve does not bend back. On the other hand, if the relationship is stronger than linear, say, exponential, then it turns out that the base solution has two values of wall speed for every wall stress below a maximum. In this case, we find that as we increase the wall speed, the wall stress increases along a 'lower branch'. Along this branch, the increase in velocity gradient is stronger than the decrease in viscosity and even though the wall stress increases it rate of ascent continues to fall. A point is reached where the wall stress reaches a maximum. With a further increase in wall speed, the wall stress actually decreases and the curve bends back thus generating an 'upper branch'. Along this branch, the decrease in viscosity is stronger than the increase in velocity gradient.

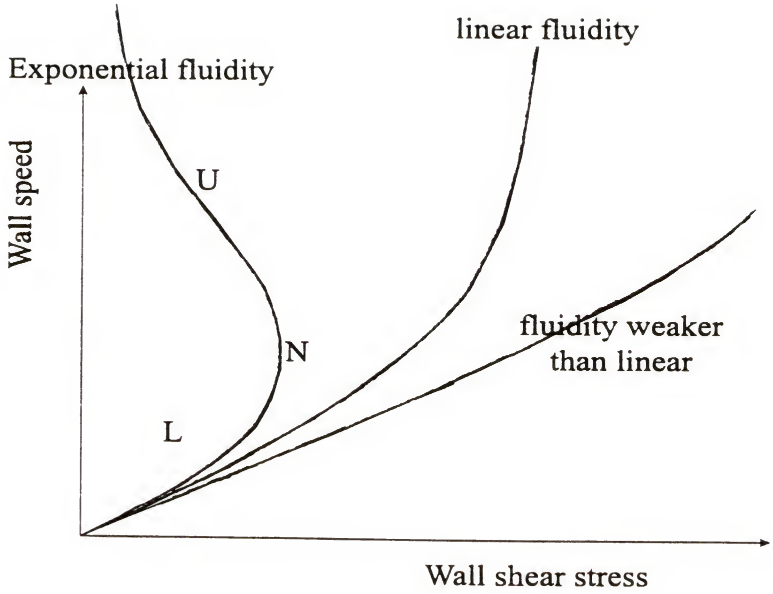

Figure 1.2: Wall speed vs. the Wall shear stress curve for various fluidities

Figure 1.2 shows how the curve of wall stress varies qualitatively with the wall speed for plane Couette flow of a fluid with a temperature dependent viscosity. It turns out that any measure of temperature rise. say the maximum temperature in the gap can replace the wall speed on the ordinate. Three different curves are depicted in the figure. The first case is for a fluidity weaker than linear, the second for a linear and the third for an exponential. On the curve for exponential fluidity. L denotes the lower branch. N the nose of the curve where the maximum shear stress is obtained and U denotes the upper branch.

While the base curve is interesting, its stability to small disturbances is even more interesting. To see this, let us ask whether a small perturbation, if imposed on the flow at any point on the base curve. will grow or decay. The answer turns out to be dependent on the requirements the perturbation must satisfy. In thinking about how and where a perturbation may be imposed, we realize that any point on the base curve may be obtained by running up the wall speed. Having reached a point on the base curve, a perturbation may be imposed such that either the velocity disturbances or the stress disturbances at the moving wall are required to vanish.

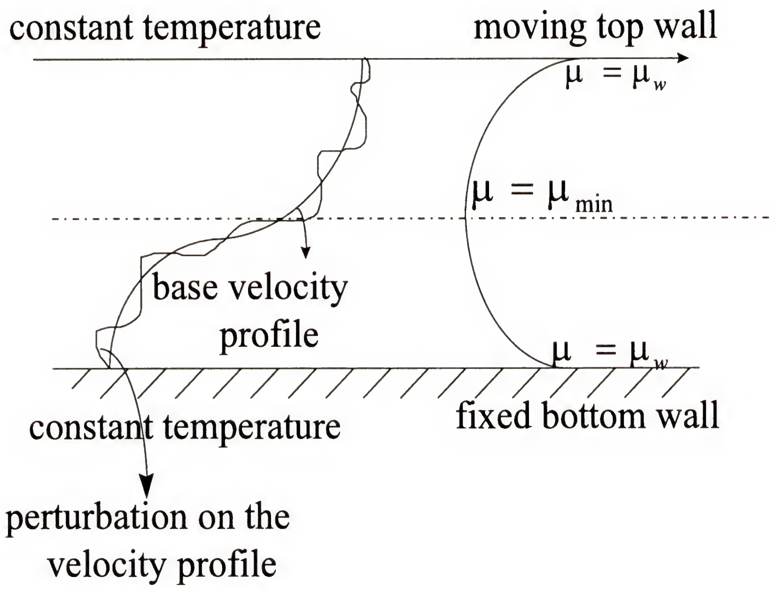

Figure 1.3: Schematic of Couette flow with arbitrary perturbations on the base velocity

Then the question arises as to whether there is any qualitative difference between these two cases.

An explanation is put forth to suggest that there is indeed a difference in the rate at which perturbations grow or decay under these two conditions and hence provides a motivation for the stability calculations to be performed under these two conditions: To understand the difference, consider a disturbance given to the velocity field. This disturbance has to diffuse through to the boundaries and the kinematic viscosity, the viscosity of the liquid divided by its density, is the diffusivity for the disturbance to be carried away to the boundaries. Now as the velocity field produces frictional heat, a perturbation to the velocity field produces a perturbation to the temperature in the gap. So, the viscosity of the liquid in the gap changes from its base viscosity profile. However, to simplify the thinking, we will assume that the disturbance imposed to be 'special' in the sense that only the velocity field is perturbed and the base temperature profile and hence the base viscosity profile are unaffected by this disturbance. As the base temperature profile has a maximum at the channel centre, it follows that the base viscosity profile has a minimum at the channel center. Therefore, assuming that the density is a constant, the diffusivity for the velocity perturbation is minimum at the channel center.

The bottom wall is fixed and hence the velocity perturbations on it vanish. Now, when the velocity perturbations vanish on the top wall too, then the velocity disturbance can diffuse through both the boundaries as there is a momentum sink on both the boundaries. On the other hand, when the stress perturbations vanish on the top wall, the velocity disturbance can leak only through the bottom wall. The wall at the top does not allow any perturbation to leak through. It is adiabatic to momentum.

Now, consider an arbitrary velocity disturbance close to the top of the channel. Under conditions of constant wall speed on the top wall, the disturbance can just diffuse through the top wall but under conditions of constant wall stress, it has to cross the entire width of the channel before it can leak out through the bottom. In doing so, it has to cross the center-line wherein the temperature is at its highest and hence the viscosity is at its lowest. Therefore, it is conceivable that a velocity disturbance would take a longer time to cross this region than in the case where the velocity perturbations die out at both walls.

It is worth recalling in the above argument that we have discarded the temperature perturbations that arise out of the imposed velocity perturbations. In other words, a purely mechanical argument, i.e., one which is based only on the decay of the velocity perturbations alone, has been put forth, suggesting that perturbations at constant wall stress persist longer than perturbations at constant wall speed.

The above picture of the decay of perturbations therefore suggests that there is indeed a difference in the rate at which perturbations decay in these two cases and hence gives us a motivation to study the stability of the problem in these two cases. In fact, this is the foundation on which we will build further to explain how perturbations grow or decay in this problem and what, if any, are the modes of instability in this flow. As all of our physical notions on the stability to disturbances in these kinds of shear flow rest on first understanding the characteristics of the base curve and its properties, we begin our study by first studying the base state. However, before proceeding to study the base state, we will discuss whether the ideas that we introduced to get a feel for the shape of the base curve and the dependence of its stability on the restrictions placed on the boundaries can be carried over to other simple shear flows like circular Couette flow and Poiseulle flow in a channel.

Earlier in this chapter, we suggested that the shape of the base curve of the wall speed vs. the wall stress is dependent on the strength of the fluidity-temperature relationship. This turns out to be true as we will see later on in this thesis. In fact it turns out that for a strong fluidity-temperature relationship like the exponential law, the wall stress initially increases with an increase in wall speed, reaches a maximum and then with a further increase in the wall speed bends back and decreases. The same behaviour carries over to shear flow situations like circular Couette flow and Poiseulle flow in a pipe. The curve of torque vs. the 'rpm' of the rotating cylinder in azimuthal flow between concentric cylinders and the curve of the pressure drop vs. the flow rate for laminar flow in a channel show a similar trend. Thus, for an exponential fluidity dependence on temperature, there is an upper bound for the torque in circular Couette flow and an upper bound for the pressure drop in Poiseulle flow beyond which no simple solutions exist.

Another aspect of the physics of the flow that we were interested in, in the main body of this chapter, is the stability of the plane Couette flow to small disturbances. We provided an argument to suggest that the case of constant wall stress is more unstable than the case of constant wall speed. Now, let us see whether this argument can be extended to circular Couette flow and Poiseulle flow in a channel.

For the case of a circular Couette flow between concentric cylinders, we can imagine running up the rpm of the rotating cylinder and then holding either the torque or the rpm of the rotating cylinder fixed at a point on the base curve. Let us assume that the outer cylinder is rotated and that the inner cylinder is fixed and let us also assume that both walls are held at constant temperature. Then extending the argument provided earlier in this chapter, it is not difficult to see that an arbitrary perturbation would take a longer time to decay if the torque on the outer cylinder is held fixed as compared to the case where the rpm of the rotating cylinder is held fixed. This is due to the fact that holding the torque fixed on the outer cylinder makes it adiabatic to momentum. Thus the stability arguments that we presented for plane Couette flow carry over to circular Couette flow: a restriction of constant torque is more unstable than a restriction of constant rpm. In fact, this turns out to be useful to know as experiments are easier to perform in a circular geometry while calculations are easier to perform in a planar geometry. Therefore, conclusions about experiments in circular Couette flow can be drawn based on calculations performed on plane Couette flow.

Extending this stability argument to Poiseulle flow in a channel is not straight forward. The reason is that one cannot imagine holding the pressure drop fixed, even in a thought experiment ! This can be seen by the following illustration: In fig.1.4 there is a flow across the horizontal section of the channel. The pressure at point A on the pipe is held constant by maintaining a constant hydrostatic head. This in turn is achieved by adding the liquid to maintain a constant level. However, the pressure at point B which is the outlet of the pipe cannot be preset, i.e., it cannot be fixed. In fact, there is no reason to believe that for a general case, the pressure at point B is not a function of the transverse position even though for laminar flow in a pipe it is so. Thus, even in a thought experiment, one can imagine only setting the flow rate fixed and not the pressure drop. The pressure drop can only be a response.

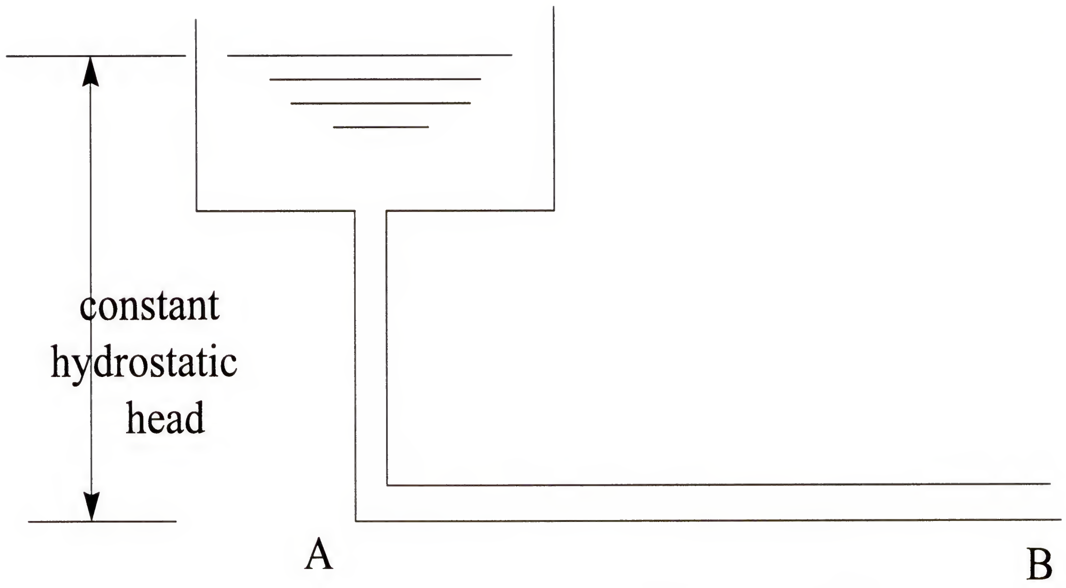

Figure 1.4: Illustration of Poiseulle flow in a pipe

Hence, the stability arguments we presented for plane Couette flow cannot be directly extended to Poiseulle flow in a channel.

CHAPTER 2
THE BASE STATE

In chapter 1, we conjectured that a nose might arise on the base curve of the wall speed vs. the wall stress if the viscosity-temperature dependence is strong enough. Further, we also presented a picture argument based only on looking at the mechanical disturbances to suggest that the rate of decay of disturbances at a point on the base curve is dependent on the restrictions placed on them. To verify the conjectures made in chapter 1, we first need to write a model to describe the base state and then make calculations based on the model to obtain the base curve. After doing this, the stability of the base state needs to be inspected by imposing a small perturbation around the base state and calculating its evolution. This chapter will focus only on the discussion of the model needed to produce the base curve and its properties. We begin by first writing the equations of motion and the equation of thermal energy that describe the base state. This will be done for both plane Couette flow and circular Couette flow, the latter being significant in running experiments. We then present a scaling which will help us shift smoothly from the circular Couette flow equations to the plane Couette flow equations as the gap width goes to zero. This scaling comes in handy as we go along as it enables us to make conclusions about the physical experiments in circular Couette flow based on calculations performed for plane Couette flow. Further, we will establish a rigorous method to predict when a nose ought to occur in the base curve of the wall speed vs. the wall stress. In addition, we will also obtain a result on how the three most important quantities in the flow, the wall speed, the maximum temperature in the gap and the shear stress across the gap are related. We will also present a rough argument based on the temporal behaviour of thermal disturbances to suggest that perturbations at constant wall stress may be more unstable than perturbations at constant wall speed. This is interesting as we will then have arrived at the same result as earlier when only mechanical perturbations were considered. The verification of these arguments for the stability of the base state will be made in the next chapters by carrying out a perturbation calculation and calculating the rate of growth or decay of perturbations.

2.1 The Model

In Chapter 1 we recognized that the definitive feature that determines the shape of the base curve is the strength of the dependence of the viscosity of the liquid on its temperature. In general, the density, heat capacity and the thermal conductivity of liquids depend less strongly on temperature than does the viscosity. Therefore, we write the model for the flow holding the density and the thermal conductivity fixed. Under these conditions, we write the equation of motion for a solenoidal velocity field as

$$\rho\frac{\partial \mathbf{v}}{\partial t} + \rho\mathbf{v}.\nabla\mathbf{v} = -\nabla p + 2\nabla\mu.D + \mu\nabla^2\mathbf{v} \tag{2.1}$$

and the equation of energy as

$$\rho C_v\frac{\partial T}{\partial t} + \rho C_v\mathbf{v}.\nabla T = k\nabla^2 T + 2\mu D : D \tag{2.2}$$

where $2D$ is $(\nabla\mathbf{v} + \nabla\mathbf{v}^T)$.

Now, the base state describes one class of solutions to the non-linear model. To obtain the base equations and hence the base solution, we look for a flow that is steady and unidirectional. Also, we look for the condition that the heat flux in the base state is transverse to the flow such that $\mathbf{v}.\nabla T = 0$. It turns out in this case that a solution can be obtained under these assumptions. When we describe the base flow, we will add the subscript zero to $\mathbf{v}, p$ and T and denote the corresponding viscosity by μ_0 which is shorthand for $\mu(T_0)$.

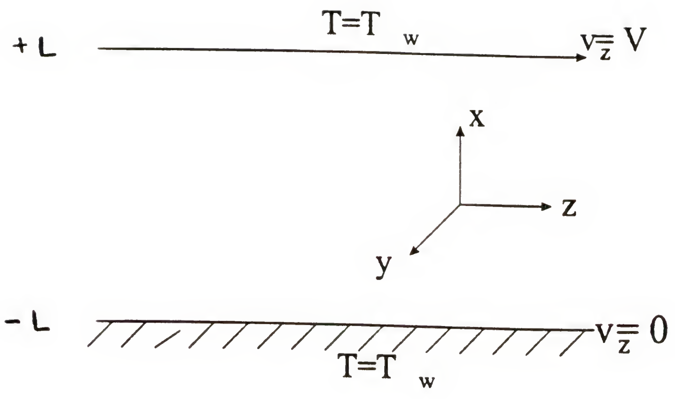

Figure 2.1: Schematic of Plane Couette flow

2.2 The Base Equations

Figure 2.1 illustrates a plane Couette flow setup where the fluid flows in the z direction in the gap. To obtain the base equations, we substitute $\mathbf{v} = v_{z_0}(x)\mathbf{k}$ and $T = T_0(x)$ into the model to get the following equations of motion in the $'x'$ and $'z'$ directions.

$$0 = -\frac{\mathrm{d}p_0}{\mathrm{d}x} \tag{2.3}$$

$$0 = \frac{\mathrm{d}}{\mathrm{d}x}\left(\mu_0 \frac{\mathrm{d}v_{z_0}}{\mathrm{d}x}\right) \tag{2.4}$$

The thermal energy equation becomes

$$0 = k\frac{\mathrm{d}^2T_0}{\mathrm{d}x^2} + \mu_0\left(\frac{\mathrm{d}v_{z_0}}{\mathrm{d}x}\right)^2 \tag{2.5}$$

The boundary conditions to be satisfied are

$$v_{z_0}(x = -L) = 0, v_{z_0}(x = +L) = V_0, T_0(x = +L) = T_w, T_0(x = -L) = T_w$$

The second differential equation tells us that the shear stress $\tau_{xz_0} = \mu_0\left(\frac{\mathrm{d}v_{z_0}}{\mathrm{d}x}\right)$ is constant across the gap and in terms of τ_{xz_0}, the model is simply

$$V_0 = \tau_{xz_0}\int_{-L}^{L}\frac{\mathrm{d}x}{\mu_0} \tag{2.6}$$

and

$$0 = k\frac{\mathrm{d}^2T_0}{\mathrm{d}x^2} + \frac{\tau_{xz_0}^2}{\mu_0} \tag{2.7}$$

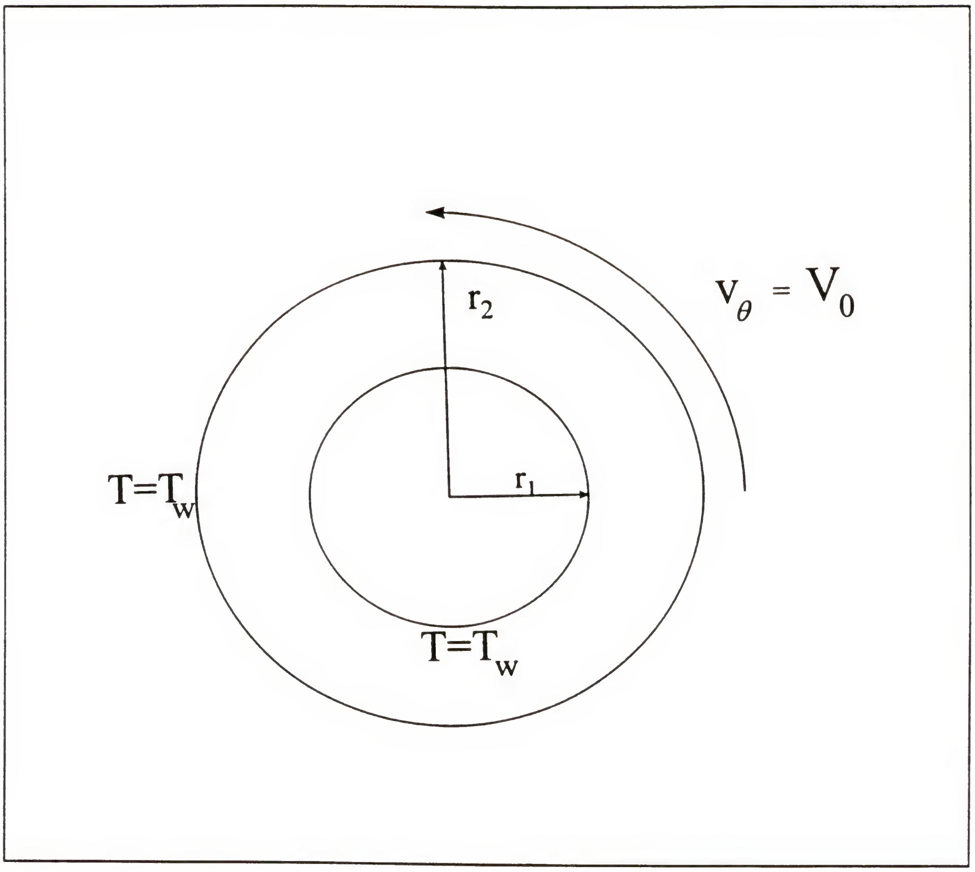

Figure 2.2: Schematic of Circular Couette flow

The first term in the temperature equation describes the rate at which heat is being conducted to the boundaries and the second term describes the heat generation by viscous dissipation. It is worth noting that this equation bears some resemblance to a model of thermal ignition in a catalyst pellet. More on this will be discussed in an endnote to this chapter.

The experiments to realize this flow are more easily performed in a circular Couette flow rather than in a plane Couette flow configuration. This being the case, the base equations for circular Couette flow will be presented alongside the corresponding equations for plane Couette flow.

Figure 2.2 illustrates a circular Couette flow setup. Here, the fluid flows in the azimuthal direction in the gap between the two concentric cylinders. The radius of the inner cylinder is r_1 and the radius of the outer cylinder is r_2. In keeping with the assumptions, we put $\mathbf{v} = v_{\theta_0}(r)\mathbf{i}_\theta$, $p = p_0(r)$ and $T = T_0(r)$ to obtain the r and θ components of the equation of motion,

$$-\frac{\rho v_{\theta_0}^2}{r} = -\frac{\mathrm{d}p_0}{\mathrm{d}r}$$

$$0 = \frac{\mathrm{d}}{\mathrm{d}r}\left[r^3 \mu_0 \frac{\mathrm{d}}{\mathrm{d}r}\left(\frac{v_{\theta_0}}{r}\right)\right]$$

with the boundary conditions

$$v_{\theta_0}(r = r_2) = V_0, v_{\theta_0}(r = r_1) = 0$$

This equation tells us that the quantity $r^3\mu_0 \frac{\mathrm{d}}{\mathrm{d}r}\left(\frac{v_{\theta_0}}{r}\right)$ is a constant across the gap and in fact $2\pi r^3 \mu_0 \frac{\mathrm{d}}{\mathrm{d}r}\left(\frac{v_{\theta_0}}{r}\right)$ is the torque per unit length.

The equation of thermal energy is

$$0 = k\frac{1}{r}\frac{\mathrm{d}}{\mathrm{d}r}\left(r\frac{\mathrm{d}T_0}{\mathrm{d}r}\right) + \mu_0\left[r\frac{\mathrm{d}}{\mathrm{d}r}\left(\frac{v_{\theta_0}}{r}\right)\right]^2$$

with the following boundary conditions

$$T_0(r = r_2) = T_w, T_0(r = r_1) = T_w$$

Let us digress a moment and make some observations about the boundary conditions on velocity. In writing the boundary conditions, we have assumed that the outer cylinder is rotated while the inner cylinder is held fixed. It may be shown for the flow of an inviscid fluid between concentric cylinders that the azimuthal flow between concentric cylinders is stable to centrifugal instability, if the angular momentum per unit volume increases with an increase in radius. The condition to be satisfied for stability is then

$$\frac{\mathrm{d}}{\mathrm{d}r}\left(\rho r^2 \Omega_0\right)^2 > 0$$

where Ω_0 is the angular speed v_{θ_0}/r. For the above choice of boundary conditions, the angular momentum is stably stratified if an inviscid fluid adopted the corresponding velocity profile. To see this, first observe that the condition to be looked at, when the density is a constant is

$$\frac{\mathrm{d}}{\mathrm{d}r}\left(r^2\Omega_0\right)^2 > 0$$

where Ω_0 is $\frac{\Omega_2 \int_{r=r_1}^{r=r} \frac{1}{\mu_0}\frac{\mathrm{d}r}{r^3}}{\int_{r=r_1}^{r=r_2} \frac{1}{\mu_0}\frac{\mathrm{d}r}{r^3}}$ when the outer cylinder is spun with an angular speed Ω_2 and the inner cylinder is held fixed. Therefore the condition becomes

$$\frac{\mathrm{d}}{\mathrm{d}r}\left(\frac{r^2\Omega_2}{\int_{r=r_1}^{r=r_2} \frac{1}{\mu_0}\frac{\mathrm{d}r}{r^3}} \int_{r=r_1}^{r=r} \frac{1}{\mu_0}\frac{\mathrm{d}r}{r^3}\right)^2 > 0$$

which yields

$$\frac{2r^2\Omega_2}{\int_{r=r_1}^{r=r_2} \frac{1}{\mu_0}\frac{\mathrm{d}r}{r^3}} \int_{r=r_1}^{r=r} \frac{1}{\mu_0}\frac{\mathrm{d}r}{r^3}\left(\frac{2r\Omega_2}{\int_{r=r_1}^{r=r_2} \frac{1}{\mu_0}\frac{\mathrm{d}r}{r^3}} \int_{r=r_1}^{r=r} \frac{1}{\mu_0}\frac{\mathrm{d}r}{r^3} + \frac{r^2\Omega_2}{\int_{r=r_1}^{r=r_2} \frac{1}{\mu_0}\frac{\mathrm{d}r}{r^3}} \frac{1}{\mu_0}\frac{1}{r^3}\right) > 0$$

where the second term within the paranthesis is obtained by the use of Leibnitz rule. Obviously, the condition is satisfied and this then ensures that the centrifugal forces cannot destabilize the base flow, at least from an argument based on the inviscid limit. Now, incorporating a finite but constant viscosity has been proved to be stabilizing in this flow[1]. We will assert that the same continues to hold even if there is a viscosity variation in the gap. This result is important as the focus of our work is not in the study of instability arising from the centrifugal forces. Rather it is to inquire whether the temperature dependence of viscosity can affect the stability of the flow which is otherwise stable and what, if any, are the modes of instability. Henceforth, unless otherwise stated, it is assumed that in all our experiments the outer cylinder is spun while keeping the inner cylinder fixed.

Getting back to the θ component of the equation of motion, we will denote the quantity $\left[r^3\mu_0\frac{\mathrm{d}}{\mathrm{d}r}\left(\frac{v_{\theta 0}}{r}\right)\right]$ as τ_0. In terms of τ_0, which has units of torque per unit length, the model is simply

$$\frac{V_0}{r_2} = \tau_0 \int_{r=r_1}^{r=r_2} \frac{1}{\mu_0}\frac{\mathrm{d}r}{r^3} \tag{2.8}$$

and

$$0 = k\frac{1}{r}\frac{\mathrm{d}}{\mathrm{d}r}\left(r\frac{\mathrm{d}T_0}{\mathrm{d}r}\right) + \frac{1}{\mu_0}\frac{{\tau_0}^2}{r^4} \tag{2.9}$$

where the first equation is obtained by integrating the θ component of the equation of motion using the condition that $v_{\theta_0} = 0$ when $r = r_1$ and $v_{\theta_0} = V_0$ when $r = r_2$.

Inspecting the base equations in circular Couette flow and their companion equations in plane Couette flow, we observe the following:

- In circular Couette flow, the torque per unit length $2\pi r^2 \tau_{r\theta_0}$ (where $\tau_{r\theta_0}$ is the shear stress, $\mu_0 r \frac{\mathrm{d}}{\mathrm{d}r}\left(\frac{v_{\theta_0}}{r}\right)$) is constant across the gap. But, in plane Couette flow, the shear stress τ_{xz_0} is constant across the gap. The extra r^2 that is seen in the torque expression in circular Couette flow is due to the fact that the shear stress has to be multiplied by the surface area $2\pi r$ to get the force per unit length. On taking the moment by multiplying with r, we obtain the torque per unit length. It is only due to this, that we see an extra term $1/r^4$ multiplying the viscous dissipation term in circular Couette flow. As the viscous dissipation is $\frac{\tau_{r\theta_0}^2}{\mu_0}$, when written in terms of τ_0, it becomes $\frac{1}{\mu_0}\frac{\tau_0^2}{r^4}$.

It will turn out that the equations in the planar geometry are easier to solve compared to the corresponding equations in circular geometry. Even though this may not be obvious in general at this stage wherein only the base equations are being discussed, there is one advantage even at this stage: the radius ratio r_1/r_2, which occurs as a parameter in equations describing circular Couette flow does not appear in the equations describing plane Couette flow. In the limit of a thin gap, the circular Couette flow equations become identical to the planar equations and the centrifugal term goes to zero. Moreover, as we have already eliminated the possibility of any instability originating from the centrifugal term by declaring that the outer cylinder is being rotated, we do not lose any relevant information by performing a thin gap approximation. Therefore, the plane Couette flow equations become valid approximations to the circular Couette flow equations in the limit of a thin gap. This enables us, as we go along, to draw some general conclusions about the experiments in circular Couette flow based on calculations performed for plane Couette flow. We will find that by scaling the circular Couette flow equations using the length scale based on the gap width $(r_2 - r_1)$, the plane Couette flow equations are recovered in the limit of a thin gap. This scaling is quite useful as it serves as a bridge between our calculations which are easier to perform in planar geometry and our experiments which are easier to conduct in circular geometry. We will demonstrate this next.

2.3 Thin Gapping the Circular Couette Flow Equations to obtain the Plane Couette Flow Equations

Let $\Delta = (r_2 - r_1)$ be the gap width between the two cylinders and $r^* = \frac{r - r_1}{r_2 - r_1}$ be the dimensionless radius such that when $r = r_1, r^* = 0$ and when $r = r_2, r^* = 1$. Using this the model equations to $O(\epsilon^2)$ become

$$V_0 \left(1 - \epsilon\right) = \tau_0 \Delta \int_{r^*=0}^{r^*=1} \frac{1}{\mu_0} \frac{1}{{r_1}^2} \left(1 - 3r^* \epsilon\right) \mathrm{d}r^* \tag{2.10}$$

and

$$0 = k \frac{\mathrm{d}^2 T_0}{\mathrm{d}r^{*2}} + k\epsilon \frac{\mathrm{d}T_0}{\mathrm{d}r^*} + \frac{1}{\mu_0} \left(\frac{\tau_0^2 \Delta^2}{r_1^4} \right) \left(1 - 4r^* \epsilon\right) \tag{2.11}$$

where $\epsilon = \Delta / r_1$. As $\epsilon \to 0$, these equations become

$$V_0 = \frac{\tau_0 \Delta}{{r_1}^2} \int_{r^*=0}^{r^*=1} \frac{1}{\mu_0} \mathrm{d}r^* \tag{2.12}$$

and

$$0 = k \frac{\mathrm{d}^2 T_0}{\mathrm{d}r^{*2}} + \frac{1}{\mu_0} \left(\frac{\tau_0^2 \Delta^2}{r_1^4} \right) \tag{2.13}$$

Now, scaling x in the velocity and in the temperature equations in plane Couette flow with respect to half the gap width, L, such that $x^* = x/L$, we obtain,[1]

$$V_0 = \tau_{xz0} L \int_{x^*=-1}^{x^*=1} \frac{1}{\mu_0} \mathrm{d}x^* \tag{2.14}$$

and

$$0 = k \frac{\mathrm{d}^2 T_0}{\mathrm{d}x^{*2}} + \frac{1}{\mu_0} \left(\tau_{xz0}^2 L^2 \right) \tag{2.15}$$

---

[1] Observe that the scaled gap width goes from 0 to 1 in circular Couette flow and it goes from -1 to 1 in plane Couette flow and this is solely due to the fact that x was chosen to run from $-L$ to L as this choice provides a symmetry in the temperature profile.

Comparing the scaled equations in circular Couette flow as $\epsilon \to 0$ to the corresponding scaled equations in plane Couette flow, we find that in the limit of a thin gap, for a fixed wall speed, V_0, the circular Couette flow can be modeled by the equations for plane Couette flow with $\tau_0\Delta/r_1^2$ in circular Couette flow, where τ_0 has units of torque/unit length, playing the role of $\tau_{xz_0}L$ in plane Couette flow. As the gap width, Δ, goes to zero, τ_0 tends to ∞ but it can be proved that the quantity $\tau_0\Delta/r_1^2$ remains bounded by proving that $\tau_{xz_0}L$ remains bounded. In fact, we can prove that the quantity $\tau_{xz_0}L$ not only remains bounded but is also a constant. To show this, we will first prove that the maximum temperature in plane Couette flow is independent of the gap width by considering the unscaled temperature equation

$$0 = k\frac{\mathrm{d}^2 T_0}{\mathrm{d}x^2} + \mu_0\left(\frac{\mathrm{d}v_{z_0}}{\mathrm{d}x}\right)^2$$

This statement might seem a little puzzling at first for the following reason: When the wall speed is held fixed and if the gap width is increased the velocity gradient which is the source of the frictional heat decreases and hence there is less heat to be conducted to the boundary. But this heat has to be conducted across a larger distance to reach the boundary. Therefore, it would seem that the maximum temperature in the gap can either increase or decrease with an increase in the gap size. However, scaling the energy equation tells us that the scaled heat generation and scaled heat conduction terms are independent of gap width. To see that, let us scale x by the gap width L such that $x^* = x/L$, the velocity v_{z_0} by the wall speed V_0 such that $v^*_{z_0} = v_{z_0}/V_0$ in the energy equation above to get

$$0 = k\frac{\mathrm{d}^2 T_0}{\mathrm{d}x^{*2}} + \mu_0 V_0^2\left(\frac{\mathrm{d}v^*_{z_0}}{\mathrm{d}x^*}\right)^2$$

Now, if the wall speed V_0 is fixed, this equation tells us that the maximum temperature in the gap is independent of the gap width: To see this, we first scale the equation for the shear stress

$$\tau_{xz_0} = \mu_0\left(\frac{\mathrm{d}v_{z_0}}{\mathrm{d}x}\right)$$

using the scale $x^* = x/L$ and $v^*_{z_0} = v_{z0}/V_0$ to obtain

$$\tau_{xz0} = \frac{\mu_0 V_0}{L}\left(\frac{\mathrm{d}v^*_{z0}}{\mathrm{d}x^*}\right)$$

Hence we obtain for the scaled velocity gradient

$$\left(\frac{\mathrm{d}v^*_{z0}}{\mathrm{d}x^*}\right) = \frac{\tau_{xz0} L}{\mu_0 V_0}$$

where we know that

$$\tau_{xz0} L = \frac{V_0}{\int_{-1}^{1} \frac{\mathrm{d}x^*}{\mu_0}}$$

Substituting this in the expression for $\frac{\mathrm{d}v^*_{z0}}{\mathrm{d}x^*}$, we obtain for the scaled velocity gradient,

$$\left(\frac{\mathrm{d}v^*_{z0}}{\mathrm{d}x^*}\right) = \frac{1}{\mu_0 \int_{-1}^{1} \frac{\mathrm{d}x^*}{\mu_0}}$$

The temperature equation therefore becomes

$$0 = k\frac{\mathrm{d}^2 T_0}{\mathrm{d}x^{*2}} + \frac{V_0^2}{\mu_0 \int_{-1}^{1} \left[\frac{\mathrm{d}x^*}{\mu_0}\right]^2}$$

Therefore, we find that the maximum temperature does not depend on the gap width. For constant temperature boundary conditions, the maximum temperature occurs at the channel centre. However, it should be observed that the same conclusion cannot be drawn if the wall shear stress is held fixed instead of the wall speed. To see this, let us rewrite the unscaled temperature equation as

$$0 = k\frac{\mathrm{d}^2 T_0}{\mathrm{d}x^2} + \frac{\tau^2_{xz0}}{\mu_0}$$

where $\mu_0 \frac{\mathrm{d}v_{z0}}{\mathrm{d}x} = \tau_{xz0}$. Once again, scaling x by the gap width L such that $x^* = x/L$, we get

$$0 = k\frac{\mathrm{d}^2 T_0}{\mathrm{d}x^{*2}} + L^2\frac{\tau^2_{xz0}}{\mu_0}$$

we find that for a fixed wall stress the the gap width L is not eliminated from the equation and therefore, the maximum temperature depends on the gap width.

Now, to obtain the conclusion that for a fixed velocity, $\tau_{xz_0}L$ is a constant, consider the equation

$$V_0 = \tau_{xz_0}L\int_{-1}^{1}\frac{\mathrm{d}x^*}{\mu_0}$$

Now for a fixed wall speed, the maximum temperature in the gap is fixed by our earlier conclusion. This therefore fixes the temperature profile across the gap and hence the fluidity profile in the gap, which is the integral. This proves that for fixed V_0, the quantity $\tau_{xz_0}L$ is fixed. Now, we know that $\tau_0\Delta/r_1^2$ approaches $\tau_{xz_0}L$ as $\Delta \to 0$. As we have just proved that $\tau_{xz_0}L$ is fixed for a fixed V_0, the conclusion then is that as $\Delta \to 0$, $\tau_0\Delta/r_1^2$ approaches a constant value.

One more question that might be posed now is whether $\tau_0\Delta/r_1^2$ approaches $\tau_{xz_0}L$ from the right or from the left in a graph of V_0 plotted on the abscissa vs. $\tau_0\Delta/r_1^2$ plotted on the ordinate. In an endnote, we will provide a calculation to show that for a fixed wall speed, the quantity $\tau_0\Delta/r_1^2$ increases as the gap width is increased from zero. This will then prove that as $\Delta \to 0$, $\tau_0\Delta/r_1^2$ approaches $\tau_{xz_0}L$ from the right.

To see how the centrifugal term is lost in the limit of $\epsilon \to 0$, scale the r component of equation of motion with respect to the gap width, to obtain

$$-\rho v_{\theta_0}^2\frac{\epsilon}{1+r^*\epsilon} = -\frac{\mathrm{d}p_0}{\mathrm{d}r^*}$$

and observe that as $\epsilon \to 0$, we obtain

$$\frac{\mathrm{d}p_0}{\mathrm{d}r^*} = 0$$

which is precisely the transverse component of the equation of motion in plane Couette flow.

We will demonstrate later on in this thesis that the circular Couette flow equations approach the plane Couette flow equations not only in the base state but even when a perturbation is carried out.

In trying to discuss the properties of the base equations and to obtain its solution, it is in some ways useful to write the problem in scaled variables as this reduces the number of variables in the model. It is to this task that we turn.

2.4 Scaling

We begin by scaling the thermal energy equation in plane Couette flow as it describes the base state. We use the following scaled variables, ${\theta_0}^* = (T_0 - T_w)/T_{\text{ref}}$, $x^* = x/L$, $v^*_{z_0} = v_{z0}/V_{\text{ref}}$ and $\mu^*_0 = \mu_0/\mu_w$, to get

$$0 = kT_{\text{ref}}\frac{\mathrm{d}^2\theta^*_0}{\mathrm{d}x^{*2}} + \mu_w V^2_{\text{ref}}\mu^*_0\left[\frac{\mathrm{d}v^*_{z0}}{\mathrm{d}x^*}\right]^2 \tag{2.16}$$

This gives

$$0 = \frac{\mathrm{d}^2\theta^*_0}{\mathrm{d}x^{*2}} + \frac{\mu_w V^2_{\text{ref}}}{kT_{\text{ref}}}\mu^*_0\left[\frac{\mathrm{d}v^*_{z0}}{\mathrm{d}x^*}\right]^2 \tag{2.17}$$

where the reference velocity V_{ref} and the reference temperature T_{ref} are yet to be chosen and where their choice decides the various scaling options for this problem[2].

In the most important scaling that we use in this thesis, we introduce the scaled fluidity via

$$f^*_0 = \frac{1}{\mu^*_0} = \frac{\mu_w}{\mu_0}$$

where μ_w denotes $\mu(T_w)$. Then the sensitivity of the fluidity to the temperature determines a useful temperature scale. To see that, let S denote $\frac{\mathrm{d}f^*_0}{\mathrm{d}T_0}$ evaluated at T_w. Then choosing the reference temperature T_{ref} to be $1/S$ gives the scaled temperature rise $\theta^*_0 = S(T_0 - T_w)$. For all fluidities that increase with an increase in temperature[3] this scaling requires in addition to $f^*_0(\theta^*_0 = 0) = 1$, that $f^{*'}_0(\theta^*_0 = 0) = 1$, where $'$ denotes differentiation with respect to θ^*_0. We then choose the reference velocity V_{ref} to be $\sqrt{(k/S\mu_w)}$ so that the term in front of the scaled viscous dissipation term becomes unity. Then the scaling of the shear stress comes out of the equation

---

[2] We will discuss one scaling option here and the rest in an endnote of this chapter.

[3] For fluids whose fluidity decreases with an increase in temperature we define $\frac{\mathrm{d}f^*_0}{\mathrm{d}T_0}$ evaluated at T_w as $-S$ where S is positive. Then choosing $T_{\text{ref}} = 1/S$ and $\theta^*_0 = S(T_0 - T_w)$, it follows that $f^{*'}_0(\theta^*_0 = 0) = -1$.

$$\tau_{xz0} = \mu_0 \frac{\mathrm{d}v_{z0}}{\mathrm{d}x}$$

The reference shear stress $\tau_{xz_{\mathrm{ref}}}$ can be calculated from this equation and it is $\tau_{xz_{\mathrm{ref}}} = \mu_w V_{ref}/L = \sqrt{k\mu_w/SL^2}$. We now write the model and its boundary condition in terms of these scaled variables as[4]

$$V_0^* = \tau_{xz0}^* \int_{-1}^{1} f_0{}^* \mathrm{d}x^* \tag{2.20}$$

$$0 = \frac{\mathrm{d}^2\theta_0^*}{\mathrm{d}x^{*2}} + \mu_0^* \left[\frac{\mathrm{d}v_{z0}^*}{\mathrm{d}x^*}\right]^2 \tag{2.21}$$

which written in terms of the scaled shear stress τ_{xz0}^* yields

$$0 = \frac{\mathrm{d}^2\theta_0^*}{\mathrm{d}x^{*2}} + f_0{}^* \tau_{xz0}^{*2} \tag{2.22}$$

There are several points that are worth noting about this scaling:

- This velocity scale is based on the physical properties of the fluid and is independent of the speed at which the plate is moved.

- For fluidity functions that have only one sensitivity parameter in them, for example, linear or exponential, there is one master curve of the scaled wall speed vs. the scaled wall stress and this curve is independent of the sensitivity, S for that relationship.

- As $S \to 0$, this scale fails to recover the case of constant viscosity. This difficulty can be overcome easily if the temperature difference scale is chosen based on the wall temperature, but this, then, is at the sacrifice of losing a master curve.

---

[4] The equations in circular Couette flow scaled in the same way become

$$V_0^* = \tau_0{}^* \int_{\eta}^{1} \frac{f_0{}^* \mathrm{d}r^*}{r^{*3}} \tag{2.18}$$

$$0 = \frac{1}{r^*}\frac{\mathrm{d}}{\mathrm{d}r^*}\left(r^* \frac{\mathrm{d}\theta_0^*}{\mathrm{d}r^*}\right) + \frac{\tau_0{}^{*2} f_0{}^*}{r^{*4}} \tag{2.19}$$

with $\theta_0^* = 0$ at $r^* = \eta, 1$.

The base temperature and velocity equations have a lot of nice properties. First, depending on the form of the fluidity an explicit formula for θ_0 as a function of x can be obtained, and when this is done V_0 is obtained with little additional work. It turns out that for the special case of linear fluidity this is true. Secondly, a prediction of when a nose ought to occur in the base curve of V_0 vs. τ_{xz_0} for a general class of fluidities can be obtained from these equations without a numerical calculation. In fact, it turns out that the base solution that we will obtain for linear fluidity provides a motivation for us to carry out this analysis for a general class of fluidities. We will therefore first get to the base solutions for linear fluidity. Henceforth, we will drop the $*$ but still work in the scaled variables.

2.5 The Base Solution for the Case of Linear Fluidity

For the case of linear fluidity, $f_0 = (1+\theta_0)$, the solution to the base temperature equation in plane Couette flow

$$0 = \frac{\mathrm{d}^2\theta_0}{\mathrm{d}x^2} + f_0\tau_{xz_0}^2$$

is simple. It is

$$\theta_0 = -1 + \frac{\cos(\tau_{xz_0}x)}{\cos(\tau_{xz_0})}$$

and V_0 is determined by τ_{xz_0} via

$$V_0 = 2\tan\tau_{xz_0}$$

This result is interesting in itself. It tells us that for every value of wall speed V_0, there corresponds a steady shearing flow. The values of wall stress corresponding to this family of shearing flows are bounded by $\tau_{xz_0} = \frac{\pi}{2}$. For values of $\tau_{xz_0} > \frac{\pi}{2}$, the base temperature equation has a solution but the temperature rise turns out to be negative over part of the flow domain. However all values of V_0 are already obtained before this happens.

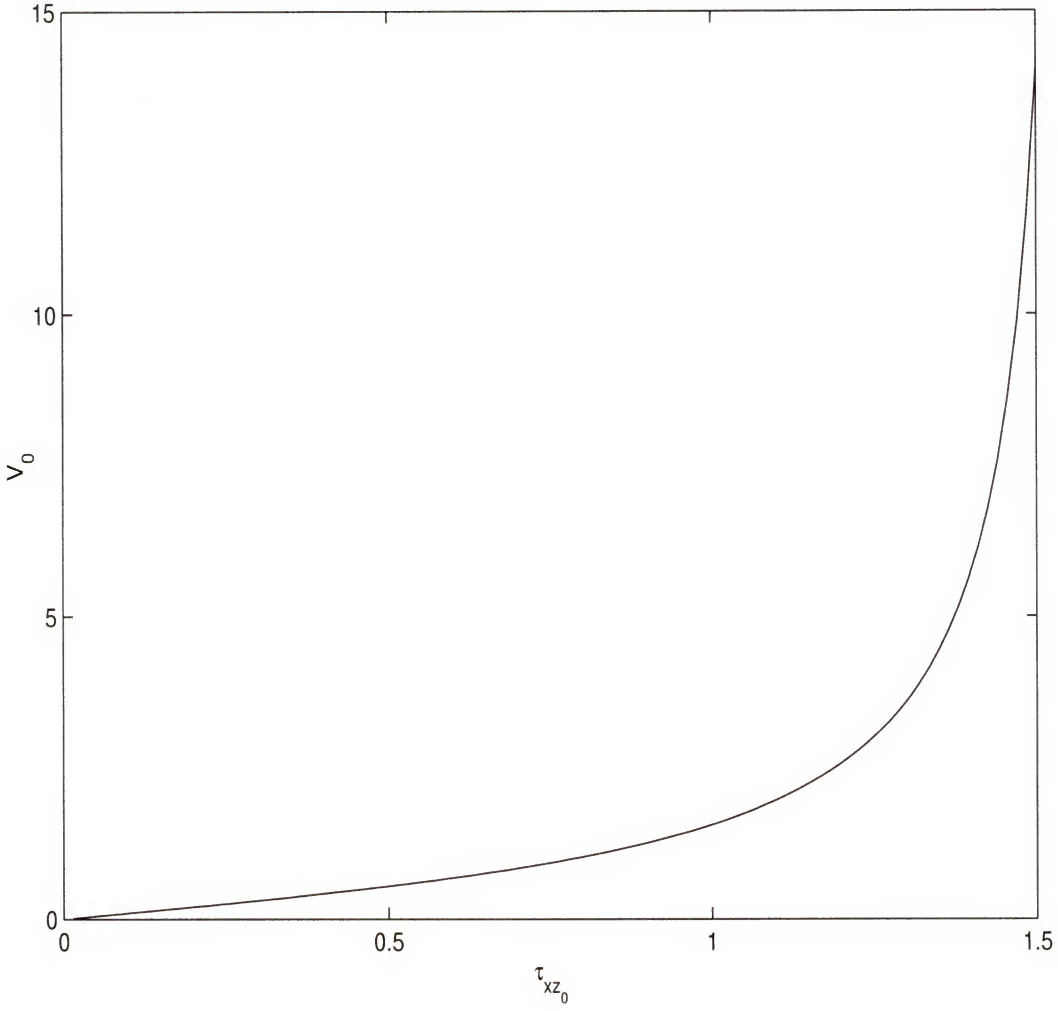

Figure 2.3: V_0 vs.τ_{xz_0} for linear fluidity

Figure 2.3 shows the plot of V_0 vs. τ_{xz_0}. The curve exhibits a lower branch and a nose, the nose lying at $\tau_{xz_0} = \frac{\pi}{2}$ where the ordinate is asymptotically infinite. This curve does not turn back and the upper branch is missing. We assert that to have an upper branch, we need $f_0{}'' > 0$ at least in some range. In other words, we conjecture that the base curve for linear fluidity with $f_0'' = 0$ uniformly lies at the edge of backward bending base curves.

Next, we will now go on to the prediction of the noses without a numerical calculation.

2.6 Prediction of the Nose on the Base Curve without performing a Numerical Calculation

To predict when a nose ought to occur in the base curve of V_0 vs. τ_{xz0}, all we have to do is to find when $\frac{\mathrm{d}V_0}{\mathrm{d}\tau_{xz0}}$ goes unbounded. Now,

$$V_0 = \tau_{xz0} \int_{-1}^{+1} f_0 \mathrm{d}x$$

Hence

$$\frac{\mathrm{d}V_0}{\mathrm{d}\tau_{xz0}} = \int_{-1}^{+1} \left[f_0 + \tau_{xz0} f_0' \frac{\mathrm{d}\theta_0}{\mathrm{d}\tau_{xz0}} \right] \mathrm{d}x$$

Therefore, it follows that to decide when $\frac{\mathrm{d}V_0}{\mathrm{d}\tau_{xz0}}$ goes unbounded, it is enough to find an equation for $\frac{\mathrm{d}\theta_0}{\mathrm{d}\tau_{xz0}}$ and inquire when it becomes unbounded. Getting an equation for $\frac{\mathrm{d}\theta_0}{\mathrm{d}\tau_{xz0}}$ is easy. It only requires us to differentiate the equation for θ_0, viz.,

$$\frac{\mathrm{d}^2\theta_0}{\mathrm{d}x^2} + f_0 \tau_{xz0}^2 = 0 \tag{2.23}$$

with

$$\theta_0(x = \pm 1) = 0$$

to obtain

$$\frac{\mathrm{d}^2\dot{\theta}_0}{\mathrm{d}x^2} + f_0' \tau_{xz0}^2 \dot{\theta}_0 + 2 f_0 \tau_{xz0} = 0 \tag{2.24}$$

with

$$\dot{\theta}_0(x = \pm 1) = 0$$

where $\dot{\theta}_0 = \frac{\mathrm{d}\theta_0}{\mathrm{d}\tau_{xz0}}$.

First observe the temperature equation which tells us that unless $\tau_{xz0} = 0$, θ_0 is positive at each interior value of x. This can be shown by contradiction, i.e., we will assume a temperature profile that is not positive everywhere in the interior and find that we end up with a contradiction. Specifically, we will assume a temperature profile which has a zero in the interior and see whether it satisfies the θ_0 equation and the boundary conditions. The temperature profile with a zero in the interior is

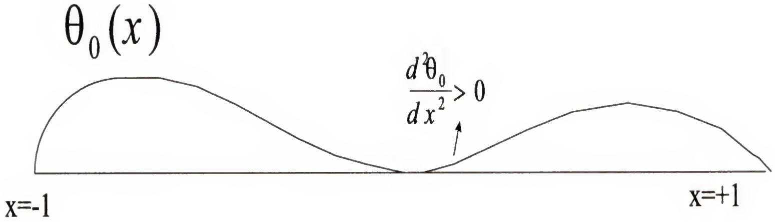

Figure 2.4: The base temperature profile with a zero in the interior.

illustrated in figure 2.4. Note that at the point where the temperature rises from zero in the interior, $\frac{\mathrm{d}^2\theta_0}{\mathrm{d}x^2} > 0$. This, however violates the requirement that $\frac{\mathrm{d}^2\theta_0}{\mathrm{d}x^2} < 0$ which the θ_0 equation demands. Therefore, we have proved by contradiction that $\theta_0 > 0$ in the interior $\tau_{xz0} > 0$.

Secondly, based on the $\dot{\theta}_0$ equation, we can conclude that each value of θ_0 in the interior increases as τ_{xz0} increases along the lower branch of the base solution curve, i.e. $\dot{\theta}_0 > 0$ along the lower branch. To see this, observe that $\dot{\theta}_0 = 0$ when $\tau_{xz0} = 0$ along the lower branch. (Note that this is not true along the upper branch, if it exists, as there the temperature rise is much higher and hence as $\tau_{xz0} \to 0$, $f_0, f_0^{'}$ might tend to ∞ thereby making it difficult to prove the sign of $\dot{\theta}_0$). This implies that a curve of θ_0 vs. τ_{xz0} begins with a slope of zero. Further, we learn that $\dot{\theta}_0 > 0$ when τ_{xz0} is small. To see this observe that when τ_{xz0} is small, the term with τ_{xz0}^2 in it can be dropped off, of course, only along the lower branch. Under this limit the $\dot{\theta}_0$ equation then is

$$\frac{\mathrm{d}^2\dot{\theta}_0}{\mathrm{d}x^2} + 2f_0\tau_{xz0} = 0$$

and this then proves that the curvature of $\dot{\theta}_0$ is negative for small τ_{xz0}. As $\dot{\theta}_0$ is zero at the boundaries, it must be positive.

Now to extend the above argument to prove that $\dot{\theta}_0 > 0$ is true along the entire lower branch, we again invoke the proof by contradiction. We look for an interior point and a value of τ_{xz0} where $\dot{\theta}_0$ just vanishes. At such a point we have

$$\frac{\mathrm{d}^2\dot{\theta}_0}{\mathrm{d}x^2} + 2f_0\tau_{xz0} = 0$$

and once again we conclude that $\dot{\theta}_0 > 0$ at each interior value of x.

To see what happens as τ_{xz_0} increases along the lower branch and reaches the nose of the curve, we introduce an eigenvalue problem. It is

$$\frac{\mathrm{d}^2\phi}{\mathrm{d}x^2} + f_0{}' \lambda^2 \phi = 0 \tag{2.25}$$

We presume that anything untoward in the behavior of $\dot{\theta}_0$ as we increase τ_{xz_0} should also show its signature in this eigenvalue problem. Now, at each point of the base curve, this eigenvalue problem must be solved. The way this calculation goes is like this: Assume a value of τ_{xz_0} corresponding to a point on the base curve. Solve the temperature equation to get $\theta_0(x)$ and from this $f_0(x)$ and hence $f_0^{'}(x)$. Once this is obtained substitute it in the eigenvalue problem and solve it. Note that this somewhat lengthy calculation procedure simplifies if $f_0^{'}$ is a constant. Fortunately, we know one fluidity where $f_0^{'}$ is a constant: It is the case of linear fluidity! In fact, for this case $f_0^{'}$ is not only a constant but $f_0^{'} = 1$. Not only that, we now know from our earlier calculations from the base equations that the nose for the linear fluidity lies at the value of $\tau_{xz_0} = \frac{\pi}{2}$. Therefore, by substituting $f_0^{'} = 1$ in the eigenvalue problem, we can check whether we get some information which points to the fact that the nose lies at $\tau_{xz_0} = \frac{\pi}{2}$ for linear fluidity. That is what we will do next.

Substituting $f_0^{'} = 1$ in the eigenvalue problem, we obtain for the eigenvalues $\lambda_1 = \frac{\pi}{2}, \lambda_2 = \pi$ and so on, and the eigenfunctions are $\phi_1 = \cos(\frac{\pi}{2}x)$ and $\phi_2 = \sin(\pi x)$ and so on. It should be noted that the linear fluidity is the only case wherein the eigenvalues and the eigenfunctions do not depend on τ_{xz_0}. And for this case if we plot $\lambda_1(\tau_{xz_0})$ which is equal to $\pi/2$ and τ_{xz_0} itself versus τ_{xz_0}, the graphs intersect at $\tau_{xz_0} = \pi/2$, the nose shear stress value of the base curve. This turns out to be true in general and introduces a useful definition of the nose of the curve. *A point of the curve is a nose if and only if* $\lambda_1(\tau_{xz_0}) = \tau_{xz_0}$. This remains to be established but in the case of linear fluidity it turns out be true as we just observed.

Now, to establish that $\lambda_1(\tau_{xz_0}) = \tau_{xz_0}$ defines a nose for a general class of fluidities, let us first see what the eigenvalues do as τ_{xz_0} increases along the lower branch of the base curve. We first observe that when $\tau_{xz_0} = 0$ then $\theta_0 = 0$ and $f_0' = 1$. So, the eigenvalues start out at linear fluidity values. To go on, we let $\dot{\phi}_i$ denote $\mathrm{d}\phi_\mathrm{i}/\mathrm{d}\tau_{\mathrm{xz}_0}$ and $\dot{\lambda_i}^2$ denote $\mathrm{d}\lambda_i^2/\mathrm{d}\tau_{xz_0}$ and differentiate the eigenvalue problem getting

$$\frac{\mathrm{d}^2\dot{\phi}_i}{\mathrm{d}x^2} + {f_0}'{\lambda_i}^2\dot{\phi}_i = -{f_0}''\dot{\theta}_0{\lambda_i}^2\phi_i - {f_0}'\dot{\lambda_i}^2\phi_i \tag{2.26}$$

with

$$\dot{\phi}_i(x = \pm 1) = 0$$

To determine $\dot{\phi}_i$ requires a solvability condition to be satisfied. It is

$$\dot{\lambda_i}^2 = -{\lambda_i}^2\frac{\int_{-1}^{1} {f_0}''\dot{\theta}_0{\phi_i}^2\mathrm{d}x}{\int_{-1}^{1} {f_0}'{\phi_i}^2\mathrm{d}x} \tag{2.27}$$

and it must be always satisfied as $\dot{\phi}_i$ could be determined by getting ϕ_i and then differentiating it with respect to τ_{xz_0}. This tells us that ${\lambda_i}^2$ decreases as τ_{xz_0} increases on the lower branch of the base curve because $\dot{\theta}_0$ is positive there. And this is true for all convex fluidities such that $f_0'' > 0$.

Now, to establish that the fundamental eigenvalue, $\lambda_1(\tau_{xz_0})$ defines the nose, observe that as τ_{xz_0} increases along the lower branch, $\lambda_1(\tau_{xz_0})$ decreases from its value of $\frac{\pi}{2}$ which it takes at $\tau_{xz_0} = 0$. As long as $\lambda_1(\tau_{xz_0})$ remains above τ_{xz_0} it continues to be true that $\dot{\theta}_0$ remains positive. But when τ_{xz_0} grows large enough such that $\lambda_1(\tau_{xz_0}) = \tau_{xz_0}$, the $\dot{\theta}_0$ equation requires that a solvability condition be satisfied before it can be solved as the corresponding homogeneous equation has solutions that are multiples of ϕ_1. This solvability condition is

$$\int_{-1}^{1} 2f_0\tau_{xz_0}\phi_1\mathrm{d}x = 0 \tag{2.28}$$

This cannot be satisfied ! The reason is that all the factors in this equation are positive and ϕ_1 is singly signed. The value of $\dot{\theta}_0$ cannot be determined and it then must be infinitely large. This then is the nose of the curve as $\dot{\theta}_0 = \frac{\mathrm{d}\theta_0}{\mathrm{d}\tau_{xz_0}}$ becomes unbounded. The problem is not with $\dot{\theta}_0$ but with τ_{xz_0}. We have reached the end of its increase along the lower branch of the base curve and it is turning back along the upper branch. The nose terminates the lower branch when $\lambda_1(\tau_{xz_0}) = \tau_{xz_0}$. This defines the value of τ_{xz0} at the nose and there, by the $\dot{\lambda}^2$ equation, the value of $\dot{\lambda}_i^2 \to -\infty$ as τ_{xz_0} tends to the nose on the lower branch. We can see how $\dot{\theta}_0$ goes to ∞ by writing the solution to $\dot{\theta}_0$ equation in terms of the solutions to the eigenvalue problem. It is

$$\dot{\theta}_0 = -\Sigma_{i=1}^{i=\infty} \frac{\int_{-1}^{+1} 2 f_0 \tau_{xz_0} \phi_i \mathrm{d}x}{\left\{\tau_{xz_0}^2 - \lambda_i^2\right\} \int_{-1}^{+1} \phi_i^2 \mathrm{d}x} \phi_i \tag{2.29}$$

and this tells us that as τ_{xz_0} tends to the nose on the lower branch $\dot{\theta}_0$ tends to $+\infty$ and the order of this is $(-1/(\tau_{xz_0}^2 - \lambda_1^2(\tau_{xz_0})))$.

At the nose τ_{xz_0} turns and decreases along the upper branch. On the upper branch we assert that $\dot{\theta}_0$ should be negative, i.e. θ_0 continues to increase as τ_{xz_0} decreases. We need to make this assumption to proceed further as we cannot mathematically prove the sign of $\dot{\theta}_0$ on the upper branch. For example, we cannot rule out the possibility that a θ_{0_m} vs. τ_{xz_0} curve may look as illustrated in figure 2.5 even though physically we know such a case is not possible. With the assertion that $\dot{\theta}_0 < 0$, we can conclude that $\dot{\lambda}_i^2$ is positive along the upper branch. As τ_{xz_0} decreases along the upper branch so too does each eigenvalue and we get a picture as shown in figure 2.6.

The possibility that on the upper branch $\dot{\theta}_0$ might again become $-\infty$ cannot be ruled out. In fact, this leads to the possibility of a second nose with $\lambda_1(\tau_{xz_0}) = \tau_{xz_0}$ on the upper branch. And, if we go on with this possibility, there can be an infinite number of noses corresponding to as and when $\dot{\theta}_0$ becomes unbounded. For an exponential fluidity in plane Couette flow, this does not happen as we will see later. In an endnote, we will see that this does not happen in circular Couette flow

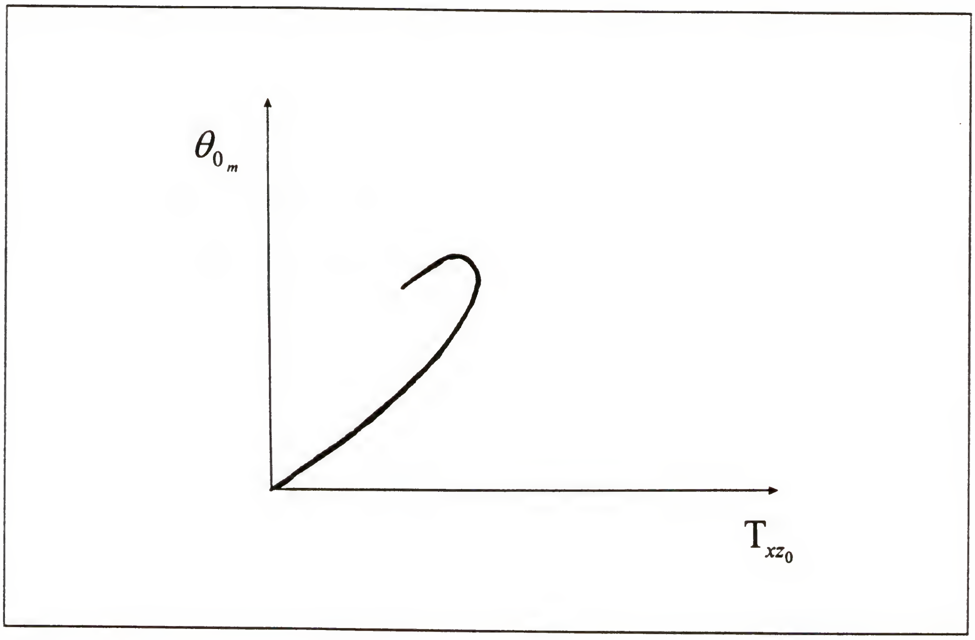

Figure 2.5: A hypothetical θ_{0_m} vs. τ_{xz_0} curve with $\dot{\theta}_0 > 0$ on the upper branch

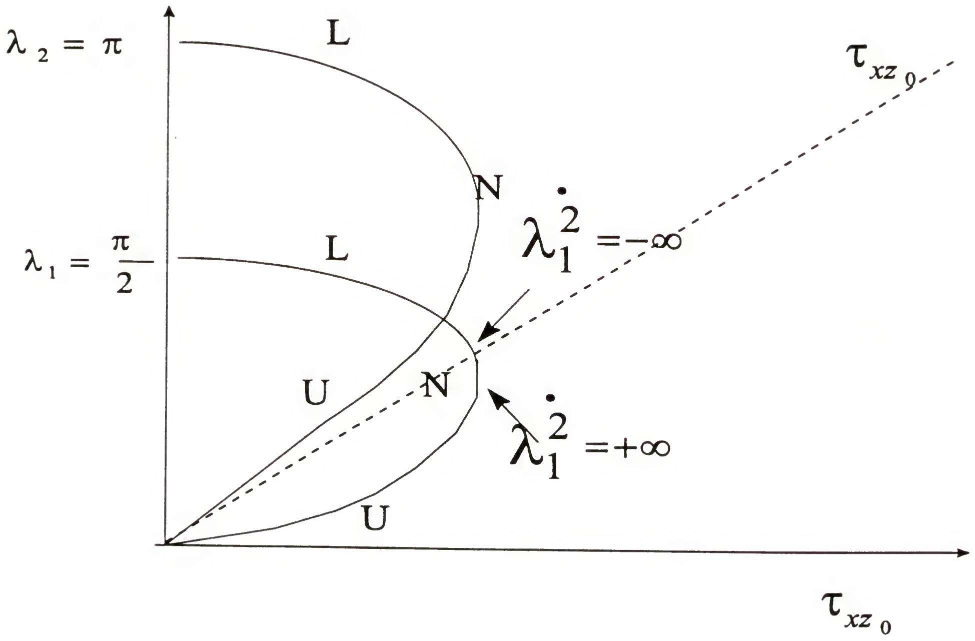
$\lambda_2 = \pi$
L
τ_{xz_0}
N
$\lambda_1 = \frac{\pi}{2}$
L
$\dot{\lambda}_1^2 = -\infty$
U
N
$\dot{\lambda}_1^2 = +\infty$
U
τ_{xz_0}

Figure 2.6: The prediction of the nose based on the second eigenvalue problem

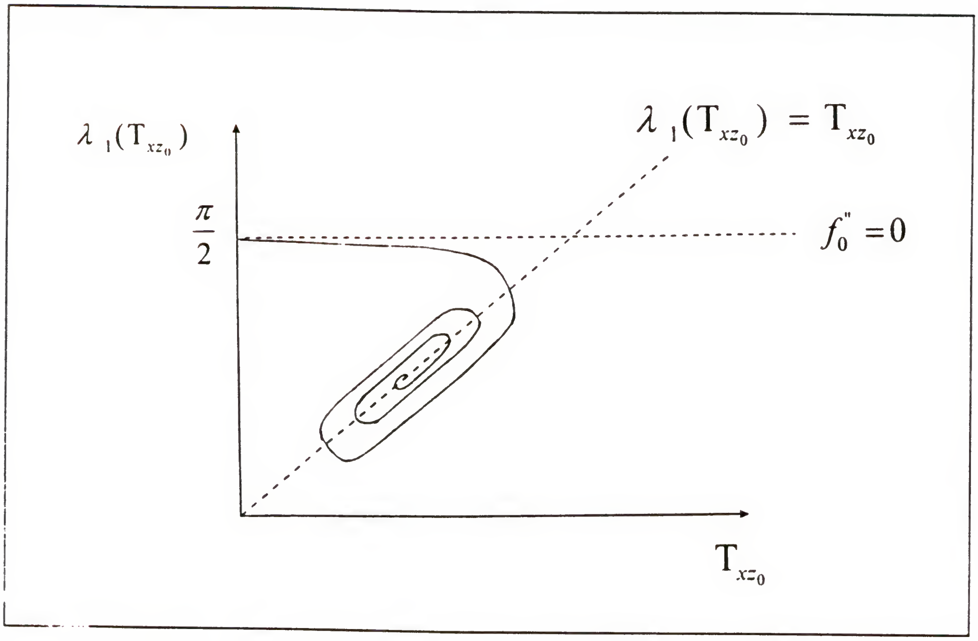

Figure 2.7: The $\lambda_1(\tau_{xz0})$ vs. τ_{xz0} curve for a case with multiple noses

either. However we cannot rule out this possibility in general. A $\lambda_1(\tau_{xz0})$ vs. τ_{xz0} for a case which has multiple noses looks as illustrated in figure 2.7:

On the upper branch, under our assertion that $\dot{\theta}_0$ is negative, $\dot{\lambda}_2^2$ remains positive and two possibilities come up. Either $\lambda_2(\tau_{xz0})$ remains above τ_{xz0} or it does not. If it does not then there is a point on the upper branch where $\lambda_2(\tau_{xz0}) = \tau_{xz0}$ and there again $\dot{\theta}_0$ goes indeterminate. But, now the solvability condition required to determine $\dot{\theta}_0$ is satisfied as ϕ_2 is an odd function and $\dot{\theta}_0$ does not become infinite as it does at the nose but it becomes multiple valued. Indeed, the solvability condition for $\dot{\theta}_0$ equation when $\lambda_2(\tau_{xz0}) = \tau_{xz0}$ is

$$\int_{-1}^{1} 2 f_0 \tau_{xz0} \phi_2 \mathrm{d}x = 0 \tag{2.30}$$

and this is satisfied as ϕ_2 is an odd function of x while f_0 is an even function. λ_2 is then called a branch point or a bifurcation point. The existence of a branch point on the upper branch is model dependent and it has to be looked at case by case.

We know for the case of linear fluidity, our prediction about the nose of the curve based on the eigenvalue problem matched our actual calculations from the base equations. Before closing this section, we will consider one more fluidity and prove the same. We will consider the case of exponential fluidity as in this case $f_0'' > 0$ and hence we should get an upper branch if our earlier assertion is correct. Unlike in linear fluidity, wherein we were able to get formulas for θ_0 vs. τ_{xz_0}, for an exponential fluidity, we might not be so lucky. However, it turns out that some useful formulas can still be obtained for a general class of fluidities. In fact, we will obtain these formulas on the way to solving the base equations for an exponential fluidity. The formulas turn out to relate the three fundamental quantities in the flow $V_0, \tau_{xz_0}, \theta_{0_m}$, where θ_{0_m} is the maximum temperature rise in the gap. One such formula which relates the maximum temperature rise in the gap and the wall speed will be used in getting the base solution for an exponential fluidity. Then, we will verify whether the eigenvalue problem predicts the nose correctly. We will also see whether there are any branch points on the upper branch for exponential fluidity, i.e., whether $\lambda_2(\tau_{xz0}) = \tau_{xz0}$ on the upper branch.

To get the relationship between the three fundamental quantities $V_0, \tau_0, \theta_{0_m}$ for a general class of fluidities, we begin by integrating the scaled temperature equation

$$\frac{\mathrm{d}^2\theta_0}{\mathrm{d}x^2} + f_0\tau_{xz_0}^2 = 0$$

once and, using the fact that the temperature profile is symmetric and hence $\frac{\mathrm{d}\theta_0}{\mathrm{d}x}(x=-1) = -\frac{\mathrm{d}\theta_0}{\mathrm{d}x}(x=+1)$, we get

$$2\frac{\mathrm{d}\theta_0}{\mathrm{d}x}(x=1) = -\tau_{xz_0}^2\int_{-1}^{+1} f_0\mathrm{d}x \tag{2.31}$$

Using $V_0 = \tau_{xz0}\int_{-1}^{+1} f_0\mathrm{d}x$ in this we get

$$2\frac{\mathrm{d}\theta_0}{\mathrm{d}x}(x=1) = -V_0\tau_{xz_0} \tag{2.32}$$

This tells us that at steady state the power dissipated by the system is carried away to the walls. We will make some stability arguments based on this formula later.

Now, multiplying the temperature equation by $\frac{\mathrm{d}\theta_0}{\mathrm{d}x}$, we get

$$\frac{1}{2}\frac{\mathrm{d}}{\mathrm{d}x}\left(\frac{\mathrm{d}\theta_0}{\mathrm{d}x}\right)^2 + f_0\tau_{xz0}^2\left(\frac{\mathrm{d}\theta_0}{\mathrm{d}x}\right) = 0 \tag{2.33}$$

Integrating this between the wall at $x = 1$ and the channel centreline wherein the temperature is maximum and taking the square root,[5] we obtain

$$\left(\frac{\mathrm{d}\theta_0}{\mathrm{d}x}\right)(x = 1) = -\sqrt{2}\tau_{xz0}\sqrt{\int_0^{\theta_{0m}} f_0 \mathrm{d}\theta_0} \tag{2.34}$$

Now, eliminating $\left(\frac{\mathrm{d}\theta_0}{\mathrm{d}x}\right)(x = 1)$ between (2.32), (2.34) we obtain

$$V_0 = 2\sqrt{2}\sqrt{\int_0^{\theta_{0m}} f_0 \mathrm{d}\theta_0} \tag{2.35}$$

Notice that τ_{xz0} also gets eliminated in the process. This equation tells us that the wall speed and the maximum temperature in the gap are increasing functions of one another. This is a confirmation of what we thought all along: when the wall speed is increased, more heat is generated by viscous dissipation. To conduct this heat to the boundary, a larger temperature gradient is required and this implies the maximum temperature has to increase. Further, we also find that for low wall speed, $f_0 \to 1$ and therefore $V_0 = 2\sqrt{2}\sqrt{\theta_{0_m}}$. This implies that the curve of V_0 vs. θ_{0_m} starts with $V_0 \propto \theta_{0_m}^{\frac{1}{2}}$.

Now, to get the base solution for the specific case of an exponential fluidity, substituting $f_0 = \mathrm{e}^{\theta_0}$ in

$$\frac{1}{2}\frac{\mathrm{d}}{\mathrm{d}x}\left(\frac{\mathrm{d}\theta_0}{\mathrm{d}x}\right)^2 + f_0\tau_{xz0}^2\left(\frac{\mathrm{d}\theta_0}{\mathrm{d}x}\right) = 0$$

then integrating it between $x = 0$, the centre of the channel and any x, i.e., an arbitrary position between $0 \leq x \leq 1$, we obtain

$$\left(\frac{\mathrm{d}\theta_0}{\mathrm{d}x}\right) = -\sqrt{2}\tau_{xz0}\sqrt{\mathrm{e}^{\theta_{0m}} - \mathrm{e}^{\theta_0}} \tag{2.36}$$

---

[5] As the temperature decreases from the channel centre $x = 0$ to the wall $x = 1$, the negative value of $\frac{\mathrm{d}\theta_0}{\mathrm{d}x}$ is chosen when taking the square root.

Integrating this once more between $x = 0$ where $\theta_0 = \theta_{0_m}$ and $x = 1$ where $\theta_0 = 0$, we get

$$\sqrt{2}\tau_{xz_0} = \frac{1}{\sqrt{e^{\theta_{0_m}}}} \ln \left[\frac{\sqrt{e^{\theta_{0_m}}} + \sqrt{e^{\theta_{0_m}} - 1}}{\sqrt{e^{\theta_{0_m}}} - \sqrt{e^{\theta_{0_m}} - 1}} \right] \tag{2.37}$$

Once θ_{0_m} is obtained, the integration may be carried out once more between $x = 0$ where $\theta_0 = \theta_{0_m}$ and $x = x$, any arbitrary position of x, to get an equation for θ_0 as a function of x. The solution of this equation will be useful to get $f_0{}'(x)$ which we will use to solve the eigenvalue problem later. For a given τ_{xz_0} less than its value at the nose, there are two values of the maximum temperature, θ_{0_m}, one on the upper branch and one on the lower branch. Depending on the solution that we seek, θ_{0_m} is limited to either the lower branch or the upper branch. Once θ_{0_m} is obtained, V_0 is calculated using the equation

$$V_0 = 2\sqrt{2}\sqrt{\int_0^{\theta_{0_m}} f_0 \mathrm{d}\theta_0}$$

substituting for the fluidity $f_0 = e^{\theta_0}$ and then integrating it to obtain

$$V_0 = 2\sqrt{2}\sqrt{e^{\theta_{0_m}} - 1} \tag{2.38}$$

Figure (2.8) depicts the solution in terms of the wall speed vs. the wall stress curve for an exponential fluidity relationship. The wall stress increases until the nose where $\tau_{xz_0} \simeq 0.94$ and then decreases thereafter.

Now, solving the eigenvalue problem for the case of exponential fluidity, by substituting for $f_0'(x)$ obtained from $\theta_0(x)$, it can be demonstrated that $\lambda_1(\tau_{xz_0}) = \tau_{xz_0}$ at the nose and $\lambda_2(\tau_{xz_0})$ remains above τ_{xz_0} along the upper branch. Table 2.1 shows the value of $\lambda_1(\tau_{xz_0})$, $\lambda_2(\tau_{xz_0})$ listed vs. τ_{xz_0} for exponential fluidity. Observe that for very low values of τ_{xz_0} on the lower branch, wherein $f_0' \simeq 1$, the eigenvalues $\lambda_1(\tau_{xz_0}), \lambda_2(\tau_{xz_0})$ very closely approach $\frac{\pi}{2}, \pi$ as expected. Moreover as predicted $\dot{\lambda}_1^2$ and $\dot{\lambda}_2^2$ approach $-\infty$ from below and are positive for values of τ_{xz_0} on the upper branch. Further, we also find that $\lambda_1(\tau_{xz_0}) \simeq \tau_{xz_0}$ for τ_{xz_0} between 0.93 and 0.94

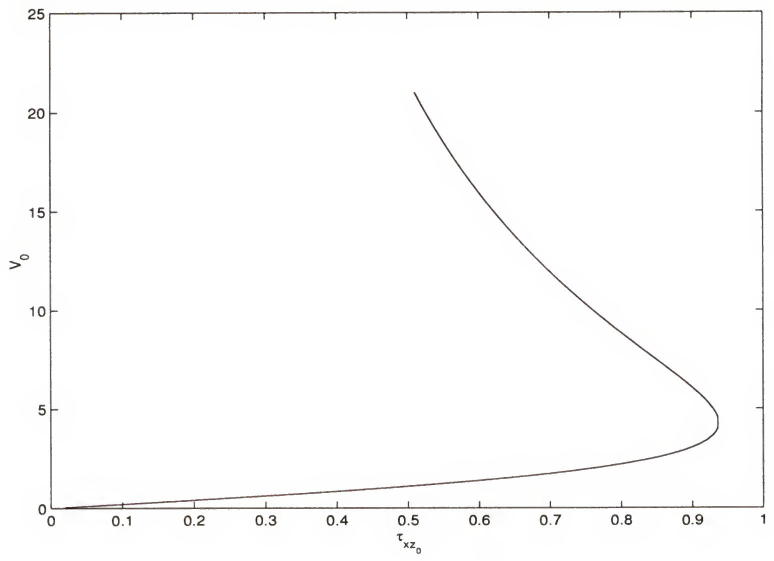

Figure 2.8: V_0 vs.τ_{xz0} for exponential fluidity

which is very close to the actual calculation from the base equations. We also find that $\lambda_2(\tau_{xz0}) > \tau_{xz0}$ along the upper branch indicating that there are no bifurcation points on the upper branch for exponential fluidity.

It might be of interest to ask what happens for fluidities slightly weaker than linear, i.e. fluids with $f_0'' < 0$. If $f_0'' < 0$, then $\dot{\lambda}_1^2$ must be positive along the lower branch where $\dot{\theta}_0$ is positive. This can be seen from the $\dot{\lambda}_i^2$ formula. Now, if there exists a nose in this case, then as τ_{xz0} tends to the nose on the lower branch, $\dot{\theta}_0$ must tend to $+\infty$. This then means that $\dot{\lambda}_1^2$ must also tend to $+\infty$ at the nose. Incorporating all this, the $\lambda_1(\tau_{xz0})$ vs. τ_{xz0} for this case can only look as shown in figure 2.9. As we see from this figure, a nose cannot arise for this case as the conditions required for a nose, viz. $\lambda_1(\tau_{xz0}) = \tau_{xz0}$ and in this case, $\dot{\lambda}_1^2 = +\infty$, cannot be simultaneously met. Therefore, the conclusion then is that for fluidities with $f_0'' < 0$, a nose does not arise. Based on this, we conclude that our earlier assertion that linear fluidity lies at the edge of backward bending base curves is correct.

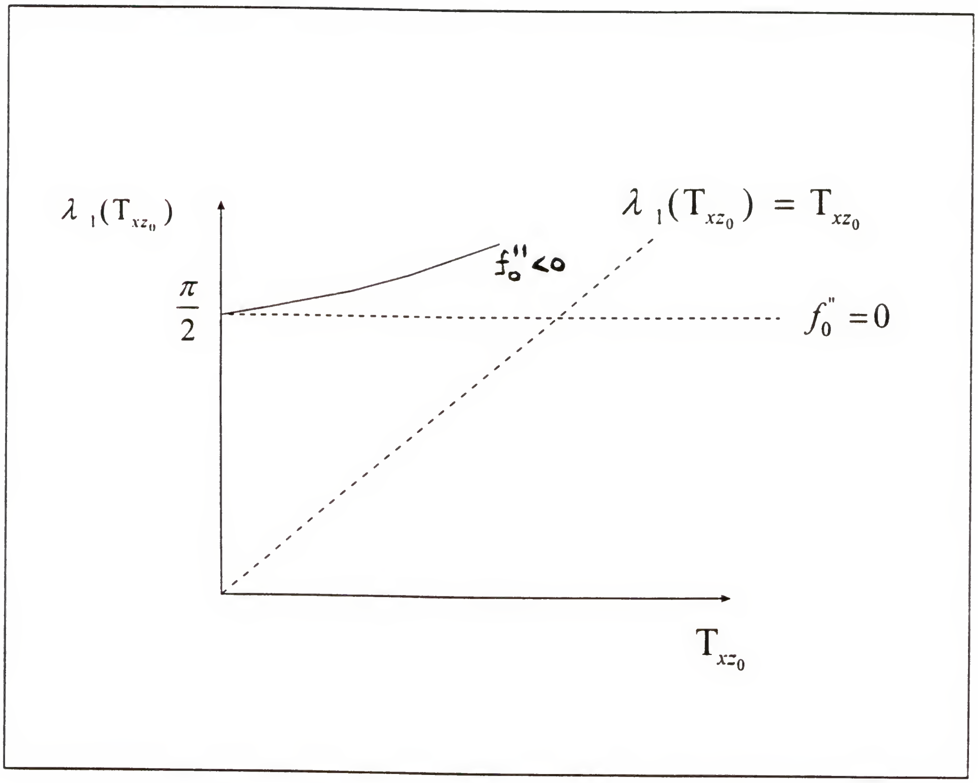

Figure 2.9: The $\lambda_1(\tau_{xz_0})$ vs. τ_{xz_0} curve for a case with $f_0'' < 0$

In an endnote, we will present one more method to predict a nose. In doing this, we will derive a formula and then use the geometric interpretation of an approximation of this formula in predicting when a nose might occur for a general class of fluidities.

2.7 Predictions about the Stability of the Base State based on a Formula

A rough argument can be made about the stability of the base state under various conditions based on the formula which states that the power dissipated is carried away to the walls

$$2\frac{\mathrm{d}\theta_0}{\mathrm{d}x}(x=1) = -V_0\tau_{xz_0}$$

In fact, this argument coupled with our earlier picture argument provides us with the motivation for studying the stability of the base state to small disturbance. To

Table 2.1: $\lambda_1(\tau_{xz0}), \lambda_2(\tau_{xz0})$ vs. τ_{xz0} for an exponential fluidity: * indicates the value of τ_{xz0} at the nose. All values above this on the table are on the lower branch and below this are on the upper branch.

τ_{xz0}	$\lambda_1(\tau_{xz0})$	$\lambda_2(\tau_{xz0})$
0.15	1.563	3.128
0.30	1.539	3.088
0.50	1.478	3.042
0.70	1.367	2.800
0.90	1.226	2.380
0.93	1.020	2.200
0.93274*	0.94174	2.058
0.93	0.851	1.893
0.90	0.740	1.686
0.70	0.436	1.079
0.50	0.261	0.696
0.30	0.132	0.385
0.15	0.0569	0.181

go ahead with the argument, first consider the case when the wall speed is held fixed and imagine a disturbance that increases the temperature in the gap. An increase in temperature causes a decrease in the average viscosity and therefore the shear stress in the gap decreases. This causes a decrease in the power dissipated in the gap and hence there is less heat to be conducted to the boundaries but a higher temperature to do it. Hence the temperature everywhere tends to decrease thus offsetting the imposed perturbation. Similarly, imagine a perturbation that decreases the temperature everywhere across the gap. A decrease in temperature causes an increase in viscosity and therefore for a fixed wall speed, the stress in the gap increases. This causes an increase in the power dissipated and hence an increase in temperature again offsetting the imposed perturbation. Thus, based on this rough argument we predict that at constant velocity any small disturbance to the temperature should decay with time and the steady state should be restored.

Now imagine a disturbance to the steady state that increases the temperature under the conditions when the wall stress is held fixed. An increase in temperature causes a decrease in viscosity. Now, to keep the stress a constant, the velocity gradient has to increase everywhere in the gap. This then means that the wall speed must increase. Consequently, the heat generated increases and hence a higher temperature is required to conduct this heat. Therefore, the temperature must increase further. Thus, we can see that there is a positive feedback and unless the heat conducted to the walls is faster than the heat that is produced by dissipation, we might conjecture that such a perturbation might grow with time. Thus, based on a purely thermal argument we have concluded that a perturbation at constant wall stress might grow with time whereas a perturbation at constant wall speed decays with time. And this result is in tune with our earlier picture argument based on the decay of mechanical disturbances from which we concluded that a perturbation at constant stress lingers longer as compared to a perturbation at constant wall speed.

In the next chapters, we will perform the stability calculations under these two input conditions to verify the suppositions made by these arguments. In doing the stability calculation, we will impose a small perturbation at every point along the base curve and see the evolution of the perturbation. For any point on the curve, if the small perturbation grows with time, then that point on the base curve is unstable. If not, it is stable. To begin with, we restrict ourselves to a perturbation that varies only in the transverse direction. In Chapter 3, we will present the perturbed equations in vector form and in Chapter 4, we will discuss the stability of these perturbed equations. Before we proceed to do that, a set of endnotes are presented that will help tie up some loose ends and settle some side issues that simply get in the way of the main theme of this chapter.

2.8 Endnotes

2.8.1 Comparison of the Couette Flow problem to the Ignition problem

The equation that models the temperature field in plane Couette flow is identical to the equation that defines the thermal ignition problem in a catalyst pellet with an exothermic zeroth order reaction under the restriction that the fluidity is exponential and the Frank-Kamnetskii approximation[2] can be made to the ignition equation.

The thermal ignition problem deals with the question of what happens to a combustible mixture if it is placed in a vessel with walls at some specified temperature. More precisely, it addresses the question of whether the heat generated by combustion is in balance with the heat loss through the walls of the vessel. The source of the heat in the thermal ignition problem is the exothermic heat of reaction and in the Couette flow problem, it is the viscous dissipation. Let us derive the base equation for the thermal ignition problem to see its similarity to the base temperature equation in the Couette flow problem.

The nonlinear equation that describes the thermal ignition problem is

$$\rho C_v \frac{\partial T}{\partial t} = k\nabla^2 T + \rho(-\Delta H_r) Q_w \frac{e^{-E/RT}}{e^{-E/RT_w}} \tag{2.39}$$

where ρ is the density of the fluid mixture, k is the thermal conductivity of the fluid mixture, (ΔH_r) is the heat released from the exothermic reaction, $Q_w e^{-E/RT}$ is the Arrhenius law for the kinetics of the reaction where Q_w is the rate at some reference temperature T_w and E is the activation energy of the reaction.

Here, we will restrict ourselves to the discussion of a one dimensional problem in a plane vessel. The equation for a 1-D plane vessel is

$$\rho C_v \frac{\partial T}{\partial t} = k\frac{\mathrm{d}^2 T}{\mathrm{d}x^2} + \frac{\rho(-\Delta H_r) Q_w}{e^{-E/RT_w}} e^{-E/RT} \tag{2.40}$$

with $T = T_w$ at $x = \pm L$. The stationary (steady) state for this problem is defined by the equation

$$0 = \frac{\mathrm{d}^2 T_0}{\mathrm{d}x^2} + \frac{\rho(-\Delta H_r)Q_w}{ke^{-E/RT_w}} e^{-E/RT_0} \tag{2.41}$$

with $T_0 = T_w$ at $x = \pm L$. To scale these equations, we might immediately realize that $x^* = x/L$ is a dimensionless length and $\theta_0 = RT_0/E$, a dimensionless temperature. The equation then becomes

$$0 = \frac{\mathrm{d}^2 \theta_0}{\mathrm{d}x^{*2}} + \frac{\rho(-\Delta H_r)Q_w L^2}{ke^{-E/RT_w}} \frac{R}{E} e^{-1/\theta_0} \tag{2.42}$$

with the boundary condition $\theta_0 = \theta_w = RT_w/E$ at $x = \pm 1$. There are two parameters in this scaling: $\kappa = \frac{\rho(-\Delta H_r)Q_w L^2}{ke^{-E/RT_w}} \frac{R}{E}$ and θ_w. A solution of the above equation is of the form

$$\theta_0 = f(x, \kappa, \theta_w)$$

A very common approximation made to this problem is called the Frank-Kamenetskii approximation. This approximation is based on the fact that in all real situations of practical importance one encounters, $RT_w/E << 1$. Use of this approximation leads to just a one parameter equation for temperature. This equation predicts the critical explosion parameter reasonably well to justify its use in all situations of practical interest.

The Frank-Kamenetskii approximation assumes a priori that if $RT_w/E << 1$, then the temperature rise $T_0 - T_w$ is also small. This is proved to be correct later. Assuming $RT_w/E << 1$ enables us to write

$$\mathrm{e}^{-E/RT_0} = \mathrm{e}^{-E/R(T_w + T_0 - T_w)} \simeq \mathrm{e}^{-E/RT_w} \mathrm{e}^{E(T_0 - T_w)/RT_w^2}$$

Now, defining a dimensionless temperature rise $\theta_0 = \frac{E}{RT_w^2}(T_0 - T_w)$ and a dimensionless length $x^* = x/L$, we rescale the problem to obtain

$$0 = \frac{\mathrm{d}^2 \theta_0}{\mathrm{d}x^{*2}} + \frac{\rho(-\Delta H_r)Q_w L^2}{k} \frac{E}{RT_w^2} e^{\theta_0} \tag{2.43}$$

with $\theta_0 = 0$ at $x = \pm 1$. Defining $\frac{\rho(-\Delta H_r)Q_w}{k}\frac{E}{RT_w^2} = \delta^2$, the equation becomes

$$0 = \frac{\mathrm{d}^2\theta_0}{\mathrm{d}x^2} + \delta^2 e^{\theta_0} \tag{2.44}$$

with $\theta_0 = 0$ at $x = \pm 1$. Thus the Frank-Kamenetskii approximation enables us to get the ignition temperature rise just as a function of one parameter viz. δ^2. The additional parameter that showed up from the boundary condition in the previous scaling is now eliminated because of the new choice of the temperature scale. In this form, the ignition equation looks identical to the temperature equation of the Couette flow problem for an exponential fluidity dependence with the ignition parameter δ taking the role of the shear stress τ_{xz_0}. However, unlike the Couette flow problem, wherein we have the possibility of studying the stability of the flow under two possible restrictions, viz. constant wall speed and constant wall stress, in the thermal ignition problem, we can imagine studying the stability under only one restriction: at constant δ. One cannot conceive a way to study the thermal ignition problem fixing the temperature in the gap. The temperature in the gap just responds to the ignition parameter δ. Hence it cannot be set.

The stability results at constant δ is available in literature[3]. In the coming chapters, we will explore whether there is some connection between the stability results for the thermal ignition problem and the Couette problem with viscous dissipation as we have already seen a similarity between the two problems just by looking at the base equations.

Now, coming back to see how a small value of $RT_w/E << 1$ relates to $(T_0 - T_w) << T_w$, realize that the maximum temperature from the temperature equation is given by $\theta_{0_m} = f(\delta)$, which implies that for a fixed δ, θ_{0_m} is a fixed. Now, rewriting the temperature scale for the maximum temperature, we obtain

$$(T_{0_m} - T_w) = \theta_{0_m} * RT_w^2/E$$

which can be rewritten as

$$(T_{0_m} - T_w)/T_w = \theta_{0_m} * RT_w/E$$

and therefore this implies that for a fixed θ_{0_m}, if $RT_w/E << 1$, then the temperature rise is also small enough, i.e. $(T_{0_m} - T_w) << T_w$.

2.8.2 Other Scaling Options

Earlier in this chapter, we discussed one option to scale the base equations. This scaling was based on $T_{\text{ref}} = 1/S$ and $V_{\text{ref}} = \sqrt{k/S\mu_w}$. However, based on other choices of V_{ref} and T_{ref}, other scaling options are possible. We will discuss them here.

In one such scaling, we choose the reference temperature $T_{\text{ref}} = T_w$. The scaled temperature rise, therefore is $\theta_0^* = (T_0 - T_w)/T_w$. The velocity scale is then chosen so as to set the term $\frac{\mu_w V_{\text{ref}}^2}{kT_w}$ to be unity. Therefore, $V_{\text{ref}} = \sqrt{(kT_w/\mu_w)}$. The shear stress scale then directly follows from this just like in the earlier scaling, i.e., $\tau_{xz_{\text{ref}}} = \mu_w V_{ref}/L = \sqrt{kT_w\mu_w/L^2}$.

The obvious advantage of this scale compared to the earlier scaling is that the case of constant viscosity can be recovered by putting $S = 0$. The price paid in deriving this advantage is that we do not have a single master curve of the scaled wall speed vs. the scaled wall stress even for one parameter fluidity-temperature models like the linear and the exponential. Instead, we have a family of curves of the scaled wall speed vs. the scaled wall stress with the sensitivity occurring as a parameter.

In another option, the velocity is scaled with respect to the wall speed. Therefore, $V_{\text{ref}} = V_0$ and the scaled velocity $v_{\theta_0}^* = v_{\theta_0}/V_0$. The stress scaling, like always, follows from the velocity scale and it is $\tau_{xz_{\text{ref}}} = \mu_w V_0/L$. Also, the reference temperature T_{ref} is chosen to be the wall temperature T_w. This generates the group, the Brinkman number, $\mathrm{Br} = \mu_{\mathrm{w}}\mathrm{V}_0^2/\mathrm{kT}_{\mathrm{w}}$, in the scaled temperature equation.

$$0 = \frac{\mathrm{d}^2\theta_0^*}{\mathrm{d}x^{*2}} + \mathrm{Br}\mu_0^* \left[\frac{\mathrm{d}v_{z_0}^*}{\mathrm{d}x^*}\right]^2 \tag{2.45}$$

where the Brinkman number, $\mathrm{Br} = \dfrac{\mu_w V_0^2}{kT_w}$. Now, integrating the scaled equation $\tau^*_{xz_0} = \mu^*_0 \frac{\mathrm{d}v^*_{z0}}{\mathrm{d}x^*}$ with the boundary condition that $V_0^* = 1$ at $x^* = 1$ and $V_0^* = 0$ at $x^* = -1$, we obtain

$$V_0^* = 1 = \tau^*_{xz_0} \int_{-1}^{1} f_0{}^* \mathrm{d}x^* \tag{2.46}$$

Therefore, $\tau^*_{xz_0}$ is given by

$$\tau^{*-1}_{xz_0} = \int_{-1}^{1} f_0{}^* \mathrm{d}x^* \tag{2.47}$$

Let $\lambda_0{}^{*^2} = \mathrm{Br}\tau^{*^2}_{xz_0}$. Then, the temperature equation above can be rewritten as

$$0 = \frac{\mathrm{d}^2\theta_0^*}{\mathrm{d}x^{*^2}} + \lambda_0{}^{*^2} f_0{}^* \tag{2.48}$$

If $\lambda_0^{*^2}$ is fixed as an input then the dimensionless temperature profile in the gap can be calculated using this equation. Once θ_0^* is known, then $\tau^*_{xz_0}$ can be calculated. From this, the Brinkman number can be calculated using the relation $\mathrm{Br} = \lambda_0^{*^2}/\tau^{*^2}_{xz_0}$. Therefore, a plot of Br vs. $\tau^*_{xz_0}$ can be obtained with the sensitivity as a parameter. The following points are noteworthy about this scaling.

- The case of constant viscosity can be recovered with this scaling.
- The scaling of the velocity with respect to the wall speed renders the scaled wall speed V_0^* unity for all cases. Therefore, in this scaling, the scaled wall speed is not a useful parameter. However, the effect of change in wall speed can be studied through the parameter, the Brinkman number.

The last option employs a new velocity scale. Multiplying and dividing the heat generation term in the temperature equation by the specific heat C_v, we obtain

$$0 = \frac{\mathrm{d}^2\theta_0^*}{\mathrm{d}x^{*2}} + \frac{\mathrm{Pr}V_{\mathrm{ref}}^2}{C_v T_{\mathrm{ref}}}\mu_0^* \left[\frac{\mathrm{d}v^*_{z0}}{\mathrm{d}x^*}\right]^2 \tag{2.49}$$

where, $\mathrm{Pr} = C_v\mu_w/k$, the Prandtl number of the liquid in the gap. Now choosing $V_{\mathrm{ref}} = \sqrt{(C_v T_{\mathrm{ref}})}$, we obtain

$$0 = \frac{\mathrm{d}^2\theta_0^*}{\mathrm{d}x^{*2}} + \mathrm{Pr}\mu_0^* \left[\frac{\mathrm{d}v^*_{z0}}{\mathrm{d}x^*}\right]^2 \tag{2.50}$$

For fluidities like the linear and exponential forms which have only one sensitivity parameter, if the choice of T_{ref} is T_w, then we have two dimensionless parameters in the scaled equation: (i) the Prandtl number, Pr, and (ii) the product ST_w, where S is the sensitivity. On the other hand, if $T_{\text{ref}} = 1/S$, then the only parameter in the model is Pr. The shear stress scaling then directly follows from the velocity scaling, i.e., $\tau_{xz_{\text{ref}}} = \mu_w V_{ref}/L = \sqrt{C_v T_w}\mu_w/L$.

The equations in this scaling are very similar to the equations arising from the scaling given in the body of this chapter with the difference that the Prandtl number of the fluid in the gap multiplies the dimensionless heat generation term in this scaling. The equations written in terms of the shear stress $\tau^*_{xz_0}$ are

$$V_0^* = \tau^*_{xz_0} \int_{-1}^{+1} f_0{}^* \mathrm{d}x \tag{2.51}$$

$$0 = \frac{\mathrm{d}^2\theta_0^*}{\mathrm{d}x^{*2}} + \mathrm{Pr}\tau^{*^2}_{xz_0} f_0{}^* \tag{2.52}$$

Therefore, we have a family of curves of V_0^* vs. $\tau^*_{xz_0}$ with Pr as a parameter. In this scaling, the velocity scale (and hence the stress scale) is independent of the thermal conductivity. We will find this scaling to be extremely useful when we view a change in the Prandtl number as the change in thermal conductivity holding the specific heat and the wall viscosity fixed.

2.8.3 Summary of the method that predicts a Nose

In this endnote, we will summarize the key ideas that we introduced earlier in this chapter to predict when a nose ought to occur in the base curve. We will begin this by declaring what we mean by a nose: we call a nose as a point on the base curve at which $\frac{\mathrm{d}V_0}{\mathrm{d}\tau_{xz_0}}$ goes unbounded. As we could prove that when $\frac{\mathrm{d}V_0}{\mathrm{d}\tau_{xz_0}}$ goes unbounded, $\frac{\mathrm{d}\theta_0}{\mathrm{d}\tau_{xz_0}}$ also goes unbounded, we decided that it is sufficient to inquire when $\frac{\mathrm{d}\theta_0}{\mathrm{d}\tau_{xz_0}}$ goes unbounded to predict a nose. To do this, we calculated the derivative of the temperature equation with respect to τ_{xz_0} to get an equation for $\frac{\mathrm{d}\theta_0}{\mathrm{d}\tau_{xz_0}}$. The equation is

$$\frac{\mathrm{d}^2\dot{\theta}_0}{\mathrm{d}x^2} + f_0{}'\tau_{xz0}^2\dot{\theta}_0 + 2f_0\tau_{xz0} = 0$$

with $\dot{\theta}_0 = 0$ at $x = \pm 1$, where $\dot{\theta}_0 = \frac{\mathrm{d}\theta_0}{\mathrm{d}\tau_{xz0}}$. This equation has a solution provided a solvability condition is satisfied. The condition is:

$$\int_{-1}^{+1} \{-2f_0\tau_{xz0}\}\, \dot{\theta}_{0,\text{homogeneous}}\mathrm{d}x = 0$$

where $\dot{\theta}_{0,\text{homogeneous}}$ is the solution to the homogeneous problem. As τ_{xz0} is increased from zero along the lower branch, the homogeneous part of the $\dot{\theta}_0$ equation has only a trivial solution as long as τ_{xz0} is less than λ_1, where λ_1 is the leading eigenvalue for the problem

$$\frac{\mathrm{d}^2\phi_1}{\mathrm{d}x^2} + f_0{}'\lambda^2\phi_1 = 0$$

with $\phi_1 = 0$ at $x = \pm 1$. Therefore, the solvability condition is automatically satisfied. But, when τ_{xz0} becomes large enough such that $\tau_{xz0} = \lambda_1$, the homogeneous part of the $\dot{\theta}_0$ has an eigensolution and the solvability condition becomes

$$\int_{-1}^{+1} \{-2f_0\tau_{xz0}\}\, \phi_1\mathrm{d}x = 0$$

This cannot be satisfied as ϕ_1 is singly signed and all the other quantities are positive. Thus, we concluded that when $\tau_{xz0} = \lambda_1$, $\dot{\theta}_0$ must become infinitely large, which by our definition is the nose of the base curve. We then determined a formula for how the eigenvalues change with respect to τ_{xz0}. It is

$$\dot{\lambda_i}^2 = -\lambda_i{}^2 \frac{\int_{-1}^{1} f_0{}''\dot{\theta}_0\phi_i{}^2\mathrm{d}x}{\int_{-1}^{1} f_0{}'\phi_i{}^2\mathrm{d}x}$$

Using this formula we were able to conclude that a nose arises on the base curve if $f_0'' \geq 0$. This conclusion was based on the following observations:

- No matter what the fluidity is, at $\tau_{xz0} = 0$ on the lower branch, the fundamental eigenvalue starts at its linear fluidity value, $\pi/2$.

- Along the lower branch $\dot{\theta}_0$ is positive, i.e. θ_0 increases with an increase in τ_{xz0}. As every other term in the $\dot{\lambda}_i^2$ formula is singly signed, it then follows that $\dot{\lambda}_i^2$ is negative[6]. Therefore, we concluded that as τ_{xz_0} is increased from zero along the lower branch λ_1 starts to decrease from $\pi/2$ until they both meet at the nose.

Thus $\dot{\lambda}_i^2$ equation turns out to be useful in understanding when a nose ought to occur on the base curve.

2.8.4 The prediction of nose for general Fluidities based on a Slope-Chord Formula

In the main body of this chapter, we introduced an eigenvalue problem to predict when a nose ought to occur in the base curve of the wall speed vs. the wall stress. We restricted ourselves to fluids with $f_0^{'} > 0, f_0^{''} \geq 0$. We concluded that the behavior of the fundamental eigenvalue λ_1 as a function of the shear stress τ_{xz0} is the key to the prediction of the nose and in fact, we defined a nose as a point at which $\lambda_1(\tau_{xz0}) = \tau_{xz0}$. In this endnote, we will derive a formula and use the geometric interpretation of this formula in the prediction of a nose. This is just one more way of looking at the problem of the prediction of the nose and in doing this, we will once again use the condition $\lambda_1(\tau_{xz0}) = \tau_{xz0}$ as the one defining the nose.

To get the formula, we substitute $\phi = \phi_1$ and $\lambda^2 = \lambda_1^2$ into the eigenvalue problem

$$\frac{\mathrm{d}^2\phi}{\mathrm{d}x^2} + f_0{'}\lambda^2\phi = 0$$

and multiply it by θ_0 and then subtract from this, the temperature equation

$$\frac{\mathrm{d}^2\theta_0}{\mathrm{d}x^2} + f_0\tau_{xz0}^2 = 0$$

multiplied by ϕ_1 and then integrate the difference over $-1 \leq x \leq 1$ to get

$$\frac{\tau_{xz0}^2}{\lambda_1^2} = \frac{\int_{-1}^{+1} f_0^{'}\phi_1\theta_0 \mathrm{d}x}{\int_{-1}^{+1} f_0\phi_1 \mathrm{d}x} \tag{2.53}$$

---

[6] For linear fluidity, $f_0^{''} = 0$ and therefore $\dot{\lambda}_i^2$ is zero.

which can be written as

$$\frac{\tau_{xz0}^2}{\lambda_1^2} = \frac{\int_{-1}^{+1} \frac{\mathrm{d}f_0}{\mathrm{d}\theta_0}\phi_1\theta_0 \mathrm{d}x}{\int_{-1}^{+1} \frac{1}{\theta_0} f_0 \phi_1 \theta_0 \mathrm{d}x} \tag{2.54}$$

This tells us that at any value of τ_{xz0}, τ_{xz0}^2 is to $\lambda_1^2(\tau_{xz0})$ as the average slope of the fluidity curve is to the average slope of the line running from the origin to the fluidity curve. The average referred to here is a special kind of average: it requires us to multiply the quantity in question at every point in the gap by the product of $\phi_1\theta_0$ at that point and then sum it all over the entire gap width. Now, if the average slope of the line running from the origin to the fluidity curve is equal to the average slope of the fluidity curve then it implies $\tau_{xz0}^2 = \lambda_1^2$, which is our definition of a nose. To use this formula to predict when a nose might occur for various fluidity types is our objective. To do this, we will pretend that this 'integral average formula' that we derived can be applied locally for a point in the gap. We will choose the point to be the centre of the channel, i.e. $x = 0$. The corresponding temperature is the maximum temperature in the gap. Therefore, the formula can be approximated to

$$\frac{\tau_{xz0}^2}{\lambda_1^2} \simeq \frac{\frac{\mathrm{d}f_0}{\mathrm{d}\theta_0}|_m}{\frac{f_0}{\theta_0}|_m}$$

Now, we can compare the slope of the fluidity curve and the slope of the line drawn from the origin to the fluidity curve at the maximum temperature and then from that conclude whether $\lambda_1(\tau_{xz0})$ is greater than or lesser than τ_{xz0}. Figure 2.10 illustrates this method for the three fluidities being considered: (a) $f_0'' > 0$ (b)$f_0'' < 0$, (c) Arrhenius fluidity. Every point along the curve corresponds to some wall speed V_0 we might set. Using this formula, we may predict whether a point on the base curve is on the lower branch or on the upper branch.

The first, f_0'' positive, is representative of the fluids of interest to us. The fluidity curve tells us that when θ_0 is small, the slope of the line from the origin to the fluidity curve is greater than the slope of the fluidity curve and hence $\lambda_1(\tau_{xz0}) > \tau_{xz0}$. However as θ_0 increases, there comes a point where the slope of the line from the

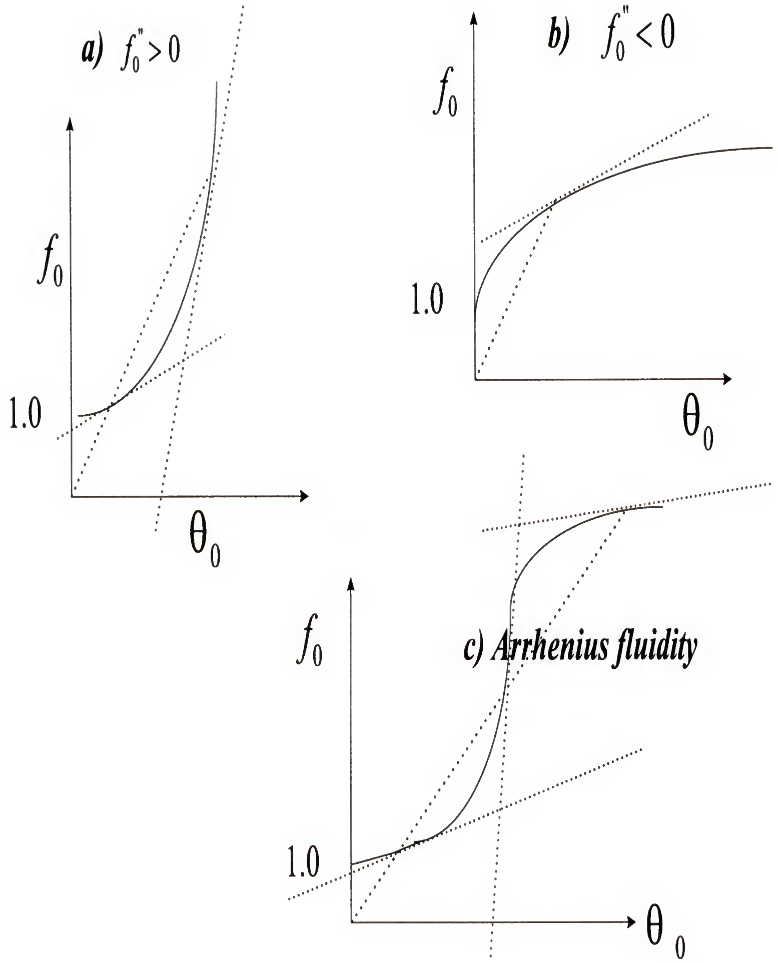

Figure 2.10: Prediction of the nose based on the Slope-Chord relationship. a)$f_0'' > 0$, b)$f_0'' < 0$, c) Arrhenius fluidity

origin to the fluidity curve is equal to the slope of the fluidity curve and hence $\lambda_1(\tau_{xz0}) = \tau_{xz0}$ and thereafter the slope of the fluidity curve is greater than the slope of the line from the origin to the fluidity curve and hence $\lambda_1(\tau_{xz0}) < \tau_{xz0}$. This is a reaffirmation of what we already know for fluids with $f_0'' > 0$.

The second case is when f_0'' is negative. Here, the slope of the fluidity curve is always less than the slope of the line to the fluidity curve and hence $\lambda_1(\tau_{xz0})$ remains above τ_{xz0}. The corresponding base solution curve cannot exhibit a nose and the lower branch continues to the right as τ_{xz0} increases indefinitely. Recall that from the $\dot{\lambda}_i^2$ formula, we arrived at the same conclusion.

The third fluidity curve suggests that an Arrhenius fluidity curve might be expected to produce two noses and indeed this is what is seen in calculations of Davis et. al.[4]. Here as the wall speed increases, the wall stress first increases, then decreases before turning again and increasing. The third branch corresponds to a slowing of the increase in the fluidity where $f_0'' < 0$.

2.8.5 A note on the Base Curve of Fluids with $f_0' < 0$

The main emphasis of this chapter was in studying the base solutions for the class of fluids whose fluidity increases with an increase in temperature. Liquids generally fall under this category. For the sake of completeness, in this endnote we will look at the class of fluids whose fluidity decreases with an increase in temperature, i.e fluids with $f_0' < 0$.

We refer to the scaled equations that describe the base velocity and temperature for plane Couette flow,

$$V_0 = \tau_{xz0} \int_{-1}^{1} f_0 \mathrm{d}x$$

and

$$0 = \frac{\mathrm{d}^2\theta_0}{\mathrm{d}x^2} + f_0 \tau_{xz0}^2$$

with the boundary condition $\theta_0(x = \pm 1) = 0$

the $\dot{\theta}_0$ equation

$$\frac{\mathrm{d}^2\dot{\theta}_0}{\mathrm{d}x^2} + f_0{}' \tau_{xz_0}^2 \dot{\theta}_0 + 2 f_0 \tau_{xz_0} = 0$$

with the boundary condition $\dot{\theta}_0(x = \pm 1) = 0$ and the corresponding homogeneous eigenvalue problem

$$\frac{\mathrm{d}^2\phi_1}{\mathrm{d}x^2} + f_0{}' \lambda_1^2 \phi_1 = 0$$

The first observation is based on the eigenvalue problem. As f_0' is negative, this equation with the boundary conditions $\phi_1(x = \pm 1) = 0$ has only the trivial solution. This then means that the solvability condition that determines $\dot{\theta}_0$ is always satisfied and $\dot{\theta}_0$ is uniquely determined and hence a nose does not arise for fluids with $f_0' < 0$.

The second observation is based on the $\dot{\theta}_0$ equation. Using this equation, we conclude that $\dot{\theta}_0 = 0$ when $\tau_{xz_0} = 0$ and then that $\dot{\theta}_0 > 0$ when τ_{xz_0} is small. To make the conclusion that $\dot{\theta}_0 > 0$ for small τ_{xz_0}, as before, we drop the term with $\tau_{xz_0}^2$ in it from the $\dot{\theta}_0$ equation. Luckily, it is also the only term in the equation with f_0' in it. Therefore, the fact that f_0' is negative now does not introduce anything new in the argument and hence, as we concluded before, we conclude that $\dot{\theta}_0$ is positive at small τ_{xz_0}. Now, to prove that $\dot{\theta}_0$ continues to remain positive as τ_{xz_0} increases, we again call for the proof by contradiction. To do this, we look for a point in the interior and for a $\tau_{xz_0} > 0$ whether setting $\dot{\theta}_0 = 0$ leads to any contradiction. Here again, setting $\dot{\theta}_0 = 0$ gets rid of f_0' from the equation. Now, a typical $\dot{\theta}_0$ profile with a zero in the interior, if it is possible, would look like in figure (2.11) Notice at the point where the temperature rises from $\dot{\theta}_0 = 0$ in the interior, $\frac{\mathrm{d}^2\dot{\theta}_0}{\mathrm{d}x^2} > 0$ but then the $\dot{\theta}_0$ equation would not allow this. As we have already proved that a nose does not arise for fluids with $f_0' < 0$, we can conclude that $\dot{\theta}_0 > 0$ for all values of τ_{xz_0} , i.e., θ_0 and τ_{xz_0} are increasing functions of one another.

We will consider the following two cases for further discussion.

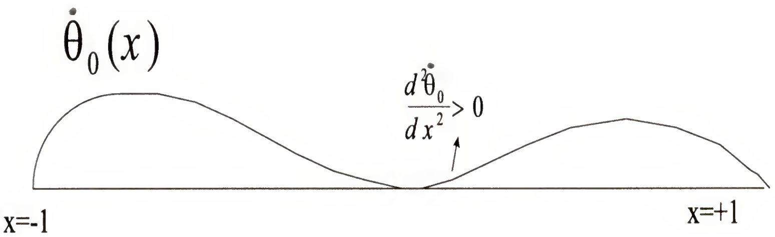

Figure 2.11: A $\dot{\theta}_0$ profile with a zero in the interior.

- Linear viscosity $\Rightarrow f_0 = \frac{1}{1+\theta_0}$
- Exponential viscosity $\Rightarrow f_0 = \mathrm{e}^{-\theta_0}$

$V - \theta_{0_m}$ relationship for fluids with $f_0' < 0$:

Using the equation

$$V_0 = 2\sqrt{2}\sqrt{\int_0^{\theta_{0_m}} f_0 \mathrm{d}\theta_0}$$

which relates the maximum temperature in the gap and the wall speed, we get for the case of linear viscosity, $\mu_0 = 1 + \theta_0$,

$$V_0 = 2\sqrt{2}\sqrt{\ln(1+\theta_{0_m})}$$

and for exponential viscosity, $\mu_0 = \mathrm{e}^{\theta_0}$:

$$V_0 = 2\sqrt{2}\sqrt{1 - \mathrm{e}^{-\theta_{0_m}}}$$

The above equations suggest that even though the scaled velocity V_0 is an increasing function of the scaled maximum temperature θ_{0_m}, the increase is sluggish. In fact, for an exponential viscosity, the scaled velocity V_0 asymptotically approaches the value of $2\sqrt{2}$.

2.8.6 The variation of $\tau_0\Delta/r_1^2$ with respect to Δ in the limit of $\Delta \to 0$

In the main body of this chapter, we proved that the quantity $\tau_0\Delta/r_1^2$, where τ_0 has the units of torque per unit length and Δ is $r_2 - r_1$, approached the value of the product $\tau_{xz_0}L$, where $\tau_{xz_0}L$ is independent of L, as the gap width goes to zero. However, we do not know whether $\tau_0\Delta/r_1^2 \to \tau_{xz_0}L$ from the right or from the left as $\Delta \to 0$. This is exactly what we will find out in this endnote. Mathematically, the problem is to calculate the sign of $\frac{\mathrm{d}}{\mathrm{d}\Delta}\left(\frac{\tau_0\Delta}{r_1^2}\right)$ as $\Delta \to 0$ for a fixed wall speed V_0. It turns out to be positive which makes us conclude that in a graph of the V_0 vs. $\tau_0\Delta/r_1^2$, $\tau_0\Delta/r_1^2$ approaches $\tau_{xz0}L$ for a fixed value of wall speed, V_0, from the right.

To perform this calculation, consider the equations that describe how the base velocity and the temperature behave for small $\epsilon = \Delta/r_1$. These are

$$V_0\,(1-\epsilon) = \tau_0\Delta \int_{r^*=0}^{r^*=1} \frac{1}{\mu_0}\frac{1}{{r_1}^2}\,(1-3r^*\epsilon)\,\mathrm{d}r^* \tag{2.55}$$

and

$$0 = k\frac{\mathrm{d}^2 T_0}{\mathrm{d}r^{*2}} + k\epsilon\frac{\mathrm{d}T_0}{\mathrm{d}r^*} + \frac{1}{\mu_0}\left(\frac{\tau_0^2\Delta^2}{r_1^4}\right)(1-4r^*\epsilon) \tag{2.56}$$

and we choose the following boundary conditions on temperature:

$$\frac{\mathrm{d}T_0}{\mathrm{d}r^*}(r^*=0) = 0, T_0(r^*=1) = 0$$

This choice of boundary condition turns out be useful to make some conclusions about the sign of $\frac{\mathrm{d}G_0}{\mathrm{d}\epsilon}(\epsilon = 0)$ as we will find out later. Let $G_0 = \tau_0\Delta/r_1^2$. It is worth noting that G_0 has the units of force per length. Then the above equations can be rewritten in terms of G_0 as

$$V_0\,(1-\epsilon) = G_0 \int_{r^*=0}^{r^*=1} \frac{1}{\mu_0}\,(1-3r^*\epsilon)\,\mathrm{d}r^* \tag{2.57}$$

$$0 = k\frac{\mathrm{d}^2 T_0}{\mathrm{d}r^{*2}} + k\epsilon\frac{\mathrm{d}T_0}{\mathrm{d}r^*} + \frac{1}{\mu_0}G_0^2\,(1-4r^*\epsilon) \tag{2.58}$$

Now, scaling these equations based on the scale that we introduced in the main body of this chapter i.e, $\theta_0 = S(T_0 - T_w)$, $\mu_0^* = \mu_0/\mu_w$, $V_0^* = \frac{V_0}{\sqrt{k/S\mu_w}}$ and $G_0^* = \frac{G_0}{\sqrt{k\mu_w/S}}$, we obtain after dropping the $*$,

$$V_0\,(1-\epsilon) = G_0 \int_{r=0}^{r=1} f_0\,(1-3r\epsilon)\,\mathrm{d}r \tag{2.59}$$

$$0 = \frac{\mathrm{d}^2\theta_0}{\mathrm{d}r^2} + \epsilon\frac{\mathrm{d}\theta_0}{\mathrm{d}r} + f_0{G_0}^2\,(1-4r\epsilon) \tag{2.60}$$

where f_0 is the fluidity, $1/\mu_0$. Now it is obvious from these equations that for a fixed V_0, G_0 varies as the gap width, ϵ, is changed. In this calculation, we aim to evaluate this variation in a certain limit. Specifically, we look for $\frac{\mathrm{d}G_0}{\mathrm{d}\epsilon}(\epsilon = 0)$. To do this, let us expand the variables in a regular perturbation series about $\epsilon = 0$. Accordingly, we write

$$\begin{aligned} G_0 &= G_0^{(0)} + \epsilon G_0^{(1)} \\ \theta_0 &= \theta_0^{(0)} + \epsilon \theta_0^{(1)} \\ f_0 &= f_0^{(0)} + \epsilon f_0^{(1)} \\ V_0 &= V_0^{(0)} + \epsilon V_0^{(1)} \end{aligned} \tag{2.61}$$

Terms of order ϵ^2 higher have been neglected under the assumption that ϵ is small. The superscript $^{(0)}$ refers to the variables evaluated at $\epsilon = 0$ and superscript $^{(1)}$ refers to $\frac{\mathrm{d}}{\mathrm{d}\epsilon}(\epsilon = 0)$. Here, $G_0^{(1)} = \frac{\mathrm{d}G_0}{\mathrm{d}\epsilon}(\epsilon = 0)$ is the quantity that we are interested in evaluating.

Now, to perform this calculation, a choice of input variable has to be declared. Fixing the wall speed as the input variable seems to the natural choice for this calculation. This then implies that no perturbations on the wall speed are allowed as we keep it fixed at $V_0^{(0)}$. Therefore, we set $V_0^{(1)} = 0$. Using the perturbation expansion for variables in the equation for velocity and temperature, we obtain

$$V_0^{(0)}\,(1-\epsilon) = (G_0^{(0)} + \epsilon G_0^{(1)}) \int_{r=0}^{r=1} (f_0^{(0)} + \epsilon f_0^{(1)})\,(1 - 3r\epsilon)\,\mathrm{d}r \tag{2.62}$$

$$0 = \frac{\mathrm{d}^2}{\mathrm{d}r^2}\left(\theta_0^{(0)} + \epsilon\theta_0^{(1)}\right) + \epsilon\frac{\mathrm{d}}{\mathrm{d}r}\left(\theta_0^{(0)} + \epsilon\theta_0^{(1)}\right) + \left(f_0^{(0)} + \epsilon f_0^{(1)}\right)\left(G_0^{(0)} + \epsilon G_0^{(1)}\right)^2 (1 - 4r\epsilon) \tag{2.63}$$

Collecting terms of order ϵ^0 and ϵ^1, we obtain for $O(\epsilon^0)$

$$V_0^{(0)} = G_0^{(0)} \int_{r=0}^{r=1} f_0^{(0)}\mathrm{d}r \tag{2.64}$$

$$0 = \frac{\mathrm{d}^2\theta_0^{(0)}}{\mathrm{d}r^2} + f_0^{(0)} G_0^{(0)^2} \tag{2.65}$$

and to $O(\epsilon^1)$

$$-V_0^{(}0) = -3G_0^{(0)} \int_{r=0}^{r=1} r f_0^{(0)} \mathrm{d}r + G_0^{(0)} \int_{r=0}^{r=1} f_0^{(0)'} \theta_0^{(1)} \mathrm{d}r + G_0^{(1)} \int_{r=0}^{r=1} f_0^{(0)} \mathrm{d}r \tag{2.66}$$

$$0 = \frac{\mathrm{d}^2\theta_0^{(1)}}{\mathrm{d}r^2} + \frac{\mathrm{d}\theta_0^{(0)}}{\mathrm{d}r} + G_0^{(0)^2} f_0^{(0)'} \theta_0^{(1)} + 2G_0^{(0)} G_0^{(1)} f_0^{(0)} - 4G_0^{(0)^2} f_0^{(0)} r \tag{2.67}$$

where $f_0^{(0)'}$ refers to $\frac{\mathrm{d}f_0^{(0)}}{\mathrm{d}\theta_0^{(0)}}$

The $0(\epsilon^1)$ equation in temperature can be rewritten as

$$\frac{\mathrm{d}^2\theta_0^{(1)}}{\mathrm{d}r^2} + G_0^{(0)^2} f_0^{(0)'} \theta_0^{(1)} = -\frac{\mathrm{d}\theta_0^{(0)}}{\mathrm{d}r} - 2G_0^{(0)} G_0^{(1)} f_0^{(0)} + 4G_0^{(0)^2} f_0^{(0)} r \tag{2.68}$$

Now, we choose the wall speed $V_0^{(0)}$ to correspond to the nose value of $G_0^{(0)}$. This choice of $V_0^{(0)}$ is very important to draw some conclusion about the sign of $G_0^{(1)}$ as any other choice would lead to only a trivial solution for the homogeneous problem. To see this, it is worth recalling that the homogeneous part of this problem directly relates to the eigenvalue problem that we introduced to predict when a nose ought to occur. Hence, choosing $V_0^{(0)}$ corresponding to any point on the lower branch would imply $\lambda_1(G_0^{(0)}) > G_0^{(0)}$ and hence we have only a trivial solution for the homogeneous problem and similarly choosing $V_0^{(0)}$ corresponding to any point on the upper branch implies $\lambda_1(G_0^{(0)}) < G_0^{(0)}$ and therefore once again we have only a trivial solution to the homogeneous problem. Only at the nose, the homogeneous problem has a non-trivial solution as there $\lambda_1(G_0^{(0)}) = G_0^{(0)}$ and therefore the $\theta_0^{(1)}$ equation has a solution only if a solvability condition is satisfied. We make of use this condition to make our predictions about the sign of $G_0^{(1)}$. The solvability condition is

$$\int_0^1 \phi_1 \left\{ -\frac{\mathrm{d}\theta_0^{(0)}}{\mathrm{d}r} - 2G_0^{(0)} G_0^{(1)} f_0^{(0)} + 4G_0^{(0)^2} f_0^{(0)} r \right\} = 0 \tag{2.69}$$

where ϕ_1 is the eigensolution to the homogeneous problem. This determines the value of $G_0^{(1)}$. It is

$$G_0^{(1)} = 2G_0^{(0)} \frac{\int_0^1 \phi_1 r f_0^{(0)} \mathrm{d}r}{\int_0^1 \phi_1 f_0^{(0)} \mathrm{d}r} - \frac{\int_0^1 \phi_1 \frac{\mathrm{d}\theta_0^{(0)}}{\mathrm{d}r} \mathrm{d}r}{2G_0^{(0)} \int_0^1 \phi_1 f_0^{(0)} \mathrm{d}r} \tag{2.70}$$

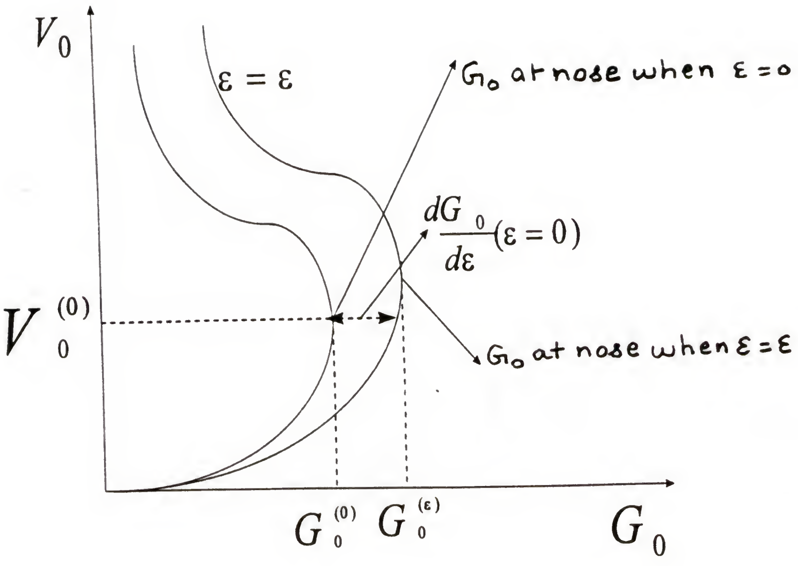
V_0
$\varepsilon = \varepsilon$
G_0 at nose when $\varepsilon = 0$
$\frac{dG_0}{d\varepsilon}(\varepsilon = 0)$
$V_0^{(0)}$
G_0 at nose when $\varepsilon = \varepsilon$
$G_0^{(0)}$
$G_0^{(\varepsilon)}$
G_0

Figure 2.12: Schematic of the variation of scaled torque with gap width in the limit of zero gap width

As ϕ_1 is singly signed and $\frac{d\theta_0^{(0)}}{dr}$ is negative, this equation tells us that that $G_0^{(1)}$ is positive. This then implies $\frac{dG_0}{d\epsilon}(\epsilon = 0) > 0$. Therefore, we have arrived at the following result: G_0 at the nose of the base problem increases as the gap width is changed from zero, holding the wall speed fixed. Figure 2.12 illustrates this result.

The following points are worth mentioning before concluding this endnote:

- The actual torque τ_0 decreases as the gap width is increased holding the wall speed fixed. Even though we did not prove this, we would expect this to be true based on physical reasoning.

- Figure 2.12 shows that the value of the wall speed at the nose increases as the gap width is increased from $\epsilon = 0$ to $\epsilon = \epsilon$. Even though we did not prove this, numerical calculations indicate such a trend.

2.8.7 A Heuristic Model for the plane Couette flow problem

In this endnote, we develop a heuristic model to describe the base flow for the plane Couette problem with frictional heating. The motivation behind developing a heuristic model for this case wherein even the rigorous model has been solved completely is simply to demonstrate that while studying complicated flow problems it might be useful to resort to a heuristic model as a screening device and then decide based on this whether a problem ought to be inspected in greater detail.

The heuristic models are not derived as much as they are written from intuition. The idea is to retain the physics of the problem with the simplest model possible. Examples of this can be found in literature[5,6,7]. Most of the examples have to do with how the flow rate in a pipe depends on the pressure drop across the pipe when the viscosity is a function of temperature. In these problems the temperature changes longitudinally, in the direction of the flow, and transversely, across the flow. The first usual step in writing a heuristic model is to approximate the transverse variation by a single temperature, some kind of average. The problem then becomes purely longitudinal. The plane Couette flow problem with frictional heating is the simplest of problems of this kind as conditions are uniform in the longitudinal direction and this therefore enables us to examine the approximation in the transverse direction in its pure form. In this endnote, we establish the fact that at least in this case, the heuristic model retains the essential physics of the problem.

To write a simple model for this without giving away anything essential, we start with the idea that in a longitudinally uniform flow, the frictional power loss comes into balance with the heat loss to the wall. In this state, the temperature of the fluid rises above the temperature of the wall and while in fact there is a transverse temperature variation, this is replaced in the simplest model by some average temperature denoted by T. Then the heat balance condition is simply

$$V\tau_{xz}WB = h\{2WB\}\{T - T_w\} \tag{2.71}$$

where the left hand side of the equation is the heat generated by viscous dissipation and the right hand side denotes how the heat is being carried away to the walls. Here h is a heat transfer coefficient whose order of magnitude can be estimated in laminar flow, B is the length of the plate and W is the width of the plate. Now, rewriting $2h$

as h the above equation can be rewritten as

$$V\tau_{xz} = h\{T - T_w\} \tag{2.72}$$

To this we add the law that describes how V depends on τ_{xz} for a transversely uniform viscosity μ. It is

$$\tau_{xz} = \mu V/L \tag{2.73}$$

This equation might roughly predict the the dependence of V on both τ_{xz} and μ where μ is evaluated at the temperature determined by the heat balance condition.

To the heat balance and the flow law we add the temperature dependence of viscosity. As before, we work in terms of fluidity, the reciprocal of viscosity and we consider two cases: linear fluidity and exponential fluidity. In each case, we write the fluidity in terms of the scaled temperature rise, denoted θ, where $\theta = S(T - T_w)$ and S describes the sensitivity of the fluidity to the temperature.

In the case of linear fluidity, the fluidity-temperature relationship is

$$\frac{\mu_w}{\mu} = 1 + \theta \tag{2.74}$$

and for exponential fluidity, it is

$$\frac{\mu_w}{\mu} = \mathrm{e}^{\theta} \tag{2.75}$$

Eliminating μ in the equation defining the stress using the fluidity-temperature relationship, and then eliminating θ in the result using the heat balance equation, we obtain for linear fluidity

$$V = \tau_{xz}\frac{L}{\mu_w}\left\{1 + \frac{\tau_{xz}VS}{h}\right\} \tag{2.76}$$

and for exponential fluidity

$$V = \mathrm{e}^{\left\{1+\frac{\tau_{xz}VS}{h}\right\}}\tau_{xz}\frac{L}{\mu_w} \tag{2.77}$$

To scale these formulas we resort to the velocity scale $\sqrt{\left\{\frac{k}{S\mu_w}\right\}}$ and therefore a stress scale of $\sqrt{\left\{\frac{k\mu_w}{SL^2}\right\}}$. Then, in scaled terms, indicated by * the equations become

$$V^* = \left\{1 + \frac{1}{\mathrm{Nu}}\tau_{xz}^* V^*\right\}\tau_{xz}^* \tag{2.78}$$

for linear fluidity and

$$V^* = \mathrm{e}^{\frac{1}{\mathrm{Nu}}\tau_{xz}^* V^*}\tau_{xz}^* \tag{2.79}$$

for exponential fluidity. Here, $\mathrm{Nu} = \frac{hL}{k}$. Taking Nu to be of order one [7] then leads to the following formulas

$$V^* = \{1 + \tau_{xz}^* V^*\}\tau_{xz}^* \tag{2.80}$$

$$V^* = \mathrm{e}^{\tau_{xz}^* V^*}\tau_{xz}^* \tag{2.81}$$

where the corresponding temperature rise can be obtained as

$$\theta = \tau_{xz}^* V^* \tag{2.82}$$

The base curve of $V^* - \tau_{xz}^*$ is illustrated graphically in figure 2.8.7. These are universal or master curves. In this scaling there is only one linear fluidity and one exponential fluidity curve. To get back to the unscaled variables, the scaling laws must be used. As τ_{xz} increases, the formulas tell us that V at first increases linearly, while $T - T_w$ increases quadratically. They also tell us that if experiments are run on geometries of various gap widths, the temperature rise will be the same in all pipes if V is held fixed but not if τ_{xz} is held fixed. It is worth recalling that this result is in tune with an earlier result in which we came to the conclusion that the maximum temperature in the gap is independent of the gap width if the velocity is held fixed and that was from a scaling argument based on the actual equations that describe the flow.

---

[7] This assumption is not necessary for what follows but is done only for the simplification obtained.

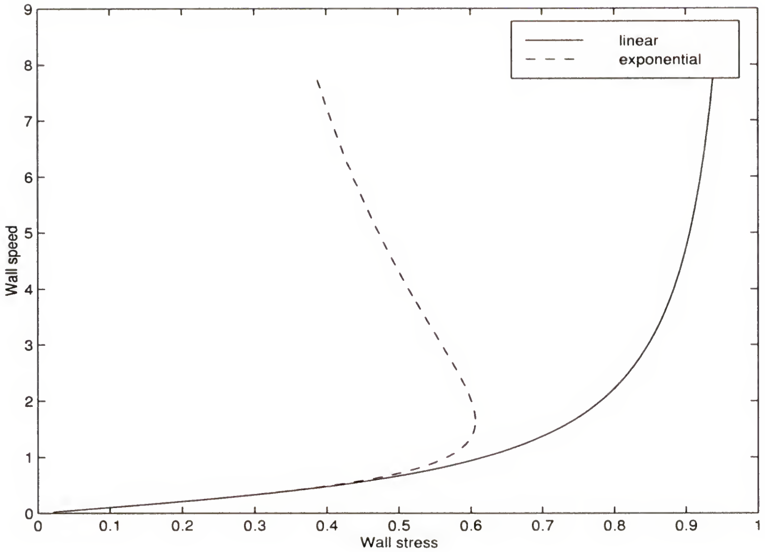

Figure 2.13: Heuristic Model: Plot of Wall speed vs. wall stress

The formulas also predict that all velocities can be obtained over a bounded range of shear stress and that the linear fluidity shear stress bounds the exponential fluidity shear stress. The exponential fluidity curve is double valued and linear fluidity would seem to be the critical fluidity at which curves go from single valued to double valued. We have seen all of this to be true from our calculations from an actual model.

Looking at the nose of the exponential fluidity curve, we conclude that if experiments are run on a series of geometries of different gap widths, the value of V at the nose will be the same in all experiments but not the value of τ_{xz}. This can be seen by observing that there is a master curve for a given fluidity and hence there is only one value for V^* and τ^*_{xz} at the nose for a given fluidity, in this case, exponential. Unscaling V^* using the velocity scale gives the actual value of V. The velocity scale is $\sqrt{k/S\mu_w}$ which is independent of the gap width. Hence, the actual value of the velocity at the nose is independent of the gap width. However, as the stress scale is $\sqrt{k\mu_w/SL^2}$, the actual value of the stress at the nose depends on the gap width.

The foregoing indicates, but of course does not prove, that simple models can describe much of what is interesting in physical processes. The predictions from these simple models can be used in the design of experiments.

The simple model used to describe frictional heating first requires the temperature rise to be proportional to the shear stress and the velocity and then requires the velocity to be proportional to the product of fluidity and the shear stress. This would seem to capture the essence of this problem and indicates the path by which heuristic models can be developed. All proportionality factors, geometric dependence, etc. take their isothermal form.

2.8.8 $V_0 - \tau_0 - \theta_{0_m}$ relationship in Circular Couette Flow

The mathematical manipulations required to get the $V - \theta_{0_m} - \tau_0$ relationships in circular Couette flow are very similar to those undertaken for plane Couette flow. However, unlike in plane Couette flow, the temperature profile in circular Couette flow is not symmetric with respect to the gap width and the position of the maximum temperature in the gap is not known. So, to help us proceed with the calculation, we make the inner wall adiabatic, i.e $\frac{\mathrm{d}\theta_0}{\mathrm{d}r}(r = \eta) = 0$, where $\eta = r_1/r_2$. This fixes the position of the maximum temperature in the gap.

Multiplying the temperature equation

$$0 = \frac{1}{r}\frac{\mathrm{d}}{\mathrm{d}r}\left(r\frac{\mathrm{d}\theta_0}{\mathrm{d}r}\right) + \frac{{\tau_0}^2 f_0}{r^4}$$

by r and integrating with the boundary condition that the inner wall is adiabatic and using the equation for velocity

$$V_0 = \tau_0 \int_\eta^1 \frac{f_0 \mathrm{d}r}{r^3}$$

in the result, we obtain

$$\frac{\mathrm{d}\theta_0}{\mathrm{d}r}(r = 1) = -V_0\tau_0 \tag{2.83}$$

Now, multiplying the temperature equation by $r^2\frac{\mathrm{d}\theta_0}{\mathrm{d}r}$ and then integrating it between $r = \eta$ and $r = 1$, we obtain,

$$\frac{1}{2}\left\{\frac{\mathrm{d}\theta_0}{\mathrm{d}r}(r=1)\right\}^2 + \tau_0^2\int_0^{\theta_{0m}}\frac{f_0\mathrm{d}\theta_0}{r^2} = 0$$

Eliminating $\frac{\mathrm{d}\theta_0}{\mathrm{d}r}$ $(r = 1)$ between the two equations above, we obtain

$$V_0^2 = 2\int_0^{\theta_{0m}}\frac{f_0\mathrm{d}\theta_0}{r^2} \tag{2.84}$$

We cannot proceed further to solve this equation analytically as we cannot write r in terms of θ_0. However, if we assume that the fluidity is exponential, i.e $f_0 = f_0' = \frac{\mathrm{d}f_0}{\mathrm{d}\theta_0}$, then it turns out that a $V_0 - \tau_0 - \theta_{0_m}$ result can still be obtained. The equation under the restriction that the fluidity is exponential becomes

$$V_0^2 = 2\int_0^{\theta_{0m}}\frac{\frac{\mathrm{d}f_0}{\mathrm{d}\theta_0}\mathrm{d}\theta_0}{r^2} \tag{2.85}$$

Integrating this equation by parts, we get

$$V_0^2 = \left[4\int_\eta^1\frac{f_0}{r^3}\mathrm{d}r\right] + 2\left[\frac{f_{0_m}}{\eta^2} - 1\right]$$

which when substituted for $V_0 = \tau_0\int_\eta^1\frac{f_0}{r^3}\mathrm{d}r$ becomes

$$V_0^2 - \frac{4V_0}{\tau_0} = 2\left[\frac{f_{0_m}}{\eta^2} - 1\right] \tag{2.86}$$

where f_{0_m} is the fluidity at the maximum temperature θ_{0_m}. Now, as the gap gets thinner, $\eta \to 1$ and $\tau_0 \to \infty$. Therefore, the equations reduce to

$$V_0 = \sqrt{2\left(f_{0_m} - 1\right)} \tag{2.87}$$

which is identical to the $V - f_{0_m}$ result for plane Couette flow if we consider just one half of the gap width, i.e. from the center-line wherein the temperature is maximum to the top of the plate where it is zero.

2.8.9 Prediction of the nose in Circular Couette Flow

To predict when a nose ought to occur in the base curve of V_0 vs. τ_0 in circular Couette flow, we follow a very similar procedure as we did in plane Couette flow. First, let us recall the base velocity and temperature equations in circular Couette flow. They are

$$V_0 = \tau_0 \int_\eta^1 \frac{f_0 \mathrm{d}r}{r^3}$$

and

$$\frac{\mathrm{d}^2\theta_0}{\mathrm{d}r^2} + \frac{1}{r}\frac{\mathrm{d}\theta_0}{\mathrm{d}r} + \frac{f_0\tau_0^2}{r^4} = 0$$

with the boundary condition $\theta_0(r = \eta, 1) = 0$. As before to predict when a nose ought to occur in the base curve of V_0 vs. τ_0, we inquire when $\frac{\mathrm{d}V_0}{\mathrm{d}\tau_0}$ goes unbounded. As we did for plane Couette flow, first let us prove that when $\frac{\mathrm{d}V_0}{\mathrm{d}\tau_0}$ goes unbounded, $\frac{\mathrm{d}\theta_0}{\mathrm{d}\tau_0}$ also goes unbounded. Differentiating the equation for V_0 proves this as seen below:

$$\frac{\mathrm{d}V_0}{\mathrm{d}\tau_0} = \int_\eta^1 \frac{\left[f_0 + \tau_0 f_0' \frac{\mathrm{d}\theta_0}{\mathrm{d}\tau_0}\right]}{r^3}\mathrm{d}r$$

Therefore, it follows out that to decide when $\frac{\mathrm{d}V_0}{\mathrm{d}\tau_0}$ goes unbounded, it is enough to find an equation for $\frac{\mathrm{d}\theta_0}{\mathrm{d}\tau_0}$ and inquire when it becomes unbounded. We will denote $\frac{\mathrm{d}\theta_0}{\mathrm{d}\tau_0}$ as $\dot{\theta}_0$. Then the $\dot{\theta}_0$ equation is

$$\frac{\mathrm{d}^2\dot{\theta}_0}{\mathrm{d}r^2} + \frac{1}{r}\frac{\mathrm{d}\dot{\theta}_0}{\mathrm{d}r} + \frac{\tau_0^2 {f_0}' \dot{\theta}_0}{r^4} + \frac{2 f_0 \tau_0}{r^4} = 0 \qquad (2.88)$$

with

$$\dot{\theta}_0(r = \eta, 1) = 0$$

We can prove that θ_0 is positive for $\tau_0 > 0$. As we did for plane Couette flow, we do it by contradiction. We will assume that there is a point in the interior where θ_0 is zero and then see whether we end with a contradiction. The temperature profile with a zero in the interior is illustrated in figure 2.14. Note that at the point where the temperature is zero in the interior, $\frac{\mathrm{d}\theta_0}{\mathrm{d}r} = 0$. Also, $\frac{\mathrm{d}^2\theta_0}{\mathrm{d}r^2} = 0$. In fact, it is a point

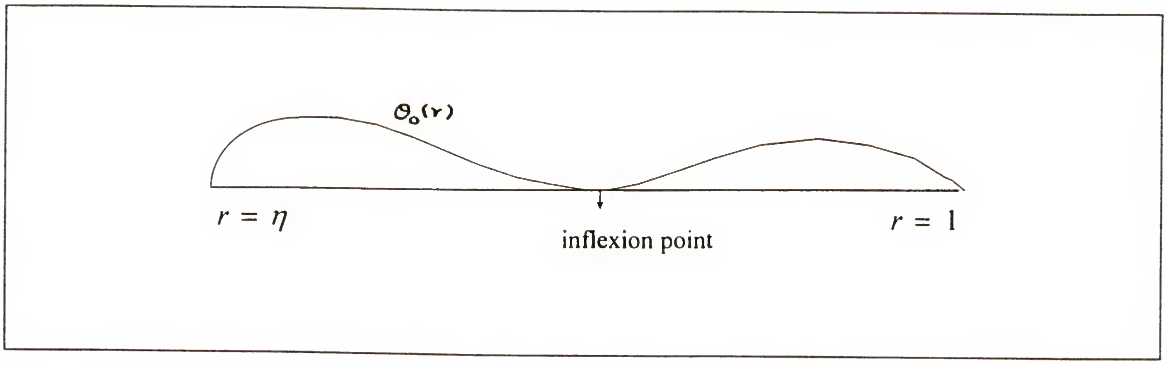

Figure 2.14: The base temperature profile with a zero in the interior

of inflexion. Therefore, putting $\frac{\mathrm{d}\theta_0}{\mathrm{d}r} = 0, \frac{\mathrm{d}^2\theta_0}{\mathrm{d}r^2} = 0$ in the temperature equation, we end with the condition $\frac{f_0^{'}\tau_0^2}{r^4} = 0$ which obviously cannot be satisfied. Therefore, we have proved that for $\tau_0 > 0$, $\theta_0 > 0$ in the interior.

Secondly, based on the $\dot{\theta}_0$ equation, we can conclude that each value of θ_0 in the interior increases as τ_0 increases along the lower branch of the base solution curve, i.e. $\dot{\theta}_0 > 0$ along the lower branch. To see this, we will assume $\dot{\theta}_0 = 0$ somewhere in the interior and see whether this leads to a contradiction. A $\dot{\theta}_0$ profile with a zero in the interior, if it exists, looks just like fig (2.14) with θ_0 replaced by $\dot{\theta}_0$. As seen in the figure, at the point where $\dot{\theta}_0 = 0, \frac{\mathrm{d}\dot{\theta}_0}{\mathrm{d}r} = 0$ and $\frac{\mathrm{d}^2\dot{\theta}_0}{\mathrm{d}r^2} = 0$ and therefore substituting these in the $\dot{\theta}_0$ equation, we end up with the condition $\frac{2f_0\tau_0}{r^4} = 0$ which obviously cannot be satisfied. Thus for every point along the lower branch of the base curve $\dot{\theta}_0 > 0$ at each point in the interior.

Thus far, we have proved that $\theta_0 > 0$ for $\tau_0 > 0$ and $\dot{\theta}_0 > 0$ for $\tau_0 > 0$ along the lower branch. To proceed further, as we did for plane Couette flow, we introduce the eigenvalue problem to see what happens as τ_0 increases along the lower branch and reaches the nose of the curve. The eigenvalue problem is

$$\frac{\mathrm{d}^2\phi}{\mathrm{d}r^2} + \frac{1}{r}\frac{\mathrm{d}\phi}{\mathrm{d}r} + \frac{\lambda^2 f_0^{'}\phi}{r^4} = 0 \tag{2.89}$$

with the boundary condition $\phi(r = \eta, 1) = 0$. Of course, the nose is defined as a point wherein $\lambda(\tau_0) = \tau_0$

Now, to determine what the eigenvalues do as τ_0 increases along the lower branch, we let $\dot{\phi}_i$ denote $\mathrm{d}\phi_{\mathrm{i}}/\mathrm{d}\tau_0$ and $\dot{\lambda}_i^{\,2}$ denote $\mathrm{d}\lambda_i^{\,2}/\mathrm{d}\tau_{xz_0}$ and differentiate the eigenvalue problem getting

$$\frac{\mathrm{d}^2\dot{\phi}}{\mathrm{d}r^2} + \frac{1}{r}\frac{\mathrm{d}\dot{\phi}_i}{\mathrm{d}r} + \frac{\lambda_i^2 {f_0}'\dot{\phi}_i}{r^4} = -\frac{\lambda_i^2 {f_0}''\dot{\theta}_0\phi}{r^4} - \frac{\dot{\lambda}_i^2 {f_0}'\phi_i}{r^4}$$

This equation requires a solvability condition to be satisfied. However, as we can always determine ϕ_i and then differentiate it with respect to τ_0 to get $\dot{\phi}_i$, the solvability condition should always be satisfied and it determines $\dot{\lambda}_i^2$ as

$$\dot{\lambda}_i^{\,2} = -{\lambda_i}^2 \frac{\int_\eta^1 {f_0}''\dot{\theta}_0 \frac{{\phi_i}^2}{r^4}\mathrm{d}r}{\int_\eta^1 {f_0}'\frac{{\phi_i}^2}{r^4}\mathrm{d}r}$$

Therefore, this equation tells us that along the lower branch, wherein we have proved that $\dot{\theta}_0 > 0$, as τ_0 is increased, the eigenvalues decrease from their linear fluidity values which they take at $\tau_0 = 0$. Again, this is true only for convex fluidities with $f_0'' > 0$. Therefore, as in plane Couette flow, we have a situation wherein as τ_0 is increased from zero, the eigenvalues decrease. As long as $\lambda_1(\tau_0) > \tau_0$, the solvability condition that determines $\dot{\theta}_0$ is satisfied as the corresponding homogeneous problem has only the trivial solution. But when τ_0 becomes large enough such that $\lambda_1(\tau_0) = \tau_0$, the solution to the $\dot{\theta}_0$ requires that a solvability condition be satisfied as the homogeneous problem has a non-trivial solution. The solvability condition is

$$\int_\eta^1 \frac{2f_0\tau_0\phi_1}{r^4}\mathrm{d}r = 0$$

and it cannot be satisfied as all the factors in this equation are positive and ϕ_1 is singly signed, it being the fundamental eigenvalue. This, in fact, is the nose of the curve and here τ_0 has reached the end of its increase along the lower branch.

Along the upper branch, τ_0 decreases. Now, if we assert that $\dot{\theta}_0$ is negative along the upper branch, then $\dot{\lambda}_i^2$ is positive. As τ_0 decreases along the upper branch, so too does each eigenvalue and we get a picture as shown in (2.15)

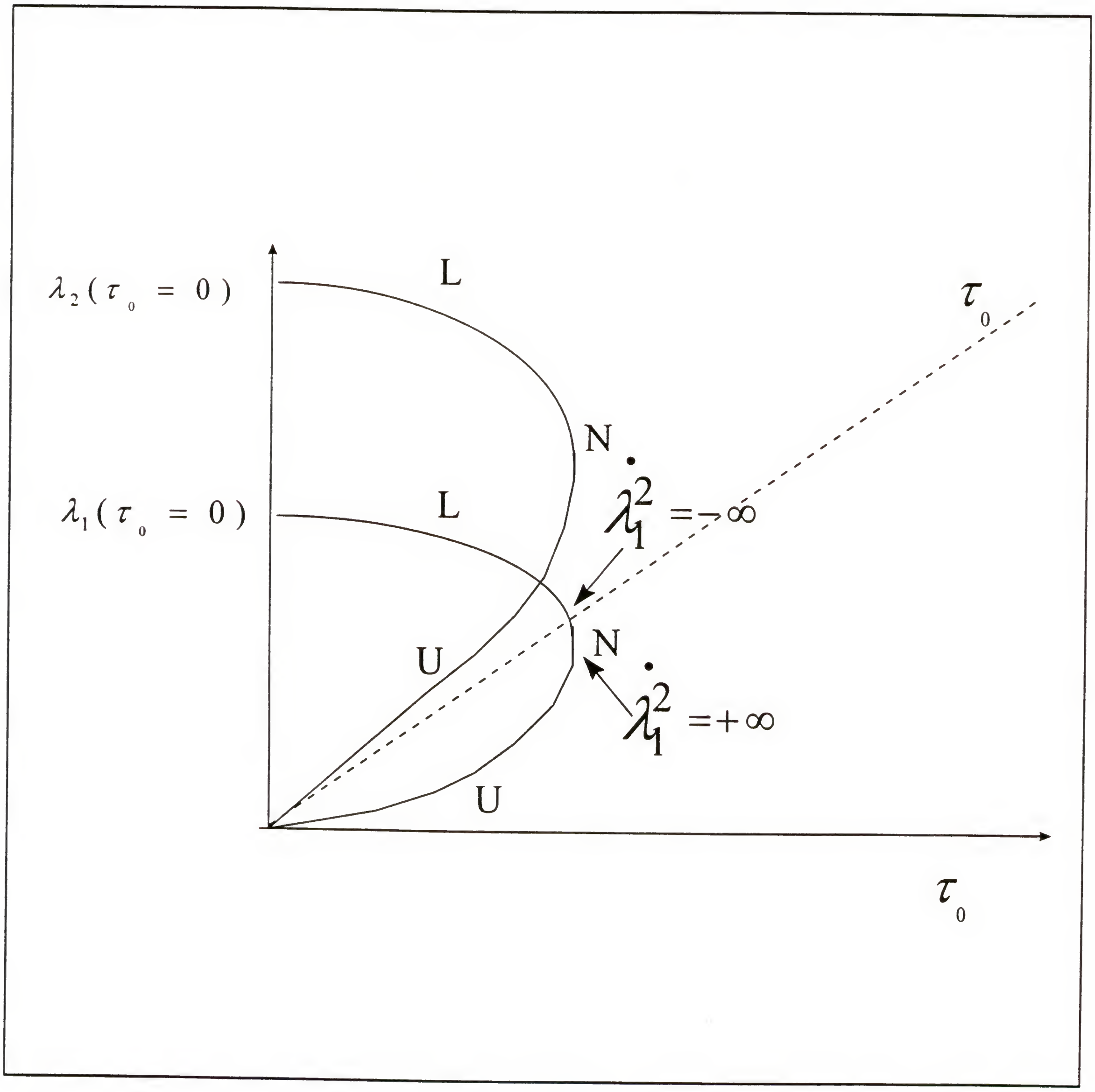

Figure 2.15: The prediction of the nose based on the eigenvalue problem: $\lambda_1(\tau_0), \lambda_2(\tau_0)$ vs. τ_0 behavior.

Table 2.2: $\lambda_1(\tau_0), \lambda_2(\tau_0)$ vs. τ_0 for an exponential fluidity for $\eta = 0.5$: * indicates the value of τ_0 at the nose. In the table, all values above the * correspond to the lower branch and below the * correspond to upper branch.

τ_0	$\lambda_1(\tau_0)$	$\lambda_2(\tau_0)$
0.25	3.14	6.28
0.50	3.10	6.21
0.75	3.04	6.11
1.00	2.95	5.97
1.25	2.83	5.76
1.75	2.33	4.90
1.88*	1.90	4.14
1.75	1.40	3.21
1.50	0.99	2.41

As we have seen thus far, there is not much difference in the analysis for the prediction of the nose in the plane Couette flow vs. the circular Couette flow. To conclude the analysis, we will calculate how $\lambda_1(\tau_0), \lambda_2(\tau_0)$ change with τ_0 along the base curve for an exponential fluidity. We will also see whether $\lambda_2(\tau_0) = \tau_0$ is possible on the upper branch. We will choose a radius ratio of 0.5 for this calculation.

Table 2.2 shows the result. We see from the table that $\lambda_1(\tau_0) \simeq \tau_0$ at $\tau_0 = 1.88$. We will later see from our calculations that $\tau_0 = 1.88$ indeed corresponds to the nose torque value. Further, we also find that along the upper branch $\lambda_2(\tau_0) > \tau_0$ indicating that a bifurcation point is not possible on the upper branch. Thus for exponential fluidity, a bifurcation point is not possible on the upper branch.

Next, we will move on to the calculation of the parameters $V_0, \tau_0, \theta_{0_m}$ using the base solutions in Circular Couette flow.

2.8.10 Calculation of $V_0, \tau_0, \theta_{0_m}$ using the Base Solutions in Circular Couette Flow

In this endnote, we will present the results of the calculation of the wall speed, torque and the maximum temperature at the nose based on the base solutions in circular Couette flow. These results will be useful in the design of experiments. Recall the base equations in circular Couette flow,

$$V_0 = \tau_0 \int_{\eta}^{1} \frac{f_0 \mathrm{d}r}{r^3} \tag{2.90}$$

$$0 = \frac{1}{r}\frac{\mathrm{d}}{\mathrm{d}r}\left(r\frac{\mathrm{d}\theta_0}{\mathrm{d}r}\right) + \frac{{\tau_0}^2 f_0}{r^4} \tag{2.91}$$

For the case of linear fluidity, $f_0 = 1 + \theta_0$, the equations become

$$0 = \frac{1}{r}\frac{\mathrm{d}}{\mathrm{d}r}\left(r\frac{\mathrm{d}\theta_0}{\mathrm{d}r}\right) + \frac{{\tau_0}^2(1+\theta_0)}{r^4} \tag{2.92}$$

$$V_0 = \tau_0 \int_{r=\eta}^{r=1} (1+\theta_0)\frac{\mathrm{d}r}{r^3} \tag{2.93}$$

The solution for the temperature is given by

$$\theta_0 = -1 + C_1 J_0(\tau_0/r) + C_2 Y_0(\tau_0/r)$$

where J_0 and Y_0 are the Bessels function of the first kind and of order zero. C_1 and C_2 are obtained from the boundary conditions on θ_0. For the case of constant temperature boundary conditions on both the walls, $\theta_0 = 0$ both at $r = \eta$ and at $r = 1$. For this case, C_1 and C_2 satisfy the following equation

$$\begin{bmatrix} J_0[\frac{\tau_0}{\eta}] & Y_0[\frac{\tau_0}{\eta}] \\ J_0[\tau_0] & Y_0[\tau_0] \end{bmatrix} \begin{bmatrix} C_1 \\ C_2 \end{bmatrix} = \begin{bmatrix} 1 \\ 1 \end{bmatrix} \tag{2.94}$$

Now, to predict when a nose ought to occur, we introduce the eigenvalue problem, which for the case of linear fluidity is

$$0 = \frac{1}{r}\frac{\mathrm{d}}{\mathrm{d}r}\left(r\frac{\mathrm{d}\phi}{\mathrm{d}r}\right) + \frac{\lambda^2 \phi}{r^4}$$

with the boundary condition $\phi(r = \eta, 1) = 0$. Once again the solution to this equation is given in terms of the Bessels functions J_0 and Y_0.

$$\phi = C_1 J_0(\lambda/r) + C_2 Y_0(\lambda/r)$$

Table 2.3: Torque at the nose for linear fluidity

η	$\lambda = \tau_{0_{\text{nose}}}$	$\tau_{0_{\text{nose}}}(1-\eta)$
0.5	3.12	1.56
0.6	4.69	1.88
0.7	7.29	2.19
0.8	12.55	2.51
0.9	28.55	2.85
0.95	59.27	2.96
0.99	314.16	3.14

where C_1 and C_2 are to be obtained from the boundary conditions. For constant temperature boundary conditions, C_1 and C_2 satisfy

$$\begin{bmatrix} J_0[\frac{\lambda}{\eta}] & Y_0[\frac{\lambda}{\eta}] \\ J_0[\lambda] & Y_0[\lambda] \end{bmatrix} \begin{bmatrix} C_1 \\ C_2 \end{bmatrix} = \begin{bmatrix} 0 \\ 0 \end{bmatrix} \tag{2.95}$$

Observe that λ is independent of τ_{xz_0} and only depends on η. A non-trivial solution to these equations exist only if the determinant of the matrix goes to zero. Therefore, λ the nose value of the τ_0 is determined by setting the determinant

$$\begin{bmatrix} J_0\left(\frac{\lambda}{\eta}\right) & Y_0\left(\frac{\lambda}{\eta}\right) \\ J_0\left(\lambda\right) & Y_0\left(\lambda\right) \end{bmatrix} \tag{2.96}$$

to zero. Obviously, λ is a function of the radius ratio η and it increases with the η. Table 2.3 indicates the nose torque values for a few radius ratios.

Observe that as $\eta \to 1$, the scaled torque at the nose $\tau_{0_{\text{nose}}}$ multiplied with the scaled gap width $(1-\eta)$ approaches the value of π and this is exactly the scaled nose shear stress value for linear fluidity in plane Couette flow if the gap width were to go from 0 to 1. To see how this result ties in with our earlier result that the quantity $\tau_0\Delta/r_1^2$ approaches the value of $\tau_{xz_0}L$ as the gap width goes to zero, let us first observe that in the earlier result τ_0 and τ_{xz_0} were unscaled whereas here they are scaled. Therefore, to make a proper comparison, we will first unscale τ_0. Now, $\tau_0(\text{scaled}) = \tau_0(\text{unscaled})/\sqrt{k\mu_w/S}r_2$. Hence, $\tau_0(\text{scaled})(1-\eta) = \tau_0(\text{unscaled})\Delta/\sqrt{k\mu_w/S}r_2^2$. Now, in the limit of a thin gap, $r_1 \simeq r_2$. Therefore, for a thin gap, $\tau_0(\text{scaled})(1-\eta) = \tau_0(\text{unscaled})\Delta/\sqrt{k\mu_w/S}r_2^2 = \tau_0(\text{unscaled})\Delta/\sqrt{k\mu_w/S}r_1^2$. Now, $\tau_{xz_0}(\text{scaled}) =$

$\tau_{xz_0}(\text{unscaled})/\sqrt{k\mu_w/SL^2}$. We have just seen from our numerical result that $\tau_0(\text{scaled})(1-\eta) = \tau_{xz_0}(\text{scaled})$ in the limit of a thin gap. This implies $\tau_0(\text{unscaled})\Delta/r_1^2 = \tau_{xz_0}(\text{unscaled})L$ which conforms with our earlier result.

For the case of exponential fluidity, $f_0 = \mathrm{e}^{\theta_0}$. So, the equations become

$$0 = \frac{1}{r}\frac{\mathrm{d}}{\mathrm{d}r}\left(r\frac{\mathrm{d}\theta_0}{\mathrm{d}r}\right) + \frac{{\tau_0}^2\mathrm{e}^{\theta_0}}{r^4} \tag{2.97}$$

$$V_0 = \tau_0\int_{r=\eta}^{r=1} e^{\theta_0}\frac{\mathrm{d}r}{r^3} \tag{2.98}$$

For this case, the formulas due to Kearsley[8] can be used. The temperature and velocity are then

$$\theta_0 = \ln\left[\frac{2m^2r^2}{{\tau_0}^2\cosh^2(m\ln r + a)}\right] \tag{2.99}$$

$$V_0 = 2m\tau_0\left\{\tanh(a) - \tanh(m\ln r + a)\right\} \tag{2.100}$$

where m, a are constants to be determined from the boundary conditions on temperature. For constant temperature boundary conditions on both walls[8]

$\theta_0 = 0$ at $r = 1 \Rightarrow m = \pm\frac{\tau_0}{\sqrt{(2)}}\cosh(\mathrm{a})$

$\theta_0 = 0$ at $r = \eta \Rightarrow \cosh(a)\eta = \cosh\left[m\ln(\eta) + a\right]$

Substituting the positive and negative values for m, we obtain the two solutions for the problem. Table 2.4 shows the value of τ_0 at the nose for various radius ratios. Here again, multiplying $\tau_{0_{\text{nose}}}$ with the gap width $1-\eta$, we observe that the shear stress τ_{xz_0} for plane Couette flow at the nose is obtained in the limit of narrow gaps. [9] Observe that the maximum temperature at the nose remains roughly a constant for a wide range of gap widths. We have not been able to prove this to be true from analytical work.

The only temperature boundary condition that we considered thus far in this chapter is that of constant temperature. In imposing this boundary condition, we

---

[8] Solutions for this problem for other temperature boundary conditions like an adiabatic boundary condition and a mixed boundary condition will follow.

[9] Observe that 1.86 is the nose shear stress value in plane Couette flow if the gap goes from zero to one.

Table 2.4: Torque, Wall speed and the maximum temperature at the nose for exponential fluidity

η	$\tau_{0_{\text{nose}}}$	$V_{0_{\text{nose}}}$	$\theta_{0_{m\,\text{nose}}}$	$\tau_{0_{\text{nose}}}(1-\eta)$
0.5	1.88	6.08	1.13	0.94
0.6	2.80	5.54	1.16	1.12
0.7	4.37	5.04	1.16	1.31
0.75	5.62	4.90	1.17	1.40
0.8	7.49	4.71	1.17	1.50
0.9	16.87	4.46	1.17	1.687
0.99	185.59	4.26	1.18	1.86

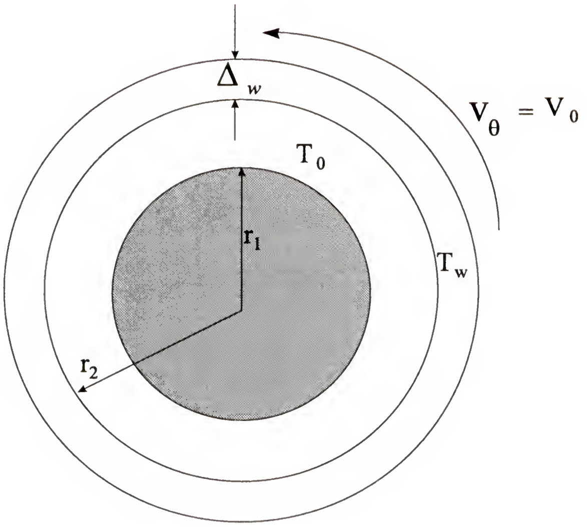

Figure 2.16: Schematic of Circular Couette flow

have tacitly assumed that the wall is of infinite thermal conductivity. But, in an actual experiment, the wall is of finite thermal conductivity. To incorporate this, let us see how to derive the boundary condition for a wall of finite thermal conductivity. For concreteness, let us assume that this boundary condition is to be derived for the outer wall.

Consider figure 2.16. The radius of the inner cylinder is r_1, the radius of the outer cylinder is r_2, the temperature profile of the fluid in the gap is denoted $T_0(r)$ and the temperature profile across the wall is denoted $T_w(r)$. The thickness of the wall is denoted Δ_w.

Writing Newton's law of cooling for the heat balance across the outer wall at r_2, we obtain:

$$k\frac{\mathrm{d}T_0}{\mathrm{d}r} + h(T_0 - T_\infty) = 0$$

where T_∞ is the ambient temperature, h is the heat transfer coefficient across the wall which can be obtained by using the boundary conditions at $r = r_2$. The conditions are that both the temperature and heat flux across r_2 must be continuous. The continuity of temperature across $r = r_2$ implies

$$T_0^{r=r_2} = T_w^{r=r_2}$$

and the continuity of heat flux across $r = r_2$ implies

$$q_0^{r=r_2} = q_w^{r=r_2}$$

Now, using $q = -k\frac{\mathrm{d}T}{\mathrm{d}r}$ in this equation we obtain

$$k\frac{\mathrm{d}T_0^{r=r_2}}{\mathrm{d}r} = k_w\frac{\mathrm{d}T_w^{r=r_2}}{\mathrm{d}r}$$

where k, k_w are the thermal conductivities of the fluid and the wall respectively. Substituting these two conditions in the Newton's law of cooling, we obtain

$$k_w\frac{\mathrm{d}T_w^{r=r_2}}{\mathrm{d}r} + h(T_w^{r=r_2} - T_\infty) = 0$$

from which it follows that

$$h = -k_w\frac{\frac{\mathrm{d}T_w^{r=r_2}}{\mathrm{d}r}}{(T_w^{r=r_2} - T_\infty)}$$

Now, to get $\frac{\mathrm{d}T_w^{r=r_2}}{\mathrm{d}r}$, we need the temperature profile across the wall. To get this, observe that the flux across the wall, q_w, is given by the solution to the equation

$$\frac{1}{r}\frac{\mathrm{d}}{\mathrm{d}r}\left[rq_w\right] = 0$$

which for a very small Δ_w compared to r_2 can be approximated as

$$\frac{\mathrm{d}q_w}{\mathrm{d}r} = 0$$

Substituting $q_w = -k\frac{\mathrm{d}T_w}{\mathrm{d}r}$ in this we obtain the equation for the temperature

$$\frac{\mathrm{d}^2T_w}{\mathrm{d}r^2} = 0$$

which when solved with the boundary condition that at $r = r_2, T = T_w$ and at $r = r_2 + \Delta_w, T = T_\infty$ yields

$$T_w = T_w^{r=r_2} - \frac{T_w^{r=r_2} - T_\infty}{\Delta_w}r$$

for the temperature profile across the wall. From this, we get

$$\frac{\mathrm{d}T_w^{r=r_2}}{\mathrm{d}r} = -\frac{(T_w^{r=r_2} - T_\infty)}{\Delta_w}$$

Substituting this in the equation for h, we obtain

$$h = k_w/\Delta_w$$

Substituting h in Newton's law of cooling, we obtain

$$\frac{\mathrm{d}T_0}{\mathrm{d}r} + \frac{k_w}{k\Delta_w}(T_0 - T_\infty) = 0$$

Now, scaling r with respect to r_2 and calling $S(T_0 - T_\infty) = \theta_0$, we obtain

$$\frac{\mathrm{d}\theta_0}{\mathrm{d}r} + \frac{k_w r_2}{k\Delta_w}\theta_0 = 0$$

Denoting the Biot number by Bi where $\mathrm{Bi} = \frac{k_w r_2}{k\Delta_w}$, the boundary condition on temperature can be denoted as

$$\frac{\mathrm{d}\theta_0}{\mathrm{d}r} + Bi\theta_0 = 0$$

We will further calculate the θ_{0_m}, V_0 τ_0 at the nose for boundary conditions other than constant temperature as this calculation gives an estimate of how they change as the boundary condition is changed. This result will be useful in the design of experiments. We will present the result for exponential fluidity as our experiments will be performed for this fluidity only.

Table 2.5: Conditions at the nose for an adiabatic inner wall and conducting outer wall

η	$\tau_{0_{\text{nose}}}$	$V_{0_{\text{nose}}}$	$\theta_{0_{m_{\text{nose}}}}$
0.5	0.82	2.95	1.15
0.75	2.66	2.38	1.16
0.9	8.26	2.19	1.16
0.99	92.60	2.12	1.17

Table 2.6: Conditions at the nose for an adiabatic inner wall and Newton's law at the outer wall

η	$\tau_{0_{\text{nose}}}$	$V_{0_{\text{nose}}}$	$\theta_{0_{m_{\text{nose}}}}$
0.50	0.69	2.68	1.16
0.75	1.83	1.83	1.11
0.90	3.95	1.24	1.07
0.99	14.82	0.4	1.00

Table 2.5 shows the conditions at the nose obtained from solving the Kearsley equations for an adiabatic inner wall and an infinitely conducting outer wall.

Table 2.6 shows the conditions at the nose obtained from solving the Kearsley equations for an adiabatic inner wall and Newton's law at the outer wall with a Bi= 6.19 which very closely corresponds to experimental conditions discussed later on in this thesis.

Further, we will calculate the actual torque, wall speed and the maximum temperature at the nose for a liquid with the following physical properties that correspond to the physical properties of the experimental fluid:

Viscosity: 5651 c.p at 25·C

Sensitivity: S=0.0757 $^{\circ}C^{-1}$ ($\mu_w/\mu = e^{S(T-T_w)}$)

Thermal conductivity : k=0.22 J/s m°C

The outer radius of the cylinder: 1"

Therefore, we obtain for the velocity, torque and the temperature scales, $V_{\text{ref}} = \sqrt{(k/S\mu_w)} = 0.72$ m/s

Table 2.7: An estimate of actual parameter values at the nose for an experiment

Boundary condition (Inner-Outer)	Torque (lb_f -in)	rpm	Max. Temp. (°C)
Conducting-Conducting	10.89	1327	40.45
Adiabatic-Conducting	5.15	644	40.32
Adiabatic-Newton's law	3.54	495	39.26

$\tau_{\text{ref}} = \sqrt{(k\mu_w r_2^2/S)} = 0.90\ \text{lb}_f\text{-in}$

$T_{\text{ref}} = 1/S = 13.2\,^{\circ}\text{C}$

respectively. Unscaling the values that we obtained at the nose for the various boundary conditions using these reference scales, we obtain the actual value of rpm, torque and the maximum temperature at the nose. Table 2.7 indicates one such set of values of rpm, torque and the maximum temperature at the nose for a 0.75 radius ratio, an outer radius of 1 inch and a length of 0.34m. The term 'Conducting' in the table refers to a wall that is infinitely conducting, thermally.

CHAPTER 3
THE PERTURBED EQUATIONS

In concluding the last chapter which was on the character of the base solution, we observed that the stability of the base solution could be inspected by subjecting it to small perturbations. The goal of this chapter then is to write the perturbed equations and we do this only in vector form. Before doing this, we rewrite the unscaled model equations of motion and energy under a solenoidal velocity field.

$$\rho\frac{\partial \mathbf{v}}{\partial t}+\rho\mathbf{v}.\nabla\mathbf{v}=-\nabla p+2\nabla.\left(\mu D\right)$$

$$\rho C_v\frac{\partial T}{\partial t}+\rho C_v\mathbf{v}.\nabla T=k\nabla^2 T+2\mu D:D$$

Now, both the velocity and temperature equations are non-linear. For a constant viscosity liquid, the non-linearity stems from the convective terms and the viscous dissipation terms. However, when viscosity is dependent on temperature, then there arises an additional non-linearity. Non-linear equations in general have more than one solution. We identified one class of solutions called the base solutions to this problem. Now, if we give a disturbance to this base solution, one of the following might happen: the disturbance might decay and the base solution may be restored or the disturbance might grow to some other solution unless something catastrophic occurs.

A stability calculation will tell us for a disturbance whether the system returns to the steady flow or evolves to a new flow or something catastrophic occurs. In doing a stability calculation, we only impart small disturbances to the base solution and see its evolution. The reason is that if a solution were unstable to large disturbances, it could still be stable to a small one; however if it were unstable to a small disturbance, it would necessarily be unstable to all disturbances. In doing a typical calculation, we look for the critical value of a system parameter at which the system either branches off to a new solution from this base state solution or ceases to have any solution at all. The former is called a branch point and the latter is called a turning point. In either case, after the critical value of the parameter is crossed, the base state ceases to predict the flow. As an example, we might imagine that the wall speed is the system parameter in question. The critical value should then depend on whether we impart disturbances such that the velocity perturbations vanish on the moving wall or the stress perturbation vanish on the moving wall as we have noticed a difference in the rate of decay of perturbations between these two cases from our physical arguments.

Having decided to impart small perturbations, we will write

$$\mathbf{v} = \mathbf{v_0} + \mathbf{v_1}, p = p_0 + p_1, T = T_0 + T_1.$$

in the model equations above and then eliminate the terms that together satisfy the base equation (order zero) and retain the terms that are linear (order one) in the perturbation variables to obtain the equations of motion as

$$\begin{aligned} \rho\frac{\partial \mathbf{v_1}}{\partial t} + \rho\mathbf{v_1}.\nabla\mathbf{v_0} + \rho\mathbf{v_0}.\nabla\mathbf{v_1} &= -\nabla p_1 + 2\nabla\mu_0.D_1 + 2{\mu_0}'\nabla T_1.D_0 \\ &+2{\mu_0}''T_1\nabla T_0.D_0 + \mu_0\nabla^2\mathbf{v_1} + {\mu_0}'T_1\nabla^2\mathbf{v_0} \end{aligned} \tag{3.1}$$

and the equation of energy as

$$\rho C_v\frac{\partial T_1}{\partial t} + \rho C_v\mathbf{v_1}.\nabla T_0 + \rho C_v\mathbf{v_0}.\nabla T_1 = k\nabla^2 T_1 + 4\mu_0 D_0 : D_1 + 2{\mu_0}'T_1 D_0 : D_0 \tag{3.2}$$

where ${\mu_0}'$ denotes $\mathrm{d}\mu(T_0)/T_0$ and $\mathbf{v_1}$ is solenoidal. Before we conclude this chapter, it would be helpful to make a few observations:

A velocity perturbation, once imposed on the base flow, has two mechanisms by which it can decay. One is purely by the diffusion of the momentum, and the kinematic viscosity, μ/ρ, of the liquid in the gap decides how long a perturbation takes to decay. For a fixed density ρ, a perturbation takes a longer time to decay if the viscosity is lower and vice-versa. The other mechanism for a velocity perturbation to decay is through the convection of the perturbation to the boundaries. The term $\rho\mathbf{v_0}.\nabla\mathbf{v_1}$ in the perturbed equations arising out of the linear perturbation of the $\rho\mathbf{v}.\nabla\mathbf{v}$ term in the Navier-Stokes' equation is responsible for the convection of velocity perturbation.

For a disturbance that varies only in the transverse direction, it turns out that all the terms arising out of the perturbation of $\rho\mathbf{v}.\nabla\mathbf{v}$ and $\rho C_v\mathbf{v}.\nabla T$ vanish and therefore the decay of disturbances is dependent only on the diffusion of the perturbations. We call this class of disturbance a zero wave number disturbance. This is for the following reason: if a Fourier expansion of the perturbed variables is carried out in anticipation of periodic behaviour in the y and z directions, then we may write $A_1(x, y, z, t) = \hat{A}_1(x)\mathrm{e}^{\sigma t}\mathrm{e}^{i\gamma z}\mathrm{e}^{i\beta y}$ for any perturbed state variable A_1 where γ, β are the wave numbers in the y, z directions respectively. If we put $\beta = 0, \gamma = 0$ in this expansion, we obtain a disturbance variable which is dependent only on the transverse direction. Thus the zero wave number disturbance that allows only transverse disturbances is a restricted case of a general class of disturbances. It is to the study of the stability of the flow to this class of disturbances that we turn next.

CHAPTER 4
THE STABILITY FOR A ZERO WAVE NUMBER DISTURBANCE

The motivation for discussing the stability of the Couette flow for a special class of disturbances, namely a disturbance of zero wave number, is two fold:

- The perturbed equations at a zero wave number disturbance are easy enough to enable us make some general conclusions about physical experiments without actually carrying out any numerical work.
- We would like to see whether the connection to the thermal ignition problem carries over when a perturbation of zero wave number is imposed on the Couette flow problem. This is because earlier we pointed out the similarity of the temperature equation of the Couette flow problem to the equation defining the thermal ignition problem. In the thermal ignition problem, the most dangerous disturbance is a disturbance of zero wave number with the nose being a point of neutral stability[1]

Figure 4.1 depicts the plane Couette flow being discussed. For a perturbation of zero wave number, the perturbation is uniform in the y and z directions. Hence, the perturbed velocity and the temperature at zero wave number are expanded as follows:

$$v_{x_1} = v_{x_1}(x,t) = \hat{v}_{x_1}(x)\mathrm{e}^{\sigma t}$$

$$v_{y_1} = v_{y_1}(x,t) = \hat{v}_{y_1}(x)\mathrm{e}^{\sigma t}$$

$$v_{z_1} = v_{z_1}(x,t) = \hat{v}_{z_1}(x)\mathrm{e}^{\sigma t}$$

---

[1] More on the stability of the Thermal Ignition problem will be presented in an endnote to this chapter.

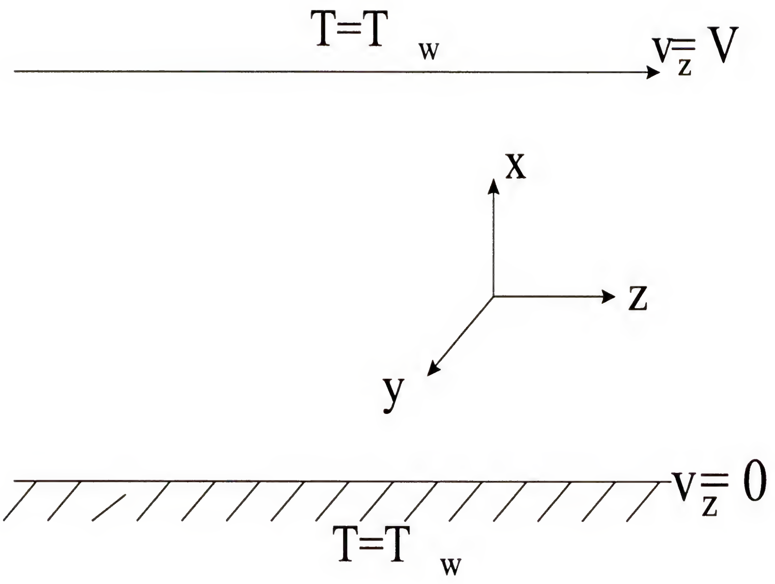

Figure 4.1: Depiction of plane Couette flow

$$T_1 = T_1(x,t) = \hat{T}_1(x)\mathrm{e}^{\sigma t}$$

where σ is the growth constant.

The first conclusion at zero wave number is that the x component of the perturbed velocity is zero. To see this, observe that the equation of continuity at zero wave number is

$$\frac{\mathrm{d}\hat{v}_{x_1}}{\mathrm{d}x} = 0$$

with the boundary condition $\hat{v}_{x_1} = 0$ at $x = \pm 1$. This therefore implies that $\hat{v}_{x_1} = 0$.

Now, let us obtain the y and z components of the equation of motion and the temperature equation by substituting

$$v_{x_1} = 0$$

$$v_{y_1} = \hat{v}_{y_1}(x)\mathrm{e}^{\sigma t}$$

$$v_{z_1} = \hat{v}_{z_1}(x)\mathrm{e}^{\sigma t}$$

$$T_1 = \hat{T}_1(x)\mathrm{e}^{\sigma t}$$

into the perturbed equations

$$\rho\frac{\partial \mathbf{v_1}}{\partial t} + \rho\mathbf{v_1}.\nabla\mathbf{v_0} + \rho\mathbf{v_0}.\nabla\mathbf{v_1} = -\nabla p_1 + 2\nabla\mu_0.D_1 + 2{\mu_0}'\nabla T_1.D_0$$

$$+2{\mu_0}''T_1\nabla T_0.D_0 + \mu_0\nabla^2\mathbf{v_1} + {\mu_0}'T_1\nabla^2\mathbf{v_0}$$

$$\rho C_v\frac{\partial T_1}{\partial t} + \rho C_v\mathbf{v_1}.\nabla T_0 + \rho C_v\mathbf{v_0}.\nabla T_1 = k\nabla^2 T_1 + 4\mu_0 D_0 : D_1 + 2{\mu_0}'T_1 D_0 : D_0$$

We obtain for the y component of the equation of motion

$$\rho\sigma\hat{v}_{y_1} = \frac{\mathrm{d}}{\mathrm{dx}}\left\{\mu_0\frac{\mathrm{d}\hat{v}_{y_1}}{\mathrm{d}x}\right\}$$

and for the z component of the equation of motion

$$\rho\sigma\hat{v}_{z_1} = \frac{\mathrm{d}}{\mathrm{dx}}\left\{\mu_0\frac{\mathrm{d}\hat{v}_{z_1}}{\mathrm{d}x} + {\mu_0}'T_1\frac{\mathrm{d}v_{z_0}}{\mathrm{d}x}\right\} \tag{4.1}$$

where ${\mu_0}' = \dfrac{\mathrm{d}\mu_0}{\mathrm{d}T_0}$
and for the temperature equation

$$\sigma\rho C_v\hat{T}_1 = k\frac{\mathrm{d}^2\hat{\mathrm{T}}_1}{\mathrm{dx}^2} + 2\mu_0\frac{\mathrm{d}v_{z_0}}{\mathrm{d}x}\frac{\mathrm{d}\hat{v}_{z_1}}{\mathrm{d}x} + {\mu_0}'\hat{T}_1\left\{\frac{\mathrm{d}v_{z_0}}{\mathrm{d}x}\right\}^2 \tag{4.2}$$

We find that the y component of the velocity stands by itself and it does not enter the z component of the equation of motion nor the temperature equation. Therefore, we conclude that at zero wave number, it is sufficient to look at the problem in $\hat{v}_{z_1}$ and $\hat{T}_1$.

The plate at $x = -L$ is fixed and therefore no velocity perturbations are allowed on it. For the plate at $x = L$, the boundary condition changes according to whether the velocity is held fixed or the stress is held fixed there. If the velocity is held fixed at $x = L$, then its perturbation at $x = L$ is zero and if the stress is the held fixed at $x = L$, then its perturbation at $x = L$ is zero. Both walls are assumed to be perfectly conducting and hence the temperature perturbation on each wall is zero. No matter whatever else we think that we are doing, the following must be true, at least theoretically: the wall speed is run up to obtain every part of the base curve. Having arrived at any point, we can inspect the stability by imposing perturbations under the requirement of either vanishing wall speed disturbances or vanishing wall stress disturbances or any other combination thereof.

Using the velocity and temperature scales that we discussed in the main body of chapter 2, i.e. choosing $V_{\text{ref}} = \sqrt{k/S\mu_w}$, so that the scaled velocity $\hat{v}^*_{z_1} = \hat{v}_{z_1}/V_{\text{ref}}$ and $T_{\text{ref}} = 1/S$ so that the scaled temperature rise $\hat{\theta}_1 = S(\hat{T}_1 - T_w)$ and further scaling the length x with L, σ with σ_{ref} such that $\sigma^* = \sigma/\sigma_{\text{ref}}$, we obtain, after dropping the $*$,

$$\frac{\rho\sigma_{\text{ref}}L^2}{\mu_{\text{ref}}}\sigma\hat{v}_{z_1} = \frac{\mathrm{d}}{\mathrm{d}x}\left[\mu_0\frac{\mathrm{d}\hat{v}_{z_1}}{\mathrm{d}x} + \left(\frac{\mathrm{d}\mu_0}{\mathrm{d}\theta_0}\right)\frac{\mathrm{d}v_{z0}}{\mathrm{d}x}\hat{\theta}_1\right] \tag{4.3}$$

$$\frac{\rho C_v\sigma_{\text{ref}}L^2}{k}\sigma\hat{\theta}_1 = \frac{\mathrm{d}^2\hat{\theta}_1}{\mathrm{d}x^2} + 2\mu_0\frac{\mathrm{d}v_{z0}}{\mathrm{d}x}\frac{\mathrm{d}\hat{v}_{z_1}}{\mathrm{d}x} + \frac{\mathrm{d}\mu_0}{\mathrm{d}\theta_0}\left\{\frac{\mathrm{d}v_{z0}}{\mathrm{d}x}\right\}^2\hat{\theta}_1 \tag{4.4}$$

Now, choosing σ_{ref} to be $\mu_w/\rho L^2$, we obtain

$$\sigma\hat{v}_{z_1} = \frac{\mathrm{d}}{\mathrm{dx}}\left\{\mu_0\frac{\mathrm{d}\hat{v}_{z_1}}{\mathrm{d}x} + \frac{\mathrm{d}v_{z0}}{\mathrm{d}x}\mu_0{}'\hat{\theta}_1\right\} \tag{4.5}$$

$$\sigma Pr\hat{\theta}_1 = \frac{\mathrm{d}^2\hat{\theta}_1}{\mathrm{dx}^2} + 2\tau_{xz0}\frac{\mathrm{d}\hat{v}_{z_1}}{\mathrm{d}x} + \mu_0{}'\hat{\theta}_1\left\{\frac{\mathrm{d}v_{z0}}{\mathrm{d}x}\right\}^2 \tag{4.6}$$

where $\tau_{xz_0} = \mu_0\mathrm{d}v_{z0}/\mathrm{d}x$ and $\mu_0{}' = \frac{\mathrm{d}\mu_0}{\mathrm{d}\theta_0}$. Here, x is the scaled gap width and it varies from -1 to $+1$. Now, for a zero wave number disturbance wherein $\hat{v}_{x_1} = 0$, the perturbed shear stress $\hat{\tau}_{xz_1}$ can be written just as a perturbation of the base shear stress $\tau_{xz_0} = \mu_0\mathrm{d}v_{z0}/\mathrm{d}x$, i.e.,

$$\hat{\tau}_{xz_1} = \mu_0\frac{\mathrm{d}\hat{v}_{z_1}}{\mathrm{d}x} + \mu_0{}'\hat{\theta}_1\frac{\mathrm{d}v_{z0}}{\mathrm{d}x} \tag{4.7}$$

Using $\tau_{xz_0} = \mu_0\mathrm{d}v_{z0}/\mathrm{d}x$ and $f_0 = 1/\mu_0$, we obtain

$$f_0\hat{\tau}_{xz_1} = \frac{\mathrm{d}\hat{v}_{z_1}}{\mathrm{d}x} - f_0{}'\tau_{xz_0}\hat{\theta}_1 \tag{4.8}$$

Now, using the definition of the perturbed shear stress, the perturbed velocity equation can be rewritten as

$$\sigma\hat{v}_{z_1} = \frac{\mathrm{d}\hat{\tau}_{\mathrm{xz}_1}}{\mathrm{dx}} \tag{4.9}$$

while the perturbed temperature equation can be rewritten as

$$\sigma Pr\hat{\theta}_1 = \frac{\mathrm{d}^2\hat{\theta}_1}{\mathrm{dx}^2} + f_0{}'\tau_{xz0}^2\hat{\theta}_1 + 2f_0\tau_{xz_0}\hat{\tau}_{xz_1} \tag{4.10}$$

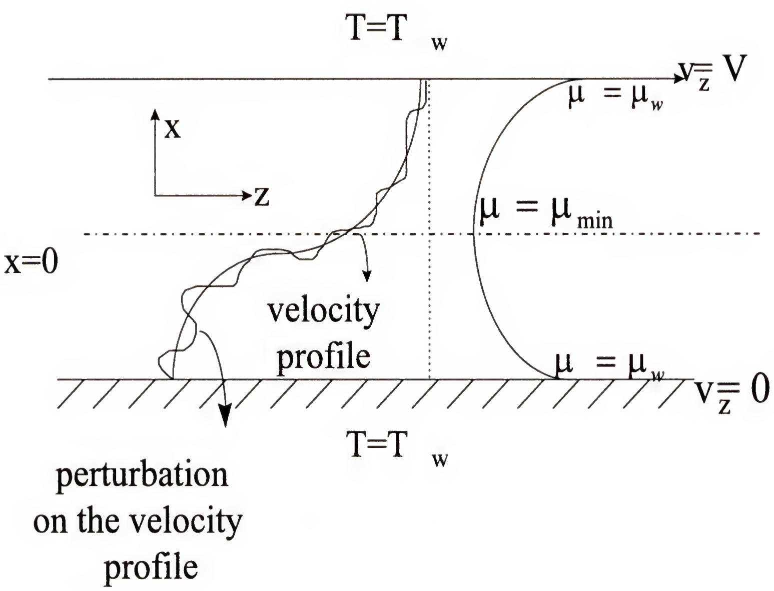

Figure 4.2: Schematic of the Couette flow with arbitrary perturbations on the base state.

where Pr is the Prandtl number, $C_v \mu_w / k$ of the fluid in the gap. The boundary conditions of the perturbed variables satisfy

$$\hat{\theta}_1(x = \pm 1) = 0, \hat{v}_{z_1}(x = -1) = 0, \hat{v}_{z_1}(x = +1) = 0$$

if the wall speed is held fixed at $x = 1$ and

$$\hat{\theta}_1(x = \pm 1) = 0, \hat{v}_{z_1}(x = -1) = 0, \hat{\tau}_{xz_1}(x = +1) = 0$$

if the wall stress is held fixed at $x = 1$[2]. Before studying the stability of the base curve to small perturbations under the two conditions, let us recall the physical explanation which was put forth earlier to explain qualitatively the difference in the rate at which perturbations decay under these two conditions.

---

[2] The rigorous way to write boundary condition at constant wall stress is to realize that in trying to keep the wall stress fixed in an experiment, we actually keep the force on the plate fixed. The boundary condition then becomes $\int_{z=0}^{z=W} \int_{y=0}^{y=B} \tau_{xz_1}(x = +1) \mathrm{d}y \mathrm{d}z = 0$. However at zero wave number as the quantities do not depend on y and z, this condition simplifies to the pointwise condition $\hat{\tau}_{xz_1} = 0$. In fact, when we will later perform the stability calculation at constant wall stress for a non-zero wave number disturbance, we will continue to use this pointwise condition as an approximation to the integral condition. More about this boundary condition will be discussed in Chapter 6

At zero wave number, there is no convective transfer of momentum as all the terms arising out of $\mathbf{v}.\nabla\mathbf{v}$ are zero. The only mechanism for the transfer of momentum is then by diffusion.

Given an arbitrary disturbance on the velocity and temperature fields, we see that under constant wall speed conditions, the velocity disturbance can diffuse through both the boundaries, there being momentum sinks there. However, under constant wall stress, the corresponding wall is 'adiabatic to momentum'. All other things being equal one might conjecture that perturbations where the stress vanishes at a wall are likely to linger longer than perturbations with vanishing speed at the wall. To determine whether our predictions are correct requires us to do some analytic work and this is the main goal of this chapter.

4.1 Stability to a Zero Wave Number Disturbance

Now, the perturbed equations at zero wave number, can be re-arranged in an operator form as follows:

$$\begin{bmatrix} 0 & \dfrac{\mathrm{d}}{\mathrm{dx}} & 0 \\ -\dfrac{\mathrm{d}}{\mathrm{dx}} & f_0 & f_0^{'}\tau_{xz0} \\ 0 & 2f_0\tau_{xz0} & \dfrac{\mathrm{d}^2}{\mathrm{dx}^2} + f_0^{'}\tau_{xz0}^2 \end{bmatrix} \begin{bmatrix} \hat{v}_{z_1} \\ \hat{\tau}_{xz_1} \\ \hat{\theta}_1 \end{bmatrix} = \sigma \begin{bmatrix} 1 & 0 & 0 \\ 0 & 0 & 0 \\ 0 & 0 & \mathrm{Pr} \end{bmatrix} \begin{bmatrix} \hat{v}_{z_1} \\ \hat{\tau}_{xz_1} \\ \hat{\theta}_1 \end{bmatrix} \tag{4.11}$$

The reason for writing the equations in this form $\mathbf{Au} = \sigma\mathbf{Bu}$ is that with very little algebraic manipulation it can be seen that the operator $\mathbf{A}$ is self-adjoint. In fact, multiplying the 1st row and the second row of the above equation by two, it turns out that the operator $\mathbf{A}$ with either of the boundary conditions is self adjoint for an exponential fluidity ($f_0 = f_0^{'}$) dependence[3]. The operator in self-adjoint form is therefore [4]

---

[3] A proof that the operator $\mathbf{A}$ is self adjoint is provided in the endnote of this chapter.

[4] The corresponding equations in operator form for the circular Couette flow are presented in an endnote to this chapter

$$\begin{bmatrix} 0 & 2\frac{\mathrm{d}}{\mathrm{dx}} & 0 \\ -2\frac{\mathrm{d}}{\mathrm{dx}} & 2f_0 & 2f_0{}'\tau_{xz_0} \\ 0 & 2f_0\tau_{xz_0} & \frac{\mathrm{d}^2}{\mathrm{dx}^2} + f_0{}'\tau_{xz_0}^2 \end{bmatrix} \begin{bmatrix} \hat{v}_{z_1} \\ \hat{\tau}_{xz_1} \\ \hat{\theta}_1 \end{bmatrix} = \sigma \begin{bmatrix} 2 & 0 & 0 \\ 0 & 0 & 0 \\ 0 & 0 & \mathrm{Pr} \end{bmatrix} \begin{bmatrix} \hat{v}_{z_1} \\ \hat{\tau}_{xz_1} \\ \hat{\theta}_1 \end{bmatrix} \tag{4.12}$$

Now, it can be proved using the self-adjointness of **A** and the positivity of the operator **B** that the eigenvalues in this case are real[5]. This implies that any arbitrary perturbation at zero wave number can either grow monotonically or decay monotonically but can never oscillate. This result will be used in determining the stability of the base solution to small disturbances. This is what we will do next.

At each point of the base solution curve, the perturbed equations determine a set of values of σ which we now know to be purely real at least for exponential fluidity and will assert this to be true for all other fluidities. Interestingly, we were not able to prove that the operator is self-adjoint for linear fluidity, even though numerical results show that the eigenvalues are real, and physically too, we believe that changing the viscosity dependence on temperature should not change the way in which a perturbation grows or decays. Now, assuming that the eigenvalues are real, if at least one of the eigenvalues turns out to be positive, then the base solution corresponding to that point is not stable. Therefore, the critical points along the curve are points where $\sigma = 0$ is an eigenvalue to the perturbed equations. Such points are called points of neutral stability and we look for those points on the base solution curve. To do this, we put $\sigma = 0$ in the perturbed equations to get the equations under neutral conditions

$$0 = \frac{\mathrm{d}\hat{\tau}_{\mathrm{xz}_1}}{\mathrm{dx}} \tag{4.13}$$

$$0 = \frac{\mathrm{d}^2\hat{\theta}_1}{\mathrm{dx}^2} + f_0{}'\tau_{xz_0}^2\hat{\theta}_1 + 2f_0\tau_{xz_0}\tau_{xz_1} \tag{4.14}$$

---

[5] The proof will be presented in an endnote.

A point on the base curve is a neutral point if a non-trivial solution to these equations exists. Our first conclusion is based on the perturbed velocity equation written for neutral conditions. This equation tells us that under neutral conditions, the perturbed shear stress remains constant across the gap, but it need not be zero. It is required to be zero only if the perturbation is carried out at constant wall stress. Then and only then does the shear stress retain its base value. We will look at the stability result under this condition first.

4.1.1 Stability Results at Constant Wall Stress

At constant wall stress, $\hat{\tau}_{xz_1} = 0$ and the perturbed temperature equation becomes

$$\frac{\mathrm{d}^2\hat{\theta}_1}{\mathrm{dx}^2} + {f_0}' \tau_{xzo}^2 \hat{\theta}_1 = 0$$

with the boundary conditions $\hat{\theta}_1(x = \pm 1) = 0$.

For any given point on the base curve, the perturbed temperature equation above tells us whether or not that point is a point of neutral stability. This can be seen by comparing this equation to the eigenvalue problem

$$\frac{\mathrm{d}^2\phi_1}{\mathrm{dx}^2} + {f_0}' \lambda^2 \phi_1 = 0$$

with $\phi_1(x = \pm 1) = 0$ that we introduced to predict when a nose ought to occur on the base curve. The temperature equation under neutral conditions has no solutions other than $\hat{\theta}_1 = 0$ along the lower branch as along the lower branch $\lambda_1(\tau_{xzo}) > \tau_{xzo}$. So, along the lower branch our assumption that $\sigma = 0$ leads to only a trivial solution. Similarly, along the upper branch where $\lambda_1(\tau_{xzo}) < \tau_{xzo}$, there are no neutral points. But the nose is a point of neutral stability as there $\lambda_1(\tau_{xzo}) = \tau_{xzo}$. There $\hat{\theta}_1$ is not equal to zero and in fact $\hat{\theta}_1 \propto \phi_1$.

Therefore, we can conclude that at constant wall stress, the lower branch is stable to small perturbations as at $\tau_{xz_0} = 0$ all the eigenvalues determined by the perturbed velocity and temperature equations are negative and they cannot rise to zero till the nose of the curve is reached. This suggests that the upper branch is unstable but does not prove it. A proof for this is presented later in this chapter [6].

Next, we will look for points of neutral stability along the base curve at constant wall speed.

4.1.2 The Stability Results at Constant Wall Speed

Rearranging the temperature equation at neutral conditions, we obtain

$$\frac{\mathrm{d}^2\hat{\theta}_1}{\mathrm{dx}^2} + f_0{}' \tau_{xz_0}^2 \hat{\theta}_1 = -2 f_0 \tau_{xz_0} \hat{\tau}_{xz_1} \tag{4.15}$$

with $\hat{\theta}_1(x = \pm 1) = 0$. Under neutral conditions $\hat{\tau}_{xz_1}$ is a constant . Now, integrating the equation that defines the perturbed shear stress

$$f_0 \hat{\tau}_{xz_1} = \frac{\mathrm{d}\hat{v}_{z_1}}{\mathrm{d}x} - f_0{}' \tau_{xz_0} \hat{\theta}_1$$

over $-1 \leq x \leq 1$, with the boundary condition that $\hat{v}_{z_1} = 0$ at $x = \pm 1$, we obtain

$$0 = \hat{\tau}_{xz_1} \int_{-1}^{+1} f_0 \mathrm{d}x + \tau_{xz_0} \int_{-1}^{+1} f_0{}' \hat{\theta}_1 \mathrm{d}x \tag{4.16}$$

Note that under neutral conditions, $\hat{\tau}_{xz_1}$ is a constant and hence can be pulled outside of the integral. Now, the objective is to see whether any non-zero solution to these equations is possible, i.e., if either $\hat{\tau}_{xz_1}$ or $\hat{\theta}_1$ is non-zero. However, it turns out that if one of them is zero, the other is also zero. To see this, observe from the perturbed temperature equation that if $\hat{\theta}_1 = 0$, then $\hat{\tau}_{xz_1} = 0$. The converse is also true, i.e., if $\hat{\tau}_{xz_1} = 0$ then $\hat{\theta}_1 = 0$. The perturbed temperature equation above tells us that this is true along the lower branch where $\lambda_1(\tau_{xz_0}) > \tau_{xz_0}$. It is also true on the upper branch where $\lambda_1(\tau_{xz_0}) < \tau_{xz_0}$. At the nose, where $\lambda_1(\tau_{xz_0}) = \tau_{xz_0}$, if $\hat{\tau}_{xz_1} = 0$, then the perturbed temperature equation above tells us that $\hat{\theta}_1 \propto \phi_1$. But then the equation

$$0 = \hat{\tau}_{xz_1} \int_{-1}^{+1} f_0 \mathrm{d}x + \tau_{xz_0} \int_{-1}^{+1} f_0{}' \hat{\theta}_1 \mathrm{d}x$$

---

[6] As the stability result at constant wall stress is identical to the stability result for a thermal ignition problem in a catalyst pellet, this raises the question "Is the thermal ignition problem a good model for the Couette flow problem with frictional heating, at least under constant wall stress conditions?" We will explore this question in detail later in the thesis.

requires the constant of proportionality to be zero as ϕ_1 is singly signed, i.e. it is an even function of x. Therefore we conclude that neither $\hat{\tau}_{xz_1}$ nor $\hat{\theta}_1$ are zero, or both are zero.

Now, let τ_{xz_0} correspond to a point on the lower branch of the base curve. To find out whether or not a solution $\hat{\tau}_{xz_1} \neq 0, \hat{\theta}_1 \neq 0$ can be found satisfying the above equations, we will write $\hat{\theta}_1 = \hat{\tau}_{xz1} \frac{\hat{\theta}_1}{\hat{\tau}_{xz_1}}$ and using the $\dot{\theta}_0$ equation

$$\frac{\mathrm{d}^2\dot{\theta}_0}{\mathrm{dx}^2} + f_0{'}\tau_{xz_0}^2\dot{\theta}_0 = -2f_0\tau_{xz_0}$$

we conclude that $\dfrac{\hat{\theta}_1}{\hat{\tau}_{xz_1}}$ under neutral conditions is equal to $\dot{\theta}_0$. This being so, $\dfrac{\hat{\theta}_1}{\hat{\tau}_{xz_1}}$ must be positive along the lower branch as $\dot{\theta}_0$ is positive along the lower branch. Now, the equation

$$0 = \hat{\tau}_{xz_1}\int_{-1}^{+1} f_0 \mathrm{d}x + \tau_{xz_0}\int_{-1}^{+1} f_0{'}\hat{\theta}_1 \mathrm{d}x$$

can be rewritten as

$$0 = \hat{\tau}_{xz_1}\int_{-1}^{+1}\left[f_0 + f_0{'}\tau_{xz0}\frac{\hat{\theta}_1}{\hat{\tau}_{xz_1}}\right]\mathrm{d}x \tag{4.17}$$

As f_0, $f_0{'}$ and τ_{xz_0} are all positive this equation can be satisfied only if $\hat{\tau}_{xz_1} = 0$. The conclusion then is that there are no points of neutral stability on the lower branch of the base solution curve as assuming $\sigma = 0$ leads us only to the trivial solution $\hat{\tau}_{xz_1} = 0$ and hence $\hat{\theta}_1 = 0$.

To move on to the upper branch, consider $\mathrm{d}V_0/\mathrm{d}\tau_{xz_0}$ where V_0 is defined as

$$V_0 = \tau_{xz0}\int_{-1}^{+1} f_0 \mathrm{d}x$$

$$\frac{\mathrm{d}V_0}{\mathrm{d}\tau_{xz_0}} = \int_{-1}^{+1}\left[f_0 + f_0{'}\tau_{xz_0}\dot{\theta}_0\right]\mathrm{d}x \tag{4.18}$$

Now the equation

$$0 = \hat{\tau}_{xz_1}\int_{-1}^{+1}\left[f_0 + f_0{'}\tau_{xz0}\frac{\hat{\theta}_1}{\hat{\tau}_{xz_1}}\right]\mathrm{d}x$$

can be rewritten by putting $\hat{\theta}_1/\hat{\tau}_{xz_1} = \dot{\theta}_0$ and then using the $\frac{\mathrm{d}V_0}{\mathrm{d}\tau_{xz_0}}$ formula in the result to obtain

$$0 = \hat{\tau}_{xz_1}\frac{\mathrm{d}V_0}{\mathrm{d}\tau_{xz_0}} \tag{4.19}$$

This equation holds on both the branches. Therefore on both the branches, the hypothesis $\hat{\tau}_{xz_1} \neq 0$ leads to the conclusion that $\hat{\tau}_{xz_1} = 0$ as along the lower branch $\mathrm{d}V_0/\mathrm{d}\tau_{xz_0}$ is positive and along the upper branch $\mathrm{d}V_0/\mathrm{d}\tau_{xz_0}$ is negative. Only the nose remains.

At the nose, the perturbed temperature equation cannot determine $\hat{\theta}_1$ unless a solvability condition is satisfied as $\lambda_1(\tau_{xz_0}) = \tau_{xz_0}$ at the nose. The solvability condition is

$$\int_{-1}^{+1} \phi_1 \left\{-2f_0\tau_{xz_0}\hat{\tau}_{xz_1}\right\} \mathrm{d}x = 0 \tag{4.20}$$

and this cannot be true unless $\hat{\tau}_{xz_1} = 0$ as ϕ_1, the fundamental eigenfunction is singly signed. This implies that the nose cannot be a point of neutral stability. Therefore, the conclusion is this: *There are no points of neutral stability on the entire base curve for perturbations of zero wave number at constant wall speed.*

The only case that we have overlooked in this analysis is that the possibility that $\lambda_2(\tau_{xz_0}) = \tau_{xz_0}$ on the upper branch. We will consider this next.

It turns out that if $\lambda_2(\tau_{xz_0}) = \tau_{xz_0}$, on the upper branch, then $\hat{\tau}_{xz_1} = 0$ does not imply $\hat{\theta}_1 = 0$. In fact, looking at the perturbed temperature equation, we can conclude that if $\hat{\tau}_{xz_1} = 0$, then $\hat{\theta}_1 \propto \phi_2$ satisfies the perturbed temperature equation and also the equation

$$0 = \hat{\tau}_{xz_1}\int_{-1}^{+1} f_0 \mathrm{d}x + \tau_{xz_0}\int_{-1}^{+1} f_0{}'\hat{\theta}_1 \mathrm{d}x$$

Such a point referred to as a 'branch point' earlier is also therefore a point of neutral stability.

The existence of a branch point on the upper branch depends on the fluidity. For exponential fluidity, we have already shown numerically in chapter 2, that along the upper branch $\lambda_2(\tau_{xz_0}) > \tau_{xz_0}$. Therefore, there is no possibility that there are neutral points at constant wall speed on the upper branch for exponential fluidity.

The stability result that we obtained at a zero wave number disturbance so far is summarized in the following statement: *"The entire base solution curve is stable to small perturbations at constant wall speed but the nose is a point of neutral stability and the upper branch is unstable at constant wall stress"*. We will explore the implications of this result in terms of a physical experiment later on in this chapter.

4.2 The rate of change of Eigenvalues with a change in the Input Variables describing the problem

Thus far, we have discussed the stability of Couette flow for a zero wave number disturbance at constant wall speed and at constant wall stress. We did this by looking for neutral points on the curve. However, in this analysis, we did not calculate the magnitude of the eigenvalues nor did we examine how they change with various parameters in this problem. This is important because in any linear stability calculation, the largest eigenvalue tells us how fast an arbitrary perturbation grows or decays with time. For example, if the largest eigenvalue is negative, it implies an arbitrary perturbation decays with time. But the sign alone does not tell us how long it takes for the perturbation to decay. The magnitude of the eigenvalue decides this. If the magnitude is very small, then it means a perturbation takes a long time to decay. On the other hand, if the magnitude is very large, then it implies that that a perturbation decays almost instantaneously. Therefore, it becomes important to estimate the magnitude of the eigenvalues along the curve for various values of parameters such as wall speed V_0 or the Prandtl number Pr and so on. With this in mind, we examine how the eigenvalues change with respect to a change in system parameters.

The perturbed equation at zero wave number can be written as

$$\mathbf{Au} = \sigma \mathbf{Bu} \tag{4.21}$$

Now, let λ be any parameter such as the Prandtl number of the fluid in the gap or the speed of the moving plate. In this section, we will be interested in seeing how the eigenvalues at zero wave number change with respect to a change in these parameters.

Let $\dot{}$ denote the derivative with respect to the parameter λ. Differentiating the above equation with respect to λ we get

$$\mathbf{A}\dot{\mathbf{u}} + \dot{\mathbf{A}}\mathbf{u} = \sigma \mathbf{B}\dot{\mathbf{u}} + \dot{\sigma}\mathbf{Bu} + \sigma \dot{\mathbf{B}}\mathbf{u} \tag{4.22}$$

Multiplying the equation $\mathbf{Au} = \sigma\mathbf{Bu}$ with $\dot{\mathbf{u}}$ and integrating it over -1 to $+1$ and subtracting it from the above equation multiplied with $\mathbf{u}$ and integrated over -1 to $+1$, we obtain

$$< \mathbf{u}, \dot{\mathbf{A}}\mathbf{u} >= \dot{\sigma} < \mathbf{u}, \mathbf{Bu} > + \sigma < \mathbf{u}, \dot{\mathbf{B}}\mathbf{u} > \tag{4.23}$$

As an example, let λ be the wall speed V_0. As the operator $\mathbf{B}$ does not depend on the wall speed V_0, $\dot{\mathbf{B}} = 0$. Therefore, we obtain

$$< \mathbf{u}, \dot{\mathbf{A}}\mathbf{u} >= \dot{\sigma} < \mathbf{u}, \mathbf{Bu} > \tag{4.24}$$

$$\dot{\sigma} = \frac{< \mathbf{u}, \dot{\mathbf{A}}\mathbf{u} >}{< \mathbf{u}, \mathbf{Bu} >} \tag{4.25}$$

where

$$\dot{A} = \begin{bmatrix} 0 & 0 & 0 \\ 0 & 2\frac{\mathrm{d}}{\mathrm{d}V_0} f_0 & 2\frac{\mathrm{d}}{\mathrm{d}V_0}\left[f_0 \tau_{xzo}\right] \\ 0 & 2\frac{\mathrm{d}}{\mathrm{d}V_0}\left[f_0 \tau_{xzo}\right] & \frac{\mathrm{d}}{\mathrm{d}V_0}\left[f_0 {\tau_{xzo}}^2\right] \end{bmatrix} \tag{4.26}$$

Substituting for $\dot{\mathbf{A}}$ in the formula for $\dot{\sigma}$, we get

$$\dot{\sigma} = \frac{2\int_{-1}^{1} \frac{\mathrm{d}}{\mathrm{d}V_0}\left[f_0\right] |\hat{\tau}_{xz_1}|^2 \mathrm{d}x + 4\int_{-1}^{+1} \frac{\mathrm{d}}{\mathrm{d}V_0}\left[f_0 \tau_{xzo}\right] \hat{\tau}_{xz_1} \hat{\theta}_1 \mathrm{d}x + \int_{-1}^{+1} \frac{\mathrm{d}}{\mathrm{d}V_0}\left[f_0 {\tau_{xzo}}^2\right] |\hat{\theta}_1|^2 \mathrm{d}x}{\mathrm{Pr}\int_{-1}^{1} |\hat{\theta}_1|^2 \mathrm{d}x + 2\int_{-1}^{1} |\hat{v}_{z_1}|^2 \mathrm{d}x} \tag{4.27}$$

Now, looking at this equation, the following observations can be made about the sign of various terms:

- As f_0 increases with θ_0 and θ_0 increases with V_0, $\frac{\mathrm{d}}{\mathrm{d}V_0}\left[f_0\right]$ is positive.

- $f_0\tau_{xz0} = \frac{\mathrm{d}v_{z0}}{\mathrm{d}x}$, the velocity gradient in the gap. As the velocity is increased, the velocity gradient has to increase in the gap and hence $\frac{\mathrm{d}}{\mathrm{d}V_0}\left[f_0\tau_{xz0}\right]$ is positive.

- $f_0{\tau_{xz0}}^2$ is the viscous dissipation term and it can be asserted that it increases with an increase in velocity. Hence, $\dfrac{\mathrm{d}}{\mathrm{d}V_0}\left[f_0{\tau_{xz0}}^2\right]$ is positive.

So, the sign of $\dot{\sigma}$ can be determined if only the sign of $\int_{-1}^{1}\hat{\theta}_1\hat{\tau}_{xz_1}$ could be determined. But it is difficult to predict the sign of $\int_{-1}^{1}\hat{\theta}_1\hat{\tau}_{xz_1}$ except for a special case and this is the case of constant wall stress and that too at the nose of the curve. Under these conditions the nose is a point of neutral stability where $\hat{\tau}_{xz_1} = 0$. Therefore the integral $\int_{-1}^{+1}\hat{\tau}_{xz_1}\hat{\theta}_1$ vanishes at the nose. This then implies that $\dot{\sigma}$ is positive as all the other terms in the right hand side of the $\dot{\sigma}$ formula are positive. It means that as the velocity is increased from its value at the nose, the largest eigenvalue increases from its value of zero. This then proves that the upper branch is unstable at constant wall stress[7].

For perturbations under constant wall speed, it is difficult to prove that the eigenvalues do increase as the wall speed is increased. A numerical calculation however indicates that they do. Table 4.1 reports the largest eigenvalues as a function of wall speed for a Prandtl number of unity. Observe from the table that the largest eigenvalue, which indicates how long a perturbation takes to decay, increases with an

---

[7] It may be of interest to note that at constant wall stress only the largest eigenvalue is positive along the upper branch. All the other eigenvalues must *always* be negative. To see this, realize that at the nose the largest eigenvalue is zero and all the other eigenvalues are negative. Now, for any eigenvalue to increase from its negative value at the nose to a positive value on the upper branch, it has to first cross zero. But we have already proved that there are no neutral points on the upper branch. Therefore, all except the largest eigenvalue must continue to remain negative even on the upper branch.

Table 4.1: The rate of decay of perturbations as a function of wall speed.

wall stress, τ_{xz_0}	wall speed, V_0	Largest eigenvalue, σ_1
0.15	0.30	-2.50
0.3	0.62	-2.40
0.5	1.10	-2.20
0.7	1.74	-1.90
0.93	3.68	-1.10
0.9362	4.02	-1.00
0.7	11.94	-0.22
0.5	21.69	-0.085
0.3	46.50	-0.022
0.15	117.9	-4.40×10^{-3}

increase in wall speed. This is due to the fact that the average viscosity in the gap decreases as the wall speed is increased and hence a perturbation takes a longer time to be carried over to the boundaries. Again, this explanation is based on the assumption that the rate of decay of perturbations is controlled by the decay of mechanical disturbances. Thus far, we have not established a methodology to determine for a given point on the curve, whether the decay of perturbations is controlled by the decay of the thermal disturbances or the decay of mechanical disturbances. We might be able to assert that as Pr → 0, the thermal disturbances die out instantaneously and the rate of the decay of perturbations is dominated by the decay of mechanical disturbances and as Pr → ∞, the decay of perturbations is dominated by the decay of thermal disturbances. The question to be addressed then is whether, for a given point on the curve and for a given Prandtl number, it is possible to determine a priori whether the decay is thermally dominated or mechanically dominated. In the next chapter, we will provide a method to answer this question. In doing this, we will find that calculating $\frac{d\sigma}{d\mathrm{Pr}}$ turns out be useful.

Returning to the stability results we conclude that:

- For vanishing wall speed perturbations, the entire base solution curve is stable to small perturbations.

- For vanishing wall stress perturbations, the nose is a point of neutral stability and the upper branch is unstable to small perturbations.

Based on the above results, we can conceive of an experiment with the following objective:

- Setting the wall speed, obtain the base solution curve. Based on our stability results, this should be possible as perturbations decay at constant wall speed.
- Once the base solution is obtained, hold the shear stress fixed at a point on the upper branch. The upper branch being unstable for a fixed wall stress, the system ought to jump to the lower branch for that value of shear stress as that is the only stable operating point for that value of shear stress.

However, as the above conclusions are based on the stability results for a zero wave number disturbance, we have to check what happens to the stability results when the restriction of a zero wave number disturbance is relaxed. For example, the following could happen for a disturbance of non-zero wave number:

- At a point on the upper branch, the base solution might become unstable for a perturbation of non-zero wave number even for constant wall speed conditions. This seems unlikely. The experiments of Sukanek[9] suggest that the base solution curve could be obtained setting the wall speed, hinting that, at least in the practically possible operating regions of a physical experiment, the upper branch is stable at constant wall speed. Nevertheless, it is important to demonstrate that for the experimental fluids used in this study that the upper branch is indeed stable under constant wall speed conditions.
- The lower branch might become unstable under constant wall stress conditions for a non-zero wave number disturbance. This is important to know because if indeed this is true, then holding the wall stress fixed even on the lower branch of the base curve becomes impossible in any physical experiment.

To check all of this, a perturbation calculation at non-zero wave number should be carried out before designing an experiment. In chapter 6, we will do this. Before that, we will address the question " What is the dominant mode of decay of perturbations for a given point on the base curve and for a given Prandtl number ?" in the next chapter. But, even before that, once again we conclude this chapter with endnotes on peripheral, but interesting and, in some cases, useful ideas that simply get in the way of the main theme of this chapter.

4.3 Endnotes

4.3.1 Proof of the Self-Adjointness of the Operator A

A self adjoint operator is defined as an operator that satisfies $\mathbf{A} = \mathbf{A}^*$ where $\mathbf{A}^*$ is the adjoint operator of $\mathbf{A}$ defined by

$$< \mathbf{Au}, \mathbf{v} >=< \mathbf{u}, \mathbf{A}^*\mathbf{v} >$$

where $\mathbf{u}, \mathbf{v}$ are two arbitrary vectors and $<>$ denotes an inner product. Here, the inner product of two vectors $< \mathbf{u}, \mathbf{v} >$ is defined as

$$< \mathbf{u}, \mathbf{v} >= \int_{-1}^{1} \overline{\mathbf{u}}.\mathbf{v}\mathrm{d}x$$

where the represents a complex conjugate.

Consider $\mathbf{Au} = \sigma\mathbf{Bu}$ for the specific case of exponential fluidity i.e.$f_0 = f_0^{'}$. It is

$$\begin{bmatrix} 0 & 2\dfrac{\mathrm{d}}{\mathrm{dx}} & 0 \\ -2\dfrac{\mathrm{d}}{\mathrm{dx}} & 2f_0 & 2f_0\tau_{xz0} \\ 0 & 2f_0\tau_{xz0} & \dfrac{\mathrm{d}^2}{\mathrm{dx}^2} + f_0\tau_{xz0}^2 \end{bmatrix} \begin{bmatrix} \hat{v}_{z1} \\ \hat{\tau}_{xz1} \\ \hat{\theta}_1 \end{bmatrix} = \sigma \begin{bmatrix} 2 & 0 & 0 \\ 0 & 0 & 0 \\ 0 & 0 & Pr \end{bmatrix} \begin{bmatrix} \hat{v}_{z1} \\ \hat{\tau}_{xz1} \\ \hat{\theta}_1 \end{bmatrix} \qquad (4.28)$$

Now, taking the inner product of the left hand side of this equation with $\mathbf{v}$ where $\mathbf{v} = \begin{bmatrix} v_1 & \tau_1 & \theta_1 \end{bmatrix}^T$, is any arbitrary vector, we obtain

$$< \begin{bmatrix} 0 & 2\dfrac{\mathrm{d}}{\mathrm{dx}} & 0 \\ -2\dfrac{\mathrm{d}}{\mathrm{dx}} & 2f_0 & 2f_0\tau_{xz0} \\ 0 & 2f_0\tau_{xz0} & \dfrac{\mathrm{d}^2}{\mathrm{dx}^2} + f_0\tau_{xz0}^2 \end{bmatrix} \begin{bmatrix} \hat{v}_{z_1} \\ \hat{\tau}_{xz_1} \\ \hat{\theta}_1 \end{bmatrix}, \begin{bmatrix} v_1 \\ \tau_1 \\ \theta_1 \end{bmatrix} > \tag{4.29}$$

when expanded this yields

$$\begin{aligned} 2\int_{-1}^{+1} \frac{\mathrm{d}\overline{\hat{\tau}}_{xz_1}}{\mathrm{d}x} v_1 \mathrm{d}x - 2\int_{-1}^{+1} \frac{\mathrm{d}\overline{\hat{v}}_{z_1}}{\mathrm{d}x}\tau_1 \mathrm{d}x + 2\int_{-1}^{+1} f_0 \overline{\hat{\tau}}_{xz_1}\tau_1 \mathrm{d}x \\ +2\textstyle\int_{-1}^{+1} f_0\tau_{xz0}\overline{\hat{\theta}}_1\tau_1 \mathrm{d}x + 2\textstyle\int_{-1}^{+1} f_0\tau_{xz0}\overline{\hat{\tau}}_{xz_1}\theta_1 \mathrm{d}x \\ +\textstyle\int_{-1}^{+1} \dfrac{\mathrm{d}^2\overline{\hat{\theta}}_1}{\mathrm{d}x^2}\theta_1 \mathrm{d}x + \displaystyle\int_{-1}^{+1} f_0{\tau_{xz0}}^2\overline{\hat{\theta}}_1\theta_1 \mathrm{d}x \end{aligned} \tag{4.30}$$

Now, the boundary condition on **v** is chosen to be the same as that of **u**. Now, if the wall speed is held fixed then

$$\hat{v}_{z_1}(x = \pm 1) = 0 = v_1(x = \pm 1), \hat{\theta}_1(x = \pm 1) = 0 = \theta_1(x = \pm 1)$$

and if the wall stress is held fixed:

$$\hat{\tau}_{xz_1}(x = +1) = 0 = \tau_1(x = +1), \hat{v}_{z_1}(x = -1) = 0 = v_1(x = -1),$$

$$\hat{\theta}_1(x = \pm 1) = 0 = \theta_1(x = \pm 1)$$

Integrating these equations with the preceding boundary condition, we get the following result both for the case of constant wall speed and for the case of constant wall stress

$$\begin{aligned} -2\int_{-1}^{+1} \frac{\mathrm{d}v_1}{\mathrm{d}x}\overline{\hat{\tau}}_{xz_1} \mathrm{d}x + 2\int_{-1}^{+1} \frac{\mathrm{d}\tau_1}{\mathrm{d}x}\overline{\hat{v}}_{z_1} \mathrm{d}x + 2\int_{-1}^{+1} f_0 \overline{\hat{\tau}}_{xz_1}\tau_1 \mathrm{d}x \\ +2\textstyle\int_{-1}^{+1} f_0\tau_{xz0}\overline{\hat{\theta}}_1\tau_1 \mathrm{d}x + 2\textstyle\int_{-1}^{+1} f_0\tau_{xz0}\overline{\hat{\tau}}_{xz_1}\theta_1 \mathrm{d}x \\ +\int_{-1}^{+1} \frac{\mathrm{d}^2\theta_1}{\mathrm{d}x^2}\overline{\hat{\theta}}_1 \mathrm{d}x + \int_{-1}^{+1} f_0{\tau_{xz0}}^2\overline{\hat{\theta}}_1\theta_1 \mathrm{d}x \end{aligned} \tag{4.31}$$

This can be rewritten as

$$< \begin{bmatrix} \hat{v}_{z_1} \\ \hat{\tau}_{xz_1} \\ \hat{\theta}_1 \end{bmatrix}, \begin{bmatrix} 0 & 2\frac{\mathrm{d}}{\mathrm{dx}} & 0 \\ -2\frac{\mathrm{d}}{\mathrm{dx}} & 2f_0 & 2{f_0}'\tau_{xz0} \\ 0 & 2f_0\tau_{xz0} & \frac{\mathrm{d}^2}{\mathrm{dx}^2} + f_0\tau_{xz0}^2 \end{bmatrix} \begin{bmatrix} v_1 \\ \tau_1 \\ \theta_1 \end{bmatrix} > \tag{4.32}$$

This equation is of the form

$$< \mathbf{u}, \mathbf{A}\mathbf{v} >$$

Therefore, we find that

$$< \mathbf{A}\mathbf{u}, \mathbf{v} >=< \mathbf{u}, \mathbf{A}\mathbf{v} >$$

Therefore, by definition of a self-adjoint operator, operator **A** is self-adjoint. Now to prove that, in this case, σ is real consider once again

$$\mathbf{A}\mathbf{u} = \sigma\mathbf{B}\mathbf{u}$$

Now taking the inner product of this equation with **u**, we obtain

$$< \mathbf{u}, \mathbf{A}\mathbf{u} >=< \mathbf{u}, \sigma\mathbf{B}\mathbf{u} > \tag{4.33}$$

Consider the left hand side of this equation which is $< \mathbf{u}, \mathbf{A}\mathbf{u} >$. It can be rewritten as $< \mathbf{A}\mathbf{u}, \mathbf{u} >$ as **A** is self-adjoint. This again can be rewritten using $\mathbf{A}\mathbf{u} = \sigma\mathbf{B}\mathbf{u}$ as $< \sigma\mathbf{B}\mathbf{u}, \mathbf{u} >$ which by the definition of the inner product can be written as $\overline{\sigma} < \mathbf{B}\mathbf{u}, \mathbf{u} >$. Thus we have

$$< \mathbf{A}\mathbf{u}, \mathbf{u} >= \overline{\sigma} < \mathbf{B}\mathbf{u}, \mathbf{u} >$$

However $< \mathbf{A}\mathbf{u}, \mathbf{u} >=< \mathbf{u}, \mathbf{A}\mathbf{u} >= \sigma < \mathbf{u}, \mathbf{B}\mathbf{u} >$. In other words,

$$(\sigma - \overline{\sigma}) < \mathbf{u}, \mathbf{B}\mathbf{u} >= 0$$

Now, $< \mathbf{u}, \mathbf{B}\mathbf{u} >$ is strictly positive unless $\mathbf{u}^T$=[0 1 0]. However $\mathbf{u}^T$= [0 1 0] in our flow corresponds to $\hat{v}_{z_1}, \hat{\theta}_1 = 0$ but $\hat{\tau}_{xz_1} \neq 0$ which is physically not possible. Hence,

$< \mathbf{u}, \mathbf{B}\mathbf{u} >$ is strictly positive for all cases of physical interest. This then implies that

$$\sigma = \overline{\sigma}$$

which implies that the eigenvalues are real.

4.3.2 The Equations at Zero Wave Number for Circular Couette Flow

In the main body of this chapter, we presented the plane Couette equations in operator form. The corresponding equations in operator form for circular Couette flow are

$$\begin{bmatrix} 0 & 2\frac{\mathrm{d}}{\mathrm{dr}} & 0 \\ -2\frac{\mathrm{d}}{\mathrm{dr}} & \frac{2f_0}{r^3} & \frac{2f_0{'}\tau_0}{r^3} \\ 0 & \frac{2f_0\tau_0}{r^3} & \frac{\mathrm{d}}{\mathrm{dr}}\left(r\frac{\mathrm{d}}{\mathrm{dr}}\right) + \frac{f_0{'}\tau_0^2}{r^3} \end{bmatrix} \begin{bmatrix} \frac{\hat{v}_{\theta_1}}{r} \\ \hat{\tau}_1 \\ \hat{\theta}_1 \end{bmatrix} = \sigma \begin{bmatrix} 2r & 0 & 0 \\ 0 & 0 & 0 \\ 0 & 0 & r\mathrm{Pr} \end{bmatrix} \begin{bmatrix} \frac{\hat{v}_{\theta_1}}{r} \\ \hat{\tau}_1 \\ \hat{\theta}_1 \end{bmatrix} \tag{4.34}$$

For an exponential fluidity dependence, this operator is self-adjoint.

4.3.3 The Plane Couette Flow Equations in the 2 × 2 formulation in $\hat{v}_{z_1}$ and $\hat{\theta}_1$

For the plane Couette problem, it turns out that it is not necessary to cast the problem where **A** is a 3 × 3 matrix that the eigenvalues are real. This can also be proved by getting a 2 × 2 matrix instead. To see that, observe that the equations in 2 × 2 look like below:

$$\begin{bmatrix} \mu_0\frac{\mathrm{d}^2}{\mathrm{d}x^2} + \frac{\mathrm{d}\mu_0}{\mathrm{d}x}\frac{\mathrm{d}}{\mathrm{d}x} & -\tau_{xzo}\frac{f_0'}{f_0}\frac{\mathrm{d}}{\mathrm{dx}} - \tau_{xzo}\frac{\mathrm{d}}{\mathrm{dx}}\left[\frac{f_0'}{f_0}\right] \\ 2\tau_{xzo}\frac{\mathrm{d}}{\mathrm{dx}} & \frac{\mathrm{d}^2}{\mathrm{d}x^2} - f_0{'}\tau_{xzo}^2 \end{bmatrix} \begin{bmatrix} \hat{v}_{z_1} \\ \hat{\theta}_1 \end{bmatrix} = \sigma \begin{bmatrix} 1 & 0 \\ 0 & \mathrm{Pr} \end{bmatrix} \begin{bmatrix} \hat{v}_{z_1} \\ \hat{\theta}_1 \end{bmatrix} \tag{4.35}$$

For exponential fluidity, $f_0 = f_0'$. Hence, the equations reduce to

$$\begin{bmatrix} \mu_0\frac{\mathrm{d}^2}{\mathrm{d}x^2} + \frac{\mathrm{d}\mu_0}{\mathrm{d}x}\frac{\mathrm{d}}{\mathrm{d}x} & -\tau_{xzo}\frac{\mathrm{d}}{\mathrm{dx}} \\ 2\tau_{xzo}\frac{\mathrm{d}}{\mathrm{dx}} & \frac{\mathrm{d}^2}{\mathrm{d}x^2} - f_0{'}\tau_{xzo}^2 \end{bmatrix} \begin{bmatrix} \hat{v}_{z_1} \\ \hat{\theta}_1 \end{bmatrix} = \sigma \begin{bmatrix} 1 & 0 \\ 0 & \mathrm{Pr} \end{bmatrix} \begin{bmatrix} \hat{v}_{z_1} \\ \hat{\theta}_1 \end{bmatrix} \tag{4.36}$$

Multiplying the 1st row by two, we obtain

$$\begin{bmatrix} 2\mu_0\dfrac{\mathrm{d}^2}{\mathrm{d}x^2} + 2\dfrac{\mathrm{d}\mu_0}{\mathrm{d}x}\dfrac{\mathrm{d}}{\mathrm{d}x} & -2\tau_{xz0}\dfrac{\mathrm{d}}{\mathrm{dx}} \\ 2\tau_{xz0}\dfrac{\mathrm{d}}{\mathrm{dx}} & \dfrac{\mathrm{d}^2}{\mathrm{d}x^2} - {f_0}'\tau_{xz0}^2 \end{bmatrix} \begin{bmatrix} \hat{v}_{z_1} \\ \hat{\theta}_1 \end{bmatrix} = \sigma \begin{bmatrix} 2 & 0 \\ 0 & \mathrm{Pr} \end{bmatrix} \begin{bmatrix} \hat{v}_{z_1} \\ \hat{\theta}_1 \end{bmatrix} \tag{4.37}$$

The operator **A** in this formulation is self-adjoint and the operator **B** is strictly positive, i.e. $< \mathbf{Bu}, \mathbf{u} >$ is greater than zero for any arbitrary non-zero **u**. Therefore σ must be real.

4.3.4 Can the sign of σ be obtained from an Energy Argument ?

In the main body of this chapter, to find out whether the base flow is stable to small perturbations at constant wall speed and at constant wall stress, we looked for neutral points by substituting $\sigma = 0$ in the perturbed equations and asked whether any non-trivial solutions exist to the equations under neutral conditions. In this section, we will see whether we can obtain the sign of σ by other methods. Specifically, we will use the energy method to see whether we can determine the sign of σ. To do this, we will multiply the first row of the matrix in the 2×2 self-adjoint formulation by $\hat{v}_{z_1}$ and integrate it between -1 to 1 with the boundary condition that $\hat{v}_{z_1}(x = \pm 1) = 0$ and $\hat{\theta}_1(x = \pm 1) = 0$ and add it to the second row multiplied by $\hat{\theta}_1$ and integrated over -1 to 1 with the boundary condition that $\hat{v}_{z_1}(x = \pm 1) = 0$ and $\hat{\theta}_1(x = \pm 1) = 0$. We obtain

$$\sigma\left[\int_{-1}^{+1}\left(2|\hat{v}_{z_1}|^2 + \mathrm{Pr}|\hat{\theta}_1|^2\right)\mathrm{d}x\right] = \int_{-1}^{1}\left(-\mu_0|\frac{\mathrm{d}v_{z_1}}{\mathrm{d}x}|^2 + 4\frac{\mathrm{d}v_{z_1}}{\mathrm{d}x}\hat{\theta}_1 - |\frac{\mathrm{d}\theta_1}{\mathrm{d}x}|^2 - f_0'\tau_{xz0}^2|\hat{\theta}_1|^2\right)\mathrm{d}x$$

Notice that we have imposed the boundary condition that the wall speed is held fixed at $x = 1$ in deriving this result. The same result would have been obtained had the boundary condition been one of constant wall stress instead of one of constant wall speed at $x = 1$. This is interesting as we now know that the stability result at constant wall stress is different from the stability result at constant wall speed. And it seems like the energy argument cannot isolate that difference. Therefore, we might expect that the energy argument will not give us anything conclusive regarding the sign of σ. In fact, this turns out be indeed true. To see this observe that the formula for σ can be rewritten as

$$\sigma = \frac{\int_{-1}^{1}\left(-\mu_0|\frac{\mathrm{d}v_{z_1}}{\mathrm{d}x}|^2 + 4\frac{\mathrm{d}v_{z_1}}{\mathrm{d}x}\hat{\theta}_1 - |\frac{\mathrm{d}\theta_1}{\mathrm{d}x}|^2 - f_0'\tau_{xz_0}^2|\hat{\theta}_1|^2\right)\mathrm{d}x}{\left[\int_{-1}^{+1}\left(2|\hat{v}_{z_1}|^2 + \mathrm{Pr}|\hat{\theta}_1|^2\right)\mathrm{d}x\right]}$$

The sign of the integral $\int_{-1}^{1}\frac{\mathrm{d}v_{z_1}}{\mathrm{d}x}\hat{\theta}_1\mathrm{d}x$ has to be known to conclude anything about the sign of σ. Therefore, we conclude that we cannot predict the sign of σ using the energy argument.

4.3.5 Neutral points for the case $f_0' < 0$

Thus far in this chapter, we looked at the stability characteristics of the class of fluids which satisfy $f_0 > 0, f_0' > 0$. Liquids, typically fall under this category. To do the stability analysis, we looked for neutral points on the base solution curve which separates stable shear flows from unstable shear flows. In this section, we look for neutral points on the base solution curve for the class of fluids with $f_0 > 0, f_0' < 0$. To do this, we refer to the equations

$$0 = \frac{\mathrm{d}\hat{\tau}_{\mathrm{xz}_1}}{\mathrm{dx}}$$

$$0 = \frac{\mathrm{d}^2\hat{\theta}_1}{\mathrm{dx}^2} + f_0{}'\tau_{xz_0}^2\hat{\theta}_1 + 2f_0\tau_{xz_0}\tau_{xz_1}$$

that describe the equation of motion and the energy balance equation under neutral conditions.

At constant wall stress, $\hat{\tau}_{xz_1} = 0$. Therefore, the equation that describes the problem under neutral conditions is:

$$\frac{\mathrm{d}^2\hat{\theta}_1}{\mathrm{dx}^2} + f_0{}'\tau_{xz_0}^2\hat{\theta}_1 = 0$$

where $\hat{\theta}_1(x = \pm 1) = 0$. As f_0' is negative, this equation has no solution except $\hat{\theta}_1 = 0$ and there are no solutions other than $\hat{\theta}_1 = \hat{\tau}_{xz_1} = 0$ when we look for points of neutral stability at constant wall stress. We conclude that there are no points of neutral stability on the entire curve at constant wall stress for fluids with $f_0' < 0$.

At constant wall speed, the equations under neutral conditions are

$$\frac{\mathrm{d}^2\hat{\theta}_1}{\mathrm{dx}^2} + f_0{}'\tau_{xz0}^2\hat{\theta}_1 = -2f_0\tau_{xz0}\hat{\tau}_{xz_1}$$

$$0 = \hat{\tau}_{xz_1}\int_{-1}^{+1}\left[f_0 + f_0{}'\tau_{xz0}\frac{\hat{\theta}_1}{\hat{\tau}_{xz_1}}\right]\mathrm{d}x$$

As before, by using the similarity of the perturbed temperature equation to the $\dot{\theta}_0$ equation, we rewrite the above equation as

$$0 = \hat{\tau}_{xz_1}\int_{-1}^{+1}\left[f_0 + f_0{}'\tau_{xz_0}\dot{\theta}_0\right]\mathrm{d}x$$

which is again rewritten as

$$0 = \hat{\tau}_{xz_1}\left[\frac{\mathrm{d}V_0}{\mathrm{d}\tau_{xz_0}}\right]$$

where $V_0 = \tau_{xz_0}\int_{-1}^{+1} f_0\mathrm{d}x$. Based on our earlier calculations of V_0 for linear and exponential viscosity dependence on temperature, we can assert that $\mathrm{d}V_0/\mathrm{d}\tau_{xz_0} > 0$ for fluids with $f_0' < 0$. This then implies $\hat{\tau}_{xz_1} = 0$ and hence $\hat{\theta}_1 = 0$. Therefore assuming $\sigma = 0$ only gives us the trivial result and hence we conclude that there are no points of neutral stability for fluids with $f_0' < 0$ under constant wall speed conditions.

CHAPTER 5
THE ROLE OF PRANDTL NUMBER

In the earlier chapters two arguments were advanced to explain the physics of the problem. The first, based on the temporal behavior of mechanical disturbances, sought to explain why perturbations at fixed wall stress linger longer than perturbations at fixed wall speed. The second, based on the temporal behavior of thermal disturbances sought to explain why thermal feedback under constant stress conditions could lead to an unstable flow state while this feedback is absent when the wall speed is held fixed. Further, in an endnote to Chapter 2, it was observed that the temperature equation in the Couette flow problem is similar to the equation defining the thermal ignition problem in a heat generating solid and the wall stress in the fluid problem was found to be the analog of the ignition parameter. In addition, our stability results at constant wall stress were found to be identical to the stability results in the thermal ignition problem with the nose being a point of neutral stability and the upper branch being unstable in both the cases. However, a close look at the stability results at constant wall stress at the nose of the curve where the similarity to the ignition problem is the most striking tells us that even at this point there is indeed both a mechanical and a thermal character to the Couette flow problem. To see this, observe that at the nose of the curve where $\sigma = 0$ and $\hat{\tau}_{xz_1} = 0$, the perturbed temperature equation looks identical to the equation defining the thermal ignition problem. However, the perturbed velocity $\hat{v}_{z_1}$ is not zero. In fact, it is related to the perturbed temperature by the relation $\frac{\mathrm{d}\hat{v}_{z_1}}{\mathrm{d}x} = f_0'\tau_{xz_0}\hat{\theta}_1$. Therefore, this result suggests that the dynamics of both the mechanical and the thermal disturbances are important to understand the physics of this problem. The goal of this chapter, then, is to learn under what conditions mechanical disturbances control the dynamics and when thermal disturbances control the dynamics in Couette flow.

The Prandtl number is the ratio of the momentum to the thermal diffusivity and so one might imagine that the Prandtl number of the fluid will decide which type of disturbance, mechanical or thermal, is important, if indeed either is dominant. To decide when the mechanical disturbances control and when thermal disturbances control using the Prandtl number, we first ask how the growth rates, σ, behave with the Prandtl number. To answer this question, we will go ahead and obtain a formula for $\frac{\mathrm{d}\sigma}{\mathrm{dPr}}$ but before doing that let us ask what we can change to change the Prandtl number. Note that in our scaling, both the wall speed and wall stress are scaled with respect to the physical properties. The wall speed is scaled with respect to $\sqrt{k/S\mu_w}$ and wall stress is scaled with respect to $\sqrt{k\mu_w/SL^2}$. Therefore, the only way to change the Prandtl number holding the actual(unscaled) value of the wall speed and the wall stress fixed would be to change the value of C_v. Hence, in this scale, we view a change in Prandtl number as a change only in C_v.

Now to obtain $\frac{\mathrm{d}\sigma}{\mathrm{dPr}}$, recall that the eigenvalue problem is

$$\mathbf{Au} = \sigma\mathbf{Bu}$$

where the matrix $\mathbf{A}$ is

$$\begin{bmatrix} 0 & 2\dfrac{\mathrm{d}}{\mathrm{dx}} & 0 \\ -2\dfrac{\mathrm{d}}{\mathrm{dx}} & 2f_0 & 2{f_0}'\tau_{xz0} \\ 0 & 2f_0\tau_{xz0} & \dfrac{\mathrm{d}^2}{\mathrm{dx}^2} + {f_0}'\tau_{xz0}^2 \end{bmatrix}$$

and the matrix $\mathbf{B}$ is

$$\begin{bmatrix} 2 & 0 & 0 \\ 0 & 0 & 0 \\ 0 & 0 & \mathrm{Pr} \end{bmatrix}$$

and $\mathbf{u} = \begin{bmatrix} v_{z_1} \\ \hat{\tau}_{xz_1} \\ \hat{\theta}_1 \end{bmatrix}$

Now, recall that we obtained a formula to see how the eigenvalues change with a system parameter. It is

$$< \mathbf{u}, \dot{\mathbf{A}}\mathbf{u} >= \dot{\sigma} < \mathbf{u}, \mathbf{B}\mathbf{u} > + \sigma < \mathbf{u}, \dot{\mathbf{B}}\mathbf{u} >$$

Now, let $\dot{\sigma}$ refer to the rate of change of σ with respect to the Prandtl number. Then, the matrix $\mathbf{A}$ is independent of Prandtl number of the liquid in the gap and therefore $\dot{\mathbf{A}}$ is zero. Therefore, we obtain

$$0 = \dot{\sigma} < \mathbf{u}, \mathbf{B}\mathbf{u} > + \sigma < \mathbf{u}, \dot{\mathbf{B}}\mathbf{u} > \tag{5.1}$$

and hence

$$\dot{\sigma} = -\sigma \frac{< \mathbf{u}, \dot{\mathbf{B}}\mathbf{u} >}{< \mathbf{u}, \mathbf{B}\mathbf{u} >} \tag{5.2}$$

where $\dot{\mathbf{B}}$ simply is

$$\begin{bmatrix} 0 & 0 & 0 \\ 0 & 0 & 0 \\ 0 & 0 & 1 \end{bmatrix}$$

Substituting for $\mathbf{B}$ and $\dot{\mathbf{B}}$ in the above equation, we obtain

$$\dot{\sigma} = -\sigma \frac{\int_{-1}^{1} |\hat{\theta}_1|^2 \mathrm{d}x}{Pr \int_{-1}^{1} |\hat{\theta}_1|^2 \mathrm{d}x + 2 \int_{-1}^{1} |\hat{v}_{z_1}|^2 \mathrm{d}x} \tag{5.3}$$

This can be rewritten as

$$\dot{\sigma} = -\sigma \frac{1}{\mathrm{Pr} + 2 \frac{\int_{-1}^{1} |\hat{v}_{z_1}|^2 \mathrm{d}x}{\int_{-1}^{1} |\hat{\theta}_1|^2 \mathrm{d}x}} \tag{5.4}$$

This equation holds both for a boundary condition of constant wall speed and for a boundary condition of constant wall stress.

The first conclusion coming from this equation is that when σ is negative, $\dot{\sigma}$ is positive and when σ is positive, $\dot{\sigma}$ is negative. A change in the Prandtl number therefore stabilizes an unstable mode and destabilizes the stable modes. This can be explained as follows: an increase in C_v increases the thermal inertia of the system, i.e., it makes the response to a thermal disturbance more sluggish thus slowing down the rate at which a disturbance grows or decays. A perturbation therefore takes a longer time to decay if it is decaying and a longer time to grow if it is growing. This is exactly what the result shows. Now, this explanation should not be interpreted to mean that only the thermal disturbances control the dynamics of the growth or the decay. In fact, it turns out that the actual magnitude of $\dot{\sigma}$ changes depending on whether the dominant mode for the decay of perturbations is thermal or mechanical. If the dominant mode is mechanical, then $\dot{\sigma}$ hardly changes. On the other hand, if the dominant mode is thermal, then $\dot{\sigma}$ changes a lot. The formula leads to a curious situation on the upper branch of the curve at constant wall stress. At constant wall stress on the upper branch, the largest eigenvalue is positive(unstable) and all the other eigenvalues are negative (stable). An increase in C_v on the upper branch therefore stabilizes an unstable mode and destabilizes all the other stable modes. However, it should be noted that the stability results are not altered as the Prandtl number is changed: a stable operating point on the curve always remains stable and an unstable point on the curve always remains unstable[1]. Only the magnitude of the growth or decay changes with a change in Prandtl number.

Next we will see to what the $\dot{\sigma}$ formula reduces to in the limit of high and low Prandtl number.

For low values of Pr, assuming that $\dfrac{\int_{-1}^{1} |\hat{v}_{z_1}|^2 \mathrm{d}x}{\int_{-1}^{1} |\hat{\theta}_1|^2 \mathrm{d}x} >>$ Pr,we obtain

$$\dot{\sigma} = -\sigma \frac{1}{2\dfrac{\int_{-1}^{1} |\hat{v}_{z_1}|^2 \mathrm{d}x}{\int_{-1}^{1} |\hat{\theta}_1|^2 \mathrm{d}x}} \tag{5.5}$$

If our earlier assertion that at low Prandtl number, the growth or decay of perturbations is dominated mainly by the growth or decay of mechanical disturbances then $\dot{\sigma}$

---

[1] This is because we know that the stability results are independent of the Prandtl number

ought to be extremely small and σ ought to remain roughly a constant at low Prandtl numbers.

For extremely large Pr, assuming that $\dfrac{\int_{-1}^{1}|\hat{v}_{z_1}|^2\mathrm{d}x}{\int_{-1}^{1}|\hat{\theta}_1|^2\mathrm{d}x} << \mathrm{Pr}$, the $\dot{\sigma}$ formula simplifies to

$$\dot{\sigma} = -\frac{\sigma}{\mathrm{Pr}} \tag{5.6}$$

We learn by integrating this equation that $\sigma\mathrm{Pr}$ is a constant for large Prandtl numbers. This implies that

$$\sigma \propto 1/\mathrm{Pr}$$

And for a fixed μ_w, k, this in turn means that $\sigma \propto 1/C_v$. Therefore, at high Prandtl numbers, the eigenvalues vary inversely with respect to the specific heat C_v and is independent of $\dfrac{\int_{-1}^{1}|\hat{v}_{z_1}|^2\mathrm{d}x}{\int_{-1}^{1}|\hat{\theta}_1|^2\mathrm{d}x}$. Or at high Pr, the growth or decay of disturbances is thermally controlled.

Table 5.1 and 5.2 indicates how the eigenvalues change as a function of the Prandtl number for a constant wall speed and conducting walls [2]. The table provides results both for a point on the lower branch and for a point on the upper branch at the same value of the dimensionless shear stress $\tau_{xz_0} = 0.5$. This table demonstrates numerically the invariance of σ at low Prandtl number and also its inverse variation with Prandtl number at high Prandtl number.

Looking at the tables, we find that at low Prandtl numbers, the eigenvalues remain roughly a constant and at high Prandtl numbers, the eigenvalues vary inversely with Prandtl number. This result is in tune with the conclusions we drew earlier from the simplification of the $\dot{\sigma}$ formula in the limit of low and high Prandtl numbers. This confirms our view that at low Prandtl number, the dominant mode for the decay of perturbations is mechanical and at high Prandtl number, it is thermal. But the Prandtl number at which the switch over from mechanical to thermal occurs

---

[2] Refer to an endnote to see how a change in Prandtl number affects the growth modes for various other combinations of temperature and momentum boundary conditions on the walls

Table 5.1: The rate of change of the largest eigenvalue with respect to the Prandtl number for $\tau_{xz0} = 0.5$ along the lower branch.

Pr	Largest eigenvalue,σ_1
0.01	-2.21
0.1	-2.21
1.0	-2.19
1.1	-2.19
1.2	-2.18
1.3	-2.01
1.4	-1.87
10.0	-2.64×10^{-1}
100	-2.64×10^{-2}
1000	-2.64×10^{-3}

Table 5.2: The rate of change of the largest eigenvalue with respect to the Prandtl number for $\tau_{xz0} = 0.5$ along the upper branch.

Pr	Largest eigenvalue,σ_1
0.01	-8.36×10^{-2}
0.1	-8.35×10^{-2}
1.0	-8.27×10^{-2}
10.0	-7.50×10^{-2}
20	-6.75×10^{-2}
40	-5.54×10^{-2}
60	-4.64×10^{-2}
80	-3.97×10^{-2}
100	-3.46×10^{-2}
1000	-4.84×10^{-3}
1×10^4	-5.01×10^{-4}
1×10^5	-5.03×10^{-5}
1×10^6	-5.03×10^{-6}

is still an unknown and is dependent on the point on the base curve. Therefore, we address this question: " Given a Prandtl number and a point on the base curve, is it possible to predict the dominant mode for the decay of perturbations *a priori* ?"

To answer this question, first obtain the base solution curve of $\theta_{0_m} - \tau_{xz_0}$ based on the equation

$$\frac{\mathrm{d}^2\theta_0}{\mathrm{d}x^2} + f_0\tau_{xz_0}^2 = 0$$

Now, for any point on the curve, the scaled minimum viscosity of the fluid in the gap is given by $1/f_{0_m}$. Once this is determined, then the Prandtl number, which is based on the wall viscosity, is then modified by using the minimum scaled viscosity. We assert that the modified Prandtl number in fact determines what time scale dominates the decay of perturbations. If the modified Prandtl number is less than one, then we assert that the mechanical disturbances control the dynamics of the perturbations. On the other hand, if the modified Prandtl number is greater than one, then we assert that the thermal disturbances control the dynamics of the perturbations. This is simply based on the rationale that it is the lowest viscosity of the liquid in the gap that determines the diffusion time scale for the growth or decay of the mechanical disturbances.

To see whether our prediction is correct, let us go back to the table. Now, for $\tau_{xz_0} = 0.5$, $\mu_{0_{\min}}$ on the lower branch is 0.87 and on the upper branch is 0.017. From the table we find that along the lower branch the Prandtl number at which σ_1 starts to change noticeably indicating that the thermal effects are getting significant is 1.3. Correcting this Prandtl number by multiplying it with the minimum scaled viscosity, 0.87, we obtain 1.131. This is very closely equal to unity justifying our assertion that the switch over from mechanical to thermal occurs at a corrected Prandtl number of roughly one. Similarly, along the upper branch we find that the percentage change in the largest eigenvalue with respect to the percentage change in the Prandtl number gets significant around a Prandtl number of 40. Correcting this Prandtl number by multiplying it with the minimum scaled viscosity, 0.017, we obtain 0.68. This is again of the order of unity justifying our assertion. Therefore, based on this idea, it is possible to predict roughly for a given point on the base curve and for a given Prandtl number, whether the dominant mode for the decay of perturbations is mechanical or thermal.

Thus, using a simple procedure in which we modify the Prandtl number by multiplying it with the minimum viscosity, we may be able to decide for a given point on the curve whether the dominant mode for the decay of disturbances is thermal or mechanical. We will now return to our original task of finding out whether relaxing the restriction of a zero wave number disturbance will modify our stability results that we obtained. Before that, a set of endnotes on calculations that are related to the main theme of this chapter will be discussed.

5.1 Endnotes

5.1.1 The purely Thermal and Mechanical limit from a Scaling Argument

In the main body of this chapter, we claimed that the rate of growth or decay of disturbances were controlled by mechanical perturbations at low Prandtl number and by thermal perturbations at high Prandtl number. The numerical results that we obtained for the largest eigenvalue as a function of Prandtl number backed this assertion. We found that at low Prandtl numbers, the eigenvalues were almost invariant with respect to the Prandtl number and at high Prandtl number, the eigenvalues varied inversely with the Prandtl number. In this endnote, we will see whether we can obtain the purely thermal and mechanical limit as a function of Prandtl number just from a scaling argument. To do this, we write the perturbed equations at zero wave number:

$$\sigma \hat{v}_{z_1} = \frac{\mathrm{d}\hat{\tau}_{\mathrm{xz}_1}}{\mathrm{dx}}$$

$$\sigma Pr \hat{\theta}_1 = \frac{\mathrm{d}^2\hat{\theta}_1}{\mathrm{dx}^2} + {f_0}' \tau_{xz_0}^2 \hat{\theta}_1 + 2 f_0 \tau_{xz_0} \hat{\tau}_{xz_1}$$

We observe that in the limit of Pr → 0 and Pr → ∞, no conclusions can be drawn from these equations about whether the thermal disturbances dominate or the mechanical disturbances dominate. However, with the scaling that we discussed in the endnote of chapter 2, i.e., with $V_{\text{ref}} = \sqrt{C_v T_{\text{ref}}}$ and $T_{\text{ref}} = 1/S$, some conclusions can be drawn in the limit of Pr → 0 and Pr → ∞. To see this, we first write the equations of motion and the energy in the base state in the new scale to obtain

$$V_0 = \tau_{xz0} \int_{-1}^{1} f_0 \mathrm{d}x$$

$$0 = \frac{\mathrm{d}^2\theta_0}{\mathrm{d}x^2} + \mathrm{Pr}\tau_{xz0}^2 f_0$$

where $\tau_{xz_0} = \mu_0 \frac{\mathrm{d}v_{z0}}{\mathrm{d}x}$

Before we proceed to discuss the perturbed temperature equations in this scaling, we might be interested in knowing how a curve of wall speed vs. the wall stress curve behaves as a function of the Prandtl number in this scaling. We will pick the specific case of an exponential fluidity to answer this question.

In this scaling, changing the Prandtl number is tantamount to changing the thermal conductivity, k. As Pr → 0, i.e. $k \to \infty$, there should be no temperature variation in the gap. Hence, there should be no viscosity variation in the gap and consequently we should recover the curve for the constant viscosity problem. However, as the Prandtl number is increased, the maximum temperature in the gap gets higher. Hence, for a fixed wall speed, the wall stress must be lower as the Prandtl number is increased. A curve of the wall speed vs. the wall stress as a function of the Prandtl number therefore should look as shown in figure 5.1.

The perturbed equations at zero wave number in this scaling are

$$\frac{\rho\sigma_{\text{ref}}L^2}{\mu_{\text{ref}}}\sigma\hat{v}_{z_1} = \frac{\mathrm{d}\hat{\tau}_{xz_1}}{\mathrm{d}x} \tag{5.7}$$

$$\frac{\rho C_v \sigma_{\text{ref}} L^2}{k}\sigma\hat{\theta}_1 = \frac{\mathrm{d}^2\hat{\theta}_1}{\mathrm{d}x^2} + \mathrm{Pr}\tau_{xz0}^2 f_0' \hat{\theta}_1 + 2\mathrm{Pr} f_0 \tau_{xz_0}\hat{\tau}_{xz_1} \tag{5.8}$$

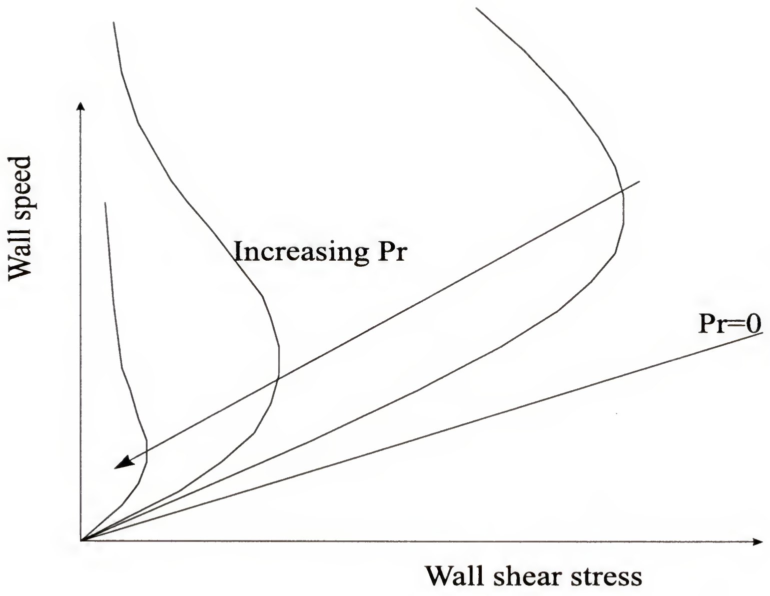

Figure 5.1: The wall speed vs. the wall stress curve as a function of the Prandtl number.

Now, to scale σ_{ref}, two options are available, one based on the viscous time scale and the second based on the thermal time scale.

If σ_{ref} is chosen such that $\sigma_{\text{ref}} = \frac{\mu_{\text{ref}}}{\rho L^2}$, then the equations become

$$\sigma \hat{v}_{z_1} = \frac{\mathrm{d}\hat{\tau}_{xz_1}}{\mathrm{d}x} \tag{5.9}$$

$$\sigma \mathrm{Pr} \hat{\theta}_1 = \frac{\mathrm{d}^2 \hat{\theta}_1}{\mathrm{d}x^2} + \mathrm{Pr} {f_0}' \tau_{xz_0}^2 \hat{\theta}_1 + 2\mathrm{Pr} f_0 \tau_{xz_0} \hat{\tau}_{xz_1} \tag{5.10}$$

On the other hand, if σ_{ref} is chosen based on the thermal diffusivity, i.e. $\sigma_{\text{ref}} = \frac{k}{\rho C_v L^2}$, then we obtain

$$\frac{\sigma}{\mathrm{Pr}} \hat{v}_{z_1} = \frac{\mathrm{d}\hat{\tau}_{xz_1}}{\mathrm{d}x} \tag{5.11}$$

$$\sigma \hat{\theta}_1 = \frac{\mathrm{d}^2 \hat{\theta}_1}{\mathrm{d}x^2} + 2\mathrm{Pr} f_0 \tau_{xz_0} \hat{\tau}_{xz_1} + \mathrm{Pr} f_0' \tau_{xz_0}^2 \hat{\theta}_1 \tag{5.12}$$

We will consider the two limiting cases, Pr → 0 and Pr → ∞.

The limit of Pr → 0 corresponds to the thermal conductivity $k \to \infty$. Therefore, we might imagine that the thermal perturbations die out instantaneously and hence only the mechanical disturbances are in control. Therefore, we will substitute Pr = 0 in the perturbed equations that are based on a viscous time scale. We then find that the temperature equation with $\hat{\theta}_1 = 0$ at the boundaries yields only the trivial solution and that the problem is therefore purely mechanical. Therefore the conclusion is that the equations scaled based on a viscous time scale provide the expected result in the limit of $Pr \to 0$.

The limit of $\mathrm{Pr} \to \infty$ corresponds to the thermal conductivity $k \to 0$ which suggests that the dominant mode of decay of perturbations is thermal. Therefore, we will put Pr=∞ in the equations arising out of the thermal time scale. We find from the equation of motion that as $\mathrm{Pr} \to \infty$, $\hat{\tau}_{xz_1}$ = constant. Further, if we assume constant wall stress conditions, then $\hat{\tau}_{xz_1} = 0$. The temperature equation then reduces to

$$\sigma\hat{\theta}_1 = \frac{\mathrm{d}^2\hat{\theta}_1}{\mathrm{d}x^2} + \mathrm{Pr} {f_0}' \tau_{xz_0}^2 \hat{\theta}_1 \tag{5.13}$$

which is identical to the equation that determines the thermal ignition problem. However, $\hat{v}_{z_1}$ is not equal to zero but related to the $\hat{\theta}_1$ by the relation

$$f_0 \frac{\mathrm{d}\hat{v}_{z_1}}{\mathrm{d}x} = {f_0}' \tau_{xz_0} \hat{\theta}_1$$

Therefore, we do not obtain the purely thermal problem in the limit of $\mathrm{Pr} \to \infty$ merely from a scaling argument even though the perturbed temperature equation looks identical to the equation for thermal ignition problem.

We can further calculate the derivative of the eigenvalues with respect to the Prandtl number in this scaling too and check to see whether we get results consistent with the results from our earlier scaling. Before we go on to do this, we will declare what we hold fixed in doing this calculation: it is the wall speed. The reason for this choice is that for a fixed wall speed, there is a wall stress corresponding to any Prandtl number one might choose. However, for a fixed wall stress, there is a range of Prandtl numbers over which there are no physically possible solutions of wall speed.

Therefore, fixing the wall speed turns out out to be the most logical thing to do in carrying out this calculation.

The equations in this scaling in operator form are

$$\begin{bmatrix} 0 & \frac{\mathrm{d}}{\mathrm{dx}} & 0 \\ -\frac{\mathrm{d}}{\mathrm{dx}} & f_0 & f_0{}' \tau_{xz0} \\ 0 & 2\mathrm{Pr} f_0 \tau_{xz0} & \frac{\mathrm{d}^2}{\mathrm{dx}^2} + \mathrm{Pr} f_0{}' \tau_{xz0}^2 \end{bmatrix} \begin{bmatrix} \hat{v}_{z1} \\ \hat{\tau}_{xz1} \\ \hat{\theta}_1 \end{bmatrix} = \sigma \begin{bmatrix} 1 & 0 & 0 \\ 0 & 0 & 0 \\ 0 & 0 & \mathrm{Pr} \end{bmatrix} \begin{bmatrix} \hat{v}_{z1} \\ \hat{\tau}_{xz1} \\ \hat{\theta}_1 \end{bmatrix} \quad (5.14)$$

The equations then can be cast in self-adjoint form by multiplying the first row by two and dividing the third row by the Prandtl number, Pr. The resulting equations in self-adjoint formulation are

$$\begin{bmatrix} 0 & 2\frac{\mathrm{d}}{\mathrm{dx}} & 0 \\ -2\frac{\mathrm{d}}{\mathrm{dx}} & 2f_0 & 2f_0{}' \tau_{xz0} \\ 0 & 2 f_0 \tau_{xz0} & \frac{1}{\mathrm{Pr}}\frac{\mathrm{d}^2}{\mathrm{dx}^2} + f_0{}' \tau_{xz0}^2 \end{bmatrix} \begin{bmatrix} \hat{v}_{z1} \\ \hat{\tau}_{xz1} \\ \hat{\theta}_1 \end{bmatrix} = \sigma \begin{bmatrix} 2 & 0 & 0 \\ 0 & 0 & 0 \\ 0 & 0 & 1 \end{bmatrix} \begin{bmatrix} \hat{v}_{z1} \\ \hat{\tau}_{xz1} \\ \hat{\theta}_1 \end{bmatrix} \quad (5.15)$$

Now, the above equations are of the form

$$\mathbf{Au} = \sigma\mathbf{Bu}$$

with σ being real as we have concluded that the operator $\mathbf{A}$ is self-adjoint. Now differentiating this equation with respect to the Prandtl number, we obtain,

$$\dot{\mathbf{A}}\mathbf{u} + \mathbf{A}\dot{\mathbf{u}} = \sigma\dot{\mathbf{B}}\mathbf{u} + \sigma\mathbf{B}\dot{\mathbf{u}} + \dot{\sigma}\mathbf{Bu}$$

where the $^{\cdot}$ represents differentiation with respect to the Prandtl number. As the operator $\mathbf{B}$ is independent of the Prandtl number, $\dot{\mathbf{B}} = 0$. Now, taking the inner product of the equation $\mathbf{Au} = \sigma\mathbf{Bu}$ with $\dot{\mathbf{u}}$ and then subtracting the result from the equation obtained by taking the inner product of the $\dot{\mathbf{A}}$ equation with $\mathbf{u}$, we obtain

$$< \mathbf{u}, \dot{\mathbf{A}}\mathbf{u} >= \dot{\sigma} < \mathbf{u}, \mathbf{Bu} >$$

from which

$$\dot{\sigma} = \frac{< \mathbf{u}, \mathbf{Au} >}{< \mathbf{u}, \mathbf{Bu} >}$$

$$\dot{\sigma} = \frac{2\int_{-1}^{1} \frac{\mathrm{d}}{\mathrm{dPr}} [f_0] \, |\hat{\tau}_{xz_1}|^2 \mathrm{d}x + 4\int_{-1}^{+1} \frac{\mathrm{d}}{\mathrm{dPr}} [f_0 \tau_{xz0}] \, \hat{\tau}_{xz_1} \hat{\theta}_1 \mathrm{d}x + \int_{-1}^{+1} \frac{\mathrm{d}}{\mathrm{dPr}} \left[f_0 {\tau_{xz0}}^2\right] |\hat{\theta}_1|^2 \mathrm{d}x}{\mathrm{Pr} \int_{-1}^{1} |\hat{\theta}_1|^2 \mathrm{d}x + 2\int_{-1}^{1} |\hat{v}_{z_1}|^2 \mathrm{d}x}$$

Now, recalling that an increase in Prandtl number in this scaling is tantamount to a decrease in the thermal conductivity, we can assert that the temperature in the gap increases with an increase in the Prandtl number, i.e., $\frac{\mathrm{d}}{\mathrm{dPr}} [f_0]$ is positive. Similarly, we can assert that an increase in Prandtl number makes the velocity gradients sharper and hence state that the quantity $\frac{\mathrm{d}}{\mathrm{dPr}} [f_0 \tau_{xz0}]$, where $f_0 \tau_{xz0} = \frac{dv_{z0}}{dx}$ is positive. And we may further assert that the viscous dissipation increases with an increase in the Prandtl number. With these assertions, we can predict the sign of $\dot{\sigma}$, if the sign of the integral $\int_{-1}^{1} \hat{\tau}_{xz_1} \hat{\theta}_1 \mathrm{d}x$ is known. Now, for a general case, it is not possible to predict the sign of $\int_{-1}^{1} \hat{\tau}_{xz_1} \hat{\theta}_1 \mathrm{d}x$. However, for the special case of constant wall stress and that too at the nose of the curve, wherein $\sigma = 0$ and $\hat{\tau}_{xz_1} = 0$, the integral $\int_{-1}^{1} \hat{\tau}_{xz_1} \hat{\theta}_1 \mathrm{d}x$ vanishes. Therefore $\dot{\sigma}$ is positive there. This result is another way of stating that the upper branch is unstable at constant stress. To see this, observe that in this scaling, for a fixed wall speed, a slight increase in Prandtl number causes the nose of a curve to shift to an upper branch of a neighbouring curve. As we have concluded that at a nose $\dot{\sigma}$ is positive, this then implies that the upper branch is unstable.

5.1.2 Rate of decay of Perturbations for various combinations of Boundary Conditions

In this endnote, we will consider Couette flow with a perfectly conducting bottom plate and an adiabatic top plate. With this combination of boundary conditions on temperature, we will compare the largest eigenvalue for the following cases:

- (a) Constant wall stress on the bottom plate and constant wall speed on the top plate.

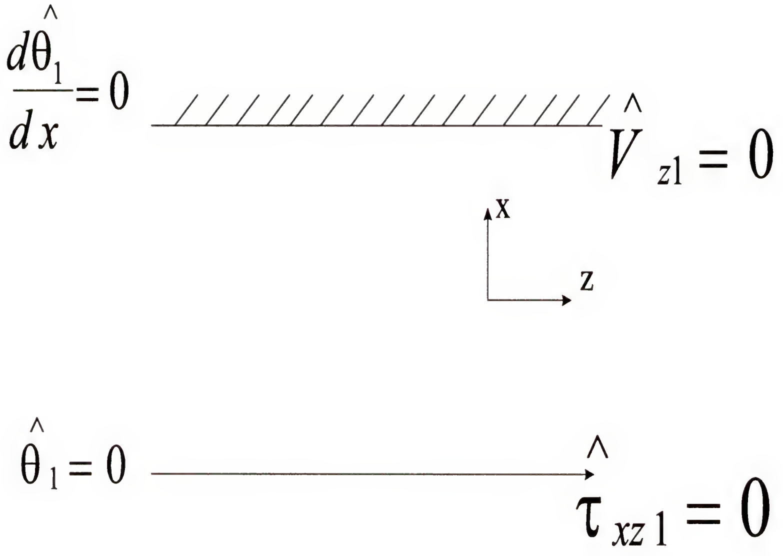

Figure 5.2: Schematic of plane Couette flow: Constant wall stress on the bottom plate and a constant wall speed on the top plate.

- (b) Constant wall speed on the bottom plate and constant wall stress on the top plate.

These two conditions are illustrated in figure 5.2 and figure 5.3

The base curve for both the cases are identical as the base state is determined purely by the temperature boundary conditions. Further, for both the cases considered, we know from the stability results in the last chapter that the lower branch is stable, the nose is a point of neutral stability and the upper branch is unstable. Therefore, the change in the boundary conditions between these two cases does not alter the stability results qualitatively. Only the actual magnitude of the eigenvalues are different between these two cases and we propose to explain this difference from a physical argument in this endnote.

Note that the perturbed shear stress $\hat{\tau}_{xz_1}$ is defined as

$$f_0 \hat{\tau}_{xz_1} = \frac{\mathrm{d}\hat{v}_{z_1}}{\mathrm{d}x} - f_0{}' \tau_{xz_0} \hat{\theta}_1$$

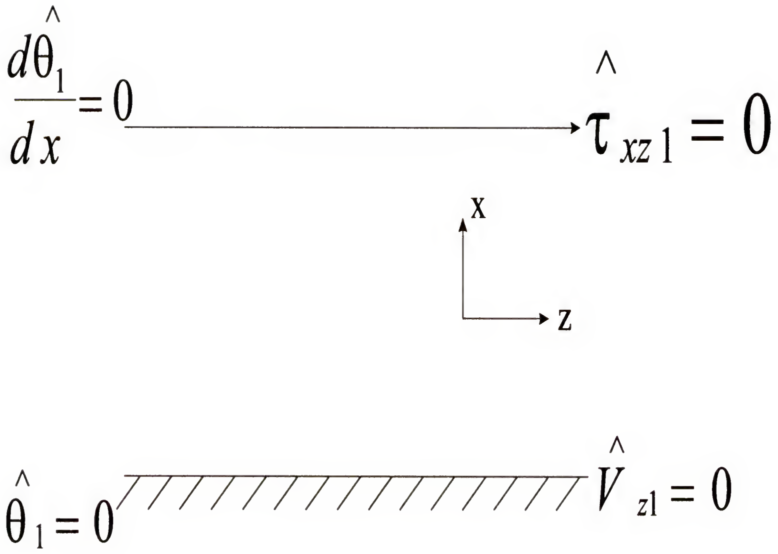

Figure 5.3: Schematic of plane Couette flow: Constant wall speed on the bottom plate and a constant wall stress on the top plate.

For a constant shear stress on a boundary, $\hat{\tau}_{xz_1}$ is zero on that boundary and hence the perturbed velocity and temperature on the plate are related by $\frac{\mathrm{d}\hat{v}_{z1}}{\mathrm{d}x} = {f_0}' \tau_{xz_0} \hat{\theta}_1$. We will use this result as we go along.

We will first present the numerical results that compare the largest eigenvalue for these two cases and then we will present an interpretation for the results obtained. Let us first consider a point on the lower branch of the base curve. This branch is stable for both the boundary conditions and the focus of our attention is therefore only to predict the difference in the rate of decay of perturbations. Table 5.1.2 shows the numerical values of the largest eigenvalue for various Prandtl numbers. Before we explain the results note that in case (a), a mechanical disturbance can leak only through the top plate. At the bottom plate $\hat{\tau}_{xz_1} = 0$ implies $\frac{\mathrm{d}\hat{v}_{z1}}{\mathrm{d}x} = 0$ as here $\hat{\theta}_1 = 0$. The bottom plate is therefore adiabatic to momentum in case (a). In case (b) however, $\hat{\tau}_{xz_1} = 0$ on the top plate does not imply $\frac{\mathrm{d}\hat{v}_{z1}}{\mathrm{d}x} = 0$ as there $\hat{\theta}_1$ is not zero.

Let us consider the limit of low Prandtl numbers first. At low values of the Prandtl number as we have concluded that the decay of disturbance is controlled by

Table 5.3: The largest eigenvalues as a function of the Prandtl number on the lower branch.

Pr	σ_1 for case (a)	σ_1 for case (b)
0.01	-1.78	-2.11
0.1	-1.75	-2.09
1.0	-1.36	-1.65
10.0	-2.19×10^{-1}	-2.21×10^{-1}
100.0	-2.25×10^{-2}	-2.23×10^{-2}
1000.0	-2.25×10^{-3}	-2.23×10^{-3}
1×10^4	-2.25×10^{-4}	-2.23×10^{-4}
1×10^5	-2.25×10^{-5}	-2.23×10^{-5}
1×10^7	-2.25×10^{-7}	-2.23×10^{-7}
1×10^9	-2.25×10^{-9}	-2.23×10^{-9}

the decay of mechanical disturbances, we can set $\hat{\theta}_1 = 0$ under the assumption that the temperature perturbations decay instantaneously. Therefore, we obtain $\frac{\mathrm{d}\hat{v}_{z1}}{\mathrm{d}x} = 0$ on the top plate for case (b). Thus, at low Prandtl numbers, we have in case (a), the bottom plate is adiabatic to momentum and in case (b), the top plate is adiabatic to momentum and the decay is controlled by the decay of mechanical disturbances. A perturbation in case (a) has to leak through the top plate wherein the temperature is the highest and hence the viscosity the lowest. Therefore, a perturbation in case (a) takes a longer time to decay as compared to a perturbation in case (b) and this is exactly what the table reports.

At high Prandtl numbers, the decay is dominated by the decay of thermal disturbances. As both the cases have identical boundary conditions on temperature perturbations, at high Prandtl numbers both the cases should have nearly the same rate of decay and the nearly same value for σ_1, the leading eigenvalue and this is what the table reports.

Next we will turn to comparing the decay of perturbations for the two cases along the upper branch. Table 5.4 reports the largest eigenvalue along the upper

Table 5.4: The largest eigenvalues as a function of the Prandtl number on the upper branch

Pr	σ_1 for case (a)	σ_1 for case (b)
0.01	3.63×10^{-2}	3.66×10^{-1}
0.1	3.63×10^{-2}	3.63×10^{-1}
1.0	3.61×10^{-2}	3.34×10^{-4}
10	3.34×10^{-1}	2.02×10^{-1}
1×10^{2}	2.08×10^{-2}	5.30×10^{-2}
1×10^{3}	5.21×10^{-3}	6.95×10^{-3}
1×10^{4}	6.42×10^{-4}	7.21×10^{-4}
1×10^{5}	6.58×10^{-5}	7.24×10^{-5}
1×10^{7}	6.60×10^{-7}	7.24×10^{-7}
1×10^{9}	6.60×10^{-9}	7.24×10^{-9}

branch. The largest eigenvalue is positive for both the cases indicating that perturbations grow along this branch. We will now explain the difference in the rate of growth along this branch.

First, consider the low Prandtl number limit. Even in this limit it is not correct to set $\hat{\theta}_1 = 0$ along the upper branch as perturbations grow along this branch. Therefore for case (b) along the upper branch at the top plate, $\frac{\mathrm{d}\hat{v}_{z1}}{\mathrm{d}x} = f_0' \tau_{xz0} \hat{\theta}_1 \neq 0$. Hence, $\frac{\mathrm{d}\hat{v}_{z1}}{\mathrm{d}x}$ can be positive or negative but not equal to zero even in the limit of $\mathrm{Pr} \to 0$. Taking $\hat{v}_{z_1}$ to be positive, if $\frac{\mathrm{d}\hat{v}_{z1}}{\mathrm{d}x} > 0$ on the top plate then it implies that a momentum perturbation is being fed from the boundaries and this case should be more unstable than case (a). On the other hand, when $\frac{\mathrm{d}\hat{v}_{z1}}{\mathrm{d}x} < 0$, then a perturbation is being consumed at the top plate and it should be more stable than case (a). The table shows that at low Prandtl number, case (b) is more unstable than case (a), i.e. perturbations grow faster in case (b) suggesting that a momentum perturbation might be fed from the boundaries in case (b). Numerical calculations for case (b) tell us that both $\hat{v}_{z_1}$ and $\frac{\mathrm{d}\hat{v}_{z1}}{\mathrm{d}x}$ are positive at the top plate implying that this is indeed true. Thus at low Prandtl number case (b) is more stable along the lower branch and more unstable along the upper branch.

At high Prandtl number, the decay is dominated by the decay of the thermal disturbances. As the perturbed temperature boundary conditions are the same in both the cases, they should show nearly the same growth rate and this is indeed what the numerical results show.

5.1.3 The Perturbed Equation in the Thermal Ignition problem

Recall that the base equation for the thermal ignition problem in a plane vessel is

$$0 = \frac{\mathrm{d}^2\theta_0}{\mathrm{d}x^2} + \delta^2 e^{\theta_0}$$

Now, the perturbed equation (scaled) for the ignition problem is

$$\sigma\hat{\theta}_1 = \frac{\mathrm{d}^2\hat{\theta}_1}{\mathrm{d}x^2} - \beta^2\hat{\theta}_1 - \gamma^2\hat{\theta}_1 + \delta^2 e^{\theta_0}\theta_1 \tag{5.16}$$

where σ is the scaled growth mode (scaled with respect to L^2/κ, where κ is the thermal diffusivity) and β, γ are the scaled wave numbers in the y, z directions respectively. It is obvious that the most dangerous disturbance is the disturbance of zero wave number, i.e. when $\beta, \gamma = 0$, as incorporating these wave numbers only facilitates the heat to be carried away by diffusion. The equation at a zero wave number disturbance is

$$\sigma\hat{\theta}_1 = \frac{\mathrm{d}^2\hat{\theta}_1}{\mathrm{d}x^2} + \delta^2 e^{\theta_0}\hat{\theta}_1 \tag{5.17}$$

It is possible to prove that the lower branch is stable to small perturbations and that the nose is a point of neutral stability using a similar approach to the one we undertook while performing the stability calculation at constant wall stress. It is also possible to prove that the upper branch is unstable at constant wall stress[3]. To do this, differentiate the base temperature equation of the ignition problem with respect to the maximum temperature θ_{0_m} to obtain

$$\frac{\mathrm{d}^2\dot{\theta}_0}{\mathrm{d}x^2} + \delta^2 e^{\theta_0}\dot{\theta}_0 = -\dot{\delta}^2 e^{\theta_0}$$

---

[3] This proof is due to Joseph[3]

where the $\dot{}$ represents differentiation with respect to θ_{0_m}. Now, multiplying this equation with respect to $\hat{\theta}_1$ and integrating the result over -1 to 1, we obtain

$$\int_{-1}^{1} \frac{\mathrm{d}^2\dot{\theta}_0}{\mathrm{d}x^2}\hat{\theta}_1 \mathrm{d}x + \int_{-1}^{1} \delta^2 e^{\theta_0}\dot{\theta}_0\hat{\theta}_1 \mathrm{d}x = -\int_{-1}^{1} \dot{\delta}^2 e^{\theta_0}\hat{\theta}_1 \mathrm{d}x$$

Similarly multiplying the $\hat{\theta}_1$ equation with $\dot{\theta}_0$ and integrating it over -1 to 1, we obtain

$$\int_{-1}^{1} \sigma\hat{\theta}_1\dot{\theta}_0 \mathrm{d}x = \int_{-1}^{1} \frac{\mathrm{d}^2\hat{\theta}_1}{\mathrm{d}x^2}\dot{\theta}_0 \mathrm{d}x + \int_{-1}^{1} \delta^2 e^{\theta_0}\hat{\theta}_1\dot{\theta}_0 \mathrm{d}x$$

Subtracting the above two equations, we obtain,

$$\frac{\sigma}{\dot{\delta}^2} = -\frac{\int_{-1}^{1} e^{\theta_0}\hat{\theta}_1 \mathrm{d}x}{\int_{-1}^{1} \hat{\theta}_1\dot{\theta}_0 \mathrm{d}x}$$

From this equation, we can conclude that σ is positive on the upper branch as $\dot{\delta}^2$ is negative on the upper branch and all the quantities in this equation are singly signed.

5.1.4 Comparison of the Perturbed Temperature Equations: Ignition vs. Couette

In chapter 2, we compared the base temperature equation in the Couette flow to the base equation in the ignition problem. Similarly the perturbed equation in the ignition problem can be compared with the perturbed temperature equation in the Couette flow problem. For an exponential fluidity dependence, the perturbed temperature equation is

$$\sigma \mathrm{Pr}\hat{\theta}_1 = \frac{\mathrm{d}^2\hat{\theta}_1}{\mathrm{d}x^2} + \tau_{xz0}^2 \mathrm{e}^{\theta_0}\hat{\theta}_1 + 2e^{\theta_0}\tau_{xz0}\hat{\tau}_{xz_1} \tag{5.18}$$

Now, comparing this equation with the perturbed equation in the thermal ignition problem, we find that there is an additional parameter, the Prandtl number and an additional variable, the perturbed shear stress, $\hat{\tau}_{xz_1}$ in this equation. For the case of constant wall stress, at the nose of the curve, wherein $\sigma = 0$ and hence $\hat{\tau}_{xz_1} = 0$, this equation looks identical to the perturbed temperature equation for the ignition problem. Everywhere else along the base curve, even though the stability behavior of the two problems match qualitatively, with the lower branch being stable and the upper branch being unstable, the actual dynamics of the Couette flow problem is different from the dynamics of the ignition problem. However, Joseph, in his paper, assumed that the perturbed temperature equation in the ignition problem is a model for the Couette flow problem *everywhere* along the base curve. And based on the perturbed temperature equation in the Ignition problem, he concluded that in Couette flow too, the nose is a neutral point and the upper branch is unstable. There are two important points to be made clear about Joseph's stability calculations and results: (i) Joseph's stability result at constant wall stress is qualitatively correct, even though it is based on an approximation to the actual model. (ii) Joseph never studied the stability at constant wall speed. The entire base curve is stable at constant wall speed. In this case, even at the nose, the perturbed temperature equation in Couette flow problem does not look identical to the perturbed temperature equation in the thermal ignition problem. Therefore, even that connection to the thermal ignition problem is lost when the boundary condition is changed from constant wall stress to constant wall speed.

CHAPTER 6
THE STABILITY FOR NON-ZERO WAVE NUMBER DISTURBANCES

In this chapter, we will discuss the stability of Couette flow to non-zero wave number disturbances. The reason for doing this is to check whether the stability results that we obtained for a zero wave number disturbance are altered when that restriction is relaxed. But, before we proceed to discuss the non-zero wave number equations and their stability in detail, let us make a few observations about how the structure of the perturbed equations get modified when the restriction of a zero wave number disturbance is relaxed.

- For a disturbance of zero wave number, all the terms arising out of the perturbation of $\mathbf{v}.\nabla\mathbf{v}$ turn out be equal to zero. Hence there is no possibility of an inertial instability. However, for a general class of disturbance which we will discuss in this chapter, the terms arising from the perturbation of $\mathbf{v}.\nabla\mathbf{v}$ do not vanish and could therefore, contribute to an inertial instability.

- For a perturbation of zero wave number, the perturbed velocity $\hat{v}_{x_1}$ is zero and $\hat{v}_{y_1}$ does not enter the problem at all. Hence, the only possibility for a new flow to emerge is again in the same direction as that of the base flow, i.e. in the z direction. However, for a non-zero wave number disturbance, $\hat{v}_{x_1}, \hat{v}_{y_1} \neq 0$ and we might therefore have flows emerging in the x, y directions.

- At zero wave number all the terms that facilitate the diffusion in the axial(z) and in the neutral (y) direction are zero. By admitting a non-zero wave number disturbance, we incorporate these effects which are stabilizing. Therefore, we have added on the one hand the convective terms which could produce instability and on the other hand, the diffusion terms which are stabilizing and consequently the stability of the flow is determined by whether the diffusion terms dominate or whether the convective terms dominate.

Now, substituting

$$\begin{aligned} v_{x_1} &= \hat{v}_{x_1} \mathrm{e}^{\sigma t} \mathrm{e}^{i\gamma z} \mathrm{e}^{i\beta y} \\ v_{y_1} &= \hat{v}_{y_1} \mathrm{e}^{\sigma t} \mathrm{e}^{i\gamma z} \mathrm{e}^{i\beta y} \\ v_{z_1} &= \hat{v}_{z_1} \mathrm{e}^{\sigma t} \mathrm{e}^{i\gamma z} \mathrm{e}^{i\beta y} \\ T_1 &= \hat{T}_1 \mathrm{e}^{\sigma t} \mathrm{e}^{i\gamma z} \mathrm{e}^{i\beta y} \end{aligned} \tag{6.1}$$

and $\mu_1 = \dfrac{\mathrm{d}\mu_0}{\mathrm{d}T_0} T_1$ where β is the wave number in the y direction and γ is the wave number in the z direction, into the perturbed equations of continuity, motion and energy, viz.

$$\nabla . \mathbf{v}_1 = 0 \tag{6.2}$$

$$\begin{aligned} \rho \frac{\partial \mathbf{v_1}}{\partial t} + \rho \mathbf{v_1} . \nabla \mathbf{v_0} + \rho \mathbf{v_0} . \nabla \mathbf{v_1} = & -\nabla p_1 + 2\nabla \mu_0 . D_1 + 2{\mu_0}' \nabla T_1 . D_0 \\ & + 2{\mu_0}'' T_1 \nabla T_0 . D_0 + \mu_0 \nabla^2 \mathbf{v_1} + {\mu_0}' T_1 \nabla^2 \mathbf{v_0} \end{aligned} \tag{6.3}$$

$$\rho C_v \frac{\partial T_1}{\partial t} + \rho C_v \mathbf{v_1} . \nabla T_0 + \rho C_v \mathbf{v_0} . \nabla T_1 = k \nabla^2 T_1 + 4\mu_0 D_0 : D_1 + 2{\mu_0}' T_1 D_0 : D_0 \tag{6.4}$$

where ${\mu_0}' = \mathrm{d}\mu(T_0)/T_0$, we obtain from the equation of continuity

$$\frac{\mathrm{d}\hat{v}_{x_1}}{\mathrm{d}x} + i\beta \hat{v}_{y_1} + i\gamma \hat{v}_{z_1} = 0 \tag{6.5}$$

and from the equations of motion

$$\begin{aligned} \rho \left(\sigma \hat{v}_{x_1} + i\gamma v_{z_0} \hat{v}_{x_1} \right) = & -\frac{\mathrm{d}\hat{p}_1}{\mathrm{d}x} + 2 \frac{\mathrm{d}\mu_0}{\mathrm{d}x} \frac{\mathrm{d}\hat{v}_{x_1}}{\mathrm{d}x} + i\gamma \left(\frac{\mathrm{d}\mu_0}{\mathrm{d}T_0} \right) \hat{T}_1 \frac{\mathrm{d}v_{z_0}}{\mathrm{d}x} \\ & + \mu_0 \left[\frac{\mathrm{d}^2 \hat{v}_{x_1}}{\mathrm{d}x^2} - \beta^2 \hat{v}_{x_1} - \gamma^2 \hat{v}_{x_1} \right] \end{aligned} \tag{6.6}$$

$$\begin{aligned}\rho\left(\sigma\hat{v}_{y_1}+i\gamma v_{z_0}\hat{v}_{y1}\right) &= -i\beta\hat{p}_1+\frac{\mathrm{d}\mu_0}{\mathrm{d}x}\left[\frac{\mathrm{d}\hat{v}_{y1}}{\mathrm{d}x}+i\beta v_{x_1}\right]\\ &\quad+\mu_0\left[\frac{\mathrm{d}^2\hat{v}_{y_1}}{\mathrm{d}x^2}-\beta^2\hat{v}_{y_1}-\gamma^2\hat{v}_{y_1}\right] \qquad (6.7)\end{aligned}$$

$$\begin{aligned}\rho\left(\sigma\hat{v}_{z_1}+i\gamma v_{z_0}\hat{v}_{z_1}+\frac{\mathrm{d}v_{z_0}}{\mathrm{d}x}\hat{v}_{x_1}\right) &= -i\gamma\hat{p}_1+\frac{\mathrm{d}\mu_0}{\mathrm{d}x}\left[\frac{\mathrm{d}\hat{v}_{z_1}}{\mathrm{d}x}+i\gamma v_{x_1}\right]+\frac{\mathrm{d}}{\mathrm{d}x}\left[\left(\frac{\mathrm{d}\mu_0}{\mathrm{d}T_0}\right)\hat{T}_1\frac{\mathrm{d}v_{z_0}}{\mathrm{d}x}\right]\\ &\quad+\mu_0\left[\frac{\mathrm{d}^2\hat{v}_{z_1}}{\mathrm{d}x^2}-\beta^2\hat{v}_{z_1}-\gamma^2\hat{v}_{z_1}\right] \qquad (6.8)\end{aligned}$$

and from the energy equation

$$\begin{aligned}\rho C_v\left[\sigma\hat{T}_1+\hat{v}_{x_1}\frac{\mathrm{d}T_0}{\mathrm{d}x}+i\gamma v_{z_0}\hat{T}_1\right] &= k\left[\frac{\mathrm{d}^2\hat{T}_1}{\mathrm{d}x^2}-\beta^2\hat{T}_1-\gamma^2\hat{T}_1\right]\\ &\quad+2\mu_0\frac{\mathrm{d}v_{z_0}}{\mathrm{d}x}\left[\frac{\mathrm{d}\hat{v}_{z_1}}{\mathrm{d}x}+i\gamma\hat{v}_{x_1}\right]+\frac{\mathrm{d}\mu_0}{\mathrm{d}T_0}\hat{T}_1\left[\frac{\mathrm{d}v_{z_0}}{\mathrm{d}x}\right]^2 \qquad (6.9)\end{aligned}$$

Now, to scale these equations, we introduce the following variables:

$$x^*=x/L,$$

$$\sigma^*=\sigma/\sigma_{\mathrm{ref}},$$

$$\hat{v}^*_{x_1}=\hat{v}_{x_1}/V_{\mathrm{ref}},$$

$$\hat{v}^*_{y_1}=\hat{v}_{y_1}/V_{\mathrm{ref}},$$

$$\hat{v}^*_{z_1}=\hat{v}_{z_1}/V_{\mathrm{ref}},$$

$$\hat{\theta}^*_1=\hat{T}_1/T_{\mathrm{ref}},$$

$${\mu_0}^*=\mu_0/\mu_{\mathrm{ref}},$$

to get

$$\frac{\mathrm{d}\hat{v}^*_{x_1}}{\mathrm{d}x}+i(\beta L)\hat{v}^*_{y_1}+i(\gamma L)v^*_{z_1}=0 \qquad (6.10)$$

$$\begin{aligned}&\rho\left(\sigma_{\mathrm{ref}}V_{\mathrm{ref}}\sigma^*\hat{v}^*_{x_1}+i\gamma V^2_{\mathrm{ref}}v^*_{z_0}\hat{v}^*_{x_1}\right)=-\frac{P_{\mathrm{ref}}}{L}\frac{\mathrm{d}\hat{p}^*_1}{\mathrm{d}x^*}+2K_v\frac{\mathrm{d}\mu^*_0}{\mathrm{d}x^*}\frac{\mathrm{d}\hat{v}^*_{x_1}}{\mathrm{d}x^*}\\ &+i(\gamma L)K_v\left(\frac{\mathrm{d}\mu^*_0}{\mathrm{d}\theta^*_0}\right)\hat{\theta}^*_1\frac{\mathrm{d}v^*_{z_0}}{\mathrm{d}x^*}+K_v\mu^*_0\left[\frac{\mathrm{d}^2\hat{v}^*_{x_1}}{\mathrm{d}{x^*}^2}-(\beta L)^2\,\hat{v}^*_{x_1}-(\gamma L)^2\,\hat{v}^*_{x_1}\right] \qquad (6.11)\end{aligned}$$

$$\begin{aligned}\rho\left(\sigma_{\text{ref}}V_{\text{ref}}\sigma^*\hat{v}^*_{y_1} + i\gamma V^2_{\text{ref}}v^*_{z_0}\hat{v}^*_{y_1}\right) &= -i\beta P_{\text{ref}}\hat{p}^*_1 + K_v\frac{\mathrm{d}\mu^*_0}{\mathrm{d}x^*}\left[\frac{\mathrm{d}\hat{v}^*_{y_1}}{\mathrm{d}x^*} + i\left(\beta L\right)v^*_{x_1}\right] \\ &\quad + K_v\mu^*_0\left[\frac{\mathrm{d}^2}{\mathrm{d}x^{*2}} - \left(\beta L\right)^2 - \left(\gamma L\right)^2\right]\hat{v}^*_{y_1} \qquad (6.12)\end{aligned}$$

$$\begin{aligned}\rho\left(\sigma_{\text{ref}}V_{\text{ref}}\sigma^*\hat{v}^*_{z_1} + i\gamma V^2_{\text{ref}}v^*_{z_0}\hat{v}^*_{z_1} + V_{\text{ref}}L\frac{\mathrm{d}v^*_{z_0}}{\mathrm{d}x^*}\hat{v}^*_{x_1}\right) &= -i\gamma P_{\text{ref}}\hat{p}^*_1 \\ + K_v\frac{\mathrm{d}\mu^*_0}{\mathrm{d}x^*}\left[\frac{\mathrm{d}\hat{v}^*_{z_1}}{\mathrm{d}x^*} + i\left(\gamma L\right)v^*_{x_1}\right] + K_v\frac{\mathrm{d}}{\mathrm{d}x^*}\left[\left(\frac{\mathrm{d}\mu^*_0}{\mathrm{d}\theta^*_0}\right)\hat{\theta}^*_1\frac{\mathrm{d}v^*_{z_0}}{\mathrm{d}x^*}\right] \\ + K_v\mu^*_0\left[\frac{\mathrm{d}^2}{\mathrm{d}x^{*2}} - \left(\beta L\right)^2 - \left(\gamma L\right)^2\right]\hat{v}^*_{z_1} \qquad (6.13)\end{aligned}$$

$$\begin{aligned}\rho C_v\left[\sigma_{\text{ref}}T_{\text{ref}}\sigma^*\hat{\theta}^*_1 + V_{\text{ref}}T_{\text{ref}}L\hat{v}^*_{x_1}\frac{\mathrm{d}\theta^*_0}{\mathrm{d}x^*} + iV_{\text{ref}}T_{\text{ref}}\gamma v^*_{z_0}\hat{\theta}^*_1\right] &= K_T\frac{\mathrm{d}^2\hat{\theta}^*_1}{\mathrm{d}x^{*2}} \\ + K_T\left\{-(\beta L)^2\hat{\theta}^*_1 - (\gamma L)^2\hat{\theta}^*_1\right\} + 2K_v\mu^*_0\frac{\mathrm{d}v^*_{z_0}}{\mathrm{d}x^*}\left[\frac{\mathrm{d}\hat{v}^*_{z_1}}{\mathrm{d}x^*} + i(\gamma L)\hat{v}^*_{x_1}\right] + K_v\frac{\mathrm{d}\mu^*_0}{\mathrm{d}\theta^*_0}\hat{\theta}_1\left[\frac{\mathrm{d}v^*_{z_0}}{\mathrm{d}x^*}\right]^2 \qquad (6.14)\end{aligned}$$

where $K_v = \dfrac{\mu_{\text{ref}}V_{\text{ref}}}{L^2}$ and $K_T = \dfrac{kT_{\text{ref}}}{L^2}$ are the scaling constants. Now, dividing the equations of motion by $\dfrac{\mu_{\text{ref}}V_{\text{ref}}}{L^2}$ and the energy equation by $\dfrac{\mathrm{k}T_{\text{ref}}}{L^2}$ and choosing $P_{\text{ref}} = \dfrac{\mu_{\text{ref}}V_{\text{ref}}}{L}$, $\sigma_{\text{ref}} = \mu_{\text{ref}}/\rho L^2$ and further employing the choice of V_{ref}, T_{ref} based on the scales used in the base state, i.e., using the scaling $\mu_{\text{ref}} = \mu_w$, $T_{\text{ref}} = 1/S$ and $V_{\text{ref}} = \sqrt{(k/S\mu_w)}$, the equations become

$$\frac{\mathrm{d}\hat{v}^*_{x_1}}{\mathrm{d}x} + i(\beta L)\hat{v}^*_{y_1} + i(\gamma L)v^*_{z_1} = 0 \qquad (6.15)$$

$$\begin{aligned}\sigma^*\hat{v}^*_{x_1} + i(\gamma L)\mathrm{Re}v^*_{z_0}\hat{v}^*_{x_1} &= -\frac{\mathrm{d}\hat{p}^*_1}{\mathrm{d}x^*} + 2\frac{\mathrm{d}\mu^*_0}{\mathrm{d}x^*}\frac{\mathrm{d}\hat{v}^*_{x_1}}{\mathrm{d}x^*} + i(\gamma L)\left(\frac{\mathrm{d}\mu^*_0}{\mathrm{d}\theta^*_0}\right)\hat{\theta}^*_1\frac{\mathrm{d}v^*_{z_0}}{\mathrm{d}x^*} \\ &\quad + \mu^*_0\left[\frac{\mathrm{d}^2\hat{v}^*_{x_1}}{\mathrm{d}x^{*2}} - (\beta L)^2\hat{v}^*_{x_1} - (\gamma L)^2\hat{v}^*_{x_1}\right] \qquad (6.16)\end{aligned}$$

$$\begin{aligned}\sigma^*\hat{v}^*_{y_1} + i(\gamma L)\mathrm{Re}v^*_{z_0}\hat{v}^*_{y_1} &= -i\beta\hat{p}^*_1 + \frac{\mathrm{d}\mu^*_0}{\mathrm{d}x^*}\left[\frac{\mathrm{d}\hat{v}^*_{y_1}}{\mathrm{d}x^*} + i\left(\beta L\right)v^*_{x_1}\right] \\ &\quad + \mu^*_0\left[\frac{\mathrm{d}^2\hat{v}^*_{y_1}}{\mathrm{d}x^{*2}} - \left(\beta L\right)^2\hat{v}^*_{y_1} - \left(\gamma L\right)^2\hat{v}^*_{y_1}\right]\end{aligned}$$

$$\begin{aligned}\sigma^*\hat{v}^*_{z_1} + i(\gamma L)\mathrm{Re}v^*_{z_0}\hat{v}^*_{z_1} + \mathrm{Re}\frac{\mathrm{d}v^*_{z_0}}{\mathrm{d}x^*}\hat{v}^*_{x_1} &= -i\gamma\hat{p}^*_1 + \frac{\mathrm{d}\mu^*_0}{\mathrm{d}x^*}\left[\frac{\mathrm{d}\hat{v}^*_{z_1}}{\mathrm{d}x^*} + i\left(\gamma L\right)v^*_{x_1}\right] \\ + \frac{\mathrm{d}}{\mathrm{d}x^*}\left[\left(\frac{\mathrm{d}\mu^*_0}{\mathrm{d}\theta^*_0}\right)\hat{\theta}^*_1\frac{\mathrm{d}v^*_{z_0}}{\mathrm{d}x^*}\right] + \mu^*_0\left[\frac{\mathrm{d}^2\hat{v}^*_{z_1}}{\mathrm{d}x^{*2}} - (\beta L)^2\hat{v}^*_{z_1} - (\gamma L)^2\hat{v}^*_{z_1}\right] \qquad (6.17)\end{aligned}$$

$$\sigma^*\mathrm{Pr}\hat{\theta}_1^* + \mathrm{RePr}\hat{v}_{x_1}^*\frac{\mathrm{d}\theta_0^*}{\mathrm{d}x^*} + i(\gamma L)\mathrm{RePr}v_{z_0}^*\hat{\theta}_1^* = \left[\frac{\mathrm{d}^2\hat{\theta}_1^*}{\mathrm{d}x^{*2}} - (\beta L)^2\hat{\theta}_1^* - (\gamma L)^2\hat{\theta}_1^*\right]$$
$$+\frac{\mathrm{d}\mu_0^*}{\mathrm{d}\theta_0^*}\hat{\theta}_1^*\left[\frac{\mathrm{d}v_{z_0}^*}{\mathrm{d}x^*}\right]^2 + 2\mu_0^*\frac{\mathrm{d}v_{z_0}^*}{\mathrm{d}x^*}\left[\frac{\mathrm{d}\hat{v}_{z_1}^*}{\mathrm{d}x^*} + i(\gamma L)\hat{v}_{x_1}^*\right] \quad (6.18)$$

Introducing $\tau_{xz_0}^* = \mu_0^*\frac{\mathrm{d}v_{z_0}^*}{\mathrm{d}x^*}$ and rewriting $\gamma L = \gamma$ and $\beta L = \beta$, we obtain

$$\frac{\mathrm{d}\hat{v}_{x_1}^*}{\mathrm{d}x} + i\beta\hat{v}_{y_1}^* + i\gamma v_{z_1}^* = 0 \quad (6.19)$$

$$\begin{aligned}\sigma^*\hat{v}_{x_1}^* + i\gamma\mathrm{Re}v_{z_0}^*\hat{v}_{x_1}^* &= -\frac{\mathrm{d}\hat{p}_1^*}{\mathrm{d}x^*} + 2\frac{\mathrm{d}\mu_0^*}{\mathrm{d}x^*}\frac{\mathrm{d}\hat{v}_{x_1}^*}{\mathrm{d}x^*} + i\gamma\tau_{xz_0}^*\left(\frac{\frac{\mathrm{d}\mu_0^*}{\mathrm{d}\theta_0^*}}{\mu_0^*}\right)\hat{\theta}_1^* \\ &\quad +\mu_0^*\left[\frac{\mathrm{d}^2\hat{v}_{x_1}^*}{\mathrm{d}x^{*2}} - \beta^2\hat{v}_{x_1}^* - \gamma^2\hat{v}_{x_1}^*\right] \end{aligned} \quad (6.20)$$

$$\begin{aligned}\sigma^*\hat{v}_{y_1}^* + i\gamma\mathrm{Re}v_{z_0}^*\hat{v}_{y_1}^* &= -i\beta\hat{p}_1^* + \frac{\mathrm{d}\mu_0^*}{\mathrm{d}x^*}\left[\frac{\mathrm{d}\hat{v}_{y_1}^*}{\mathrm{d}x^*} + i\beta v_{x_1}^*\right] \\ &\quad +\mu_0^*\left[\frac{\mathrm{d}^2\hat{v}_{y_1}^*}{\mathrm{d}x^{*2}} - \beta^2\hat{v}_{y_1}^* - \gamma^2\hat{v}_{y_1}^*\right] \end{aligned} \quad (6.21)$$

$$\sigma^*\hat{v}_{z_1}^* + i\gamma\mathrm{Re}v_{z_0}^*\hat{v}_{z_1}^* + \mathrm{Re}\frac{\mathrm{d}v_{z_0}^*}{\mathrm{d}x^*}\hat{v}_{x_1}^* = -i\gamma\hat{p}_1^* + \frac{\mathrm{d}\mu_0^*}{\mathrm{d}x^*}\left[\frac{\mathrm{d}\hat{v}_{z_1}^*}{\mathrm{d}x^*} + i\gamma v_{x_1}^*\right]$$
$$+\tau_{xz_0}^*\frac{\mathrm{d}}{\mathrm{d}x^*}\left[\left(\frac{\frac{\mathrm{d}\mu_0^*}{\mathrm{d}\theta_0^*}}{\mu_0^*}\right)\hat{T}_1^*\right] + \mu_0^*\left[\frac{\mathrm{d}^2\hat{v}_{z_1}^*}{\mathrm{d}x^{*2}} - \beta^2\hat{v}_{z_1}^* - \gamma^2\hat{v}_{z_1}^*\right] \quad (6.22)$$

$$\sigma^*\mathrm{Pr}\hat{\theta}_1^* + \mathrm{RePr}\hat{v}_{x_1}^*\frac{\mathrm{d}\theta_0^*}{\mathrm{d}x^*} + i\gamma\mathrm{RePr}v_{z_0}^*\hat{\theta}_1^* = \left[\frac{\mathrm{d}^2\hat{\theta}_1^*}{\mathrm{d}x^{*2}} - \beta^2\hat{\theta}_1^* - \gamma^2\hat{\theta}_1^*\right]$$
$$+\tau_{xz_0}^{*2}\frac{\frac{\mathrm{d}\mu_0^*}{\mathrm{d}\theta_0^*}}{\mu_0^{*2}}\hat{\theta}_1^* + 2\tau_{xz_0}^*\left[\frac{\mathrm{d}\hat{v}_{z_1}^*}{\mathrm{d}x^*} + i\gamma\hat{v}_{x_1}^*\right] \quad (6.23)$$

Now, to inquire about the stability of these equations for any given point on the base curve, we have to calculate the eigenvalues σ for an input Re, Pr, γ, β. If the real part of σ is negative, then the flow is stable to small perturbations for this combination of parameter values. On the other hand, if the real part of σ is positive, then the flow is unstable.

For constant viscosity plane Couette flow, Squire's transformation, which translates the three dimensional problem into an equivalent two dimensional problem, is possible. Using this transformation it can be demonstrated that for the case of isoviscous plane Couette flow two dimensional disturbances are the most dangerous. Therefore an argument can be made to prove that it is indeed sufficient to look at the stability of the flow for two dimensional disturbances. However for Couette flow with viscous dissipaton and a temperature-dependent viscosity, we are unable to get a Squires's transformation. This implies that we have to look at the stability of the complete three dimensional problem. But this is not what we propose to do. Instead, we assert that even in this case, the 2D disturbances are the most dangerous and hence we look into the two dimensional problem in x and z setting $\hat{v}_{y_1} = 0$ and $\beta = 0$. With this simplification, the perturbed equations after dropping the $*$ look as follows

$$\frac{\mathrm{d}\hat{v}_{x_1}}{\mathrm{d}x} + i\gamma\hat{v}_{z_1} = 0 \tag{6.24}$$

$$\begin{aligned} \sigma\hat{v}_{x_1} + i\gamma\mathrm{Re}v_{z_0}\hat{v}_{x_1} &= -\frac{\mathrm{d}\hat{p}_1}{\mathrm{d}x} + 2\frac{\mathrm{d}\mu_0}{\mathrm{d}x}\frac{\mathrm{d}\hat{v}_{x_1}}{\mathrm{d}x} + i\gamma\tau_{xz0}\left(\frac{\frac{\mathrm{d}\mu_0}{\mathrm{d}\theta_0}}{\mu_0}\right)\hat{\theta}_1 \\ &+\mu_0\left[\frac{\mathrm{d}^2\hat{v}_{x_1}}{\mathrm{d}x^2} - \gamma^2\hat{v}_{x_1}\right] \end{aligned} \tag{6.25}$$

$$\begin{aligned} \sigma\hat{v}_{z_1} + i\gamma\mathrm{Re}v_{z_0}\hat{v}_{z_1} + \mathrm{Re}\frac{\mathrm{d}v_{z_0}}{\mathrm{d}x}\hat{v}_{x_1} &= -i\gamma\hat{p}_1 + \frac{\mathrm{d}\mu_0}{\mathrm{d}x}\left[\frac{\mathrm{d}\hat{v}_{z_1}}{\mathrm{d}x} + i\gamma v_{x_1}\right] \\ &+\tau_{xz0}\frac{\mathrm{d}}{\mathrm{d}x}\left[\left(\frac{\frac{\mathrm{d}\mu_0}{\mathrm{d}\theta_0}}{\mu_0}\right)\hat{\theta}_1\right] + \mu_0\left[\frac{\mathrm{d}^2\hat{v}_{z_1}}{\mathrm{d}x^2} - \gamma^2\hat{v}_{z_1}\right] \end{aligned} \tag{6.26}$$

$$\begin{aligned} \sigma\mathrm{Pr}\hat{\theta}_1 + \mathrm{RePr}\hat{v}_{x_1}\frac{\mathrm{d}\theta_0}{\mathrm{d}x} + i\mathrm{RePr}\gamma v_{z_0}\hat{\theta}_1 &= \frac{\mathrm{d}^2\hat{\theta}_1}{\mathrm{d}x^2} - \gamma^2\hat{\theta}_1 + \tau_{xz0}^2\frac{\frac{\mathrm{d}\mu_0}{\mathrm{d}\theta_0}}{\mu_0^2}\hat{\theta}_1 \\ &+2\tau_{xz0}\left[\frac{\mathrm{d}\hat{v}_{z_1}}{\mathrm{d}x} + i\gamma\hat{v}_{x_1}\right] \end{aligned} \tag{6.27}$$

where γL has been redefined as γ. Hence forth, we will be interested only in exponential fluidity as the experiments in this study were performed for liquids with an exponential dependence of fluidity on temperature. Substituting $\mu_0 = \mathrm{e}^{-\theta_0} = -\frac{\mathrm{d}\mu_0}{\mathrm{d}\theta_0}$ in the above equations, we obtain

$$\frac{\mathrm{d}\hat{v}_{x1}}{\mathrm{d}x} + i\gamma\hat{v}_{z_1} = 0 \tag{6.28}$$

$$\begin{aligned}\sigma\hat{v}_{x_1} + i\gamma\mathrm{Re}v_{z_0}\hat{v}_{x_1} &= -\frac{\mathrm{d}\hat{p}_1}{\mathrm{d}x} + 2\frac{\mathrm{d}\mu_0}{\mathrm{d}x}\frac{\mathrm{d}\hat{v}_{x_1}}{\mathrm{d}x} - i\gamma\tau_{xz_0}\hat{\theta}_1 \\ &\quad + \mu_0\left[\frac{\mathrm{d}^2\hat{v}_{x_1}}{\mathrm{d}x^2} - \gamma^2\hat{v}_{x_1}\right]\end{aligned} \tag{6.29}$$

$$\begin{aligned}\sigma\hat{v}_{z_1} + i\gamma\mathrm{Re}v_{z_0}\hat{v}_{z_1} + \mathrm{Re}\frac{\mathrm{d}v_{z0}}{\mathrm{d}x}\hat{v}_{x_1} &= -i\gamma\hat{p}_1 + \frac{\mathrm{d}\mu_0}{\mathrm{d}x}\left[\frac{\mathrm{d}\hat{v}_{z_1}}{\mathrm{d}x} + i\gamma v_{x_1}\right] \\ &\quad -\tau_{xz_0}\hat{\theta}_1 + \mu_0\left[\frac{\mathrm{d}^2\hat{v}_{z_1}}{\mathrm{d}x^2} - \gamma^2\hat{v}_{z_1}\right]\end{aligned} \tag{6.30}$$

$$\begin{aligned}\sigma\mathrm{Pr}\hat{\theta}_1 + \mathrm{RePr}\hat{v}_{x_1}\frac{\mathrm{d}\theta_0}{\mathrm{d}x} + i\mathrm{RePr}\gamma v_{z_0}\hat{\theta}_1 &= \frac{\mathrm{d}^2\hat{\theta}_1}{\mathrm{d}x^2} - \gamma^2\hat{\theta}_1 + \tau_{xz0}^2\frac{\frac{\mathrm{d}\mu_0}{\mathrm{d}\theta_0}}{\mu_0^2}\hat{\theta}_1 \\ &\quad +2\tau_{xz0}\left[\frac{\mathrm{d}\hat{v}_{z_1}}{\mathrm{d}x} + i\gamma\hat{v}_{x_1}\right]\end{aligned} \tag{6.31}$$

with the boundary conditions

$\hat{\theta}_1(x = \pm 1) = 0$, $\hat{v}_{z_1} = \hat{v}_{x_1} = 0$ at $x = -1$, $\hat{v}_{z_1} = \hat{v}_{x_1} = 0$ at $x = +1$

if the wall speed is held fixed at $x = 1$ and

$\hat{\theta}_1(x = \pm 1) = 0$, $\hat{v}_{z_1} = \hat{v}_{x_1} = 0$ at $x = -1$, $\hat{v}_{x_1} = \frac{\mathrm{d}\hat{v}_{z1}}{\mathrm{d}x} = 0$ at $x = +1$

if the wall stress is held fixed [1] at $x = +1$

Before inspecting the stability of the above equations in general, we will see whether we can get some results without a numerical calculation, at least in some limiting cases as this will help us in anticipating the stability behavior for a general set of parameters. We will therefore try to obtain analytically:

- The rate of change of the eigenvalues with respect to the wave number γ in the limit of zero wave number, i.e $\frac{\mathrm{d}\sigma}{\mathrm{d}\gamma}|_{\gamma=0}$. As we know how the eigenvalues behave at zero wave number, performing this calculation will help us in anticipating the stability behavior when the wave number is changed slightly from zero.

---

[1] The pointwise boundary condition for wall stress, $\frac{\mathrm{d}\hat{v}_{z1}}{\mathrm{d}x} = 0$ at $x = +1$, actually is an approximation to the actual boundary condition at constant wall stress which is an integral condition. A detailed discussion about this is provided in an endnote

- The stability of the flow at Pr = 0. We know that for a perturbation of zero wave number, the limit Pr = 0 corresponds to a purely mechanical problem as the thermal disturbances die out instantaneously. Assuming the same to be true even for non-zero wave number disturbances, we will see whether we are able to get the stability results in this limit.

Turning first to the analysis of the stability of the flow for small wave number disturbances, we proceed to get $\frac{\mathrm{d}\sigma}{\mathrm{d}\gamma}|_{\gamma=0}$. This term will tell us about the stability behavior of the flow for a slightly non zero wave number disturbance as

$$\sigma_\gamma = \sigma_{\gamma=0} + \frac{\mathrm{d}\sigma}{\mathrm{d}\gamma}|_{\gamma=0}\gamma$$

up to $O(\gamma^2)$. Now, let . denote differentiation with respect to the wave number γ. Differentiating the perturbed equations with respect to the wave number, we obtain

$$\frac{\mathrm{d}\dot{\hat{v}}_{x_1}}{\mathrm{d}x} + i\gamma\dot{\hat{v}}_{z_1} + i\hat{v}_{z_1} = 0 \tag{6.32}$$

$$\begin{aligned}\dot{\sigma}\hat{v}_{x_1} + \sigma\dot{\hat{v}}_{x_1} + i\mathrm{Re}v_{z_0}\hat{v}_{x_1} + i\gamma\mathrm{Re}v_{z_0}\dot{\hat{v}}_{x_1} &= -\frac{\mathrm{d}\dot{\hat{p}}_1}{\mathrm{d}x} + 2\frac{\mathrm{d}\mu_0}{\mathrm{d}x}\frac{\mathrm{d}\dot{\hat{v}}_{x_1}}{\mathrm{d}x} \\ &\quad -i\gamma\tau_{xz0}\dot{\hat{\theta}}_1 - i\hat{\theta}_1 + \mu_0\left[\frac{\mathrm{d}^2\dot{\hat{v}}_{x_1}}{\mathrm{d}x^2} - \gamma^2\dot{\hat{v}}_{x_1} - 2\gamma\hat{v}_{x_1}\right]\end{aligned} \tag{6.33}$$

$$\begin{aligned}\dot{\sigma}\hat{v}_{z_1} + \sigma\dot{\hat{v}}_{z_1} + i\gamma\mathrm{Re}v_{z_0}\dot{\hat{v}}_{z_1} + i\mathrm{Re}v_{z_0}\hat{v}_{z_1} + \mathrm{Re}\frac{\mathrm{d}v_{z0}}{\mathrm{d}x}\dot{\hat{v}}_{x_1} &= -i\hat{p}_1 - i\gamma\dot{\hat{p}}_1 \\ &\quad +\frac{\mathrm{d}\mu_0}{\mathrm{d}x}\left[\frac{\mathrm{d}\dot{\hat{v}}_{z_1}}{\mathrm{d}x} + iv_{x_1} + i\gamma\dot{\hat{v}}_{z_1}\right] - \tau_{xz0}\frac{\mathrm{d}\dot{\hat{\theta}}_1}{\mathrm{d}x} \\ &\quad +\mu_0\left[\frac{\mathrm{d}^2\dot{\hat{v}}_{z_1}}{\mathrm{d}x^2} - \gamma^2\dot{\hat{v}}_{z_1} - 2\gamma\hat{v}_{z_1}\right]\end{aligned} \tag{6.34}$$

$$\begin{aligned}\sigma\mathrm{Pr}\dot{\hat{\theta}}_1 + \dot{\sigma}\mathrm{Pr}\hat{\theta}_1 + \mathrm{RePr}\frac{\mathrm{d}\theta_0}{\mathrm{d}x}\dot{\hat{v}}_{x_1} + i\gamma\mathrm{RePr}v_{z_0}\dot{\hat{\theta}}_1 + i\mathrm{RePr}v_{z_0}\hat{\theta}_1 &= \frac{\mathrm{d}^2\dot{\hat{\theta}}_1}{\mathrm{d}x^2} \\ &\quad -\gamma^2\dot{\hat{\theta}}_1 - 2\gamma\hat{\theta}_1 + \tau_{xz0}^2\frac{\frac{\mathrm{d}\mu_0}{\mathrm{d}\theta_0}}{\mu_0^2}\dot{\hat{\theta}}_1 + 2\tau_{xz0}\left[\frac{\mathrm{d}\dot{\hat{v}}_{z_1}}{\mathrm{d}x} + i\gamma\dot{\hat{v}}_{x_1} + i\hat{v}_{x_1}\right]\end{aligned} \tag{6.35}$$

with the following boundary conditions:

$$\dot{\hat{v}}_{z_1}(x=\pm 1)=0, \dot{\hat{v}}_{x_1}(x=\pm 1)=0, \dot{\hat{\theta}}_1(x=\pm 1)=0$$

if the wall speed is held fixed and

$$\frac{\mathrm{d}\dot{\hat{v}}_{z_1}}{\mathrm{d}x}(x=1)=0, \dot{\hat{v}}_{z_1}(x=-1)=0, \dot{\hat{v}}_{x_1}(x=\pm 1)=0, \dot{\hat{\theta}}_1(x=\pm 1)=0$$

if the wall stress is held fixed.

As we are interested in calculating $\dot{\sigma}$ in the limit of a zero wave number disturbance, we put $\gamma = 0$ in the above equations. Recall that at zero wave number $\hat{v}_{x_1} = 0$ from the equation of continuity and $\frac{\mathrm{d}\hat{p}_1}{\mathrm{d}x} = 0$ from the x component of the equation of motion. This then implies that $\hat{p}_1$ is a constant. In fact, as we know that all the eigenfunctions at zero wave number must be real[2], $\hat{p}_1$ must be a real constant. For this analysis, we will choose this constant to be zero. Any non-zero $\hat{p}_1$ will not change our result qualitatively.

The z component of the equation of motion and the energy equation at zero wave number are

$$\sigma\hat{v}_{z_1} = \mu_0\frac{\mathrm{d}^2\hat{v}_{z_1}}{\mathrm{d}x^2} + \frac{\mathrm{d}\mu_0}{\mathrm{d}x}\frac{\mathrm{d}\hat{v}_{z_1}}{\mathrm{d}x} - \tau_{xz0}\frac{\mathrm{d}\hat{\theta}_1}{\mathrm{d}x} \tag{6.36}$$

$$\sigma\mathrm{Pr}\hat{\theta}_1 = \frac{\mathrm{d}^2\hat{\theta}_1}{\mathrm{d}x^2} + \tau_{xz0}^2\frac{\frac{\mathrm{d}\mu_0}{\mathrm{d}\theta_0}}{\mu_0^2}\hat{\theta}_1 + 2\tau_{xz0}\frac{\mathrm{d}\hat{v}_{z_1}}{\mathrm{d}x} \tag{6.37}$$

and putting $\gamma = 0$, $\hat{v}_{x_1} = 0$, $\hat{p}_1 = 0$ in the equations for $\dot{\hat{v}}_{x_1}, \dot{\hat{v}}_{z_1}$ and $\dot{\hat{\theta}}_1$ we obtain

$$\frac{\mathrm{d}\dot{\hat{v}}_{x_1}}{\mathrm{d}x} = -i\hat{v}_{z_1} \tag{6.38}$$

$$\sigma\dot{\hat{v}}_{x_1} = -\frac{\mathrm{d}\dot{\hat{p}}_1}{\mathrm{d}x} + 2\frac{\mathrm{d}\mu_0}{\mathrm{d}x}\frac{\mathrm{d}\dot{\hat{v}}_{x_1}}{\mathrm{d}x} - i\tau_{xz_0}\dot{\hat{\theta}}_1 + \mu_0\frac{\mathrm{d}^2\dot{\hat{v}}_{x_1}}{\mathrm{d}x^2} \tag{6.39}$$

$$\dot{\sigma}\hat{v}_{z_1} + \sigma\dot{\hat{v}}_{z_1} + i\mathrm{Re}v_{z_0}\hat{v}_{z_1} + \mathrm{Re}\frac{\mathrm{d}v_{z_0}}{\mathrm{d}x}\dot{\hat{v}}_{x_1} = \mu_0\frac{\mathrm{d}^2\dot{\hat{v}}_{z_1}}{\mathrm{d}x^2} + \frac{\mathrm{d}\mu_0}{\mathrm{d}x}\frac{\mathrm{d}\dot{\hat{v}}_{z_1}}{\mathrm{d}x} - \tau_{xz0}\frac{\mathrm{d}\dot{\hat{\theta}}_1}{\mathrm{d}x} \tag{6.40}$$

---

[2] Observe that in the equation at zero wave number $\mathbf{Au} = \sigma\mathbf{Bu}$, σ is real and both the operators **A** and **B** are real. Therefore **u** must be real.

$$\sigma\mathrm{Pr}\dot{\hat{\theta}}_1 + \dot{\sigma}\mathrm{Pr}\hat{\theta}_1 + \mathrm{RePr}\frac{\mathrm{d}\theta_0}{\mathrm{d}x}\dot{\hat{v}}_{x_1} + i\mathrm{RePr}v_{z_0}\hat{\theta}_1 = \frac{\mathrm{d}^2\dot{\hat{\theta}}_1}{\mathrm{d}x^2} + \tau_{xz_0}^2\frac{\frac{\mathrm{d}\mu_0}{\mathrm{d}\theta_0}}{\mu_0^2}\dot{\hat{\theta}}_1 + \tau_{xz_0}\frac{\mathrm{d}\dot{\hat{v}}_{z_1}}{\mathrm{d}x} \quad (6.41)$$

where $\tau_{xz_0} = \mu_0\frac{\mathrm{d}v_{z_0}}{\mathrm{d}x}$. Now multiply the $\dot{\hat{\theta}}_1$ equation with $\hat{\theta}_1$ and integrate over -1 to 1 and subtract it from the temperature equation at zero wave number multiplied with $\dot{\hat{\theta}}_1$ and integrated over -1 to 1 to obtain

$$\begin{aligned}\dot{\sigma}\mathrm{Pr}\int_{-1}^{1}\hat{\theta}_1^2\mathrm{d}x + \mathrm{RePr}\int_{-1}^{1}\frac{\mathrm{d}\theta_0}{\mathrm{d}x}\dot{\hat{v}}_{x_1}\hat{\theta}_1\mathrm{d}x + i\mathrm{RePr}\int_{-1}^{1}v_{z_0}\hat{\theta}_1^2\mathrm{d}x \\ = 2\tau_{xz_0}\left[\int_{-1}^{1}\left\{\frac{\mathrm{d}\dot{\hat{v}}_{z_1}}{\mathrm{d}x}\hat{\theta}_1 - \frac{\mathrm{d}\hat{v}_{z_1}}{\mathrm{d}x}\dot{\hat{\theta}}_1\right\}\right]\mathrm{d}x \quad (6.42)\end{aligned}$$

Similarly, multiply the equation for $\dot{\hat{v}}_{z_1}$ with $\hat{v}_{z_1}$ and integrate it over -1 to 1 and then subtract it from the velocity equation at zero wave number multiplied by $\dot{\hat{v}}_{z_1}$ and integrated over -1 to 1 to obtain

$$\begin{aligned}\dot{\sigma}\int_{-1}^{1}\hat{v}_{z_1}^2\mathrm{d}x + \mathrm{Re}\int_{-1}^{1}\frac{\mathrm{d}v_{z_0}}{\mathrm{d}x}\dot{\hat{v}}_{x_1}\hat{\theta}_1\mathrm{d}x + i\mathrm{Re}\int_{-1}^{1}v_{z_0}\hat{v}_{z_1}^2\mathrm{d}x \\ = -\tau_{xz_0}\left[\int_{-1}^{1}\left\{\frac{\mathrm{d}\dot{\hat{\theta}}_1}{\mathrm{d}x}\hat{v}_{z_1} - \frac{\mathrm{d}\hat{\theta}_1}{\mathrm{d}x}\dot{\hat{v}}_{z_1}\right\}\right]\mathrm{d}x \quad (6.43)\end{aligned}$$

Integrating the right hand side of the above equation by parts, we obtain

$$\begin{aligned}\dot{\sigma}\int_{-1}^{1}\hat{v}_{z_1}^2\mathrm{d}x + \mathrm{Re}\int_{-1}^{1}\frac{\mathrm{d}v_{z_0}}{\mathrm{d}x}\dot{\hat{v}}_{x_1}\hat{\theta}_1\mathrm{d}x + i\mathrm{Re}\int_{-1}^{1}v_{z_0}\hat{v}_{z_1}^2\mathrm{d}x \\ = -\tau_{xz_0}\left[\int_{-1}^{1}\left\{-\frac{\mathrm{d}\hat{v}_{z_1}}{\mathrm{d}x}\dot{\hat{\theta}}_1 + \frac{\mathrm{d}\dot{\hat{v}}_{z_1}}{\mathrm{d}x}\hat{\theta}_1\right\}\right]\mathrm{d}x \quad (6.44)\end{aligned}$$

It should be noted that these results are obtained irrespective of whether the boundary condition is constant wall speed or constant wall stress. Now, multiplying the above equation by two and adding it to the equation for $\hat{\theta}_1^2$, we get

$$\begin{aligned}\dot{\sigma}\left[2\int_{-1}^{1}\hat{v}_{z_1}^2\mathrm{d}x + \mathrm{Pr}\int_{-1}^{1}\hat{\theta}_1^2\mathrm{d}x\right] &= -\mathrm{Re}\left[2\int_{-1}^{1}\frac{\mathrm{d}v_{z_0}}{\mathrm{d}x}\dot{\hat{v}}_{x_1}\hat{v}_{z_1}\mathrm{d}x + Pr\int_{-1}^{1}\frac{\mathrm{d}\theta_0}{\mathrm{d}x}\dot{\hat{v}}_{x_1}\hat{\theta}_1\mathrm{d}x\right] \\ &\quad + i\mathrm{Re}\left[2\int_{-1}^{1}v_{z_0}\hat{v}_{z_1}^2\mathrm{d}x + Pr\int_{-1}^{1}v_{z_0}\hat{\theta}_1^2\mathrm{d}x\right] \quad (6.45)\end{aligned}$$

Therefore,

$$\dot{\sigma} = \frac{-\mathrm{Re}\left[\int_{-1}^{1}\dot{\hat{v}}_{x_1}\left(2\frac{\mathrm{d}v_{z_0}}{\mathrm{d}x}\hat{v}_{z_1} + \mathrm{Pr}\frac{\mathrm{d}\theta_0}{\mathrm{d}x}\hat{\theta}_1\right)\mathrm{d}x\right] + i\mathrm{Re}\left[\int_{-1}^{1}v_{z_0}\left(2\hat{v}_{z_1}^2 + \mathrm{Pr}\hat{\theta}_1^2\right)\mathrm{d}x\right]}{2\int_{-1}^{1}\hat{v}_{z_1}^2\mathrm{d}x + \mathrm{Pr}\int_{-1}^{1}\hat{\theta}_1^2\mathrm{d}x} \quad (6.46)$$

where $\dot{\hat{v}}_{x_1}$ in the limit of $\gamma = 0$ is obtained from the equation

$$\dot{\hat{v}}_{x_1}(x) = -i\int_{-1}^{\xi=x} \hat{v}_{z_1}(\xi)\mathrm{d}\xi \tag{6.47}$$

Now, as all the eigenfunctions at the zero wave number should be real, the equation for $\dot{\sigma}$ tells us that it is purely imaginary[3]. Now, the $\dot{\sigma}$ equation tells us that for an infinitesimal change in the wave number from zero, the eigenvalues develop a purely oscillatory component. This result is interesting because earlier for a zero wave number disturbance we concluded that the eigenvalues are real. Now, for a small change in the wave number from zero, the real part of the eigenvalue does not change but there is an addition of an oscillatory component. As this result is valid both at constant wall speed and at constant wall stress, it leads to a curious situation at the nose of the curve. For a perturbation of zero wave number at constant wall stress, the nose of the curve is a point of neutral stability ($\sigma = 0$). Now, from this result for an infinitesimal wave number disturbance, the nose becomes a point of Hopf bifurcation, i.e $\sigma = 0 + ib$, where b is some real constant. This result makes us restate our stability result at the nose for constant wall stress: For an arbitrary disturbance, the system evolves to a new flow and this flow might be either steady or oscillatory depending on the wave number at which the base flow goes unstable. If the base flow goes unstable to $\gamma = 0$, then the emerging flow is steady and if the base flow goes unstable to small wave numbers, then the emerging flow is oscillatory.

Next, we will turn to the analysis of the perturbed equations in the limit of $\mathrm{Pr} = 0$. It turns out that under the assumption that $\hat{\theta}_1 \to 0$ in the limit of $\mathrm{Pr} = 0$, the resulting equations are identical to the Orr-Sommerfield equation for a variable viscosity fluid. To see this, we will introduce the stream function $\hat{\psi}_1$ which satisfies the equation of continuity such that $\hat{v}_{z_1} = -\frac{\mathrm{d}\hat{\psi}_1}{\mathrm{d}x}$ and $\hat{v}_{x_1} = i\gamma\hat{\psi}_1$. The x and z

---

[3] Observe that this result is not due to the effect of viscosity-temperature coupling. It can be observed even at constant viscosity.

components of the equation of motion combine to give

$$\sigma\frac{\mathrm{d}^2\hat{\psi}_1}{\mathrm{d}x^2}-\sigma\gamma^2\hat{\psi}=\frac{\mathrm{d}^2}{\mathrm{d}x^2}\left[\mu_0\frac{\mathrm{d}^2\hat{\psi}_1}{\mathrm{d}x^2}\right]-2\gamma^2\frac{\mathrm{d}}{\mathrm{d}x}\left[\mu_0\frac{\mathrm{d}\hat{\psi}_1}{\mathrm{d}x}\right]-i\gamma\mathrm{Re}v_{z_0}\frac{\mathrm{d}^2\hat{\psi}_1}{\mathrm{d}x^2}$$
$$\left[i\gamma^3\mathrm{Re}v_{z_0}+i\gamma\mathrm{Re}\frac{\mathrm{d}^2v_{z_0}}{\mathrm{d}x^2}+\gamma^4\mu_0+\gamma^2\frac{\mathrm{d}^2\mu_0}{\mathrm{d}x^2}\right]\hat{\psi}_1+\tau_{xzo}\frac{\mathrm{d}^2\hat{\theta}_1}{\mathrm{d}x^2}+\gamma^2\tau_{xz_0}\theta_1 \qquad (6.48)$$

and the energy equation yields

$$\sigma\mathrm{Pr}\hat{\theta}_1+i\gamma\mathrm{RePr}\hat{\psi}_1\frac{\mathrm{d}\theta_0}{\mathrm{d}x}+i\gamma\mathrm{RePr}v_{z_0}\hat{\theta}_1=\frac{\mathrm{d}^2\hat{\theta}_1}{\mathrm{d}x^2}-\gamma^2\hat{\theta}_1+\tau_{xzo}^2\frac{\frac{\mathrm{d}\mu_0}{\mathrm{d}\theta_0}}{\mu_0^2}\hat{\theta}_1$$
$$-2\tau_{xzo}\left[\frac{\mathrm{d}^2\hat{\psi}_1}{\mathrm{d}x^2}+\gamma^2\hat{\psi}_1\right] \qquad (6.49)$$

with the boundary conditions

$\hat{\theta}_1(x=\pm1)=0$, $\hat{\psi}_1=\frac{\mathrm{d}\hat{\psi}_1}{\mathrm{d}x}=0$ at $x=-1$, $\hat{\psi}_1=\frac{\mathrm{d}\hat{\psi}_1}{\mathrm{d}x}=0$ at $x=+1$

if the wall speed is held fixed at $x=1$ and

$\hat{\theta}_1(x=\pm1)=0$, $\hat{\psi}_1=\frac{\mathrm{d}\hat{\psi}_1}{\mathrm{d}x}=0$ at $x=-1$, $\hat{\psi}_1=\frac{\mathrm{d}^2\hat{\psi}_1}{\mathrm{d}x^2}=0$ at $x=+1$

if the wall stress is held fixed at $x=+1$.

Now, in the limit of $\mathrm{Pr}=0$, we anticipate the mechanical disturbances to be dominant. This is based purely on our results at zero wave number. Therefore, we will put $\hat{\theta}_1=0$ in these equations to obtain[4]

$$\sigma\frac{\mathrm{d}^2\hat{\psi}_1}{\mathrm{d}x^2}-\sigma\gamma^2\hat{\psi}=\frac{\mathrm{d}^2}{\mathrm{d}x^2}\left[\mu_0\frac{\mathrm{d}^2\hat{\psi}_1}{\mathrm{d}x^2}\right]-2\gamma^2\frac{\mathrm{d}}{\mathrm{d}x}\left[\mu_0\frac{\mathrm{d}\hat{\psi}_1}{\mathrm{d}x}\right]-i\gamma\mathrm{Re}v_{z_0}\frac{\mathrm{d}^2\hat{\psi}_1}{\mathrm{d}x^2}$$
$$+\left[i\gamma^3\mathrm{Re}v_{z_0}+i\gamma\mathrm{Re}\frac{\mathrm{d}^2v_{z_0}}{\mathrm{d}x^2}+\gamma^4\mu_0+\gamma^2\frac{\mathrm{d}^2\mu_0}{\mathrm{d}x^2}\right]\hat{\psi}_1 \qquad (6.50)$$

Note that this equation is indeed the Orr-Sommerfield equation for a viscous fluid with an arbitrary viscosity variation. Now, based on this equation if we can predict whether the flow is stable or not, then we can later explore the role of Prandtl number and how it alters the stability results by admitting finite Prandtl numbers in the analysis. The limit of Pr → 0 therefore provides us with a convenient starting point to think about the stability of this complicated problem.

---

[4] Similarly, one might look at the purely thermal problem by putting $\hat{\psi}_1=0$ even though physically it is not possible to say what limit it corresponds to. It can be easily seen using an energy argument that under this limit, the flow is stable.

To find out the sign of σ, multiply this equation by $\overline{\psi}_1$, where $\overline{\psi}_1$ is the complex conjugate of ψ_1 to obtain

$$-\sigma\left(\int_{-1}^{+1}|\frac{\mathrm{d}\hat{\psi}_1}{\mathrm{d}x}|^2+\gamma^2|\hat{\psi}|^2\mathrm{d}x\right)=\int_{-1}^{+1}\mu_0|\frac{\mathrm{d}^2\hat{\psi}_1}{\mathrm{d}x^2}|^2\mathrm{d}x$$
$$+2\gamma^2\int_{-1}^{+1}\mu_0|\frac{\mathrm{d}\hat{\psi}_1}{\mathrm{d}x}|^2\mathrm{d}x+\int_{-1}^{+1}\left[\gamma^4\mu_0+\gamma^2\frac{\mathrm{d}^2\mu_0}{\mathrm{d}x^2}\right]|\hat{\psi}_1|^2\mathrm{d}x$$
$$-i\gamma\mathrm{Re}\int_{-1}^{+1}v_{z0}\frac{\mathrm{d}^2\hat{\psi}_1}{\mathrm{d}x^2}\overline{\psi}_1\mathrm{d}x+\int_{-1}^{+1}\left[i\gamma^3\mathrm{Re}v_{z0}+i\gamma\mathrm{Re}\frac{\mathrm{d}^2v_{z0}}{\mathrm{d}x^2}\right]|\hat{\psi}_1|^2\mathrm{d}x \tag{6.51}$$

Therefore, the real part of σ is given by

$$\mathrm{Real}(\sigma)=\frac{-\int_{-1}^{+1}\left\{\mu_0|\frac{\mathrm{d}^2\hat{\psi}_1}{\mathrm{d}x^2}|^2+2\gamma^2\mu_0|\frac{\mathrm{d}\hat{\psi}_1}{\mathrm{d}x}|^2+\left(\gamma^4\mu_0+\gamma^2\frac{\mathrm{d}^2\mu_0}{\mathrm{d}x^2}\right)|\hat{\psi}_1|^2\right\}\mathrm{d}x}{\int_{-1}^{+1}\left\{|\frac{\mathrm{d}\hat{\psi}_1}{\mathrm{d}x}|^2+\gamma^2|\hat{\psi}_1|^2\right\}\mathrm{d}x} \tag{6.52}$$

$$+\frac{\mathrm{Real}(i\gamma Re\int_{-1}^{+1}v_{z0}\frac{\mathrm{d}^2\hat{\psi}_1}{\mathrm{d}x^2}\overline{\hat{\psi}}_1\mathrm{d}x)}{\int_{-1}^{+1}\left\{|\frac{\mathrm{d}\hat{\psi}_1}{\mathrm{d}x}|^2+\gamma^2|\hat{\psi}_1|^2\right\}\mathrm{d}x} \tag{6.53}$$

and the imaginary part of σ is given by[5]

$$\mathrm{Imag}(\sigma)=-\frac{\int_{-1}^{+1}\left[\gamma^3\mathrm{Re}v_{z0}+\gamma\mathrm{Re}\frac{\mathrm{d}^2v_{z0}}{\mathrm{d}x^2}\right]|\hat{\psi}_1|^2\mathrm{d}x}{\int_{-1}^{+1}\left\{|\frac{\mathrm{d}\hat{\psi}_1}{\mathrm{d}x}|^2+\gamma^2|\hat{\psi}_1|^2\right\}\mathrm{d}x} \tag{6.54}$$

$$+\frac{\mathrm{Imag}(i\gamma Re\int_{-1}^{+1}v_{z0}\frac{\mathrm{d}^2\hat{\psi}_1}{\mathrm{d}x^2}\overline{\hat{\psi}}_1\mathrm{d}x)}{\int_{-1}^{+1}\left\{|\frac{\mathrm{d}\hat{\psi}_1}{\mathrm{d}x}|^2+\gamma^2|\hat{\psi}_1|^2\mathrm{d}x\right\}\mathrm{d}x} \tag{6.55}$$

The real part of σ is negative unless there is a positive contribution from

$$\frac{\mathrm{Real}(i\gamma Re\int_{-1}^{+1}v_{z0}\frac{\mathrm{d}^2\hat{\psi}_1}{\mathrm{d}x^2}\overline{\hat{\psi}}_1\mathrm{d}x)}{\int_{-1}^{+1}\left\{|\frac{\mathrm{d}\hat{\psi}_1}{\mathrm{d}x}|^2+\gamma^2|\hat{\psi}|^2\mathrm{d}x\right\}\mathrm{d}x}$$

In fact, even if there is a positive contribution from this term, it might turn out that the flow is still stable. Without performing a numerical calculation this is as far as we can go. Now, it is well known from numerical calculations in the past literature[10] that for constant viscosity plane Couette flow, wherein v_{z_0} is a linear function of x, the Orr-Sommerfield equations predict stability for all finite Reynolds number at constant wall speed. For constant viscosity plane Poiseulle flow, wherein v_{z_0} is a quadratic function of x, the critical Reynolds number at the onset of instability is 5772 and the corresponding wave number γ is 1.02[10]. The mechanism by which an instability sets in Poiseulle flow has not been clearly explained in literature, even though it is attributed to the gradients in base flow interacting with the perturbations. Notice that, in the constant viscosity plane Couette flow, the gradient in velocity is a constant everywhere across the gap and in constant viscosity plane Poiseulle flow, the gradient in velocity is maximum at the wall and zero at the centre. Now, with a viscosity dependence on temperature, the velocity gradient in plane Couette flow is given by $\frac{\mathrm{d}v_{z0}}{\mathrm{d}x} = f_0 \tau_{xz0}$. Therefore, for a given value of shear stress τ_{xz0}, the maximum velocity gradient is given by $\frac{\mathrm{d}v_{z0}}{\mathrm{d}x}|_m = f_{0_m} \tau_{xz0}$ where f_{0_m} is the fluidity at the maximum temperature. Now, the ratio of the value of f_{0_m} in the upper branch vs. the lower branch for a scaled $\tau_{xz0} = 0.15$ is about 1500. This gives an idea of the steepness in velocity gradient introduced by the viscosity variation of temperature. Therefore, we would presume that along the upper branch where the velocity gradients are sharper, there is more possibility for the instability to set in if we believe that a sharper gradient in the velocity profile might lead to an instability. While all of these suppositions are interesting, if our objective is to understand the reasons for an instability at non-zero wave number, our primary interest in this chapter is to find out whether the conclusions drawn from our stability results at a zero wave number disturbance are modified when a non-zero wave number disturbance is imposed. We will therefore check this by performing a stability calculation for a non-zero wave number disturbance. To be concrete, we will choose the properties of the liquid that will used in the experiments for the numerical calculation.

---

[5] An observation is worth mentioning here: Lord Rayleigh's inflexion point theorem for inviscid fluids states that for an inviscid liquid, a necessary condition for instability is for the velocity profile to have an inflexion point in the gap, i.e. $\frac{\mathrm{d}^2v_{z0}}{\mathrm{d}x^2}$ should change sign somewhere in the interior. If one were to extend the inflexion point theorem to viscous fluids, one would expect the term $\frac{\mathrm{d}^2v_{z0}}{\mathrm{d}x^2}$ to be important in determining the stability of the flow. However, observe from the energy argument that the term with $\frac{\mathrm{d}^2v_{z0}}{\mathrm{d}x^2}$ is only in the imaginary part of σ. Simply based on this observation, we may conclude that an inflexion point may not be necessary for an instability in viscous shear flows. More about this point will be discussed in an endnote.

For numerically calculating the eigenvalues for a general set of parameters, the equations in the stream function formulation

$$\sigma\frac{\mathrm{d}^2\hat{\psi}_1}{\mathrm{d}x^2}-\sigma\gamma^2\hat{\psi}=\frac{\mathrm{d}^2}{\mathrm{d}x^2}\left[\mu_0\frac{\mathrm{d}^2\hat{\psi}_1}{\mathrm{d}x^2}\right]-2\gamma^2\frac{\mathrm{d}}{\mathrm{d}x}\left[\mu_0\frac{\mathrm{d}\hat{\psi}_1}{\mathrm{d}x}\right]-i\gamma\mathrm{Re}v_{z_0}\frac{\mathrm{d}^2\hat{\psi}_1}{\mathrm{d}x^2}$$

$$\left[i\gamma^3\mathrm{Re}v_{z_0}+i\gamma\mathrm{Re}\frac{\mathrm{d}^2v_{z0}}{\mathrm{d}x^2}+\gamma^4\mu_0+\gamma^2\frac{\mathrm{d}^2\mu_0}{\mathrm{d}x^2}\right]\hat{\psi}_1+\tau_{xz0}\frac{\mathrm{d}^2\hat{\theta}_1}{\mathrm{d}x^2}+\gamma^2\tau_{xz_0}\hat{\theta}_1 \qquad (6.56)$$

$$\sigma\mathrm{Pr}\hat{\theta}_1+i\gamma\mathrm{RePr}\hat{\psi}_1\frac{\mathrm{d}\theta_0}{\mathrm{d}x}+i\gamma\mathrm{RePr}v_{z_0}\hat{\theta}_1=\frac{\mathrm{d}^2\hat{\theta}_1}{\mathrm{d}x^2}-\gamma^2\hat{\theta}_1+\tau_{xz0}^2\frac{\frac{\mathrm{d}\mu_0}{\mathrm{d}\theta_0}}{\mu_0^2}\hat{\theta}_1$$

$$-2\tau_{xz0}\left[\frac{\mathrm{d}^2\hat{\psi}_1}{\mathrm{d}x^2}+\gamma^2\hat{\psi}_1\right] \qquad (6.57)$$

with the boundary conditions

$\hat{\theta}_1(x=\pm1)=0$, $\hat{\psi}_1=\frac{\mathrm{d}\hat{\psi}_1}{\mathrm{d}x}=0$ at $x=-1$, $\hat{\psi}_1=\frac{\mathrm{d}\hat{\psi}_1}{\mathrm{d}x}=0$ at $x=+1$

if the wall speed is held fixed at $x=1$ and

$\hat{\theta}_1(x=\pm1)=0$, $\hat{\psi}_1=\frac{\mathrm{d}\hat{\psi}_1}{\mathrm{d}x}=0$ at $x=-1$, $\hat{\psi}_1=\frac{\mathrm{d}^2\hat{\psi}_1}{\mathrm{d}x^2}=0$ at $x=+1$

if the wall stress is held fixed at $x=+1$ are finite differenced. A central scheme is employed for the finite differencing. Using this scheme, the infinite dimensional differential equations are truncated to a finite dimensional system of equations. The equations that result can be cast in the form $\mathbf{Au}=\sigma\mathbf{Bu}$, where $\mathbf{A}$ and $\mathbf{B}$ are now algebraic matrices. The eigenvalues of this system of algebraic equations are then calculated.

The liquid used in our experiment has a viscosity of $\mu_w=5651$ c.p at 25°C. The sensitivity to temperature, S is 0.0757°C^{-1} and the thermal conductivity k is 0.22 J/s m C. Therefore, the velocity scale corresponding to this set of physical properties is $V_{\mathrm{ref}}=\sqrt{k/S\mu_w}=0.72$ m/s. The gap width used in an experiment is typically of the order of 1 cm. The density of the liquid used in the experiment is around 1000kg/m^3. Hence, the Reynolds number in this scaling is $\mathrm{Re}=LV_{\mathrm{ref}}\rho/\mu_w=1.30$. The specific heat of the liquid is 2000 J/kg/K and therefore the Prandtl number is $\mathrm{Pr}=C_v\mu_w/k=51500$. We will address the stability questions specifically for this set of parameter values.

First, we will consider the case of constant wall stress. For this case, we know that for a zero wave number disturbance, the lower branch is stable, the nose is a point of neutral stability and the upper branch is unstable. The question would then be to ask whether there is a point on the lower branch that is unstable to a non-zero wave number disturbance at constant wall stress, for the set of parameter values that we have chosen. To answer this question, we will choose a point on the base curve corresponding to a scaled shear stress value of $\tau_{xz_0} = 0.93$ and a scaled velocity $V_0 = 3.67$. This point is on the lower branch of the base curve and very close to the nose. If our earlier conclusion that we drew for a zero wave number disturbance, viz. that the eigenvalues increase with an increase in the wall speed, holds good even for non-zero wave number disturbances then ensuring the stability of this chosen point on the curve would ensure that the flow is stable to all points on the lower branch which have lower wall speeds.

Table 6.1 shows the value of the real part of the largest eigenvalue with respect to the wave number. We see from the table that the real part remains negative for a range of wave numbers thus confirming that the lower branch is stable to small perturbations at constant wall stress, at least under the chosen experimental conditions[6].

Next, we will check whether at constant wall speed, the upper branch is stable to small disturbances for the chosen experimental conditions. Note that the wall speed along the upper branch goes all the way up to infinity. However, we are only interested in ensuring the stability of the flow for the maximum wall speeds that we can expect in our experiment. The experiments, as mentioned before, are run in circular Couette flow with an outer radius of one inch. Typical maximum speeds

---

[6] One might be curious to know about the stability at constant wall stress for a non-zero wave number disturbance on the upper branch. However, as we already know that at constant wall stress, the flow is unstable for a zero wave number disturbance for all Prandtl numbers, the result of a stability calculation for a non-zero wave number disturbance will not alter the stability picture on the upper branch. Therefore, we did not perform the stability calculation at constant wall stress on the upper branch.

Table 6.1: Stability at constant wall stress: The real part of the largest eigenvalue vs. the wave number for a point on the lower branch for the chosen experimental conditions.

wave number	Real part of the largest eigenvalue
0.5	-2.3×10^{-2}
1.0	-3.6×10^{-2}
2.0	-5.8×10^{-2}
3.0	-7.6×10^{-2}
4.0	-9.3×10^{-2}
5.0	-1.1×10^{-1}

Table 6.2: The stability at constant wall speed: The plot of the largest eigenvalue vs. the wave number for a point on the upper branch and for properties based on our experimental liquid.

wave number	Real part of the largest eigenvalue
0.5	-2.3×10^{-2}
1.0	-3.5×10^{-2}
2.0	-5.5×10^{-2}
3.0	-7.2×10^{-2}
4.0	-8.8×10^{-2}
5.0	-1.0×10^{-1}

expected in the experiment are around 2000 rpm. This translates to a linear speed of 5.32 m/s for this geometry. Hence, scaling this velocity with respect to the reference velocity, we obtain for the scaled velocity $V_0 = 7.39$. This corresponds to a point on the upper branch of the base curve with the corresponding scaled shear stress $\tau_{xz_0} = 0.853$. If this point is stable at constant wall speed then we can ensure that for the experimental conditions the flow is stable at constant wall speed.

Table 6.2 shows the value of the largest eigenvalue as a function of the wave number for the chosen point on the base curve and for the set of chosen parameters corresponding to the experiment. The table shows that the real part of the largest eigenvalue is negative for a range of wave numbers thus ensuring that the flow is stable at constant wall speed under the experimental conditions.

Thus the conclusion from our stability results is that for the chosen experimental conditions, the lower branch is stable both at constant wall speed and at constant wall stress conditions. The upper branch is stable at constant wall speed but unstable at constant wall stress. Therefore, we find that the stability results for a non-zero wave number disturbance do not alter the conclusions that we drew based on the stability results for a zero wave number disturbance. This then directly leads us on to exploring the possibility of performing an experiment with the objective that we originally had at the end of chapter 4:

- Setting the wall speed, obtain the base solution curve. Once the base solution is obtained, hold the wall stress fixed at a point on the upper branch. The upper branch being unstable for a fixed wall stress, the system ought to jump to the lower branch for that value of wall stress as that is the only stable operating point for that value of wall stress.

However, we first have to conceive of an experimental plan to attain these objectives and this is what we will do in chapter 7. But, before that, as in the earlier chapters, here again we conclude this part with endnotes on peripheral, but interesting and, in some cases, useful issues that otherwise simply get in our way.

6.1 Endnotes

6.1.1 The Thin Gapping of Perturbed Equations in Circular Couette flow

In chapter 2, we showed that in the limit of the gap width going to zero, the base equations in circular Couette flow become identically equal to the base equations in plane Couette flow. In this endnote, we will prove that the same holds true even when a perturbation is carried out. Now, the perturbed equations in the circular Couette flow are obtained by introducing

$$v_{r_1} = \hat{v}_{r_1}(r)\mathrm{e}^{\sigma t}\mathrm{e}^{im\theta}\mathrm{e}^{i\beta z}$$

$$v_{\theta_1} = \hat{v}_{\theta_1}(r)\mathrm{e}^{\sigma t}\mathrm{e}^{im\theta}\mathrm{e}^{i\beta z}$$

$$v_{z_1} = \hat{v}_{z_1}(r)\mathrm{e}^{\sigma t}\mathrm{e}^{im\theta}\mathrm{e}^{i\beta z}$$

$$p_1 = \hat{p}_1(r)\mathrm{e}^{\sigma t}\mathrm{e}^{im\theta}\mathrm{e}^{i\beta z}$$

$$T_1 = \hat{T}_1(r)\mathrm{e}^{\sigma t}\mathrm{e}^{im\theta}\mathrm{e}^{i\beta z}$$

into the perturbed equations

$$\nabla.\mathbf{v}_1 = 0 \tag{6.58}$$

$$\rho\frac{\partial \mathbf{v_1}}{\partial t} + \rho\mathbf{v_1}.\nabla\mathbf{v_0} + \rho\mathbf{v_0}.\nabla\mathbf{v_1} = -\nabla p_1 + 2\nabla\mu_0.D_1 + 2{\mu_0}^{'}\nabla T_1.D_0$$
$$+2{\mu_0}^{''}T_1\nabla T_0.D_0 + \mu_0\nabla^2\mathbf{v_1} + {\mu_0}^{'}T_1\nabla^2\mathbf{v_0} \tag{6.59}$$

$$\rho C_v\frac{\partial T_1}{\partial t} + \rho C_v\mathbf{v_1}.\nabla T_0 + \rho C_v\mathbf{v_0}.\nabla T_1 = k\nabla^2 T_1 + 4\mu_0 D_0 : D_1 + 2{\mu_0}^{'}T_1 D_0 : D_0 \tag{6.60}$$

where ${\mu_0}^{'} = \mathrm{d}\mu(T_0)/T_0$, we obtain

Here, m is the wave number in the azimuthal direction and β is the wave number in the z direction. As a result, we see that the continuity equation reduces to

$$\frac{1}{r}\frac{\mathrm{d}}{\mathrm{d}r}\left[r\hat{v}_{r_1}\right] + \frac{i\mathrm{m}}{r}\hat{v}_{\theta_1} + i\beta\hat{v}_{z_1} = 0 \tag{6.61}$$

while the r, θ, z component of the equation of motion become

$$\rho\left(\sigma\hat{v}_{r_1} + i\mathrm{m}\frac{v_{\theta_0}}{r}\hat{v}_{r_1} - 2\frac{v_{\theta_0}\hat{v}_{\theta_1}}{r}\right)^{7} = -\frac{\mathrm{d}\hat{p}_1}{\mathrm{d}r} + 2\frac{\mathrm{d}\mu_0}{\mathrm{d}r}\frac{\mathrm{d}\hat{v}_{r_1}}{\mathrm{d}r}$$
$$+\mu_0\left[\frac{\mathrm{d}^2}{\mathrm{d}r^2} + \frac{1}{r}\frac{\mathrm{d}}{\mathrm{d}r} - \frac{1}{r^2} - \frac{m^2}{r^2} - \beta^2\right]\hat{v}_{r_1} + \frac{\mathrm{d}\mu_0}{\mathrm{d}T_0}\hat{T}_1 i\mathrm{m}\frac{\mathrm{d}}{\mathrm{d}r}\left[\frac{\hat{v}_{\theta_0}}{r}\right] - 2\mu_0 i\mathrm{m}\frac{\hat{v}_{\theta_1}}{r^2} \tag{6.62}$$

$$\rho\left(\sigma\hat{v}_{\theta_1} + \hat{v}_{r_1}\frac{\mathrm{d}v_{\theta_0}}{\mathrm{d}r} + i\mathrm{m}\frac{v_{\theta_0}\hat{v}_{\theta_1}}{r} + \frac{\hat{v}_{\theta_0}\hat{v}_{r_1}}{r}\right) = -i\frac{m}{r}\hat{p}_1 + \frac{\mathrm{d}\mu_0}{\mathrm{d}r}\left[\frac{\mathrm{d}\hat{v}_{\theta_1}}{\mathrm{d}r} + \frac{i\mathrm{m}}{r}\hat{v}_{r_1}\right]$$
$$+\mu_0\left[\frac{\mathrm{d}^2}{\mathrm{d}r^2} + \frac{1}{r}\frac{\mathrm{d}}{\mathrm{d}r} - \frac{1}{r^2} - \frac{m^2}{r^2} - \beta^2\right]\hat{v}_{\theta_1}$$
$$+\frac{\mathrm{d}}{\mathrm{d}r}\left[r\frac{\mathrm{d}\mu_0}{\mathrm{d}T_0}\hat{T}_1\frac{\mathrm{d}}{\mathrm{d}r}\left(\frac{v_{\theta_0}}{r}\right)\right] + 2\frac{\mu_0 i\mathrm{m}}{r^2}\hat{v}_{r_1} - \frac{\mathrm{d}\mu_0}{\mathrm{d}r}\frac{\hat{v}_{\theta_1}}{r} \tag{6.63}$$

$$\rho\left(\sigma\hat{v}_{z_1} + i\mathrm{m}\frac{v_{\theta_0}}{r}\hat{v}_{z_1}\right) = -i\beta\hat{p}_1 + \frac{\mathrm{d}\mu_0}{\mathrm{d}r}\frac{\mathrm{d}\hat{v}_{z_1}}{\mathrm{d}r}$$
$$+\mu_0\left[\frac{\mathrm{d}^2}{\mathrm{d}r^2} + \frac{1}{r}\frac{\mathrm{d}}{\mathrm{d}r} - \frac{1}{r^2} - \frac{m^2}{r^2} - \beta^2\right]\hat{v}_{z_1} \tag{6.64}$$

The energy equation turns into

$$\rho\left(\sigma\hat{T}_1+\hat{v}_{r_1}\frac{\mathrm{d}T_0}{\mathrm{d}r}+im\frac{v_{\theta_0}\hat{T}_1}{r}\right)=k\left[\frac{\mathrm{d}^2}{\mathrm{d}r^2}+\frac{1}{r}\frac{\mathrm{d}}{\mathrm{d}r}-\frac{1}{r^2}-\frac{m^2}{r^2}-\beta^2\right]\hat{T}_1$$
$$+\frac{\mathrm{d}\mu_0}{\mathrm{d}T_0}\hat{T}_1\left[r\frac{\mathrm{d}}{\mathrm{d}r}\left(\frac{v_{\theta_0}}{r}\right)\right]^2+2\mu_0r^2\frac{\mathrm{d}}{\mathrm{d}r}\left(\frac{v_{\theta_0}}{r}\right)\frac{\mathrm{d}}{\mathrm{d}r}\left(\frac{\hat{v}_{\theta_1}}{r}\right)+2\mu_0\frac{\mathrm{d}}{\mathrm{d}r}\left(\frac{v_{\theta_0}}{r}\right)im\hat{v}_{r_1}\qquad(6.65)$$

Now, scaling these equations using $r^*=(r-r_1)/\Delta$ where $\Delta=(r_2-r_1)$ and multiplying the equation of continuity by Δ and the momentum and energy equations by Δ^2 throughout, the equation of continuity becomes

$$\frac{1}{(r^*\Delta+r_1)}\frac{\mathrm{d}}{\mathrm{d}r^*}\left[(r^*\Delta+r_1)\hat{v}_{r_1}\right]+i(m\Delta)\frac{\hat{v}_{\theta_1}}{(r^*\Delta+r_1)}+i(\beta\Delta)\hat{v}_{z_1}=0\qquad(6.66)$$

and the equations of motion become

$$\rho\left(\sigma\Delta^2\hat{v}_{r_1}+im\Delta^2\frac{v_{\theta_0}}{(r^*\Delta+r_1)}\hat{v}_{r_1}-2\frac{v_{\theta_0}\hat{v}_{\theta_1}\Delta^2}{(r^*\Delta+r_1)}\right)=-\Delta\frac{\mathrm{d}\hat{p}_1}{\mathrm{d}r^*}+2\frac{\mathrm{d}\mu_0}{\mathrm{d}r^*}\frac{\mathrm{d}\hat{v}_{r_1}}{\mathrm{d}r^*}$$
$$+\mu_0\left[\frac{\mathrm{d}^2}{\mathrm{d}r^{*2}}+\frac{\Delta}{(r^*\Delta+r_1)}\frac{\mathrm{d}}{\mathrm{d}r^*}-\frac{\Delta^2}{(r^*\Delta+r_1)^2}-\frac{m^2\Delta^2}{(r^*\Delta+r_1)^2}-(\beta\Delta)^2\right]\hat{v}_{r_1}$$
$$+\frac{\mathrm{d}\mu_0}{\mathrm{d}T_0}\hat{T}_1im\Delta\frac{\mathrm{d}}{\mathrm{d}r^*}\left[\frac{v_{\theta_0}}{(r^*\Delta+r_1)}\right]-2\mu_0im\frac{\hat{v}_{\theta_1}}{(r^*\Delta+r_1)^2}\qquad(6.67)$$

$$\rho\left(\sigma\Delta^2\hat{v}_{\theta_1}+\Delta\hat{v}_{r_1}\frac{\mathrm{d}v_{\theta 0}}{\mathrm{d}r^*}+im\Delta^2\frac{v_{\theta_0}\hat{v}_{\theta_1}}{(r^*\Delta+r_1)}+\Delta^2\frac{\hat{v}_{\theta_0}\hat{v}_{r_1}}{(r^*\Delta+r_1)}\right)=-i\frac{m\Delta^2}{(r^*\Delta+r_1)}\hat{p}_1$$
$$+\mu_0\left[\frac{\mathrm{d}^2}{\mathrm{d}r^{*2}}+\frac{\Delta}{(r^*\Delta+r_1)}\frac{\mathrm{d}}{\mathrm{d}r^*}-\frac{\Delta^2}{(r^*\Delta+r_1)^2}-\frac{m^2\Delta^2}{r^2}+(\beta\Delta)^2\right]\hat{v}_{\theta_1}$$
$$+\frac{\mathrm{d}\mu_0}{\mathrm{d}r^*}\left[\frac{\mathrm{d}\hat{v}_{\theta_1}}{\mathrm{d}r^*}+\frac{im\Delta}{(r^*\Delta+r_1)}\hat{v}_{r_1}\right]+\frac{\mathrm{d}}{\mathrm{d}r^*}\left[(r^*\Delta+r_1)\frac{\mathrm{d}\mu_0}{\mathrm{d}T_0}\hat{T}_1\frac{\mathrm{d}}{\mathrm{d}r^*}\left(\frac{v_{\theta_0}}{(r^*\Delta+r_1)}\right)\right]$$
$$+2\frac{\mu_0im\Delta^2}{(r^*\Delta+r_1)^2}\hat{v}_{r_1}-\Delta\frac{\mathrm{d}\mu_0}{\mathrm{d}r^*}\frac{\hat{v}_{\theta_1}}{(r^*\Delta+r_1)}\qquad(6.68)$$

$$\rho\left(\sigma\Delta^2\hat{v}_{z_1}+im\Delta^2\frac{v_{\theta_0}}{(r^*\Delta+r_1)}\hat{v}_{z_1}\right)=-i\beta\Delta^2\hat{p}_1+\frac{\mathrm{d}\mu_0}{\mathrm{d}r^*}\frac{\mathrm{d}\hat{v}_{z_1}}{\mathrm{d}r^*}$$
$$+\mu_0\left[\frac{\mathrm{d}^2}{\mathrm{d}r^{*2}}+\frac{\Delta}{(r^*\Delta+r_1)}\frac{\mathrm{d}}{\mathrm{d}r^*}-\frac{\Delta^2}{(r^*\Delta+r_1)^2}-\frac{m^2\Delta^2}{(r^*\Delta+r_1)^2}-\beta\Delta^2\right]\hat{v}_{z_1}\qquad(6.69)$$

and the energy equation becomes

$$\rho\left(\sigma\Delta^2\hat{T}_1+\hat{v}_{r_1}\Delta\frac{\mathrm{d}T_0}{\mathrm{d}r^*}+im\Delta^2\frac{v_{\theta_0}\hat{T}_1}{(r^*\Delta+r_1)}\right)=k\left[\frac{\mathrm{d}^2}{\mathrm{d}r^{*2}}+\frac{\Delta}{(r^*\Delta+r_1)}\frac{\mathrm{d}}{\mathrm{d}r^*}\right]\hat{T}_1$$

$$-k\left[\frac{\Delta^2}{(r^*\Delta+r_1)^2}+\frac{m^2\Delta^2}{(r^*\Delta+r_1)^2}+(\beta\Delta)^2\right]\hat{T}_1+\frac{\mathrm{d}\mu_0}{\mathrm{d}T_0}\hat{T}_1\left[(r^*\Delta+r_1)\Delta\frac{\mathrm{d}}{\mathrm{d}r^*}\left(\frac{v_{\theta_0}}{r^*\Delta+r_1}\right)\right]^2$$

$$+2\mu_0(r^*\Delta+r_1)^2\frac{\mathrm{d}}{\mathrm{d}r^*}\left[\frac{v_{\theta_0}}{(r^*\Delta+r_1)}\right]\frac{\mathrm{d}}{\mathrm{d}r^*}\left[\frac{\hat{v}_{\theta_1}}{(r^*\Delta+r_1)}\right]+2\mu_0\frac{\mathrm{d}}{\mathrm{d}r^*}\left[\frac{v_{\theta_0}}{(r^*\Delta+r_1)}\right]im\Delta\hat{v}_{r_1} \tag{6.70}$$

Let $\Delta/r_1=\epsilon$. Redefine $\mathrm{m}/r_1=\gamma$ to obtain the equation of continuity as

$$\frac{\mathrm{d}\hat{v}_{r_1}}{\mathrm{d}r^*}+\frac{\epsilon\hat{v}_{r_1}}{(1+\epsilon r^*)}+i(\gamma\Delta)\frac{\hat{v}_{\theta_1}}{(1+\epsilon r^*)}+i(\beta\Delta)\hat{v}_{z_1}=0 \tag{6.71}$$

the equations of motion as

$$\rho\left(\sigma\Delta^2\hat{v}_{r_1}+i(\gamma\Delta)\Delta\frac{v_{\theta_0}}{(1+r^*\epsilon)}\hat{v}_{r_1}-2\epsilon\Delta\frac{v_{\theta_0}\hat{v}_{\theta_1}}{(1+r^*\epsilon)}\right)=-\Delta\frac{\mathrm{d}\hat{p}_1}{\mathrm{d}r^*}+2\frac{\mathrm{d}\mu_0}{\mathrm{d}r^*}\frac{\mathrm{d}\hat{v}_{r_1}}{\mathrm{d}r^*}$$

$$+\mu_0\left[\frac{\mathrm{d}^2}{\mathrm{d}r^{*2}}+\frac{\epsilon}{(1+r^*\epsilon)}\frac{\mathrm{d}}{\mathrm{d}r^*}-\frac{\epsilon^2}{(1+r^*\epsilon)^2}-\frac{(\gamma\Delta)^2}{(1+r^*\epsilon)^2}-(\beta\Delta)^2\right]\hat{v}_{r_1}$$

$$+\frac{\mathrm{d}\mu_0}{\mathrm{d}T_0}\hat{T}_1 i(\gamma\Delta)\frac{\mathrm{d}}{\mathrm{d}r^*}\left[\frac{\hat{v}_{\theta_0}}{(1+r^*\epsilon)}\right]-2\mu_0 i(\gamma\Delta)\epsilon\frac{\hat{v}_{\theta_1}}{(1+r^*\epsilon)^2} \tag{6.72}$$

$$\rho\left(\sigma\Delta^2\hat{v}_{\theta_1}+\Delta\hat{v}_{r_1}\frac{\mathrm{d}v_{\theta_0}}{\mathrm{d}r^*}+i(\gamma\Delta)\epsilon\frac{v_{\theta_0}\hat{v}_{\theta_1}}{(r^*\Delta+r_1)}+\Delta^2\frac{\hat{v}_{\theta_0}\hat{v}_{r_1}}{(1+r^*\epsilon)}\right)=-i\Delta\frac{\gamma\Delta}{(1+r^*\epsilon)}\hat{p}_1$$

$$+\mu_0\left[\frac{\mathrm{d}^2}{\mathrm{d}r^{*2}}+\frac{\epsilon}{(1+r^*\epsilon)}\frac{\mathrm{d}}{\mathrm{d}r^*}-\frac{\epsilon^2}{(1+r^*\epsilon)^2}-\frac{\gamma^2\Delta^2}{(1+r^*\epsilon)^2}+(\beta\Delta)^2\right]\hat{v}_{\theta_1}$$

$$+\frac{\mathrm{d}\mu_0}{\mathrm{d}r^*}\left[\frac{\mathrm{d}\hat{v}_{\theta_1}}{\mathrm{d}r^*}+i\frac{\gamma\Delta}{(1+r^*\epsilon)}\hat{v}_{r_1}\right]+\frac{\mathrm{d}}{\mathrm{d}r^*}\left[(r^*\Delta+r_1)\frac{\mathrm{d}\mu_0}{\mathrm{d}T_0}\hat{T}_1\frac{\mathrm{d}}{\mathrm{d}r^*}\left(\frac{v_{\theta_0}}{(r^*\Delta+r_1)}\right)\right]$$

$$+2\mu_0 i\gamma\Delta(1+r^*\epsilon)^2\hat{v}_{r_1}-\epsilon\frac{\mathrm{d}\mu_0}{\mathrm{d}r^*}\frac{\hat{v}_{\theta_1}}{(1+r^*\Delta)} \tag{6.73}$$

$$\rho\left(\sigma\Delta^2\hat{v}_{z_1}+i(\gamma\Delta)\Delta\frac{v_{\theta_0}}{(r^*\Delta+r_1)}\hat{v}_{z_1}\right)=-i(\beta\Delta)\Delta\hat{p}_1+\frac{\mathrm{d}\mu_0}{\mathrm{d}r^*}\frac{\mathrm{d}\hat{v}_{z_1}}{\mathrm{d}r^*}$$

$$+\mu_0\left[\frac{\mathrm{d}^2}{\mathrm{d}r^{*2}}+\frac{\epsilon}{(1+r^*\epsilon)}\frac{\mathrm{d}}{\mathrm{d}r^*}-\frac{\epsilon^2}{(1+r^*\epsilon)^2}-\frac{(\gamma\Delta)^2}{(1+r^*\epsilon)^2}-(\beta\Delta)^2\right]\hat{v}_{z_1} \tag{6.74}$$

and the energy equation as

$$\rho\left(\sigma\Delta^2\hat{T}_1+\hat{v}_{r_1}\Delta\frac{\mathrm{d}T_0}{\mathrm{d}r^*}+i(\gamma\Delta)\Delta\frac{v_{\theta_0}\hat{T}_1}{(1+r^*\epsilon)}\right)=k\left[\frac{\mathrm{d}^2}{\mathrm{d}r^{*2}}+\frac{\epsilon}{(1+r^*\epsilon)}\frac{\mathrm{d}}{\mathrm{d}r^*}\right]\hat{T}_1$$

$$-k\left[\frac{\epsilon^2}{(1+r^*\epsilon)^2}+\frac{(\gamma\Delta)^2}{(1+r^*\epsilon)^2}+(\beta\Delta)^2\right]\hat{T}_1+\frac{\mathrm{d}\mu_0}{\mathrm{d}T_0}\hat{T}_1\left[(1+r^*\epsilon\Delta)\frac{\mathrm{d}}{\mathrm{d}r^*}\left(\frac{v_{\theta_0}}{(1+r^*\epsilon)}\right)\right]^2$$

$$+2\mu_0(1+r^*\epsilon)^2\frac{\mathrm{d}}{\mathrm{d}r^*}\left(\frac{v_{\theta_0}}{(1+r^*\epsilon)}\right)\frac{\mathrm{d}}{\mathrm{d}r^*}\left(\frac{\hat{v}_{\theta_1}}{(1+r^*\epsilon)}\right)+2\mu_0\frac{\mathrm{d}}{\mathrm{d}r^*}\left(\frac{v_{\theta_0}}{(1+r^*\epsilon)}\right)i(\gamma\Delta)\hat{v}_{r_1} \tag{6.75}$$

As the gap width $\Delta = (r_2 - r_1)$ goes to zero, $\epsilon \to 0$ and the equation of continuity reduces to

$$\frac{\mathrm{d}\hat{v}_{r1}}{\mathrm{d}r^*} + i(\gamma\Delta)\hat{v}_{\theta_1} + i(\beta\Delta)\hat{v}_{z_1} = 0 \tag{6.76}$$

and the equations of motion reduce to

$$\begin{aligned}\rho\left(\sigma\Delta^2\hat{v}_{r_1} + i(\gamma\Delta)\Delta v_{\theta_0}\hat{v}_{r_1}\right) = -\Delta\frac{\mathrm{d}\hat{p}_1}{\mathrm{d}r^*} + 2\frac{\mathrm{d}\mu_0}{\mathrm{d}r^*}\frac{\mathrm{d}\hat{v}_{r_1}}{\mathrm{d}r^*} + \frac{\mathrm{d}\mu_0}{\mathrm{d}T_0}\hat{T}_1 i(\gamma\Delta)\frac{\mathrm{d}\hat{v}_{\theta_0}}{\mathrm{d}r^*} \\ +\mu_0\left[\frac{\mathrm{d}^2}{\mathrm{d}r^{*2}} - (\gamma\Delta)^2 - (\beta\Delta)^2\right]\hat{v}_{r_1}\end{aligned} \tag{6.77}$$

$$\begin{aligned}\rho\left(\sigma\Delta^2\hat{v}_{\theta_1} + \Delta\hat{v}_{r_1}\frac{\mathrm{d}v_{\theta_0}}{\mathrm{d}r^*} + i(\gamma\Delta)\Delta\hat{v}_{\theta_0}\hat{v}_{\theta_1}\right) = -i\Delta(\gamma\Delta)\hat{p}_1 + \frac{\mathrm{d}}{\mathrm{d}r^*}\left[\frac{\mathrm{d}\mu_0}{\mathrm{d}T_0}\hat{T}_1\frac{\mathrm{d}v_{\theta_0}}{\mathrm{d}r^*}\right] \\ +\frac{\mathrm{d}\mu_0}{\mathrm{d}r^*}\left[\frac{\mathrm{d}\hat{v}_{\theta_1}}{\mathrm{d}r^*} + i(\gamma\Delta)\hat{v}_{r_1}\right] + \mu_0\left[\frac{\mathrm{d}^2}{\mathrm{d}r^{*2}} - (\gamma\Delta)^2 - (\beta\Delta)^2\right]\hat{v}_{\theta_1}\end{aligned} \tag{6.78}$$

$$\rho\left(\sigma\Delta^2\hat{v}_{z_1} + i(\gamma\Delta)\Delta v_{\theta_0}\hat{v}_{z_1}\right) = -i(\beta\Delta)\Delta\hat{p_1} + \frac{\mathrm{d}\mu_0}{\mathrm{d}r^*}\frac{\mathrm{d}\hat{v}_{z_1}}{\mathrm{d}r^*} + \mu_0\left[\frac{\mathrm{d}^2}{\mathrm{d}r^{*2}} - (\gamma\Delta)^2 - (\beta\Delta)^2\right]\hat{v}_{z_1} \tag{6.79}$$

while the energy equation reduces to

$$\begin{aligned}\rho\left(\sigma\Delta^2\hat{T}_1 + \hat{v}_{r_1}\Delta\frac{\mathrm{d}T_0}{\mathrm{d}r^*} + i(\gamma\Delta)\Delta\frac{v_{\theta_0}\hat{T}_1}{(1 + r^*\epsilon)}\right) = k\left[\frac{\mathrm{d}^2}{\mathrm{d}r^{*2}} - (\gamma\Delta)^2 - (\beta\Delta)^2\right]\hat{T}_1 \\ +\frac{\mathrm{d}\mu_0}{\mathrm{d}T_0}\hat{T}_1\left[\frac{\mathrm{d}v_{\theta_0}}{\mathrm{d}r^*}\right]^2 + 2\mu_0\frac{\mathrm{d}v_{\theta_0}}{\mathrm{d}r^*}\left[\frac{\mathrm{d}\hat{v}_{\theta_1}}{\mathrm{d}r^*} + i(\gamma\Delta)\hat{v}_{r_1}\right]\end{aligned} \tag{6.80}$$

Now, scaling x in the unscaled plane Couette equations given in the main body of this chapter with respect to the gap width L we obtain for the equation of continuity

$$\frac{\mathrm{d}\hat{v}_{x1}}{\mathrm{d}x^*} + i(\beta L)\hat{v}_{y_1} + i(\gamma L)\hat{v}_{z_1} = 0 \tag{6.81}$$

and for the equations of motion

$$\begin{aligned}\rho\left(\sigma L^2\hat{v}_{x_1} + i(\gamma L)v_{z_0}\hat{v}_{x_1}\right) &= -L\frac{\mathrm{d}\hat{p}_1}{\mathrm{d}x^*} + 2\frac{\mathrm{d}\mu_0}{\mathrm{d}x^*}\frac{\mathrm{d}\hat{v}_{x1}}{\mathrm{d}x^*} + i(\gamma L)\left(\frac{\mathrm{d}\mu_0}{\mathrm{d}T_0}\right)\hat{T}_1\frac{\mathrm{d}v_{z_0}}{\mathrm{d}x^*} \\ &\quad +\mu_0\left[\frac{\mathrm{d}^2\hat{v}_{x1}}{\mathrm{d}x^{*2}} - (\beta L)^2\hat{v}_{x_1} - (\gamma L)^2\hat{v}_{x_1}\right]\end{aligned} \tag{6.82}$$

$$\begin{aligned}\rho\left(\sigma L^2\hat{v}_{y_1} + i(\gamma L)v_{z_0}\hat{v}_{y_1}\right) &= -i(\beta L)L\hat{p}_1 + \frac{\mathrm{d}\mu_0}{\mathrm{d}x^*}\left[\frac{\mathrm{d}\hat{v}_{y1}}{\mathrm{d}x^*} + i(\beta L)v_{x_1}\right] \\ &\quad +\mu_0\left[\frac{\mathrm{d}^2\hat{v}_{y1}}{\mathrm{d}x^{*2}} - (\beta L)^2\hat{v}_{y_1} - (\gamma L)^2\hat{v}_{y_1}\right]\end{aligned} \tag{6.83}$$

Table 6.3: Correspondence between circular Couette flow and the plane Couette flow

Circular Couette flow	plane Couette flow
θ component	z component
r component	x component
z component	y component

$$\rho\left(\sigma L^2\hat{v}_{z_1} + i(\gamma L)Lv_{z_0}\hat{v}_{z_1} + L\frac{\mathrm{d}v_{z0}}{\mathrm{d}x^*}\hat{v}_{x_1}\right) = -i(\gamma L)L\hat{p}_1 + \frac{\mathrm{d}\mu_0}{\mathrm{d}x^*}\left[\frac{\mathrm{d}\hat{v}_{z_1}}{\mathrm{d}x^*} + i(\gamma L)v_{x_1}\right]$$
$$+\frac{\mathrm{d}}{\mathrm{d}x^*}\left[\left(\frac{\mathrm{d}\mu_0}{\mathrm{d}T_0}\right)\hat{T}_1\frac{\mathrm{d}v_{z_0}}{\mathrm{d}x^*}\right] + \mu_0\left[\frac{\mathrm{d}^2\hat{v}_{z_1}}{\mathrm{d}x^{*2}} - (\beta L)^2\hat{v}_{z_1} - (\gamma L)^2\hat{v}_{z_1}\right] \quad (6.84)$$

and for the energy equation

$$\rho C_v\left[\sigma L^2\hat{T}_1 + L\hat{v}_{x_1}\frac{\mathrm{d}T_0}{\mathrm{d}x^*} + i(\gamma L)Lv_{z_0}\hat{T}_1\right] = k\left[\frac{\mathrm{d}^2\hat{T}_1}{\mathrm{d}x^{*2}} - (\beta L)^2\hat{T}_1 - (\gamma L)^2\hat{T}_1\right]$$
$$+2\mu_0\frac{\mathrm{d}v_{z_0}}{\mathrm{d}x^*}\left[\frac{\mathrm{d}\hat{v}_{z_1}}{\mathrm{d}x^*} + i(\gamma L)\hat{v}_{x_1}\right] + \frac{\mathrm{d}\mu_0}{\mathrm{d}T_0}\hat{T}_1\left[\frac{\mathrm{d}v_{z_0}}{\mathrm{d}x^*}\right]^2 \quad (6.85)$$

Inspecting the equations in circular Couette flow as $\epsilon \to 0$ and the corresponding equations in plane Couette flow, we find that as the gap width goes to zero, the circular equations reduce to plane Couette equations in this scaling with the following correspondence between them as indicated in table 6.3

6.1.2 The Boundary Condition at Constant Wall Stress

In the main body of this chapter, we used the following boundary condition at constant wall stress at $x = +1$ at constant temperature: $\frac{\mathrm{d}\hat{v}_{z1}}{\mathrm{d}x}(x = +1) = 0$. We will learn in this endnote that this is a simplification of the real situation at constant wall stress and it was done purely to obtain an easier calculation procedure. To see what the correct boundary condition at constant wall stress is, let us first consider the perturbed equations in $v_{z_1}, v_{z_1}, p_1, \theta_1$. These equations are partial differential equations in x, z and t. Now, the average shear stress on the fluid layer at $x = +1$ can be held constant by holding the the force on the plate constant. The boundary condition is then

$$\int_{z=0}^{z=W} \frac{\mathrm{d}\hat{v}_{z_1}}{\mathrm{d}x}\mathrm{d}z = 0$$

where $v_{z_1}(x = +1)$ cannot be a function of z as the plate is rigid. This problem with this boundary condition is well posed and though difficult, can be solved. The difficulty, one might observe, stems from the fact that partial differential equations have to be solved. Now, to simplify the calculation, if one introduces Fourier modes to reduce the partial differential equations to ordinary differential equations, it leads to a problem at the wall as the wall velocity cannot change with z. Now, there is an approximation which makes the calculation a lot easier. In this, we first reduce the partial differential equations to ordinary differential equations by introducing Fourier modes. This, of course, is done pretending that the wall does not exist. Then, we assume that the integral condition that arises at constant force can be applied pointwise, i.e., we assume that there is no variation in the shear stress at $x = +1$ across z. This simplification not only leads to a well posed problem but also to a calculation that is a lot easier. This in fact was the simplification used in calculating the stability at constant wall stress.

6.1.3 The Stability of the Perturbed Equations when the Wave Number, $\gamma = 0, \beta \neq 0$

In the main body of this chapter, we asserted that it is enough to consider the two dimensional problem in x and z and carried out our stability calculation for this problem. In this endnote, we will consider its companion two dimensional problem in x and y and see whether it is stable. If indeed it is stable, then it will further fortify our original supposition that it is not necessary to consider the stability of the complete three dimensional flow for this problem.

The two dimensional problem in x and y with the wave number $\gamma = 0, \beta \neq 0$ ought to be stable for the following reason: The equations at $\gamma = 0, \beta \neq 0$ correspond to the narrow gap limit of the problem that describes the the circular Couette flow between concentric cylinders. However, the biggest difference is that the centrifugal term that causes the Taylor instability in the circular Couette flow is lost due to thin gapping. This would then mean that this flow should be stable to small disturbances provided the viscosity variation with temperature does not affect the stability. To see whether this is true, let us first consider the perturbed equations at $\beta \neq 0$ and $\gamma = 0$

$$\frac{\mathrm{d}\hat{v}_{x_1}}{\mathrm{d}x} + i\beta\hat{v}_{y_1} = 0 \tag{6.86}$$

$$\sigma\hat{v}_{x_1} = -\frac{\mathrm{d}\hat{p}_1}{\mathrm{d}x} + 2\frac{\mathrm{d}\mu_0}{\mathrm{d}x}\frac{\mathrm{d}\hat{v}_{x_1}}{\mathrm{d}x} + \mu_0\left[\frac{\mathrm{d}^2\hat{v}_{x_1}}{\mathrm{d}x^2} - \beta^2\hat{v}_{x_1}\right] \tag{6.87}$$

$$\sigma\hat{v}_{y_1} = -i\beta\hat{p}_1 + \frac{\mathrm{d}\mu_0}{\mathrm{d}x}\left[\frac{\mathrm{d}\hat{v}_{y_1}}{\mathrm{d}x} + i\beta v_{x_1}\right] + \mu_0\left[\frac{\mathrm{d}^2\hat{v}_{y_1}}{\mathrm{d}x^2} - \beta^2\hat{v}_{y_1}\right] \tag{6.88}$$

$$\sigma\hat{v}_{z_1} + \mathrm{Re}\frac{\mathrm{d}v_{z_0}}{\mathrm{d}x}\hat{v}_{x_1} = \frac{\mathrm{d}\mu_0}{\mathrm{d}x}\left[\frac{\mathrm{d}\hat{v}_{z_1}}{\mathrm{d}x}\right] + \frac{\mathrm{d}}{\mathrm{d}x}\left[\left(\frac{\mathrm{d}\mu_0}{\mathrm{d}\theta_0}\right)\hat{\theta}_1\frac{\mathrm{d}v_{z_0}}{\mathrm{d}x}\right] + \mu_0\left[\frac{\mathrm{d}^2\hat{v}_{z_1}}{\mathrm{d}x^2} - \beta^2\hat{v}_{z_1}\right] \tag{6.89}$$

$$\sigma\mathrm{Pr}\hat{\theta}_1 + \mathrm{RePr}\hat{v}_{x_1}\frac{\mathrm{d}\theta_0}{\mathrm{d}x} = \frac{\mathrm{d}^2\hat{\theta}_1}{\mathrm{d}x^2} - \beta^2\hat{\theta}_1 + \frac{\mathrm{d}\mu_0}{\mathrm{d}\theta_0}\hat{\theta}_1\left[\frac{\mathrm{d}v_{z_0}}{\mathrm{d}x}\right]^2 + 2\mu_0\frac{\mathrm{d}v_{z_0}}{\mathrm{d}x}\frac{\mathrm{d}\hat{v}_{z_1}}{\mathrm{d}x} \tag{6.90}$$

Note that in the above set of equations, only $\hat{v}_{x_1}, \hat{v}_{y_1}$ and $\hat{p}_1$ can be determined independent of $\hat{v}_{z_1}$ and $\hat{\theta}_1$. Now, it is possible to prove that the eigenvalues that determine $\hat{v}_{x_1}$ and $\hat{v}_{y_1}$ are negative. To do this, we first eliminate pressure, by multiplying the x component by $-i\beta$, and then differentiating the y component and adding them to obtain.

$$\begin{aligned}\rho\sigma\left[\frac{\mathrm{d}\hat{v}_{y_1}}{\mathrm{d}x} - i\beta\hat{v}_{x_1}\right] = {} & \frac{\mathrm{d}^2\mu_0}{\mathrm{d}x^2}\left[i\beta\hat{v}_{x_1} + \frac{\mathrm{d}\hat{v}_{y_1}}{\mathrm{d}x}\right] + \frac{\mathrm{d}\mu_0}{\mathrm{d}x}\left[i\beta\frac{\mathrm{d}\hat{v}_{x_1}}{\mathrm{d}x} + \frac{\mathrm{d}^2\hat{v}_{y_1}}{\mathrm{d}x^2}\right] \\ & + \mu_0\left[\frac{\mathrm{d}^3\hat{v}_{y_1}}{\mathrm{d}x^3} - \beta^2\frac{\mathrm{d}\hat{v}_{y_1}}{\mathrm{d}x}\right] + \frac{\mathrm{d}\mu_0}{\mathrm{d}x}\left[\frac{\mathrm{d}^2\hat{v}_{y_1}}{\mathrm{d}x^2} - \beta^2\hat{v}_{y_1}\right] \\ & - i\beta\mu_0\left[\frac{\mathrm{d}^2\hat{v}_{x_1}}{\mathrm{d}x^2} - \beta^2\hat{v}_{x_1}\right] - 2i\beta\frac{\mathrm{d}\mu_0}{\mathrm{d}x}\frac{\mathrm{d}\hat{v}_{x_1}}{\mathrm{d}x}\end{aligned} \tag{6.91}$$

Introducing the stream function $\hat{\Psi}_1$ such that $\hat{v}_{y_1} = \frac{\mathrm{d}\hat{\Psi}_1}{\mathrm{d}x}$ and $\hat{v}_{x_1} = -i\beta\hat{\Psi}_1$ where the stream function satisfies the equation of continuity, we obtain,

$$\begin{aligned}\rho\sigma\left[\frac{\mathrm{d}^2\hat{\Psi}_1}{\mathrm{d}x^2} - \beta^2\hat{\Psi}_1\right] = {} & \frac{\mathrm{d}^2\mu_0}{\mathrm{d}x^2}\left[\beta^2\hat{\psi}_1 + \frac{\mathrm{d}^2\hat{\Psi}_1}{\mathrm{d}x^2}\right] + \frac{\mathrm{d}\mu_0}{\mathrm{d}x}\left[\frac{\mathrm{d}^3\hat{\Psi}_1}{\mathrm{d}x^3} + \beta^2\hat{\Psi}_1\right] \\ & + \mu_0\left[\frac{\mathrm{d}^4\hat{\Psi}_1}{\mathrm{d}x^4} - \beta^2\frac{\mathrm{d}^2\hat{\Psi}_1}{\mathrm{d}x^2}\right] + \frac{\mathrm{d}\mu_0}{\mathrm{d}x}\left[\frac{\mathrm{d}^3\hat{\Psi}_1}{\mathrm{d}x^3} - \beta^2\frac{\mathrm{d}\hat{\Psi}_1}{\mathrm{d}x}\right] \\ & - \beta^2\mu_0\frac{\mathrm{d}^2\hat{\Psi}_1}{\mathrm{d}x^2} + \beta^4\mu_0\hat{\Psi}_1 - 2\beta^2\frac{\mathrm{d}\mu_0}{\mathrm{d}x}\frac{\mathrm{d}\hat{\Psi}_1}{\mathrm{d}x}\end{aligned} \tag{6.92}$$

Simplifying, we obtain,

$$\rho\sigma\left[\frac{\mathrm{d}^2\hat{\Psi}_1}{\mathrm{d}x^2}-\beta^2\hat{\Psi}_1\right]=\frac{\mathrm{d}^2}{\mathrm{d}x^2}\left[\mu_0\frac{\mathrm{d}^2\hat{\Psi}_1}{\mathrm{d}x^2}\right]-2\beta^2\frac{\mathrm{d}}{\mathrm{d}x}\left[\mu_0\frac{\mathrm{d}\hat{\Psi}_1}{\mathrm{d}x}\right] \\ +\beta^4\mu_0\hat{\Psi}_1+\beta^2\frac{\mathrm{d}^2\mu_0}{\mathrm{d}x^2}\hat{\Psi}_1 \tag{6.93}$$

The boundary conditions are

$$x=\pm 1, \hat{\psi}_1=\frac{\mathrm{d}\hat{\psi}_1}{\mathrm{d}x}=0$$

Now, to prove that the eigenvalues determined by this equation are negative, multiply the equation by $\overline{\hat{\Psi}_1}$, where $\overline{\hat{\Psi}_1}$ denotes the complex conjugate of $\hat{\Psi}_1$ and $\hat{\Psi}_1\overline{\hat{\Psi}_1}=|\hat{\Psi}_1|^2$ and integrate it between -1 to 1 to obtain

$$\sigma\left[-\int_{-1}^{+1}|\frac{\mathrm{d}\hat{\Psi}_1}{\mathrm{d}x}|^2\mathrm{d}x-\beta^2\int_{-1}^{+1}|\hat{\Psi}_1|^2\mathrm{d}x\right]=\int_{-1}^{+1}\mu_0|\frac{\mathrm{d}^2\hat{\Psi}_1}{\mathrm{d}x^2}|^2\mathrm{d}x+\beta^2\int_{-1}^{+1}\frac{\mathrm{d}^2\mu_0}{\mathrm{d}x^2}|\hat{\Psi}_1|^2\mathrm{d}x \\ +\beta^4\int_{-1}^{+1}\mu_0|\hat{\Psi}_1|^2\mathrm{d}x+2\beta^2\int_{-1}^{+1}\mu_0|\frac{\mathrm{d}\hat{\Psi}_1}{\mathrm{d}x}|^2\mathrm{d}x \tag{6.94}$$

Therefore,

$$\sigma=-\frac{\int_{-1}^{+1}\left\{\mu_0|\frac{\mathrm{d}^2\hat{\Psi}_1}{\mathrm{d}x^2}|^2+\beta^2\frac{\mathrm{d}^2\mu_0}{\mathrm{d}x^2}|\hat{\Psi}_1|^2+\beta^4\mu_0|\hat{\Psi}_1|^2+2\beta^2\mu_0|\frac{\mathrm{d}\hat{\Psi}_1}{\mathrm{d}x}|^2\right\}\mathrm{d}x}{\left[\int_{-1}^{+1}|\frac{\mathrm{d}\hat{\Psi}_1}{\mathrm{d}x}|^2\mathrm{d}x+\beta^2\int_{-1}^{+1}|\hat{\Psi}_1|^2\mathrm{d}x\right]} \tag{6.95}$$

This equation shows that the eigenvalues that determine $\hat{v}_{x_1}$ and $\hat{v}_{y_1}$ are negative. This then means $\hat{v}_{x_1}$ and $\hat{v}_{y_1}$ must decay with time, no matter what $\hat{v}_{z_1}$ and $\hat{\theta}_1$ do. Now, observe the z component of the equation of motion and the energy equation. In addition to $\hat{v}_{z_1}$ and $\hat{\theta}_1$, these equations also have $\hat{v}_{x_1}$ in them. Now, all the eigenvalues that correspond to a non-zero value of $\hat{v}_{x_1}$ have already been determined. Therefore, to determine the remaining eigenvalues for this flow, we may put $\hat{v}_{x_1}=0$ in these two equations. When we do this, these equations become independent of $\hat{v}_{x_1}$ and $\hat{v}_{y_1}$. Not only that, they look very similar to the zero wave number equations with an extra added diffusion term due to β. Now, we know that at zero wave number, the flow is stable at constant wall speed. The extra added diffusion term can only further stabilize the flow. The conclusion then is that the eigenvalues that determine $\hat{v}_{z_1}$ and $\hat{\theta}_1$ must also be negative. This then means that the flow is stable to disturbances $\gamma = 0$, $\beta \neq 0$ at constant wall speed. This result further fortifies our original belief that the y component of the equation of motion does not affect the stability of the flow and hence need not be considered while studying the stability.

6.1.4 A comment on the Non-Zero Wave Number Equations in the limit $\gamma \to 0$

Earlier in this chapter, we made a calculation to prove that as the wave number changes from zero, the eigenvalues develop a purely oscillatory component. To check this result, one might calculate the eigenvalues at very small wave numbers and see whether the real part of the eigenvalues from such a calculation match with those from a zero wave number calculation. It turns out that one has to be extremely careful while interpreting the result from such a calculation at low wave numbers. To see why, let us first write the non-zero wave number equations in the stream function formulation. The equations are

$$\sigma \frac{\mathrm{d}^2\hat{\psi}_1}{\mathrm{d}x^2} - \sigma\gamma^2\hat{\psi} = \frac{\mathrm{d}^2}{\mathrm{d}x^2}\left[\mu_0 \frac{\mathrm{d}^2\hat{\psi}_1}{\mathrm{d}x^2}\right] - 2\gamma^2 \frac{\mathrm{d}}{\mathrm{d}x}\left[\mu_0 \frac{\mathrm{d}\hat{\psi}_1}{\mathrm{d}x}\right] - i\gamma\mathrm{Re}v_{z_0}\frac{\mathrm{d}^2\hat{\psi}_1}{\mathrm{d}x^2}$$
$$\left[i\gamma^3\mathrm{Re}v_{z_0} + i\gamma\mathrm{Re}\frac{\mathrm{d}^2 v_{z_0}}{\mathrm{d}x^2} + \gamma^4\mu_0 + \gamma^2\frac{\mathrm{d}^2\mu_0}{\mathrm{d}x^2}\right]\hat{\psi}_1 + \tau_{xz0}\frac{\mathrm{d}^2\hat{\theta}_1}{\mathrm{d}x^2} + \gamma^2\tau_{xz_0}\theta_1 \qquad (6.96)$$

$$\sigma\mathrm{Pr}\hat{\theta}_1 + i\gamma\mathrm{RePr}\hat{\psi}_1\frac{\mathrm{d}\theta_0}{\mathrm{d}x} + i\gamma\mathrm{RePr}v_{z_0}\hat{\theta}_1 = \frac{\mathrm{d}^2\hat{\theta}_1}{\mathrm{d}x^2} - \gamma^2\hat{\theta}_1 + \tau_{xz0}^2\frac{\frac{\mathrm{d}\mu_0}{\mathrm{d}\theta_0}}{\mu_0^2}\hat{\theta}_1$$
$$-2\tau_{xz0}\left[\frac{\mathrm{d}^2\hat{\psi}_1}{\mathrm{d}x^2} + \gamma^2\hat{\psi}_1\right] \qquad (6.97)$$

Let us take the specific case of constant wall speed. Under this condition, the boundary conditions are

$\hat{\theta}_1(x = \pm 1) = 0$, $\hat{\psi}_1 = \frac{\mathrm{d}\hat{\psi}_1}{\mathrm{d}x} = 0$ at $x = \pm 1$.

A key point about the boundary condition is worth mentioning here: Note that the condition $\hat{\psi}_1 = 0$ at $x = \pm 1$ directly comes from the fact that $\hat{v}_{x_1} = 0$ at $x = \pm 1$. Now, by definition of a stream function, the difference between its value at any two points gives the net flow between those two points. Now, the stream function is zero both at $x = -1$ and $x = +1$. This then means that there cannot be any net flow in the perturbation at non-zero wave number. All the eigenvalues in the two dimensional flow therefore correspond to no net flow.

At zero wave number, the flow is one dimensional as $\hat{v}_{x_1}$ is zero. Therefore, writing the zero wave number equations in the stream function formulation is unnecessary. However, if one chooses to do so, the equations are then:

$$\sigma \frac{\mathrm{d}^2 \hat{\psi}_1}{\mathrm{d}x^2} = \frac{\mathrm{d}^2}{\mathrm{d}x^2}\left[\mu_0 \frac{\mathrm{d}^2 \hat{\psi}_1}{\mathrm{d}x^2}\right] + \tau_{xz0} \frac{\mathrm{d}^2 \hat{\theta}_1}{\mathrm{d}x^2} \tag{6.98}$$

$$\sigma \mathrm{Pr} \hat{\theta}_1 = \frac{\mathrm{d}^2 \hat{\theta}_1}{\mathrm{d}x^2} + \tau_{xz0}^2 \frac{\frac{\mathrm{d}\mu_0}{\mathrm{d}\theta_0}}{\mu_0^2} \hat{\theta}_1 - 2\tau_{xz0} \frac{\mathrm{d}^2 \hat{\psi}_1}{\mathrm{d}x^2} \tag{6.99}$$

Let us turn to the boundary conditions: The condition that the wall speed is held fixed at $x = \pm 1$ leads to $\frac{\mathrm{d}\hat{\psi}_1}{\mathrm{d}x} = 0$ at $x = \pm 1$. Constant temperature on both the walls yield $\hat{\theta}_1 = 0$ at $x = \pm 1$. Now, as $\hat{v}_{x_1}$ does not appear at zero wave number writing $\hat{\psi}_1 = 0$ at $x = \pm 1$ is not a valid boundary condition. To get the other two boundary conditions, realize that at zero wave number and for an exponential fluidity,

$$\sigma \hat{v}_{z_1} = \frac{\mathrm{d}}{\mathrm{d}x}\left[\mu_0 \frac{\mathrm{d}\hat{v}_{z_1}}{\mathrm{d}x} - \tau_{xz0} \hat{\theta}_1\right]$$

Substituting $\hat{v}_{z_1} = -\frac{\mathrm{d}\hat{\psi}_1}{\mathrm{d}x}$ in this equation, we obtain

$$\sigma \frac{\mathrm{d}\hat{\psi}_1}{\mathrm{d}x} = \frac{\mathrm{d}}{\mathrm{d}x}\left[\mu_0 \frac{\mathrm{d}^2 \hat{\psi}_1}{\mathrm{d}x^2} + \tau_{xz0} \hat{\theta}_1\right]$$

Now setting $\frac{\mathrm{d}\hat{\psi}_1}{\mathrm{d}x} = 0$ at $x = \pm 1$, which is tantamount to using $\hat{v}_{z_1} = 0$ at $x = \pm 1$ once again, yields $\frac{\mathrm{d}}{\mathrm{d}x}\left[\mu_0 \frac{\mathrm{d}^2 \hat{\psi}_1}{\mathrm{d}x^2} + \tau_{xz0} \hat{\theta}_1\right] = 0$ at $x = \pm 1$. These are the other two boundary conditions to be used for the zero wave number equations in stream function formulation. This then is the correct model for calculating the eigenvalues at zero wave number in the fourth order stream function formulation.

Now, let us see what happens as we substitute very low values of the wave number in the non-zero wave number equations and try to recover the eigenvalues

Table 6.4: The comparison of the first few eigenvalues from a zero wave number calculation with those arising from setting $\gamma = 0.01$ in the non-zero wave number equations. The chosen parameter values are $\tau_{xz0} = 0.5, V_0 = 1.09$, Re=1, Pr=1.

The eigenvalues at zero wave number	The real part of the eigenvalues at non-zero wave number	The corresponding imaginary part
-2.19		
-2.61	-2.61	-5.5×10^{-3}
-8.95	-8.95	-5.5×10^{-3}
-9.98	-9.70	-5.5×10^{-3}
-20.20	-18.55	-5.5×10^{-3}
-22.27	-22.27	-5.5×10^{-3}
-35.94	-35.97	-5.5×10^{-3}

at zero wave number. Before that, once again recall that at zero wave number, the flow is one dimensional. There is no restriction on the flow to turn and repeat itself periodically. Consequently, it is possible that there are modes which allow net flow. Now, by using $\hat{\psi}_1 = 0$ at $x = \pm 1$ in a non-zero wave number calculation, we look only for those eigenvalues that allow no net flow. Therefore, in this calculation, as $\gamma \to 0$, we will lose those eigenvalues that correspond to a net flow. Indeed this is exactly what we observed in our calculations when we set very low values of γ in the non-zero wave number equations and compared the eigenvalues with those arising from a zero wave number calculation that are based on a correct model. Table 6.1.4 shows a comparison of the first few eigenvalues at zero wave number with those from a non-zero wave number with $\gamma = 0.01$. We chose $\tau_{xz0} = 0.5, V_0 = 1.098$ and $\mathrm{Re} = 1, \mathrm{Pr} = 1$ for this calculation. The eigenvalues are arranged based on decreasing real part.

From the table observe that the eigenvalue -2.19 at zero wave number is missing in the non-zero wave number calculation. This in fact is the eigenvalue that corresponds to a net flow in the perturbation. The real part of the other eigenvalues match with those from a zero wave number calculation. This then is in agreement with our earlier analytical result that the real part of the eigenvalue does not change as the wave number is changed slightly from zero.

6.1.5 Is an Inflexion point necessary for an Instability in Viscous Shear Flows?

Lord Rayleigh's inflexion point theorem for inviscid fluids states that the necessary condition for an instability in a shear flow is that the base profile should have a point of inflexion. Mathematically, an inflexion point in the velocity profile can be defined as follows: If the velocity v_{z_0} is a function of x, then the point where $\frac{\mathrm{d}^2 v_{z0}}{\mathrm{d}x^2}$ changes sign is a point of inflexion in the velocity profile. Now, an inflexion point is a necessary condition but not a sufficient condition for an instability, i.e., a flow with an inflexion point in its base velocity profile may still be stable. All this is true in the inviscid limit. Now, incorporating a finite viscosity, one might assume, is stabilizing. However, it turns out that this is not true for shear flows of these kind. In fact, a small amount of viscosity turns out be destabilizing in a flow where the totally inviscid limit is stable! A classic example wherein this is true is the case of isoviscous plane Poiseulle flow, which has a parabolic velocity profile. For this case, in scaled terms, the velocity v_{z_0} can be written as $1-x^2$, where x is the scaled gap width which is zero at the channel centre and one at the wall. There are no inflexion points in the base profile as $\frac{\mathrm{d}^2 v_{z0}}{\mathrm{d}x^2}$ in this case is equal to a constant, -2. However, it turns out from a numerical calculation that this flow goes unstable to small disturbances for a Reynolds number of 5772. The conclusion therefore is that an inflexion point is not necessary for an instability in viscous shear flows. In fact, we checked this to be true for the Couette flow problem with a temperature dependent viscosity and with an adiabatic top wall and a conducting bottom wall as illustrated in fig(6.1). The base velocity profile arising out of this combination of temperature boundary conditions does not have a point of inflexion as $\frac{\mathrm{d}^2 v_{z0}}{\mathrm{d}x^2}$ in this case is equal to $\tau_{xz0}\frac{\mathrm{d}f_0}{\mathrm{d}x}$ and $\frac{\mathrm{d}f_0}{\mathrm{d}x} \geq 0$. However, our numerical calculations for this case show that the flow indeed does go unstable at constant wall speed. Of course, the value at which an instability sets in corresponds to an rpm which is well beyond the realms of a physical experiment.

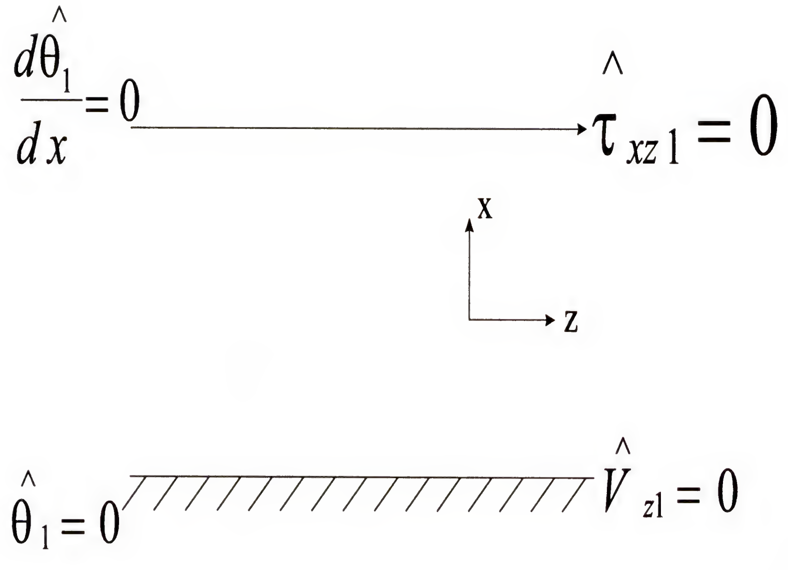

Figure 6.1: Schematic of plane Couette flow with an adiabatic top wall and a conducting bottom wall

The point here is just to prove it is not necessary to have an inflexion point in the base profile for an instability to develop in viscous shear flows.

6.1.6 Comparison of our Stability Results with an earlier work

In this endnote, we will check to see whether we are able to reproduce the stability results of earlier workers Yueh and Weng[11] from our calculations as doing this successfully would fortify our belief in the numerical scheme that we follow. To do this, the first observation we make is that in their work, Yueh and Weng employ a different velocity and temperature scale. In fact, the scaling option that we discussed in an endnote of chapter 2 with the wall speed as the velocity scale and the wall temperature as the temperature scale is the basis for their scaling. The scaled base temperature and velocity equations in this scaling are

$$0=\frac{\mathrm{d}^2\theta_0}{\mathrm{d}x^2}+\mathrm{Br}\tau_{xz_0}^2 f_0$$

$$v_{z_0}(x=+1)-v_{z_0}(x=-1)=1/2-(-1/2)=1=\tau_{xz_0}\int_{-1}^{1} f_0\mathrm{d}x$$

respectively where $\mathrm{Br}=\frac{\mu_w V_0^2}{kT_w}$ is Brinkmann number. Observe that we have used the velocity boundary condition that the top wall moves with a velocity of $V_0/2$ and the bottom wall moves with a velocity of $-V_0/2$ while integrating the definition of shear stress. Yueh and Weng follow this convention, possibly for the symmetry in the velocity profile that results. To make a proper comparison with their result we too follow the same convention here even though this is different from that we have been following thus far, viz., assuming that the bottom wall is fixed and the top wall moves with a velocity V_0. The scaled velocity in this scaling therefore goes from $-1/2$ to $1/2$.

Even though Yueh and Weng have considered both exponential and Arrhenius fluidity for their stability calculation, we will consider only the case of exponential fluidity dependence for comparison as that is the case of the most interest to us. For exponential dependence of viscosity on temperature, f_0 in this scaling is equal to $\mathrm{e}^{\alpha\theta_0}$ where α is the sensitivity.

The perturbed equations in this scaling for an exponential dependence of viscosity on temperature are

$$\frac{\mathrm{d}\hat{v}_{x_1}}{\mathrm{d}x} + i\gamma\hat{v}_{z_1} = 0 \tag{6.100}$$

$$\begin{aligned} \sigma\hat{v}_{x_1} + i\gamma\mathrm{Re}v_{z_0}\hat{v}_{x_1} &= -\frac{\mathrm{d}\hat{p}_1}{\mathrm{d}x} + 2\frac{\mathrm{d}\mu_0}{\mathrm{d}x}\frac{\mathrm{d}\hat{v}_{x_1}}{\mathrm{d}x} - i\alpha\gamma\tau_{xz_0}\hat{\theta}_1 \\ &\quad +\mu_0\left[\frac{\mathrm{d}^2\hat{v}_{x_1}}{\mathrm{d}x^2} - \gamma^2\hat{v}_{x_1}\right] \end{aligned} \tag{6.101}$$

$$\begin{aligned} \sigma\hat{v}_{z_1} + i\gamma\mathrm{Re}v_{z_0}\hat{v}_{z_1} + \mathrm{Re}\frac{\mathrm{d}v_{z_0}}{\mathrm{d}x}\hat{v}_{x_1} &= -i\gamma\hat{p}_1 + \frac{\mathrm{d}\mu_0}{\mathrm{d}x}\left[\frac{\mathrm{d}\hat{v}_{z_1}}{\mathrm{d}x} + i\gamma v_{x_1}\right] \\ &\quad -\alpha\tau_{xz_0}\hat{\theta}_1 + \mu_0\left[\frac{\mathrm{d}^2\hat{v}_{z_1}}{\mathrm{d}x^2} - \gamma^2\hat{v}_{z_1}\right] \end{aligned} \tag{6.102}$$

$$\begin{aligned} \sigma\mathrm{Pr}\hat{\theta}_1 + \mathrm{RePr}\hat{v}_{x_1}\frac{\mathrm{d}\theta_0}{\mathrm{d}x} + i\gamma\mathrm{RePr}v_{z_0}\hat{\theta}_1 &= \frac{\mathrm{d}^2\hat{\theta}_1}{\mathrm{d}x^2} - \gamma^2\hat{\theta}_1 + \mathrm{Br}\tau_{xz_0}^2\frac{\frac{\mathrm{d}\mu_0}{\mathrm{d}\theta_0}}{\mu_0^2}\hat{\theta}_1 \\ &\quad +2\mathrm{Br}\tau_{xz_0}\left[\frac{\mathrm{d}\hat{v}_{z_1}}{\mathrm{d}x} + i\gamma\hat{v}_{x_1}\right] \end{aligned} \tag{6.103}$$

The boundary conditions on these variables satisfy

$$\hat{v}_{z_1}(x = \pm 1) = 0, \hat{v}_{x_1}(x = \pm 1) = 0, \hat{\theta}_1(x = \pm 1) = 0$$

if the wall speed is held fixed and

$$\frac{\mathrm{d}\hat{v}_{z1}}{\mathrm{d}x}(x=+1)=0, \hat{v}_{z_1}(x=-1)=0, \hat{v}_{x_1}(x=\pm 1)=0, \hat{\theta}_1(x=\pm 1)=0$$

if the wall stress is held fixed. In their work, Yueh and Weng have considered only the case of constant wall speed. Hence, that is the only case we will consider in this endnote. Now, writing the equations in stream function formulation with the stream function $\hat{\psi}_1$ which satisfies the equation of continuity such that $\hat{v}_{z_1} = -\frac{\mathrm{d}\hat{\psi}_1}{\mathrm{d}x}$ and $\hat{v}_{x_1} = i\gamma\hat{\psi}_1$. The x and z components of the equation of motion then combine to give

$$\sigma\frac{\mathrm{d}^2\hat{\psi}_1}{\mathrm{d}x^2} - \sigma\gamma^2\hat{\psi} = \frac{\mathrm{d}^2}{\mathrm{d}x^2}\left[\mu_0\frac{\mathrm{d}^2\hat{\psi}_1}{\mathrm{d}x^2}\right] - 2\gamma^2\frac{\mathrm{d}}{\mathrm{d}x}\left[\mu_0\frac{\mathrm{d}\hat{\psi}_1}{\mathrm{d}x}\right] - i\gamma\mathrm{Re}v_{z_0}\frac{\mathrm{d}^2\hat{\psi}_1}{\mathrm{d}x^2}$$
$$\left[i\gamma^3\mathrm{Re}v_{z_0} + i\gamma\mathrm{Re}\frac{\mathrm{d}^2v_{z0}}{\mathrm{d}x^2} + \gamma^4\mu_0 + \gamma^2\frac{\mathrm{d}^2\mu_0}{\mathrm{d}x^2}\right]\hat{\psi}_1 + \alpha\tau_{xz0}\frac{\mathrm{d}^2\hat{\theta}_1}{\mathrm{d}x^2} + \alpha\gamma^2\tau_{xz_0}\hat{\theta}_1 \quad (6.104)$$

and the energy equation is

$$\sigma\mathrm{Pr}\hat{\theta}_1 + i\gamma\mathrm{RePr}\hat{\psi}_1\frac{\mathrm{d}\theta_0}{\mathrm{d}x} + i\gamma\mathrm{RePr}v_{z_0}\hat{\theta}_1 = \frac{\mathrm{d}^2\hat{\theta}_1}{\mathrm{d}x^2} - \gamma^2\hat{\theta}_1 + \mathrm{Br}\tau_{xz_0}^2\frac{\frac{\mathrm{d}\mu_0}{\mathrm{d}\theta_0}}{\mu_0^2}\hat{\theta}_1$$
$$-2\mathrm{Br}\tau_{xz0}\left[\frac{\mathrm{d}^2\hat{\psi}_1}{\mathrm{d}x^2} + \gamma^2\hat{\psi}_1\right] \quad (6.105)$$

with the boundary condition

$\hat{\psi}_1 = \frac{\mathrm{d}\hat{\psi}_1}{\mathrm{d}x} = \hat{\theta}_1 = 0$ at $x = \pm 1$

if the wall speed is held fixed at $x = 1$.

Note that these equations look identical to those in the scaling that we work with except for the group Br and the sensitivity parameter α. Also, the scaled base velocity and base viscosity profiles are different in this scaling as compared to our scaling.

Yueh and Weng have plotted a stability curve of the critical Reynolds number vs. the wave number for a chosen value of $\mathrm{Br} = 20, \mathrm{Pr} = 50$, for a liquid with an exponential fluidity dependence with the sensitivity $\alpha = 5$. We will check this result

Table 6.5: Comparison of the result of Yueh and Weng with our calculations: The critical Reynold's number vs. the wave number for $\mathrm{Br} = 20, \mathrm{Pr} = 50$.

	The critical wave number, γ	
Re	as read from Yueh's graph	Our calculation
20	0.62	0.63
50	0.22	0.22
100	0.11	0.11
120	0.16	0.16

with our numerical calculation. Table 6.1.6 shows the comparison. From the table we find that our numerical results match well with the result of Yueh and Weng.

Now, we will check to see whether the scaled wall speed V_0 corresponding to the above critical parameter values are possible in an experiment. It turns out that the wall speed can be obtained from the formula $V_0 = \sqrt{\frac{\mathrm{Br}}{\mathrm{Pr}}} \times \sqrt{C_v T_w}$. Now, choosing a specific heat C_v =2000 J/kg K and a reference temperature of 25 C, we obtain for the wall speed, $V_0 = 488$ m/s which corresponds to an rpm of 1.32×10^5 in our experiment ! Therefore, we conclude that the stability results of Yueh and Weng is only of theoretical interest.

6.1.7 A note on the stability of Isoviscous Plane Couette Flow

Thus far, we discussed the stability of the plane Couette flow with a temperature dependent viscosity. We examined the stability both at constant wall speed and at constant wall stress. For the sake of completion, we will discuss the stability of constant viscosity plane Couette flow both at constant wall speed and constant wall stress in this endnote.

It is well known in literature[10] that isoviscous plane Couette flow is stable for all finite Reynolds number at constant wall speed. However, the stability results at constant wall stress are not available in literature. In this section, we will present the result of a numerical calculation of the real part of the largest eigenvalue vs. the wave number for a range of Reynolds numbers both under constant wall speed and constant wall stress conditions.

The Orr-Sommerfield equation for isoviscous plane Couette flow for which v_{z_0} is a linear function of x is

$$\begin{aligned}\sigma\frac{\mathrm{d}^2\hat{\psi}_1}{\mathrm{d}x^2} - \sigma\gamma^2\hat{\psi} = \frac{\mathrm{d}^4\hat{\psi}_1}{\mathrm{d}x^4} - 2\gamma^2\frac{\mathrm{d}^2\hat{\psi}_1}{\mathrm{d}x^2} &- i\gamma\mathrm{Re}v_{z_0}\frac{\mathrm{d}^2\hat{\psi}_1}{\mathrm{d}x^2} \\ &+ i\gamma^3\mathrm{Re}v_{z_0}\hat{\psi}_1 + \gamma^4\hat{\psi}_1 \qquad (6.106)\end{aligned}$$

with the boundary condition
$\hat{\psi}_1 = \frac{\mathrm{d}\hat{\psi}_1}{\mathrm{d}x} = 0$ at $x = \pm 1$ if the wall speed is held fixed at $x = +1$ and
$\hat{\psi}_1 = \frac{\mathrm{d}\hat{\psi}_1}{\mathrm{d}x} = 0$ at $x = -1$ and $\hat{\psi}_1 = \frac{\mathrm{d}^2\hat{\psi}_1}{\mathrm{d}x^2} = 0$ at $x = +1$
if the wall stress is held fixed at $x = +1$. Here $\mathrm{Re} = LV_0\rho/\mu$ where V_0 is the velocity of the wall, μ is the viscosity of the liquid, ρ is the density of the liquid and L is the gap width. σ has been scaled with respect to L^2/ν, where ν is the kinematic viscosity. This infinite dimensional differential equation is truncated to a finite dimensional system of equations by finite differencing the equations. The equations that result can be cast as $\mathbf{Au} = \sigma\mathbf{Bu}$, where $\mathbf{A}$ and $\mathbf{B}$ are matrices. The eigenvalues of this system is then calculated.

Figure 6.2 shows the plot of the real part of the largest eigenvalue vs. the wave number for a range of Reynolds number for conditions of constant wall speed. The real part is negative for a range of wave numbers indicating that the flow is stable. Similarly, fig(6.3) shows the plot of the real part of the largest eigenvalue vs. the wave number for a range of Reynolds number for conditions of constant wall stress. Again, the real part is negative indicating that the flow is stable at constant wall stress too. Also, note that the real part of the largest eigenvalue in this case is less negative as compared to the case of constant wall speed, once again indicating that constant wall stress is more unstable than constant speed.

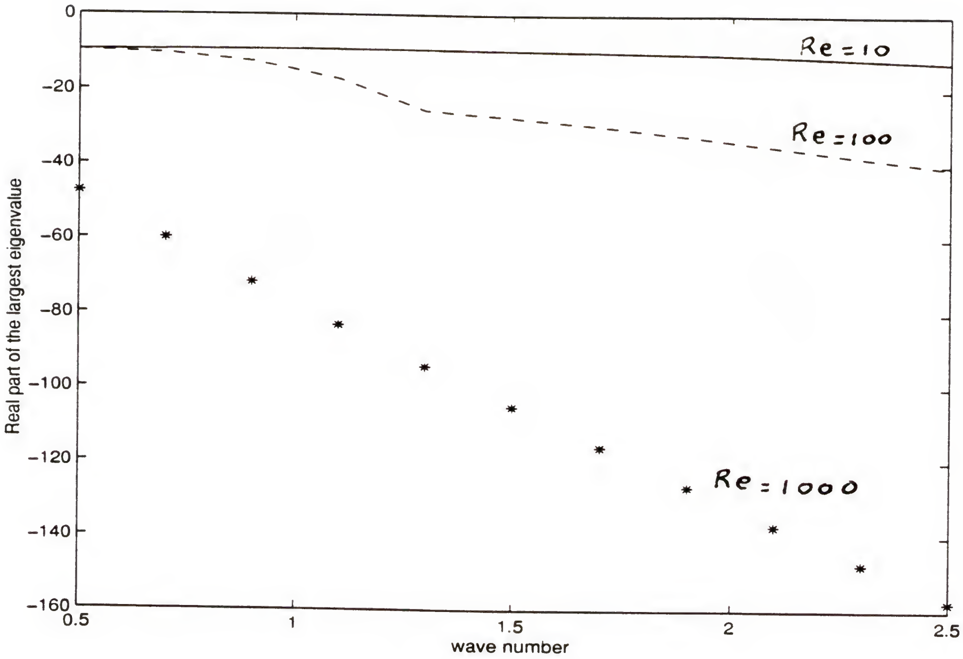

Figure 6.2: Isoviscous plane Couette flow: The plot of the largest eigenvalue vs. the wavenumber for a range of Reynolds numbers for conditions of constant wall speed.

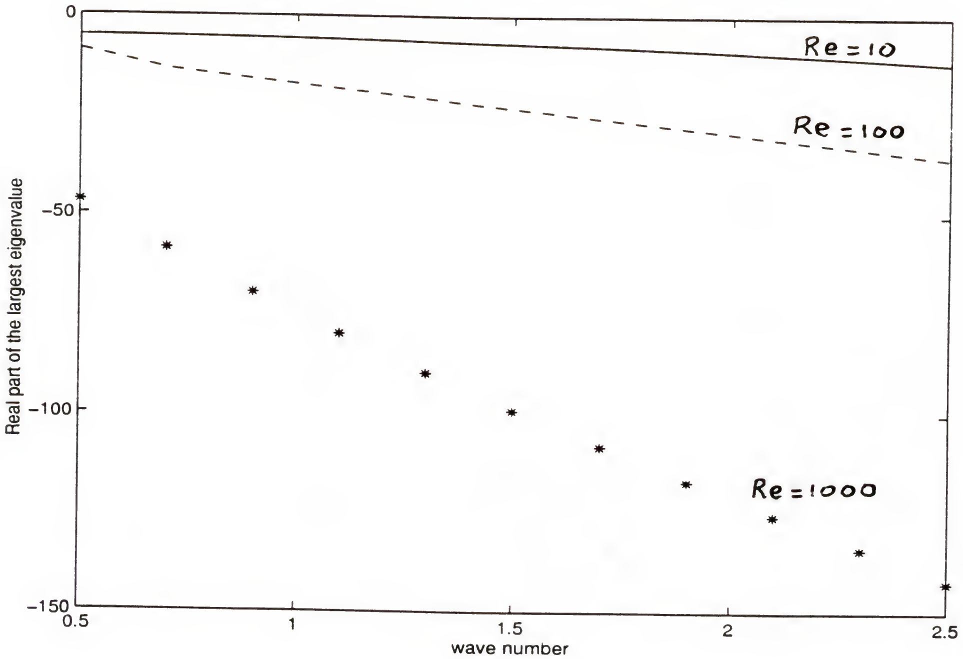

Figure 6.3: Isoviscous plane Couette flow: The plot of the largest eigenvalue vs. the wavenumber for a range of Reynolds numbers for conditions of constant wall stress.

CHAPTER 7
OVERVIEW OF AN EXPERIMENT AND CONCLUSIONS DRAWN FROM IT

At the end of the last chapter, we presented an objective for an experiment based on our stability results at constant wall speed and at constant wall stress. It was this: To obtain the base curve from an experiment and at any point along it hold the wall stress fixed thereafter determining its stability. In trying to decide how this objective is to be achieved, we will discuss the configuration of an experiment in this chapter. In doing this, we will not discuss anything specific such as the nature of an experimental liquid or the geometric dimensions and so on. These details have to be decided only after confirming that we can actually perform the experiment that we intended to.

Figure 7.1 illustrates a typical experimental setup. *In this setup, observe that the power from the motor is an input to the system and the rpm of the cylinder and the torque exerted by the fluid on the cylinder are measured as output.* Now, our earlier view was that the entire base curve could be traced holding the wall speed as an input variable. This was based on our stability result at constant wall speed, viz. small perturbations decay at constant wall speed. However, as we now realize that power is the input variable, a stability calculation at constant power must therefore be performed as only the result of such a calculation will really tell us whether the base curve can be obtained in an experiment. This is the task to which we now turn.

Now, to study the stability of the flow under constant power input, we ought to consider the power from the electric source going into the motor which drives the belt to shear the flow. The efficiency of the motor, then, has to be taken into account to calculate the power coming out of the motor and the efficiency of a motor is a

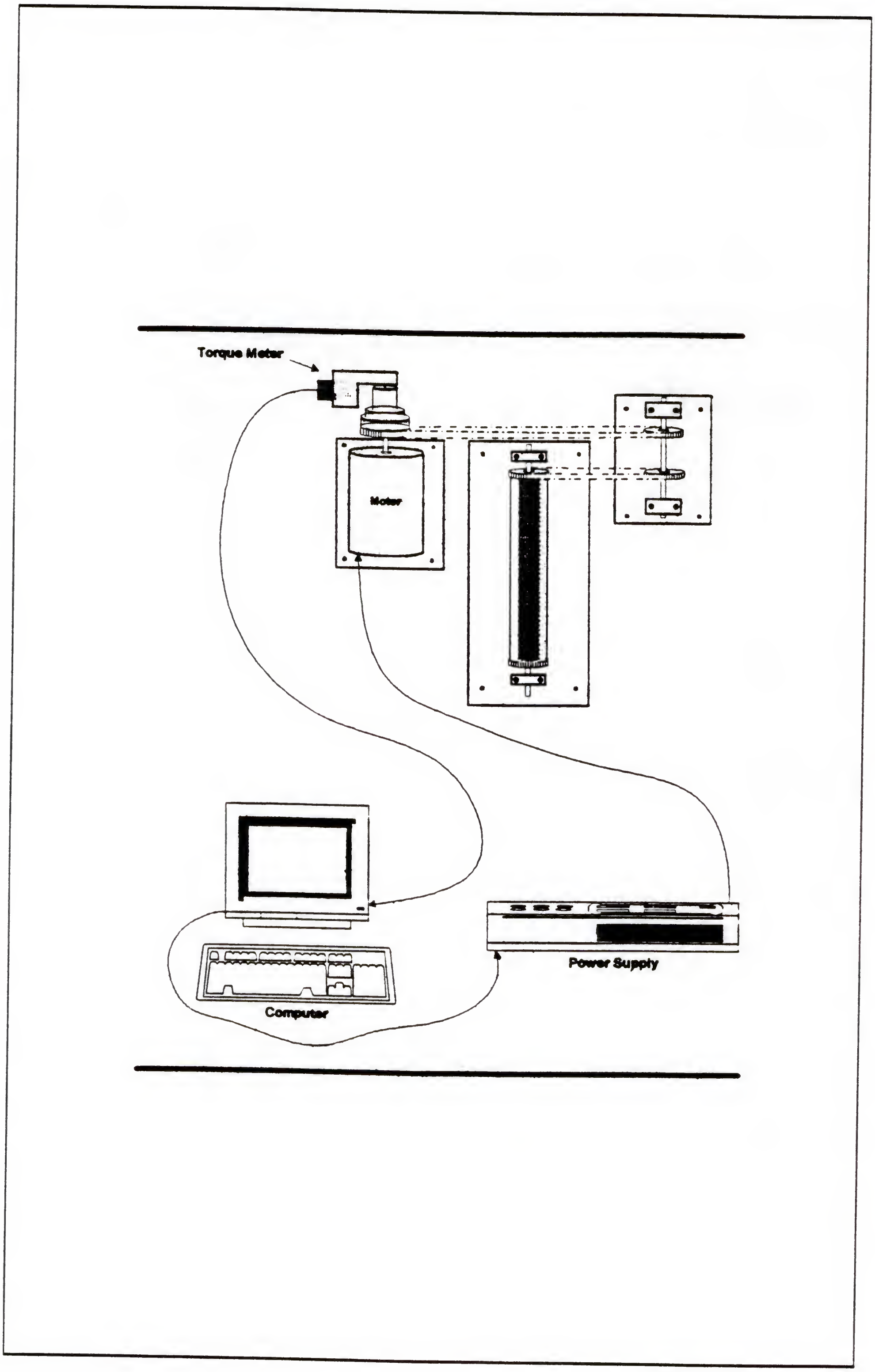

Figure 7.1: Experimental setup

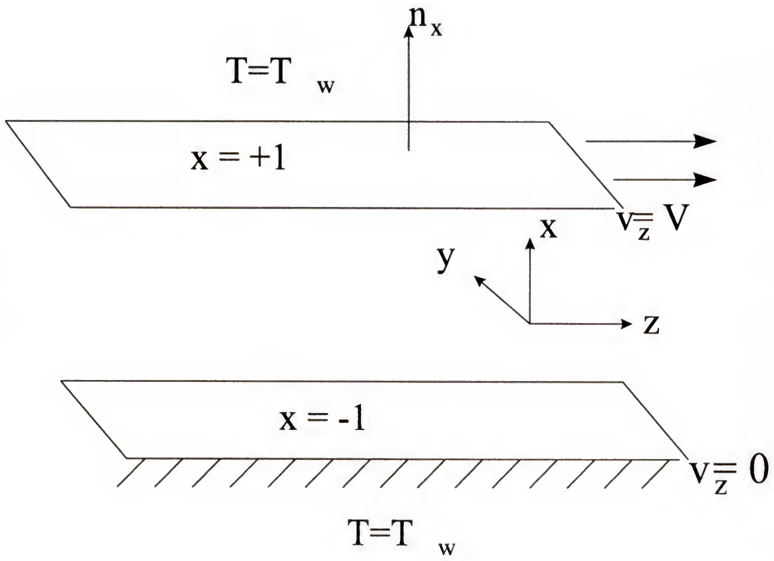

Figure 7.2: A schematic of the constant power input for plane Couette flow

function of its rotating speed! To avoid this complication, we consider the power coming out of the motor as the basis. Further, if we also ignore losses along the way, this will also be the power going to shear the fluid. Consequently, the stability calculation will be performed at constant power to shear the fluid. And as always, we will perform the stability calculation for plane Couette flow and based on this draw our conclusions for the circular Couette flow experiment.

Figure 7.2 illustrates a plane Couette flow experiment. If the power input, P, at the wall $x = L$ is fixed, then we have the following condition to be satisfied:

$$P = \int_S \left[\vec{v}.\left(\vec{\vec{\tau}}.\vec{n}\right)\right]_{x=L} \mathrm{d}S = \text{constant}$$

where $\vec{\vec{\tau}}$ is the stress tensor, $\vec{n}$ is the unit vector normal to the surface dS. For the plane Couette flow depicted in figure 7.2, $\vec{n} = \vec{i}_x$. Further, as the velocity components v_x, v_y are zero on the plate at $x = L$, we obtain

$$\int_S \left[\vec{v}.\left(\vec{\vec{\tau}}.\vec{n}\right)\right]_{x=L} \mathrm{d}S = \int_{y=0}^{y=B} \int_{z=0}^{z=W} v_z \tau_{xz}|_{x=L} \mathrm{d}y \mathrm{d}z$$

where B, W are the lengths in the y, z directions respectively.

At the base state, let the power input be denoted by P_0. Therefore,

$$\int_{y=0}^{y=B}\int_{z=0}^{z=W} V_0\tau_{xz_0}(x=L)\mathrm{d}y\mathrm{d}z = P_0$$

where $V_0 = v_{z_0}(x=L)$. In the base state, the quantities V_0, τ_{xz_0} do not depend on y, z. The above equations then reduce to

$$V_0\tau_{xz_0}WB = P_0$$

Notice that this equation is unscaled. Now, to scale this, using the length scale L such that $W^* = W/L, B^* = B/L$ where L is the gap width and further using $V_0^* = V_0/V_{\text{ref}}, \tau_{xz_0}^* = \tau_{xz_0}/\tau_{xz_{\text{ref}}}$ where $\tau_{xz_{\text{ref}}} = \mu_w V_{\text{ref}}/L$ and $P_0^* = P_0/P_{\text{ref}}$, where $P_{\text{ref}} = V_{\text{ref}}\tau_{xz_{\text{ref}}}L^2$, we obtain,

$$V_0^*\tau_{xz_0}^*W^*B^* = P_0^*$$

After dropping the $*$, we write this equation as

$$V_0\tau_{xz_0} = P_0/WB$$

Redefine $P_0/WB = P_0$ to obtain

$$V_0\tau_{xz_0} = P_0$$

Now, carrying out a perturbation of the variables about the base state, we obtain up to $O(\epsilon^2)$

$$v_z = v_{z_0}(x) + v_{z_1}(x,y,z,t)$$

$$V = V_0 + V_1(t)$$

$$\tau_{xz} = \tau_{xz_0} + \tau_{xz_1}(x,y,z,t)$$

$$P = P_0 + P_1(x,y,z,t)$$

where $V_1 = v_{z_1}(x=1)$. The perturbed equations at constant power input must satisfy

$$\int_{z=0}^{z=W}\int_{y=0}^{y=B}\left\{V_1\tau_{xz_0}(x=1) + V_0\tau_{xz_1}(x=1)\right\}\mathrm{d}y\mathrm{d}z = 0$$

Now, the perturbed equations for $v_{x_1}, v_{y_1}, v_{z_1}, p_1, T_1$ are partial differential equations in x, y, z and t subject to the above integral boundary condition[1] leads to a well posed problem. However, it is difficult to solve. We therefore look for conditions under which the problem becomes easily solvable. It turns out that when we expand the perturbed variables assuming a zero wave number disturbance, the problem becomes easy. At zero wave number, the variables can be expanded as

$$v_z = v_{z0} + \hat{v}_{z_1} e^{\sigma t}$$

$$V = V_0 + \hat{V}_1 e^{\sigma t}$$

$$\tau_{xz} = \tau_{xz0} + \hat{\tau}_{xz_1} e^{\sigma t}$$

$$P = P_0 + \hat{P}_1 e^{\sigma t}$$

The boundary condition on the perturbed variables at zero wave number reduces to

$$\hat{V}_1 \tau_{xz0} + \hat{\tau}_{xz1_{x=1}} V_0 = 0 \tag{7.1}$$

where $\hat{V}_1$ and $\hat{\tau}_{xz1_{x=1}}$ are constants. It should be noted that only at zero wave number, does the integral condition reduce to a simple algebraic equation and to a pointwise, instead of the averaged equation.

Now, this equation is a linear combination of the boundary condition at constant wall speed and the boundary condition at constant wall stress. Therefore, based on our earlier physical explanation of the rate of decay of perturbations at constant wall speed vs. constant wall stress, it would seem that the eigenvalues corresponding to the perturbations under a constant power must be between the value for constant wall speed and the value for constant stress. This would then mean that there might be a point of neutral stability ($\sigma = 0$) on the upper branch for constant power as under constant wall speed, the upper branch is stable (σ=negative) to small perturbations and for constant wall stress, the upper branch is unstable (σ=positive) to small perturbations. To check this, let us see whether there are any neutral points on the base solution curve at constant power and at zero wave number.

---

[1] Refer to an endnote to learn more about this integral boundary condition

The equations to be considered are the perturbed velocity equation and the perturbed temperature equation at neutral conditions,

$$0 = \frac{\mathrm{d}\hat{\tau}_{\mathrm{xz}1}}{\mathrm{dx}}$$

$$0 = \frac{\mathrm{d}^2\hat{\theta}_1}{\mathrm{dx}^2} + f_0{}'\tau_{xz0}^2\hat{\theta}_1 + 2f_0\tau_{xz0}\hat{\tau}_{xz_1}$$

respectively. The first equation tells us that the perturbed shear stress is a constant across the gap. Using this and integrating the equation

$$\frac{\mathrm{d}\hat{v}_{z_1}}{\mathrm{d}x} = f_0\hat{\tau}_{xz_1} + \tau_{xz0}f_0{}'\hat{\theta}_1$$

across the gap using at $x = 1, \hat{v}_{z_1} = \hat{V}_1$ and at $x = -1, \hat{v}_{z_1} = 0$, we get

$$\hat{V}_1 = \hat{\tau}_{xz_1}\int_{-1}^{+1} f_0\mathrm{d}x + \tau_{xz0}\int_{-1}^{+1} f_0{}'\hat{\theta}_1\mathrm{d}x \tag{7.2}$$

where under neutral conditions, as the perturbed shear stress $\hat{\tau}_{xz_1}$ is constant across the gap, $\hat{\tau}_{xz_1}(x = 1)$ can be replaced by $\hat{\tau}_{xz_1}$ anywhere across the gap. With this simplification, rearranging the boundary condition at $x = 1$, we obtain

$$\hat{V}_1 = -\hat{\tau}_{xz_1}V_0/\tau_{xz0} \tag{7.3}$$

Now, using this in the equation above, we obtain

$$-\frac{V_0}{\tau_{xz0}} = \int_{-1}^{+1} f_0\mathrm{d}x + \tau_{xz0}\int_{-1}^{+1} f_0{}'\frac{\hat{\theta}_1}{\hat{\tau}_{xz_1}}\mathrm{d}x \tag{7.4}$$

Now, as explained before, under neutral conditions, $\frac{\hat{\theta}_1}{\hat{\tau}_{xz_1}} = \dot{\theta}_0$ and hence the above equation can be rewritten as

$$-\frac{V_0}{\tau_{xz0}} = \int_{-1}^{+1} f_0\mathrm{d}x + \tau_{xz0}\int_{-1}^{+1} f_0{}'\dot{\theta}_0\mathrm{d}x \tag{7.5}$$

The right hand side of this equation is identically equal to $\frac{\mathrm{d}V_0}{\mathrm{d}\tau_{xz0}}$ where V_0 is defined by $V_0 = \tau_{xz0}\int_{-1}^{+1} f_0\mathrm{d}x$. Therefore this equation can be rewritten as

$$-\frac{V_0}{\tau_{xz0}} = \frac{\mathrm{d}V_0}{\mathrm{d}\tau_{xz0}} \tag{7.6}$$

Along the lower branch, $\frac{\mathrm{d}V_0}{\mathrm{d}\tau_{xz0}}$ is positive. Therefore, the right hand side of this equation is positive but the left hand side is negative. So, this equation can never be satisfied along the lower branch and hence $\sigma = 0$ is not possible along the lower branch. As $\dfrac{\mathrm{d}V_0}{\mathrm{d}\tau_{xz0}}$ is negative along the upper branch, it may happen that this equation can be satisfied as both the left hand side and the right hand side of this equation are negative. But, it turns out that this is not so. To see this, consider the following plausible statement: "An increase in wall speed is obtained by increasing the wall power[2]". In mathematical terms, it is

$$\frac{\mathrm{d}}{\mathrm{d}V_0}\left(V_0\tau_{xz0}\right) > 0 \tag{7.7}$$

This implies

$$\begin{aligned}
\tau_{xz0} + V_0\frac{\mathrm{d}\tau_{xz0}}{\mathrm{d}V} &> 0 &(7.8)\\
\Rightarrow \frac{\mathrm{d}\tau_{xz0}}{\mathrm{d}V_0} &> -\frac{\tau_{xz0}}{V_0} &(7.9)\\
\Rightarrow \frac{\mathrm{d}V_0}{\mathrm{d}\tau_{xz0}} &< -\frac{V_0}{\tau_{xz0}} &(7.10)
\end{aligned}$$

Therefore, we learn from this equation[3] that the condition for neutral stability can never be satisfied along the upper branch of the base curve. This then means that there are no points of neutral stability on either branches. This only leaves the nose of the curve to be examined.

At the nose, the equation

$$0 = \frac{\mathrm{d}^2\hat{\theta}_1}{\mathrm{dx}^2} + f_0{}'\tau_{xz0}^2\hat{\theta}_1 + 2f_0\tau_{xz0}\hat{\tau}_{xz1}$$

---

[2] In an endnote it will be shown that this statement is true along the lower branch, the nose and at least for some distance along the upper branch

[3] Observe that $\frac{\mathrm{d}V_0}{\mathrm{d}\tau_{xz0}} > -\frac{V_0}{\tau_{xz0}}$ on the lower branch and $\frac{\mathrm{d}V_0}{\mathrm{d}\tau_{xz0}} < -\frac{V_0}{\tau_{xz0}}$ on the upper branch. Based on this one might be wrongly led to think $\frac{\mathrm{d}V_0}{\mathrm{d}\tau_{xz0}} = -\frac{V_0}{\tau_{xz0}}$ at the nose and therefore wrongly conclude that nose is a neutral point. However, it should be remembered that $\frac{\mathrm{d}V_0}{\mathrm{d}\tau_{xz0}}$ starts out positive along the lower branch, becomes positive infinity at the nose and then starts out at negative infinity along the upper branch and then increases to finite negative values.

cannot determine $\hat{\theta}_1$ unless a solvability condition is satisfied as there $\tau_{xz0} = \lambda_1(\tau_{xz0})$. The solvability condition is

$$\int_{-1}^{+1} \phi_1 \left\{-2\tau_{xz0} f_0 \hat{\tau}_{xz_1}\right\} \mathrm{d}x = 0 \tag{7.11}$$

and this requires $\hat{\tau}_{xz_1} = 0$ as ϕ_1 is singly signed. If $\hat{\tau}_{xz_1} = 0$, then $\hat{V}_1 = 0$ from the equation

$$\hat{V}_1 \tau_{xz0} + \hat{\tau}_{xz1_{x=1}} V_0 = 0$$

and also $\hat{\theta}_1 = 0$ from the equation

$$\hat{V}_1 = \hat{\tau}_{xz_1} \int_{-1}^{+1} f_0 \mathrm{d}x + \tau_{xz_0} \int_{-1}^{+1} f_0{}' \hat{\theta}_1 \mathrm{d}x$$

Therefore, at the nose, only the solution $\hat{V}_1, \hat{\tau}_{xz_1}, \hat{\theta}_1 = 0$ is possible to the eigenvalue problem when σ is put to zero and therefore $\sigma = 0$ is not an eigenvalue at the nose. The stability result at constant input power is then: *The entire base solution curve is stable to small perturbations as σ starts out negative at $\tau_{xz0} = 0$ and it never rises to zero anywhere along the base curve.*

Now, before we proceed any further, recognize that the power is not directly put into the fluid but instead onto a plate and in any physical experiment, the mass of the plate that moves and generates the shear is finite. But, thus far in our calculations, we have neglected the inertia of the plate by assuming that it is of zero mass. Therefore, we will see how a finite mass of the plate affects our stability results. To do this, we will have to incorporate the dynamics of the wall at $x = L$ in the stability calculation. Let m_w be the mass of the plate and V its velocity. Let F be the force applied on the plate and $\tau_{xz}(x = L)$ be the shear stress on the fluid and let A be the area of the plate. Accordingly, we can write for the dynamics of the wall,

$$m_w \frac{\mathrm{d}V}{\mathrm{d}t} = F - \int_{y=0}^{y=B} \int_{z=0}^{z=W} \tau_{xz}(x = L) \mathrm{d}y \mathrm{d}z \tag{7.12}$$

where the force F is related to the input power P by the relation

$$P = FV \tag{7.13}$$

Now, at the base state, denoted by subscript zero, we have

$$P_0 = F_0 V_0$$

where

$$F_0 = \tau_{xz_0}(x = L)A$$

For a zero wave number perturbation, we write up to $O(\epsilon^2)$

$$V = V_0 + \hat{V}_1 \mathrm{e}^{\sigma t}$$

$$\tau_{xz} = \tau_{xz_0} + \hat{\tau}_{xz_1} \mathrm{e}^{\sigma t}$$

$$F = F_0 + \hat{F}_1 \mathrm{e}^{\sigma t}$$

$$P = P_0 + \hat{P}_1 \mathrm{e}^{\sigma t}$$

As the perturbation is carried out at constant input power, we set $\hat{P}_1 = 0$. Now, perturbing $P = FV$ about the base state, we obtain, at constant power

$$0 = \hat{F}_1 V_0 + \hat{F}_0 V_1$$

$$\hat{F}_1 = -\hat{V}_1 F_0 / V_0 = -\hat{V}_1 P_0 / V_0^2$$

Therefore, the boundary condition on the plate at $x = L$ becomes

$$\sigma m_w \hat{V}_1 = -\hat{V}_1 P_0 / V_0^2 - \hat{\tau}_{xz_1}(x = L)A \tag{7.14}$$

Notice that the term

$$\int_{y=0}^{y=B} \int_{z=0}^{z=W} \tau_{xz}(x = L)\mathrm{d}y\mathrm{d}z$$

has reduced to $\hat{\tau}_{xz_1}(x = L)A$ in the limit of a zero wave number where $A = BW$. Now, scaling the length by L, where L is the gap width, V by V_{ref}, the shear stress τ_{xz} by $\tau_{xz_{\text{ref}}} = \mu_w V_{\text{ref}}/L$, the power by the product of $\tau_{xz_{\text{ref}}} V_{\text{ref}} L^2$, the growth rate by $\sigma_{\text{ref}} = \mu_w/(\rho L^2)$, where ρ is the density of the fluid and μ_w is the viscosity at the wall temperature T_w, we obtain

$$\frac{m_w}{\rho A L}\sigma^* \hat{V}_1^* = -\frac{L^2}{A}\hat{V}_1^* P_0^* / V_0^{*^2} - \hat{\tau}_{xz_1}^*(x^* = 1) \tag{7.15}$$

As ρAL is the mass of the fluid m_f in the gap, we can rewrite the equations, after dropping the $*$ as

$$\frac{m_w}{m_f}\sigma\hat{V}_1 = -\frac{L^2}{A}\hat{V}_1 P_0/V_0^2 - \hat{\tau}_{xz_1}(x=1) \tag{7.16}$$

Therefore, the ratio of the mass of the plate with respect to the mass of the fluid in the gap, affects σ, the rate of decay of perturbations. We find that as $m_w \to 0$, the dynamics corresponding to the constant power conditions without incorporating the mass of the wall are approached. This indeed serves as a check for this calculation as we obtain the expected result in the limit of $m_w \to 0$. On the other hand, as the mass $m_w \to \infty$, the dynamics corresponding to the constant wall speed conditions are approached. Therefore, one might conclude that for a massy wall, the dynamics of the flow approaches constant wall speed conditions even though the experiment may be run under constant power. In an endnote, we will show that this is indeed true by considering the problem of Taylor instability in circular Couette flow.

Summarizing what we learnt this chapter: we have realized that the only input variable in this problem is the power to shear the fluid. The wall speed and wall stress are output variables. Based on this, we conclude that an experiment to trace the entire base curve can be performed by setting the power and measuring the torque and the rpm. This conclusion is not only based on our belief that the power is the input variable but also due to the stability result at constant power: small perturbations decay at constant power. Further, we also found out that the dynamics of the flow at constant power to the plate depends on the ratio of the mass of the moving plate with respect to the mass of the fluid: An extremely massy plate as compared to the mass of the fluid leads to a dynamics corresponding to constant wall speed conditions.

We will now turn to the other objective for an experiment that we set ourselves earlier, viz. to hold the wall stress fixed on the upper branch to see whether we can experimentally realize that the upper branch is unstable at constant wall stress.

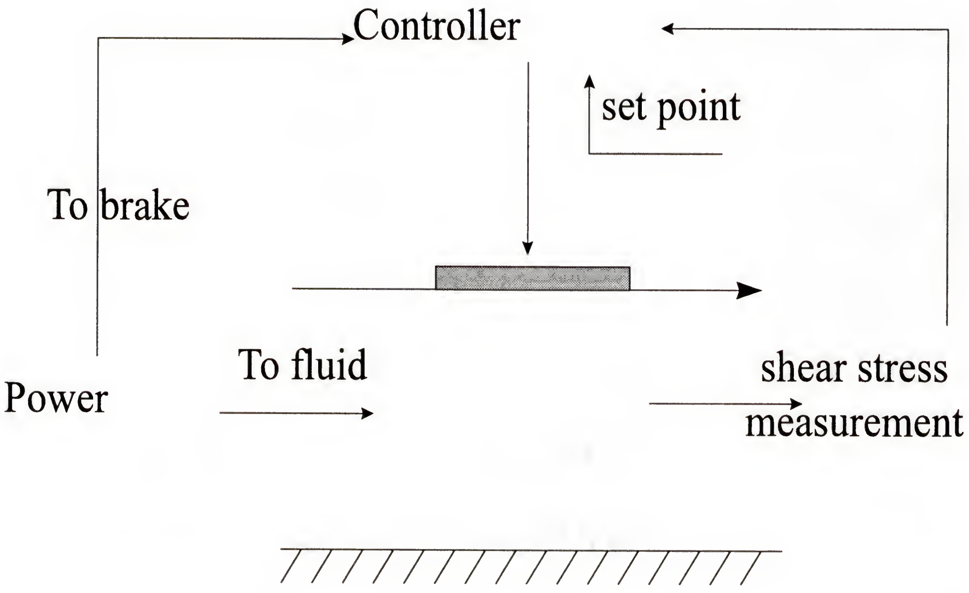

Figure 7.3: Illustration of Couette flow with a braking mechanism to control the wall stress

What we expect to see in an experiment is this: As the upper branch is unstable at constant wall stress, the system should jump to the lower branch for that wall stress. Now, before trying to achieve this in an experiment, first observe that our earlier calculations, which formed the motivation for this experiment, were performed pretending that the wall stress is the input variable. However, we now believe that the only input variable in this experiment is power. Hence, we now realize that in an experiment, the wall stress, an output variable can only be set using the power to the fluid. Keeping this in mind, we conceive the following scheme for an experiment in plane Couette flow as illustrated in figure 7.3.

Figure 7.3 shows the plane Couette flow experiment with a braking mechanism. Power from the source is split into two: One portion goes to shear the flow and the other portion goes to a braking mechanism. The shear stress exerted by the fluid on the wall is measured and compared with the wall shear stress set point. Depending on the difference between these two, the brake is either applied or released thereby either decreasing or increasing the power which in turn brings the wall stress close to the set point. Notice that in this control scheme the power to the fluid is not fixed.

It has to be adjusted to keep the wall stress close to the set point. How close depends on the sensitivity of the instrument that we use to measure the shear stress. For example if the set point shear stress is 2 units and the sensitivity of the instrument is 0.05 units, any shear stress value in the range from 1.95 to 2.05 may be seen by the instrument as 2 units. Now, the question is "If the wall stress is kept close to the set point by adjusting the power on the upper branch, will the flow jump to the lower branch?" To answer this question, let us go through a thought-experiment. In this, we will first impose a perturbation on the wall shear stress. Of course, the perturbation imposed must be such that the instrument can 'see' it as different from the set point, i.e., the perturbation should be greater than the sensitivity of the instrument. Then, the next step will be to bring the wall stress back to the set point by adjusting the power. The objective then is to see whether as a consequence of this sequence of actions, the flow goes to the lower branch. To see this, let us turn to the first step: to impose a perturbation. While a perturbation may be arbitrary, we consider only a specific kind: We consider a perturbation holding the power to the fluid fixed. A perturbation that increases the wall shear stress should therefore decrease the wall speed and vice-versa. To get a feel for how a perturbation may be imposed at constant power to the fluid, let us draw the base curve with a series of constant power lines as in figure 7.4. First observe from this figure that the constant power curve can intersect the base curve only at one point. Multiple solutions are not possible as the condition that the power has to increase for an increase in the wall speed requires that along the upper branch the slope of the base curve be less than the slope of the curve of constant power at the point of intersection and only one solution can satisfy this requirement[4].

Figure 7.5 shows a perturbation at constant power from point S on the base curve. Two possible scenarios are illustrated. Point 1 illustrates a perturbation that

---

[4] Recall that the same condition that the power has to increase with an increase in the wall speed was used earlier to prove that there are no neutral points on the upper branch at constant power.

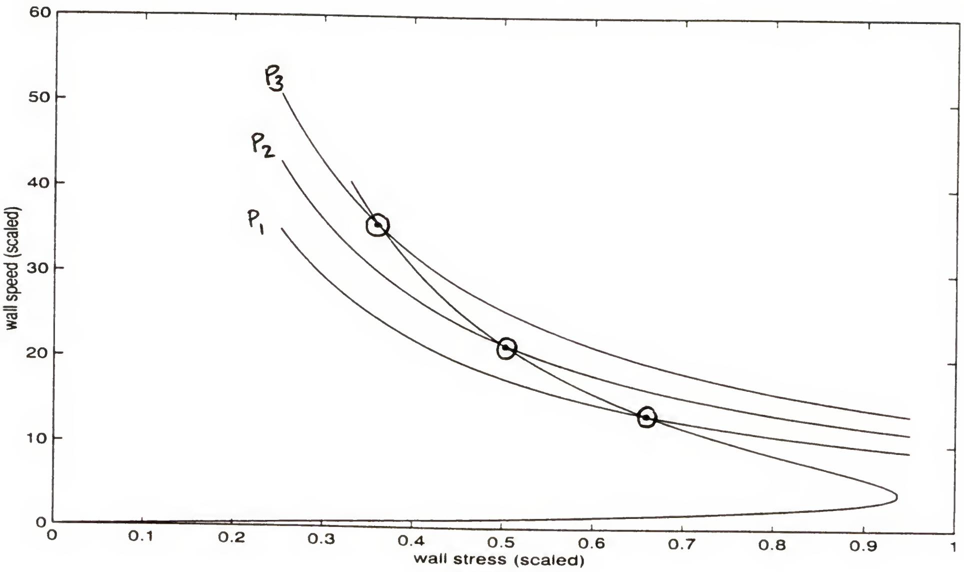

Figure 7.4: The Base curve drawn along with a series of constant power curves

decreases the wall stress and point 2 illustrates a perturbation that increases the wall stress.

Let us first consider the scenario wherein the perturbation is such that it decreases the wall stress and hence increases the wall speed from its set point. Now the first question one might have is "Should the power to the fluid be increased or decreased to increase the wall stress back to the set point?" Now, we know that along the upper branch, the steady state behavior is such that an increase in power increases the wall speed and decreases the wall stress and similarly a decrease in power decreases the wall speed and increases the wall stress. However, that is a long time behavior. We do not know how these variables respond in a transient as the power is changed. As our objective is to keep the wall stress close to the set point for all times, our interest is in the short time response of the wall stress for a step change in power. Now, to calculate this, the unsteady nonlinear equations of motion and energy have to be solved with the imposed boundary conditions, in this case, a step change in power. An endnote describes the details of this calculation. The result from the calculation is this: For a step increase in power on the upper branch, both

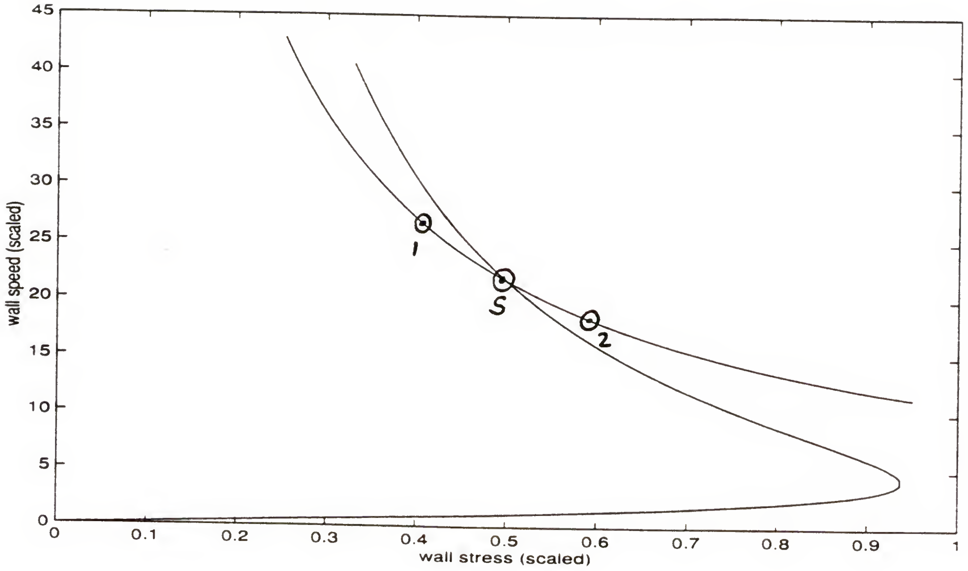

Figure 7.5: Two possible kinds of perturbation at constant power

the wall speed and the wall stress increase spontaneously, the percentage increase in wall stress being higher than the percentage increase in the wall speed. However as time progresses, the wall stress starts to decrease and the wall speed starts to increase further till finally they both reach the steady state corresponding to this higher power. Similarly, for a step decrease in power on the upper branch[5], both the wall speed and the wall stress decrease spontaneously, the percentage decrease in the wall stress being higher than the percentage decrease in the wall speed. And as time progresses, the wall speed drops further and the wall stress starts to increase till finally they both reach the steady state corresponding to this lower power. Now, what this result tells us is that for the case under consideration, where the perturbation has decreased the wall stress from its set point, the power to the fluid must be increased to increase the wall stress back to the set point. However, the rate at which the power has to be increased may be chosen arbitrarily. Depending on our choice, we can end up slightly to the north of the set point or much farther north of the set point. Once the power is adjusted to bring the wall stress back to within the sensitivity range

---

[5] assuming that the lower power also corresponds to a steady state point on the upper branch

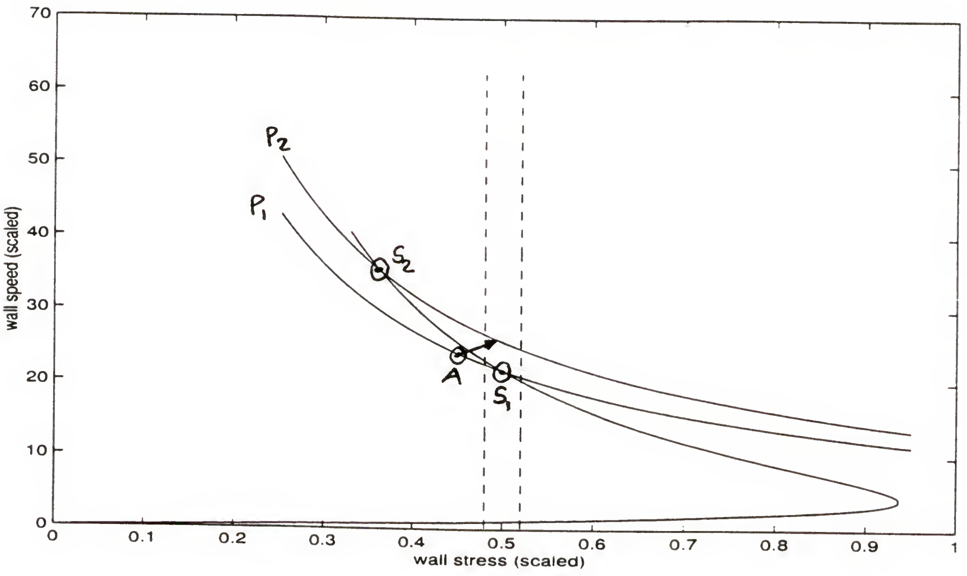

Figure 7.6: A perturbation that decreases the wall stress at constant power and a control action to bring the wall stress back.

of the instrument, a further change of power is not required. We would therefore hold the power constant till the wall stress once again deviates. Now, look at figure 7.6. Let us say, as a response to a perturbation from S_1 to A, the power is increased from P_1 to P_2 to bring the wall stress back to the set point. Now, at constant power, P_2, the steady state point on the base curve is S_2. We would therefore expect the long time response of the flow to be in the direction of S_2, i.e. in the direction of increasing wall speed and decreasing wall stress along the P_2 curve. It is however difficult to predict what happens for short times. There are two possibilities: The wall stress might start to move to the right initially and the retrace its path towards S_2 or it might monotonically move towards S_2. We will consider both these cases to see what might happen when the wall stress is controlled. We will go on and make our predictions for these cases. Later, in an endnote, we will make a calculation to check our predictions.

Let us first consider the case where the initial response of the system at constant power is away from the steady state. Figure 7.7 illustrates a probable response

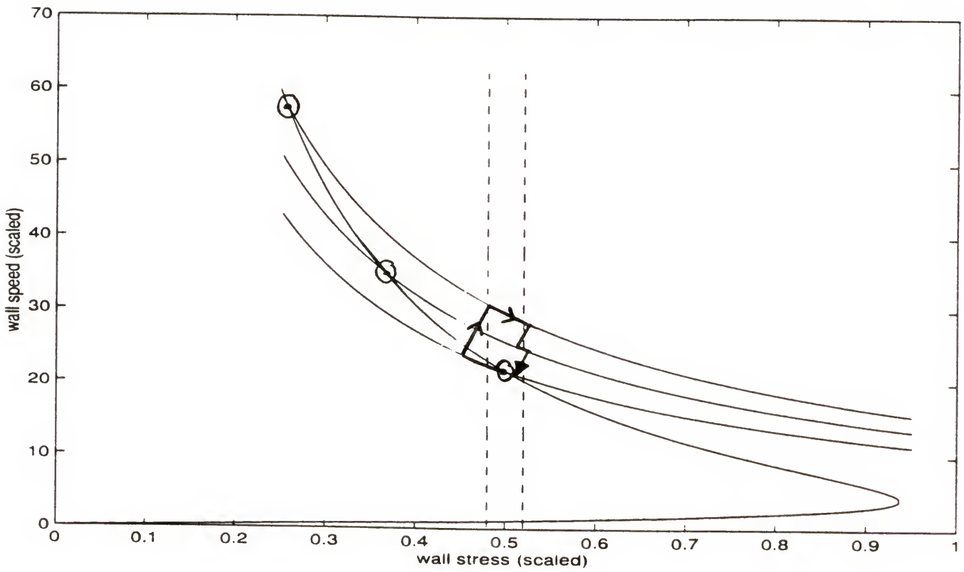

Figure 7.7: Dynamic behavior when wall stress is controlled after imposing a perturbation that decreases the wall stress from the set point: The case where the initial response of the flow at constant power is away from its steady state

for one such case. From figure 7.7, observe that the control action eventually brings the wall speed back close to the initial set point. Therefore. one might conclude that in this case, if we try to control the wall stress on the upper branch. the flow does not leave the upper branch. It stays close to the set point with an offset.

Now, let us consider the other possibility: the response of the flow at constant power is spontaneously towards the steady state. Figure 7.8 shows a probable response of a control action for one such case. Here, an attempt to control the wall stress eventually takes us in the direction of higher power and hence higher wall speeds. This might go all the way up to infinity[6]. Thus, in both these situations, we do not get to the lower branch. In the former case, we remain close to the set point and in the latter case, the wall speed might go all the way up to infinity.

One can go on and see what happens if the initial perturbation is one that increases the wall stress and decreases the wall speed. Figure 7.9 illustrates this

---

[6] Our dynamic calculation for this case actually simulated this behavior. We will discuss that in an endnote

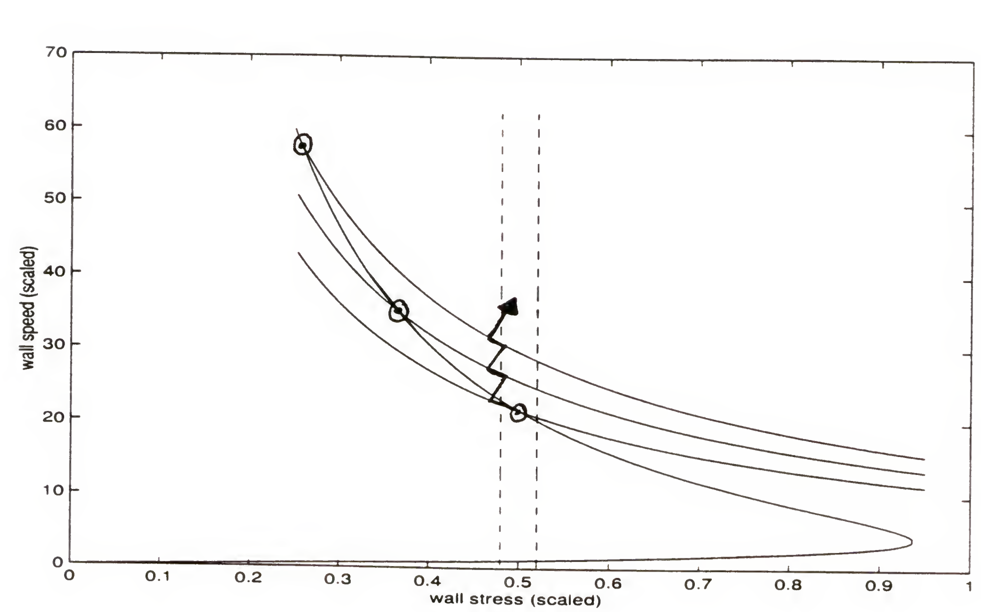

Figure 7.8: Dynamic behavior when wall stress is controlled after imposing a perturbation that decreases the wall stress from the set point: The case where the initial response of the flow at constant power is towards its steady state

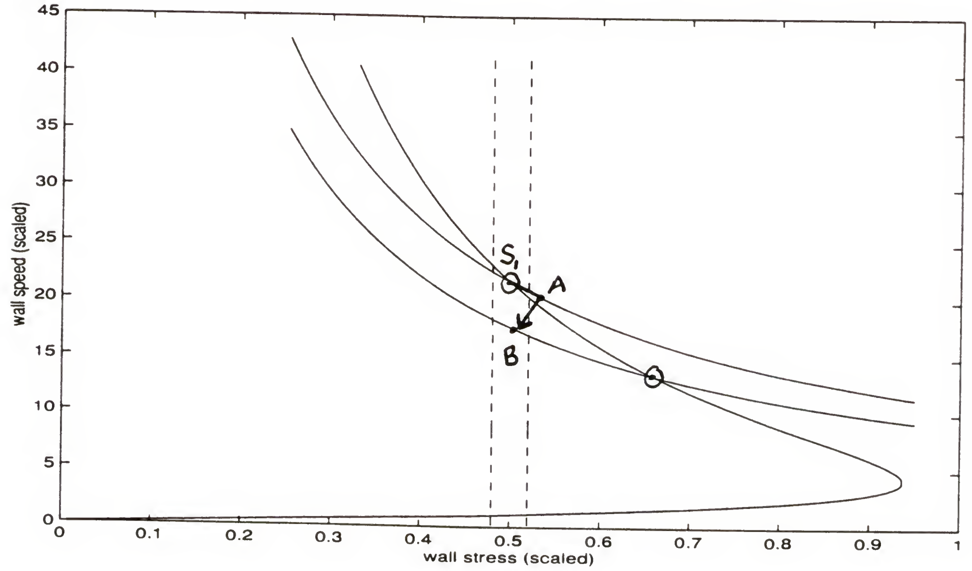

Figure 7.9: A perturbation that increases the wall stress and a control action to bring the wall stress back to the set point.

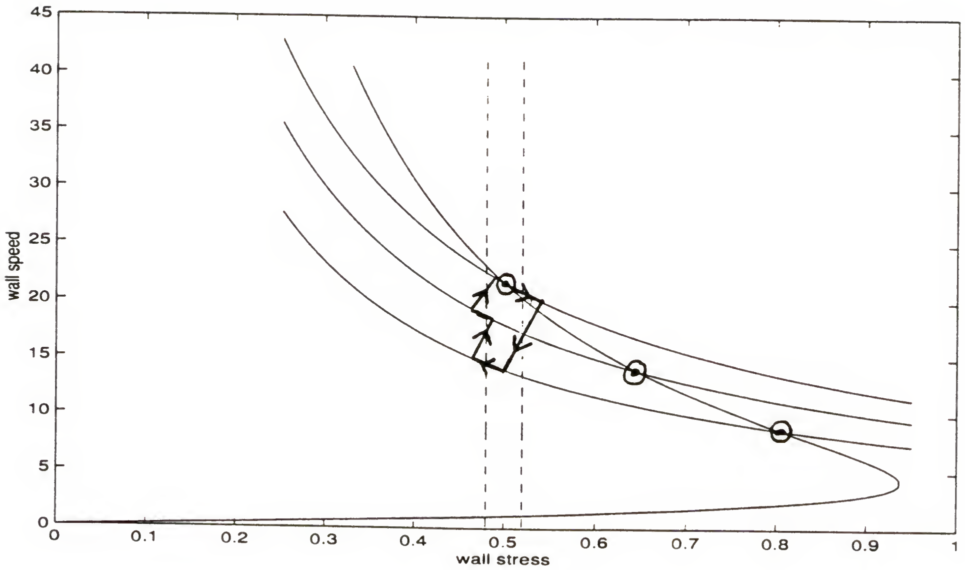

Figure 7.10: Dynamic behavior when wall stress is controlled after imposing a perturbation that increases the wall stress: The case where the wall stress starts to move away from the set point at constant power

scenario. The perturbation at constant power increases the wall stress from S_1 to A. At A, a control action is taken to bring the wall stress back to B which is along a constant power curve P_2. Once again, we have two possibilities depending on how the flow responds at constant power. Let us first consider the case where the wall stress initially moves away from the set point. Figure 7.10 shows a possible response of a control action for this case. In figure 7.10 we see that the the control action eventually brings the wall stress back to within the sensitivity range of the instrument. Therefore, in this case, trying to control the wall stress, we do not leave the upper branch.

Let us next consider the case where the initial response of the wall stress at constant power is towards the steady state. Figure 7.11 shows the probable response of a control action for one such case. In this case, we see that the control action takes us all the way to the lower branch point corresponding to that wall stress[7]. Thus we find that in only one of the four possible scenarios that we discussed, the

---

[7] Our dynamic calculation for this case actually simulates this behavior.

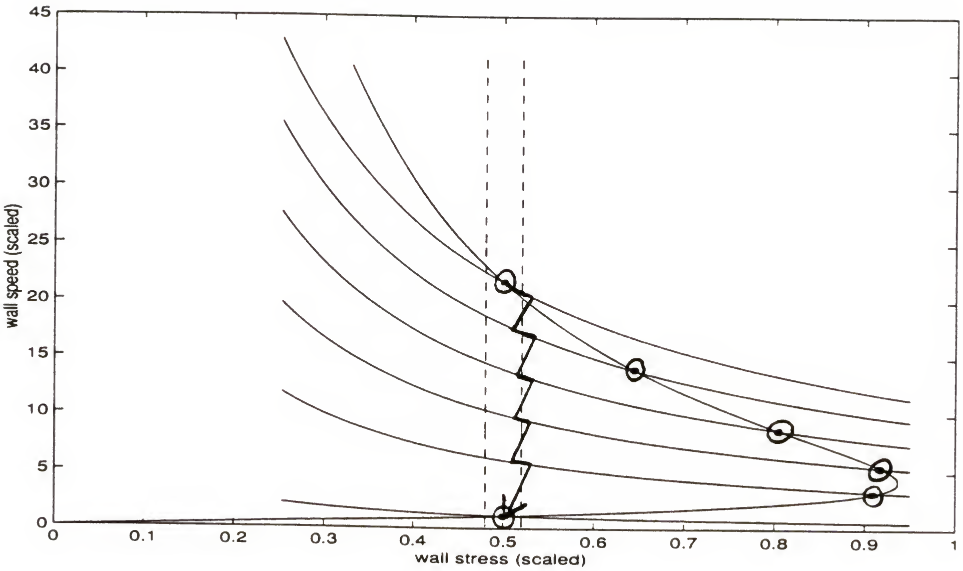

Figure 7.11: Dynamic behavior when wall stress is controlled after imposing a perturbation that increases the wall stress: The case where the wall stress starts to move towards the set point at constant power

flow gets to the lower branch and that too not in a way we initially conjectured. Our original conjecture was: If we hold the wall stress constant on the upper branch, the flow jumps to the lower branch. In making this conjecture, we assumed that the wall stress is an input variable. However, in reality it is an output variable. Therefore, even if the flow gets to the lower branch, it will not be a jump as we thought initially. The flow goes through a series of stages in which at each stage we adjust the power to keep the wall stress close to the set point and once the wall stress is within the set point range of the instrument we hold the flow at constant power till the flow starts to once again deviate from the set point. The dynamics of this step is decided by the fluid properties. Once again we respond to this deviation by adjusting the power. The sequence goes on till the steady state point on the lower branch is reached. Thus the dynamics of the flow going from the upper branch to the lower branch is not as dramatic as we initially conjectured. An experimental verification of this thought-experiment was not carried out.

to keep the wall stress close to the set point and once the wall stress is within the set point range of the instrument we hold the flow at constant power till the flow starts to once again deviate from the set point. The dynamics of this step is decided by the fluid properties. Once again we respond to this deviation by adjusting the power. The sequence goes on till the steady state point on the lower branch is reached. Thus the dynamics of the flow going from the upper branch to the lower branch is not as dramatic as we initially conjectured. An experimental verification of this thought-experiment was not carried out.

In the next chapter, we will discuss the experimental design to achieve the objective of obtaining the base curve. We will also compare our experimental base curve with the theoretical predictions. Before we proceed to do that, a set of endnotes that are related to the discussion in the main body of this chapter are provided.

7.1 Endnotes

7.1.1 A note about the Boundary Condition at Constant Power

In the main body of this chapter, while we were discussing the perturbed equations at constant power, we introduced the following boundary condition at constant power

$$\int_{z=0}^{z=W} \int_{y=0}^{y=B} \{V_1 \tau_{xz_0}(x=1) + V_0 \tau_{xz_1}(x=1)\} \, \mathrm{d}y \mathrm{d}z = 0$$

As we proceeded to the zero wave number limit of the perturbed equations, this integral condition reduced to a pointwise condition. In this endnote, we will make some observations about the integral condition as it stands. First observe that if we pretend to send the power directly to the fluid instead of a plate, then the perturbed velocity at $x = 1$, V_1, may be a function of y and z. Under these conditions, the above integral condition does not lead to a well posed problem as more than one variation of V_1 and τ_{xz_1} can satisfy this equation. However, in an experiment if we actually send power to the plate that shears the fluid. Then V_1 cannot be a function of y and z. The boundary condition then simplifies to

$$\int_0^W \left[\frac{\mathrm{d}v_{z_1}}{\mathrm{d}x} V_0\right]_{x=1} \mathrm{d}z = -V_1 \tau_{xz_0}$$

if we assume infinitely conducting walls. Here, V_1 is an unknown constant and is determined as a part of the solution. In this formulation, the problem is solvable. However, we did not solve the problem in this formulation and proceeded to the zero wave number limit of these equations as we anticipated to obtain analytical results at zero wave number. This is in view of the fact that earlier we obtained analytical results both at constant wall speed and at constant wall stress for a zero wave number disturbance.

Now, if we include the wall in the model, we cannot expand the variables in a Fourier mode to reduce the partial differential equations to ordinary differential equations: the wall is rigid and it cannot allow any spatial variation in its velocity. Now, to simplify the calculation and at the same time not lose the essence of the model, the following approximation may be useful. The equations in the domain may be expanded in Fourier mode pretending that the wall does not exist. And while writing the boundary condition at constant power, replace the integral condition by a pointwise condition under the assumption that the power input is uniform. The resulting model is a set of ordinary differential equation with a pointwise boundary condition for power. This in fact is the model that we will use when we solve the problem of Taylor instability at constant power input.

7.1.2 A Proof to show that Wall Speed increases with Power

In this endnote, we will try to prove that an increase in power to the fluid ought to produce an increase in the wall speed. To do this, first recall that we have already proved in chapter 2 that as the power increases, the temperature gradient at the wall increases. Mathematically this condition is seen from the equation

$$V_0 \tau_{xz_0} = -2\frac{\mathrm{d}\theta_0}{\mathrm{d}x}(x = 1)$$

Now, if we can could assert that as the temperature gradient at the wall increases, the temperature everywhere in the gap increases, then we would have the following result: With an increase in power, the temperature in the gap increases. Now, if we could further prove that with an increase in the temperature of the fluid in the gap, the wall speed increases, then we would have proved that with an increase in power, the wall speed increases. To do this, first consider the temperature equation

$$\frac{\mathrm{d}^2\theta_0}{\mathrm{d}x^2} + f_0\tau_{xz_0}^2 = 0 \tag{7.17}$$

with

$$\theta_0(x = \pm 1) = 0$$

Differentiating this equation with respect to V_0, we obtain

$$\frac{\mathrm{d}^2\dot{\theta}_0}{\mathrm{d}x^2} + f_0{}'\tau_{xz_0}^2\dot{\theta}_0 = -2f_0\tau_{xz_0}\dot{\tau}_{xz_0} \tag{7.18}$$

with

$$\dot{\theta}_0(x = \pm 1) = 0$$

where $\dot{\theta}_0 = \frac{\mathrm{d}\theta_0}{\mathrm{d}V_0}$. Now, at $\tau_{xz_0} = 0$, this equation along with the boundary condition tells us that $\dot{\theta}_0$ is zero. This implies that the θ_0 vs. V_0 curve starts with a slope of zero. For small values of τ_{xz_0} along the lower branch, assuming that the term with $\tau_{xz_0}^2$ can be neglected, it follows that $\dot{\theta}_0$ is positive as the curvature of $\dot{\theta}_0$ is negative and it is zero at the boundaries. Now, it can be further shown that for any value of τ_{xz_0} along the lower branch, $\dot{\theta}_0$ is positive. We do this again with a proof by contradiction. To do this, we will assume that $\dot{\theta}_0 = 0$ somewhere in the interior and see whether we end up with a contradiction. Putting $\dot{\theta}_0 = 0$ in the $\dot{\theta}_0$ equation leads to the condition that its curvature must be negative at that point. Now as $\dot{\theta}_0$ rises from zero at this point, its curvature is positive which is in contradiction to the condition that we obtained by setting $\dot{\theta}_0 = 0$. Therefore we have proved by contradiction that $\dot{\theta}_0$ is positive along the lower branch.

At the nose, $\dot{\tau}_{xz_0} = 0$ and therefore $\dot{\theta}_0 \propto \phi_1$. To obtain the proportionality constant, differentiate the equation

$$V_0 = \tau_{xz0} \int_{-1}^{1} f_0 \mathrm{d}x$$

with respect to V_0 to obtain

$$1 = \tau_{xz0} \int_{-1}^{1} f_0' \dot{\theta}_0 \mathrm{d}x$$

Putting $\dot{\theta}_0 = K\phi_1$ in this equation, we obtain for the proportionality constant

$$K = \frac{1}{\tau_{xz0} \int_{-1}^{+1} f_0' \phi_1 \mathrm{d}x}$$

from which we obtain for $\dot{\theta}_0$,

$$\dot{\theta}_0 = \frac{\phi_1}{\tau_{xz0} \int_{-1}^{+1} f_0' \phi_1 \mathrm{d}x}$$

Obviously, $\dot{\theta}_0$ is positive at the nose as all the quantities in this equation are positive. Thus we have proved that $\dot{\theta}_0$ is positive up to and including the nose. It is therefore certain that $\dot{\theta}_0$ remains positive at least for some distance along the upper branch. Therefore we conclude that as the power to shear the fluid is increased, the wall speed increases, at least for some distance along the upper branch.

7.1.3 A comment on Stability at Constant Input Power

In the main body of this chapter, we found out that the entire base solution curve is stable to small perturbations at constant power. This result does raise the following question: "Why don't we see any neutral points along the upper branch at constant power as the constant power boundary condition is a linear combination of the boundary condition at constant wall speed and boundary condition at constant wall stress and we know that at constant wall stress, σ is positive along the upper branch and at constant wall speed σ is negative along the upper branch?" To answer this question, consider the mixed boundary condition at $x = 1$,

$$\hat{V}_1 + K\hat{\tau}_{xz_1} = 0$$

where K is an arbitrary positive constant. We can readily attach a physical significance to this boundary condition for the following cases:

- When $K \to 0$, we recover the case of constant wall speed.
- When $K \to \infty$, we recover the case of constant wall stress.
- When $K = V_0/\tau_{xz_0}$, then we recover the case of constant input power.

For any other value of K, we may not be able to attach a physical significance for this boundary condition. Nevertheless, studying the stability of the flow for an arbitrary value of K, throws some light on the stability results that we obtained at constant input power.

As before, we look for points of neutral stability along the base solution curve with this boundary condition. Following the same procedure adapted for the constant power boundary condition and using the fact that $\hat{V}_1/\hat{\tau}_{xz_1} = -K$ now, we get the following condition for neutral stability everywhere along the base curve except at the nose.

$$\frac{\mathrm{d}V_0}{\mathrm{d}\tau_{xz_0}} = -K_c \tag{7.19}$$

where K_c is the critical value of K at which $\sigma = 0$. As K is positive, this condition can never be satisfied along the lower branch as $\mathrm{d}V_0/\mathrm{d}\tau_{xz_0}$ is positive along the lower branch. But along the upper branch, the condition required by this equation can be satisfied as along this branch $\mathrm{d}V_0/\mathrm{d}\tau_{xz_0}$ is negative. By comparing the above equation with the equation

$$\mathrm{d}V_0/\mathrm{d}\tau_{xz_0} < -\frac{V_0}{\tau_{xz_0}}$$

it is obvious that $K_c > V_0/\tau_{xz_0}$. This explains why we never encountered any points of neutral stability on the upper branch for the case of constant power input, i.e. when $K = V_0/\tau_{xz_0}$.

Table 7.1.3 below shows $K_c = \mathrm{d}V_0/\mathrm{d}\tau_{xz_0}$ calculated numerically for a few points along the upper branch along with the value of V_0/τ_{xz_0} for those points. This

Table 7.1: Comparison of the critical value of K, $K_c = \mathrm{d}V_0/\mathrm{d}\tau_{xz_0}$ with V_0/τ_{xz_0} on the upper branch for a mixed boundary condition

τ_{xz_0}	V_0/τ_{xz_0}	K_c
0.93	5.3	-53.5
0.9	6.7	-30.6
0.7	17.0	-34.52
0.5	43.3	-69.8
0.3	154.7	-216.7
0.15	783.0	-1012.7

table numerically confirms the reason for the absence of neutral points on the upper branch.

7.1.4 A comment on the Taylor Instability Problem

In the main body of this chapter, we learned that the dynamics of the Couette flow experiments may approach the constant wall speed conditions if the system is massy compared to the fluid. In this endnote, we will show that this is indeed true by considering one of the classical problems in fluid dynamics: the problem of centrifugal instability between concentric cylinders. The stability calculation for the boundary conditions of constant wall speed and constant power conditions for this problem will be performed and the critical rpm at the onset of Taylor instability will then be calculated. We will then compare the result of the critical rpm obtained from these calculations with that of the experimentally observed rpm at the onset of instability. We will find that the experimental result for the critical rpm matches the numerical results for the condition of constant wall speed thus confirming that the inertia of the system makes the dynamics approach the constant wall speed conditions.

What we mean by the constant power condition ought to be made clear before proceeding any further: In performing the stability calculation, we carry out a Fourier series expansion of the variables pretending that the solid wall does not exist and while writing the boundary conditions for the wall at which the power is fixed, replace the integral expression by an algebraic expression that would have been obtained were the power input be uniform. With this simplification, the problem becomes easily solvable and we assume that this is a reasonable approximation and would give us results which are close to what exactly goes on in a real situation.

While studying the problem of centrifugal instability, we will restrict ourselves to the case of constant viscosity. The perturbed equations for this case will be written for axisymmetric conditions, as we observe in our experiments that at the onset of Taylor instability, the flow is axisymmetric. Under these conditions, the perturbed equations are

$$\frac{\partial v_{r_1}}{\partial r} + \frac{v_{r_1}}{r} + \frac{\partial v_{z_1}}{\partial z} = 0 \tag{7.20}$$

$$\frac{\partial v_{r_1}}{\partial t} - \frac{2 v_{\theta_0} v_{\theta_1}}{r} = -\frac{\partial p_1/\rho}{\partial r} + \nu \left(\nabla^2 v_{r_1} - \frac{v_{r_1}}{r^2} \right) \tag{7.21}$$

$$\frac{\partial v_{\theta_1}}{\partial t} + \left(\frac{\mathrm{d} v_{\theta_0}}{\mathrm{d} r} + \frac{v_{\theta_0}}{r} \right) v_{r_1} = \nu \left(\nabla^2 v_{r_1} - \frac{v_{\theta_1}}{r^2} \right) \tag{7.22}$$

$$\frac{\partial v_{z_1}}{\partial t} = -\frac{\partial p_1/\rho}{\partial z} + \nu \nabla^2 v_{z_1} \tag{7.23}$$

where $\nabla^2 = \frac{\partial^2}{\partial r^2} + \frac{1}{r}\frac{\partial}{\partial r} + \frac{\partial^2}{\partial z^2}$ where ν is the kinematic viscosity μ/ρ. Now, anticipating periodic solutions, we write[8]

$$v_{r_1} = \hat{v}_{r_1} \mathrm{e}^{\sigma t} \cos(\beta z)$$

$$v_{\theta_1} = \hat{v}_{\theta_1} \mathrm{e}^{\sigma t} \cos(\beta z)$$

$$v_{z_1} = \hat{v}_{z_1} \mathrm{e}^{\sigma t} \sin(\beta z)$$

$$p_1 = \hat{p}_1 \mathrm{e}^{\sigma t} \cos(\beta z)$$

in the perturbed equations to obtain the equation of continuity:

$$D_* \hat{v}_{r_1} + \beta \hat{v}_{z_1} = 0 \tag{7.24}$$

---

[8] Observe that the z direction in circular Couette flow is analogous to the y direction in plane Couette flow. Hence the wave number β is chosen in the z direction in circular Couette flow to be consistent with our earlier definition of the wave number, β in the y direction for plane Couette flow.

r component of the equation of motion:

$$\nu\left(DD_* - \beta^2 - \frac{\sigma}{\nu}\right)\hat{v}_{r_1} + 2\frac{v_{\theta_0}}{r}v_{\theta_1} = \frac{\mathrm{d}}{\mathrm{d}r}\left(\frac{\hat{p}_1}{\rho}\right) \tag{7.25}$$

θ component of the equation of motion:

$$\nu\left(DD_* - \beta^2 - \frac{\sigma}{\nu}\right)\hat{v}_{\theta_1} - (D_* v_{\theta_0})(\hat{v}_{r_1}) = 0 \tag{7.26}$$

z component of the equation of motion:

$$\nu\left(D_* D - \beta^2 - \frac{\sigma}{\nu}\right)\hat{v}_{z_1} = -\beta\frac{\hat{p}_1}{\rho} \tag{7.27}$$

where $D = \frac{\mathrm{d}}{\mathrm{d}r}$ and $D_* = \frac{\mathrm{d}}{\mathrm{d}r} + \frac{1}{r}$

Now, first eliminating $\hat{v}_{z_1}$ using the z component of the equation of motion and the equation of continuity, we obtain for the pressure

$$\frac{\nu}{\beta^2}\left[DD_* - \beta^2 - \frac{\sigma}{\nu}\right]D_*\hat{v}_{r_1} = \frac{\hat{p_1}}{\rho}$$

Inserting this expression for $\hat{p_1}$ in the r component of the equation of motion, we obtain

$$\frac{\nu}{\beta^2}\left[DD_* - \beta^2 - \frac{\sigma}{\nu}\right]\left[DD_* - \beta^2\right]\hat{v}_{r_1} = 2\frac{v_{\theta_0}}{r}\hat{v}_{\theta_1}$$

This equation together with the θ component of the equation of motion

$$\nu\left(DD_* - \beta^2 - \frac{\sigma}{\nu}\right)\hat{v}_{\theta_1} = (D_* v_{\theta_0})(\hat{v}_{r_1})$$

must be solved to get σ for any given conditions of v_{θ_0}, β, ν. For a constant viscosity liquid $v_{\theta_0} = Ar + B/r$ where A, B are constants to be obtained from the boundary conditions. If the outer cylinder rotates with an angular speed Ω_2 and the inner cylinder rotates with an angular speed Ω_1, then $A = -\Omega_1\eta^2\frac{1-\omega/\eta^2}{1-\eta^2}$ and $B = \Omega_1 R_1^2\frac{(1-\omega)}{1-\eta^2}$ where $\omega = \Omega_2/\Omega_1$.

Now, scaling r with respect to r_2 such that $r^* = r/r_2$, β with respect to r_2 such that $\beta^* = \beta r_2$ and scaling σ with respect to r_2^2/ν such that $\sigma^* = \sigma r_2^2/\nu$, we obtain after dropping the *,

$$\left[DD_* - \beta^2 - \sigma\right]\left[DD_* - \beta^2\right]\hat{v}_{r_1} = \frac{2\beta^2 B}{\nu}\left(\frac{1}{r^2} + \frac{AR_2^2}{B}\right)\hat{v}_{\theta_1}$$

and

$$\left[DD_* - \beta^2 - \sigma\right] \hat{v}_{\theta_1} = \frac{2A}{\nu} R_2^2 \hat{v}_{r_1}$$

Now, making the transformation,

$$\frac{2AR_2^2}{\nu} \hat{v}_{r_1} = \hat{v}_{r_1}$$

the equations become

$$\left[DD_* - \beta^2 - \sigma\right] \left[DD_* - \beta^2\right] \hat{v}_{r_1} = -4T \frac{\eta^4 (1-\omega)(1-\omega/\eta^2)}{((1-\eta^2)^2)} \beta^2 \left(\frac{1}{r^2} - \kappa\right) \hat{v}_{\theta_1}$$

and

$$\left[DD_* - \beta^2 - \sigma\right] \hat{v}_{\theta_1} = \hat{v}_{r_1}$$

where

$$T = \frac{\Omega_1^2 R_2^4}{\nu^2}$$

and

$$\kappa = \frac{1-\omega/\eta^2}{1-\omega}$$

Now, we do not know whether σ is indeed real in these equations. However, at the onset of Taylor instability, the experiments show that the emerging flow is steady. Therefore, we assume σ is real and look for points where the base flow goes unstable by setting $\sigma = 0$ in these equations. At $\sigma = 0$, the equations become

$$\left[DD_* - \beta^2\right]^2 \hat{v}_{r_1} = -4T \frac{\eta^4 (1-\omega)(1-\omega/\eta^2)}{((1-\eta^2)^2)} \beta^2 \left(\frac{1}{r^2} - \kappa\right) \hat{v}_{\theta_1} \tag{7.28}$$

and

$$\left[DD_* - \beta^2\right] \hat{v}_{\theta_1} = \hat{v}_{r_1} \tag{7.29}$$

The boundary conditions on these variables are

$$\hat{v}_{r_1}(r = \eta, 1) = D\hat{v}_{r_1}(r = \eta, 1) = \hat{v}_{\theta_1}(r = \eta, 1) = 0$$

if the rpm is held fixed at $r = \eta$ and

$$\hat{v}_{r_1}(r = \eta) = D\hat{v}_{r_1}(r = \eta) = -\frac{(3-\eta^2)}{\eta(1-\eta^2)} \hat{v}_{\theta_1}(r = \eta) + D\hat{v}_{\theta_1}(r = \eta) = 0$$

and

$$\hat{v}_{r_1}(r=1) = D\hat{v}_{r_1}(r=1) = \hat{v}_{\theta_1}(r=1) = 0$$

if the power is held fixed at $r = \eta$. Observe that under both the limits $\eta \to 0, 1$, the boundary conditions at constant wall speed are recovered.

From these equations, for a given radius ratio η and for a given ratio of Ω_2/Ω_1, we can obtain the critical Taylor number at which the flow goes unstable. To get this, we finite difference the equations and write the resulting equations at neutral conditions in the form $\mathbf{A}\mathbf{u} = T\mathbf{B}\mathbf{u}$ and obtain the Taylor number, T as the eigenvalue.

We perform the calculation for the specific case of the inner cylinder rotating and the outer cylinder fixed. For this case $\Omega_2 = 0$ and hence $\kappa = 1$. Table 7.1.4 shows the result both for the conditions of constant wall speed and constant wall power for this case. Now before we go on to compare the numerical results with the experimental results, there is an extremely interesting aspect of the result that is worth explaining: The critical Taylor number has a minimum for a radius ratio of 0.5 both at constant rpm and constant power. Now, this implies there are possibly two different effects which resist an instability to set in in this problem: one dominating at high radius ratios and the other dominating at low radius ratios and both these effects have their least significant at $\eta = 0.5$ which is neither a thin gap nor a thick gap. Hence at $\eta = 0.5$, the critical Taylor number shows a minimum. Therefore, we will consider the two limits, $\eta \to 0$ and $\eta \to 1$ and explain why the critical rpm should be high in both the limits. In this argument, we will fix the outer radius, r_2 as this would ensure that for a fixed fluid, an increase in Taylor number $\Omega_1^2 R_2^4/\nu^2$ is tantamount to an increase in rpm, Ω_1. First, let us consider low radius ratios. For a fixed r_2, when $\eta \to 0$, r_1 is small. This then means that for a fixed Ω_1 the centrifugal force, $\rho\Omega_1^2 r_1$, that causes the instability, is small. Consequently, a high enough rpm is required to generate the instability. On the other hand, at high radius ratios, r_1 is

Table 7.2: The critical Taylor number for various radius ratios at constant rpm and at constant power

	The critical Taylor number, T^* at		
η	Constant rpm	Constant power	percentage difference
0.95	1.51×10^7	1.20×10^7	20.0
0.75	2.09×10^5	1.72×10^5	17.7
0.50	7.43×10^4	6.40×10^4	13.9
0.35	9.46×10^4	8.44×10^4	10.8
0.25	1.76×10^5	1.62×10^4	8.0
0.15	6.78×10^5	6.46×10^5	4.7
0.10	2.43×10^6	2.36×10^6	2.9

very close to r_2 and hence it is difficult for the fluid to turn over in the small gap of $r_2 - r_1$. Therefore, once again a very high rpm is required to generate the instability.

Now, getting back to the comparison of the numerical predictions with the experimental results, we find that for a radius ratio of 0.75, the Taylor number at constant wall speed is 2.09×10^5 and at constant power is 1.72×10^5. For a liquid of 100 centistokes and for a geometry with an outer radius of 1 inch, this translates an rpm of 678 at constant wall speed and 555 at constant power. Now, we find from our experiments that the critical rpm for the onset of Taylor instability is 677 which matches the theoretical results at constant speed. Hence, we conclude that the dynamics of our system approaches the constant wall speed conditions even though the power is the input and this is due to the large inertia of the system.

Before we close this endnote, it is worth recalling that our bifurcation parameter in this calculation was the Taylor number which when unscaled for a fixed outer radius and for a fixed fluid yields the critical rpm at the onset of instability. Therefore, it follows that for a fixed fluid and fixed outer radius, the critical rpm also behaves qualitatively like the critical Taylor number, having a minimum at $\eta = 0.5$. Now, it might be of some interest to see what some other parameters like the linear speed, the torque, the angular momentum per unit volume and the power to the fluid behave at the onset of instability as a function of radius ratio, η. Therefore, we will calculate these quantities at the onset of instability next. We will look at the case of constant wall speed boundary condition to do this calculation. A brief note about how each of these variables is calculated may be useful.

The critical rpm is obtained form the Taylor number, T using the formula

$$\Omega_1 = \sqrt{T^*}\nu/R_2^2$$

The linear speed, V_1 is obtained from the formula

$$V_1 = \Omega_1 R_1$$

and the critical Torque τ using

$$\tau = 4\pi\mu R_2^2 L \frac{\eta^2}{1-\eta^2}\Omega_1$$

The angular momentum per unit volume A is calculated using the formula

$$A = \rho r_1^2 \Omega_1$$

and the power, P using the formula

$$P = \tau\Omega_1$$

Table 7.3 reports the critical parameters as a function of radius ratio for a geometry with an outer radius of 1 inch and a length of 34 cm.

From the table, we find that the torque and the angular momentum at the onset decrease monotonically with a decrease in radius ratio whereas the power to the fluid and the linear speed show a similar trend as the rpm initially decreasing with a decrease in radius ratio and thereafter increasing with a decrease in radius ratio. However compared to their initial drop, these quantities do not rise much above the minimum.

η	β	Taylor no.	Ω_1,rpm	V_1, m/s	τ,lb-in	A,kg/m^{2}s	Power, hp
0.95	62.8	1.51×10^7	5752	14.00	13.6	350	1.24
0.75	12.56	2.09×10^5	678	1.35	0.22	25.7	2.36×10^{-3}
0.50	6.32	7.43×10^4	403	0.53	0.034	6.81	2.15×10^{-4}
0.35	4.92	9.46×10^4	454	0.42	0.017	3.76	1.16×10^{-4}
0.25	4.32	1.76×10^5	621	0.42	0.018	2.61	1.03×10^{-4}
0.15	3.90	7.35×10^5	1217	0.49	0.0072	1.82	1.38×10^{-4}
0.10	3.73	2.43×10^6	2309	0.61	0.0060	1.56	2.18×10^{-4}

Table 7.3: The critical parameters for various radius ratios at constant rpm

7.1.5 Simulation of the dynamics of the Nonlinear Equations

In this section, we will provide the results of the numerical calculations that simulate the dynamic behavior of the wall speed and the wall stress for various imposed conditions on power. To do the calculation, we consider the scaled nonlinear equations and put $\mathbf{v} = v_z(x,t)$ and $\theta = \theta(x,t)$ in them. Under these assumptions, the scaled equations of motion and energy become

$$\frac{\mathrm{d}v_z}{\mathrm{d}t} = \frac{\mathrm{d}}{\mathrm{d}x}\left[\mu \frac{\mathrm{d}v_z}{\mathrm{d}x}\right]$$

$$\mathrm{Pr}\frac{\mathrm{d}\theta}{\mathrm{d}t} = \frac{\mathrm{d}^2\theta}{\mathrm{d}x^2} + \mu\left[\frac{\mathrm{d}v_z}{\mathrm{d}x}\right]^2$$

respectively. We assume perfectly conducting walls at the bottom and at the top. Hence, $\theta(x = \pm 1) = 0$ for all times. The bottom wall is fixed and therefore $v_z(x = -1) = 0$ for all times. We choose a $\mathrm{Pr} = 1$ for this calculation. A finite difference scheme on both the position and time is used for the calculation.

The first calculation simulates the dynamics of the wall speed and the wall stress for a step increase in power. To do this calculation, we start from a steady state operating point on the upper branch, S_1, that corresponds to a wall speed $V_1 = 21.69$, the wall stress, $\tau_{xz_1} = 0.5$ and power $P_1 = 10.845$ and then provide a step increase in power to S_2 that corresponds to $V_2 = 35.02$, $\tau_{xz_2} = 0.3667$, $P_2 = 12.845$. Figure 7.12 shows the initial and final steady states.

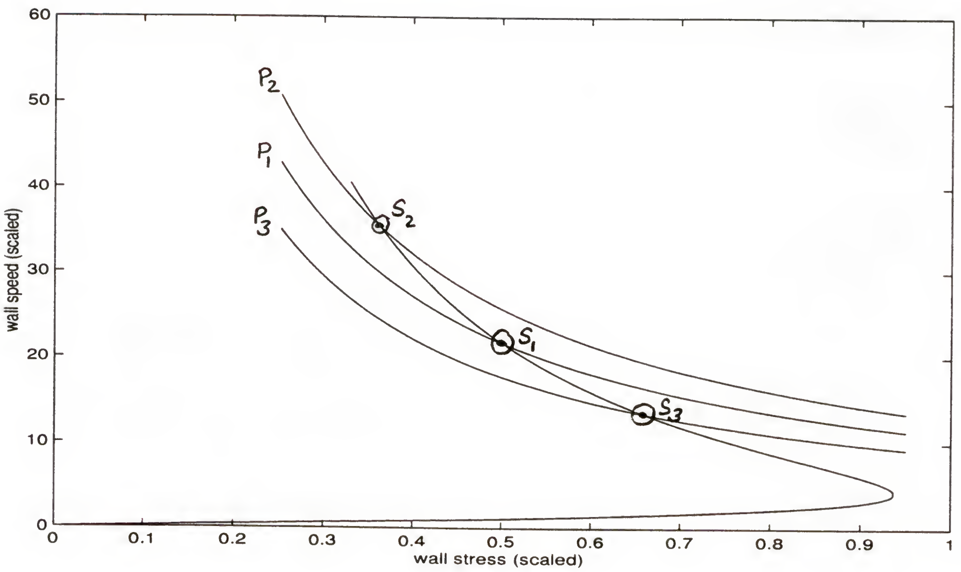

Figure 7.12: Step change in power: The initial and the final steady state points

Figure 7.13 shows the evolution of the wall speed and figure 7.14 shows the evolution of the wall stress when a step increase is made to the power. We see from the graph that both the wall speed and the wall stress initially increase with an increase in the power. The percentage change in wall stress is however much larger than the percentage change in the wall speed. As time progresses, the wall stress decreases and the wall speed increases further and the system eventually reaches the steady state corresponding to the new power, P_2. Likewise, we considered a case where a step decrease is made in power from S_1 to S_3, where S_3 corresponds to $V_3 = 13.41$, $\tau_{xz_3} = 0.6598$, $P_3 = 8.845$ in figure 7.12. Figure 7.15 shows the evolution of the wall speed and figure 7.16 of the wall stress.

Our next calculation simulates the response of the wall speed and the wall stress as we control the wall stress on the upper branch. To do this calculation, we first have to impose a perturbation holding the power constant. To do this, we assume that our instrument can read the wall shear stress with a sensitivity of 1%. Therefore, we choose the initial perturbation in shear stress to be larger than 1%. A set point wall stress of 0.5 on the upper branch is chosen. The steady state velocity

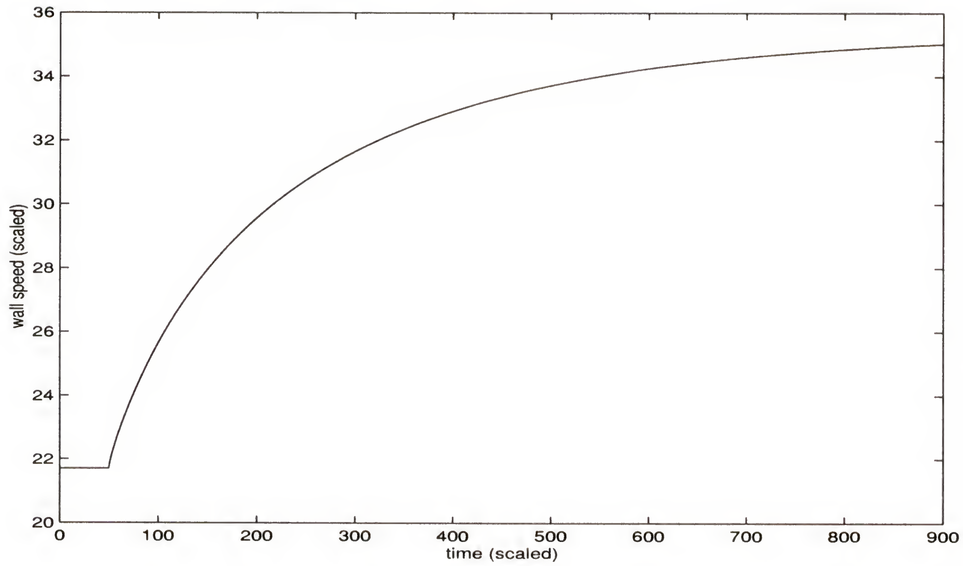

Figure 7.13: Step increase in power: The response of wall speed.

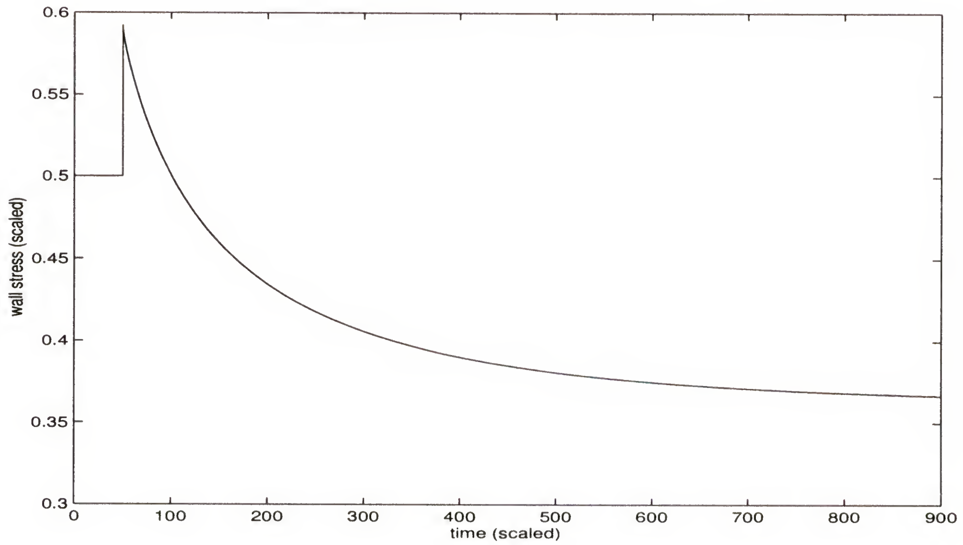

Figure 7.14: Step increase in power: The response of wall stress.

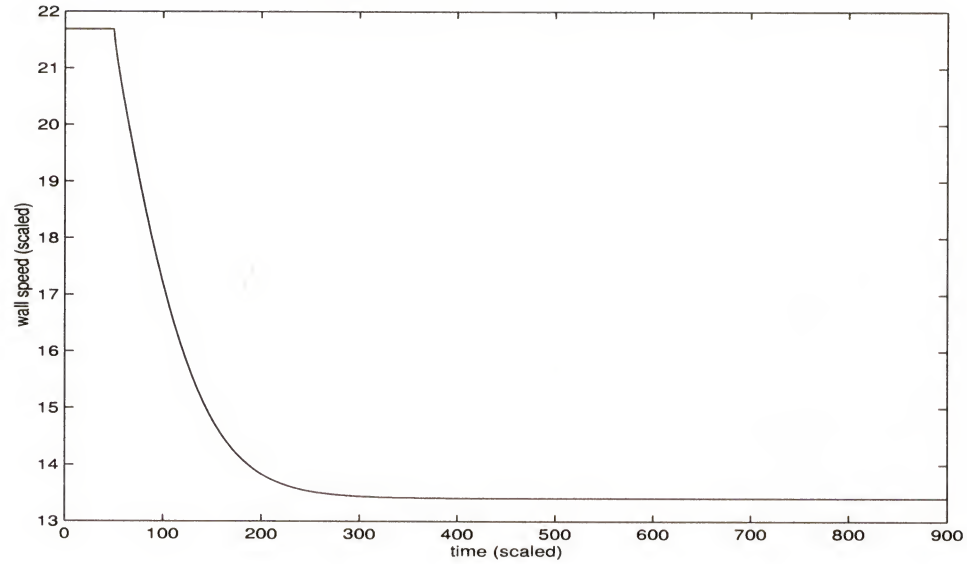

Figure 7.15: Step decrease in power: The response of wall speed.

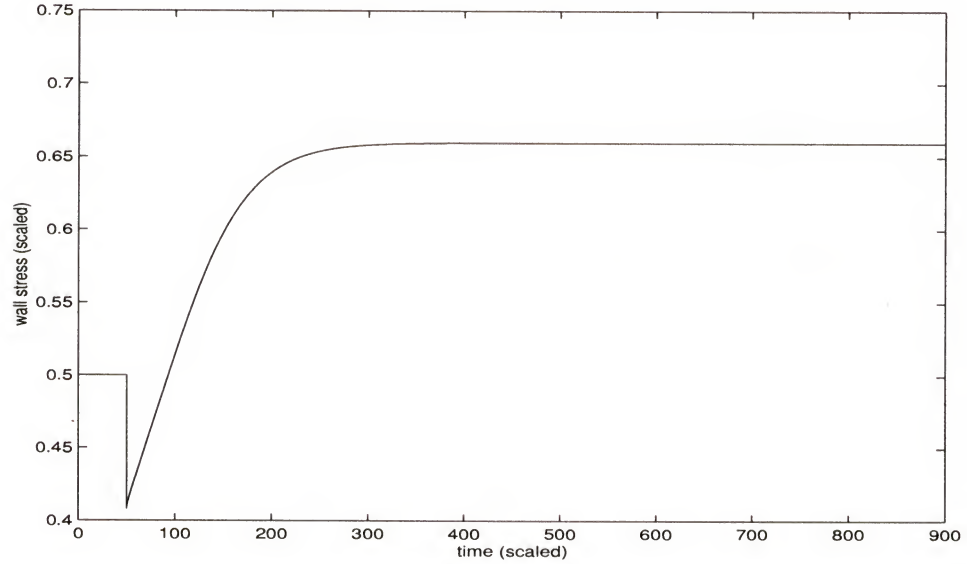

Figure 7.16: Step decrease in power: The response of wall stress.

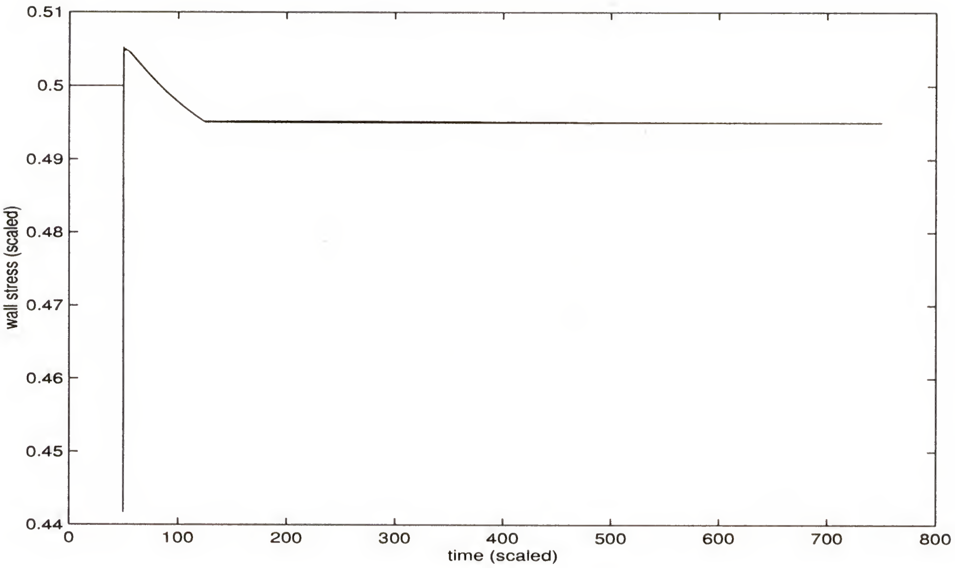

Figure 7.17: The dynamics of the wall stress when a perturbation that decreases the wall stress is imposed and a control action is then instituted to keep the wall stress close to the set point

corresponding to this wall stress is 21.69 and the steady state power is 10.845. In doing this calculation, first a perturbation that decreases the wall stress is imposed. As a response, the power is increased to bring the wall stress back to the set point. Then the system is run at constant power till the wall stress once again moves away from the set point. Figure 7.17 shows the evolution of the wall stress and figure 7.18 shows the evolution of the wall speed for this sequence of actions. Observe from figure 7.18 that the velocity monotonically increases with time. Thus in this case, as we attempt to control the wall stress, the wall speed goes all the way up to infinity.

Next we considered a perturbation that increases the wall stress at constant power and carried out a calculation to simulate the response of the wall speed and the wall stress as we control the wall stress. Figure 7.19 shows the evolution of the wall stress and figure 7.20 shows the evolution of the wall speed for this case. As we see from the dynamics of the wall speed, the flow goes to the lower branch in this case.

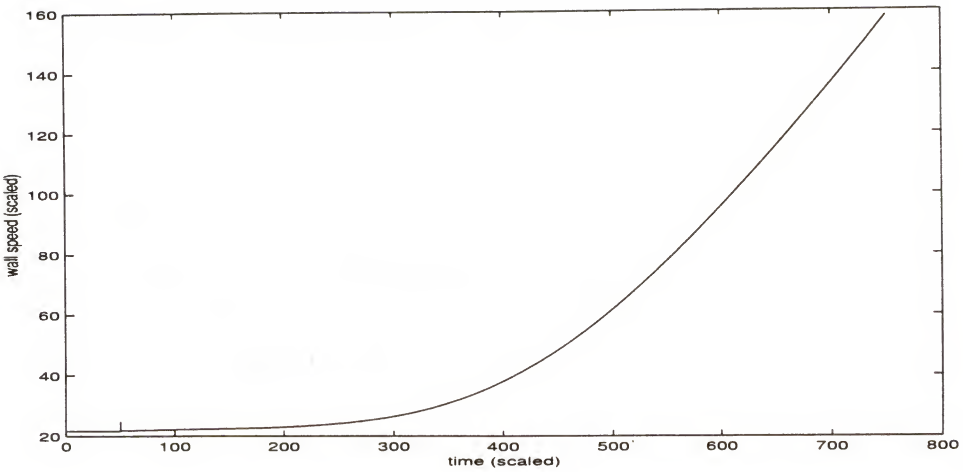

Figure 7.18: The dynamics of the wall speed when a perturbation that decreases the wall stress is imposed and a control action is then instituted to keep the wall stress close to the set point.

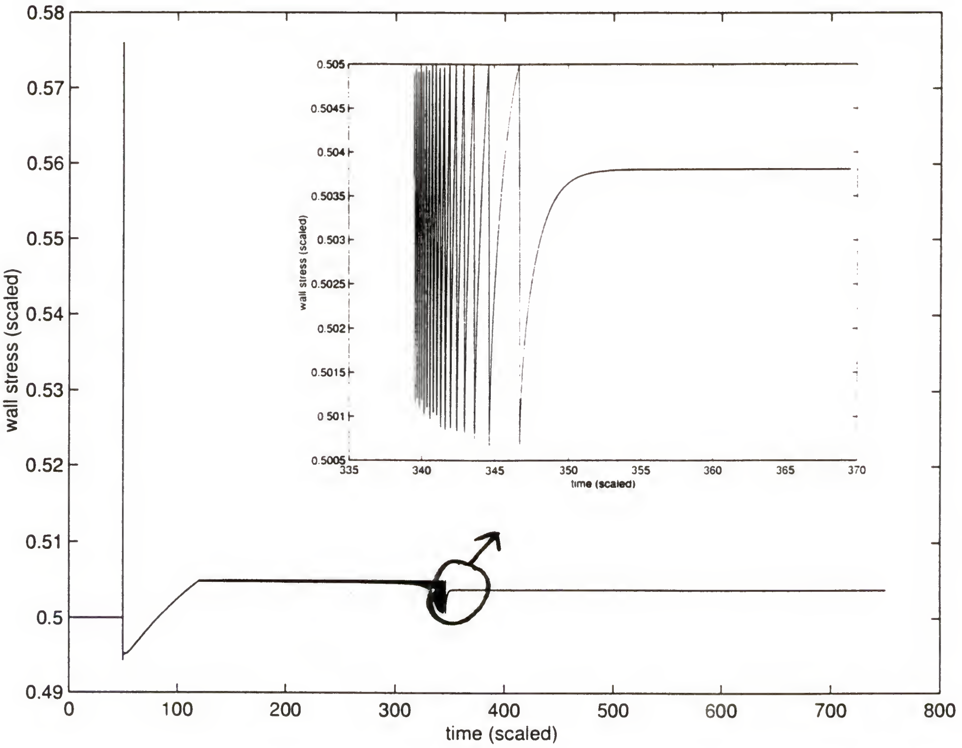

Figure 7.19: The dynamics of the wall stress when a perturbation that increases the wall stress is imposed and a control action is then instituted to keep the wall stress close to the set point. Inset shows a magnified view of the dynamics of the wall stress for a scaled time between $t = 335$ and $t = 370$.

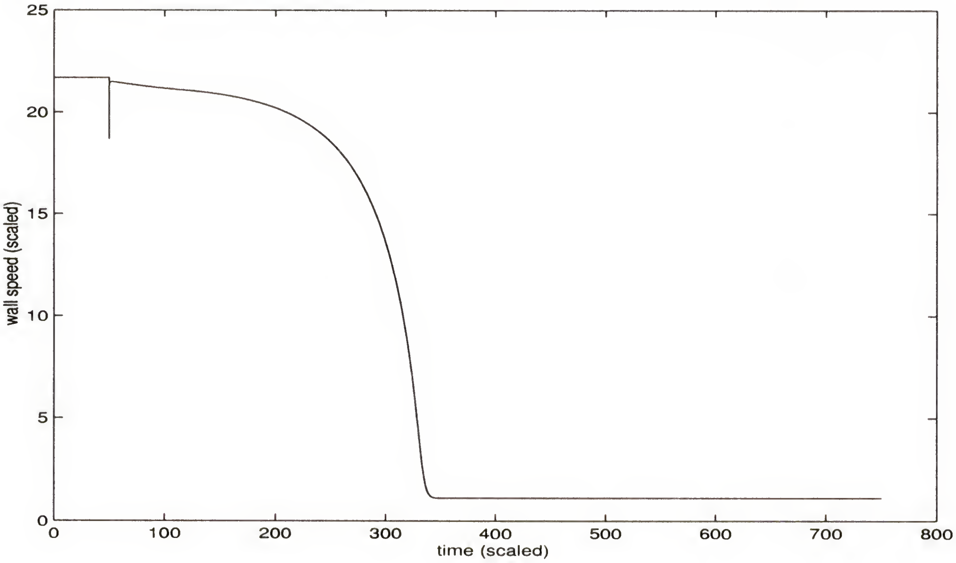

Figure 7.20: The dynamics of the wall speed when a perturbation that increases the wall stress is imposed and a control action is then instituted to keep the wall stress close to the set point.

CHAPTER 8
EXPERIMENTAL DESIGN AND RESULTS

In the previous chapter, we concluded that it is indeed possible to obtain the base curve in a circular Couette flow experiment by inputting the power and measuring the output variables, viz. the torque and the rpm. This conclusion was based on the result that the flow is stable under constant power input. In this chapter, we will first discuss the design of an experiment to achieve this objective. Then we will compare the curve of the torque vs. rpm obtained from an experiment with the curve from a theoretical prediction. It turns out that there is a good agreement between the experimental results and the theoretical predictions.

Figure 8.1 is a depiction of the experiment. Power from the motor is put in to run the outer cylinder.[1] The torque and the rpm are then the measured output variables. Now, in a typical experiment like this, we are practically constrained by the maximum rotational speeds that we can go to. One of the important objectives of our experimental design is therefore to help us get to the nose of the base curve and beyond with a minimum expenditure on rpm. A suitable choice of an experimental liquid turns out be critical in meeting this objective. Now, before we go on to look for the properties of the liquid that affect our objective, the following statement may be treated as a rough guideline to predict the shape of the base curve: the torque increases roughly as the product of the average viscosity and the rpm. With this statement in mind observe that with an increase in rpm, the temperature in the gap increases. Therefore, the average viscosity falls. Hence, depending on whether the increase in rpm is stronger or the decrease in the average viscosity is stronger,

---

[1] To avoid Taylor instability, we spin the outer cylinder, keeping the inner cylinder fixed.

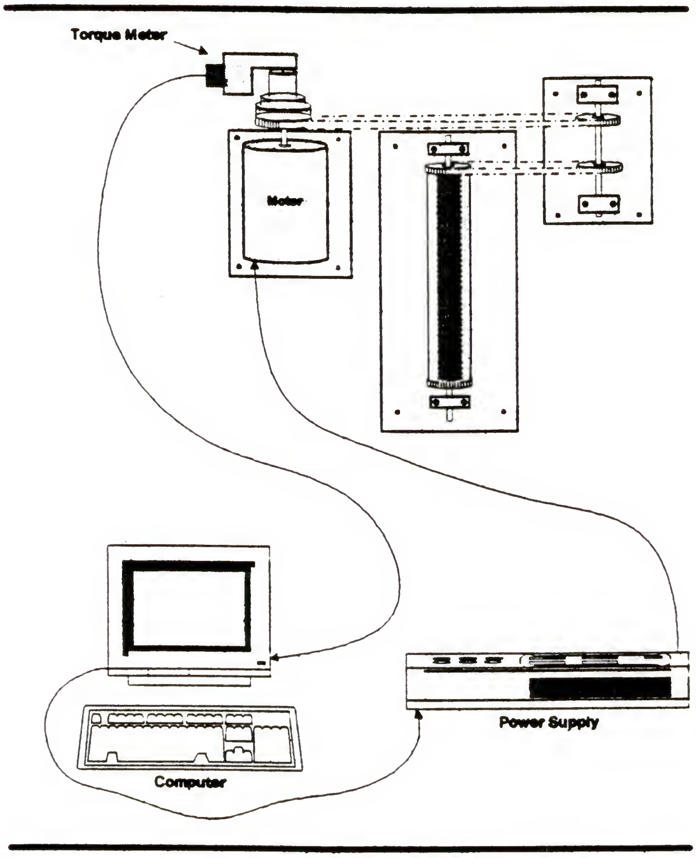

Figure 8.1: Experimental Setup

the torque either increases or decreases with an increase in rpm. Hence, any design measure we take towards decreasing the viscosity of the liquid for a given rpm works in favor of our objective.

The two most important properties that dictate the choice of an experimental liquid are the following: (1) Sensitivity of its viscosity-temperature relationship. (2) Its viscosity at room temperature. Now, the viscosity of liquids typically decrease exponentially with an increase in temperature. Therefore, for a given viscosity at room temperature, it is obvious that the higher the sensitivity of the viscosity-temperature relationship, the lower the rpm at which a nose occurs. However, it is not enough for the liquid just to have a strong temperature dependence on viscosity. It must also have a reasonably high viscosity at room temperature. This is required to generate enough heat to raise its temperature appreciably. Only then will the viscosity drop low enough so as to generate a nose at a lower rpm.

Sukanek, in his experiments to obtain the base curve, used Arochlor as the experimental liquid. Arochlor has an extremely strong viscosity dependence on temperature and has a high viscosity at room temperature. Its viscosity at 25°C is 4×10^4 poise and drops by a factor of four for every 5°C. This makes it an ideal choice for an experiment. However, at present, the use of Arochlor is banned. Alternately, we found that a viscosity standard S-2000 supplied by the Cannon Company meets these two requirements reasonably well. Table 8.1 shows the viscosity-temperature data for S-2000. An exponential sensitivity was fit to the data using $\frac{\mu_{\text{ref}}}{\mu} = e^{S(T-T_{\text{ref}})}$. The sensitivity S between 25°C and 66°C was found to be 0.0757. Figure 8.2 shows the plot of the fit along with the data. Table 8.2 shows the comparison of the viscosity data with the fit at various temperatures. From the table observe that the fit overpredicts the viscosity till 47°C and underpredicts it beyond 47° C. We will elaborate on this when the design calculations are discussed. Now, it turns out that S-2000 is a mixture of polybutenes. Therefore, we assumed its thermal conductivity to be

Table 8.1: The viscosity-temperature data for the experimental liquid.

T ˙C	μ, c.p
20	8961
25	5651
32	3117
37.78	1969
40	1664
47	1004
54	632
60	438
66	311

Table 8.2: The comparison of the viscosity data with the fit.

T °C	μ, c.p (data)	μ, c.p (fit)
25	5651	5651
32	3117	3326
37.78	1969	2147
40	1664	1815
47	1004	1068
54	632	629
60	438	399
66	311	253

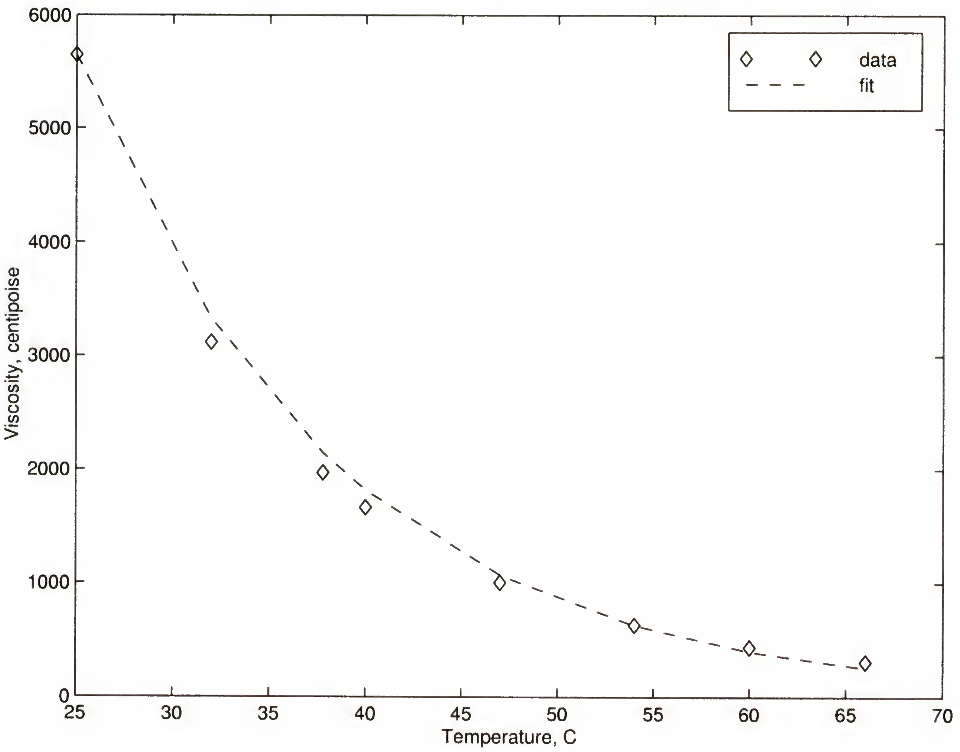

Figure 8.2: Viscosity-temperature data for the experimental liquid plotted along with an exponential fit.

that of polybutene and chose $k = 0.22$ J/s m C in our design calculations. For a given viscosity-temperature relationship, a lower thermal conductivity enables us to get to the nose at a lower rpm. This is due to the fact that a less conducting liquid requires a stronger temperature gradient to conduct the heat. Therefore the temperature in the gap increases and hence the average viscosity falls. Hence it is possible to generate a nose at a lower rpm for a liquid with a lower thermal conductivity. The thermal conductivity of polybutene is low: it is less than half that of water. This, in fact, works in favor of our design objective even though we did not consider it as our primary requirement.

For a given fluid, it is possible to advance the nose rpm by choosing an adiabatic wall instead of a conducting wall. For a given rpm, the average temperature in the gap is higher for an adiabatic inner wall as compared to a conducting inner wall. Therefore, the average viscosity is lower. Thus it is possible to get to the nose at a lower rpm with an adiabatic wall than with a conducting wall. Therefore, we chose a wooden inner cylinder which for all practical purposes is adiabatic.

The outer cylinder was made of lucite. The thermal conductivity of lucite, $k_w = 0.17$ J/s m °C. The thickness of the lucite wall used in the experiment, $\Delta_w =$ 3.17 mm. We chose the radius of the outer cylinder, $r_2 = 1$ inch. Hence, the Biot number of the outer wall, $Bi = \frac{k_w r_2}{k \Delta_w}$, turns out to be 6.19. The radius ratio was chosen to be 0.75.[2] The length of the cylinder was chosen to be 0.34m. The length to gap width ratio in this experiment is 54. This ensures that end effects can be neglected.

Table 8 shows the steady state torque vs. rpm data obtained from our experiment. Along with this, we also measured the temperature of the ambient air close to the outer wall for every run. The scaled temperature rise θ_0 which we calculate

---

[2] An endnote explains the choice of this radius ratio.

Table 8.3: The torque and the ambient temperature at various rpms in an experiment with r_2=1 inch, $\eta = 0.75$, L=0.34m.

rpm	Torque, $\mathrm{lb_f}$-in	$\mathrm{T_{amb}}$,°C
250	2.82	26.0
300	2.87	27.0
350	2.95	27.0
400	2.88	27.5
450	2.71	29.1
600	2.70	30.0
1000	2.60	33.2

from the Kearsley formula is actually $\theta_0 = S(T_0 - T_{\mathrm{amb}})$. Therefore, to unscale the temperature, the ambient temperature, T_{amb}, is needed.

The torquemeter used for the measurement in the experiment has a sensitivity of 0.05 $\mathrm{lb_f}$-in. Now, when one sees an experimental torque of 2.82 $\mathrm{lb_f}$-in at 250 rpm, it might be puzzling as it would seem that we have obtained torque data that is more accurate than what the instrument can possibly measure. However, it should be noted that the value of the torque and the ambient temperature reported here is an average over a period of time. For example, at 250 rpm when one sees a reading of 2.82 lb_f-in, it should be interpreted as the average of the slight fluctuations in the torque between 2.80$\mathrm{lb_f}$-in and 2.85$\mathrm{lb_f}$-in.

Next, let us see how the experimental results compare with the theoretical predictions. Recall that the scaled temperature and the wall speed are calculated using the Kearsley formulas:

$$\theta_0 = \ln\left[\frac{2m^2r^2}{\tau_0{}^2\cosh^2(m\ln r + a)}\right] \tag{8.1}$$

$$V_0 = 2m\tau_0\left\{\tanh(a) - \tanh(m\ln r + a)\right\} \tag{8.2}$$

respectively, where m, a are constants to be determined from the boundary conditions on temperature.[3] The temperature boundary conditions in this case are

---

[3] An endnote in Chapter 2, 2.8.10, page 69, discusses how m, a typically are calculated for a given boundary condition.

$\frac{d\theta_0}{dr} = 0$ at $r = \eta$ and $\frac{d\theta_0}{dr} + \mathrm{Bi}\theta_0 = 0$ at $r = 1$, where Bi is the Biot number. The following reference scales were used to unscale the temperature, velocity and torque respectively:

$$T_{\mathrm{ref}} = \frac{1}{S}$$

$$V_{\mathrm{ref}} = \sqrt{k/S\mu_{\mathrm{ref}}}$$

$$\tau_{\mathrm{ref}} = \sqrt{k\mu_{\mathrm{ref}}r_2^2/S}$$

Now, there is an important consideration when selecting a value of sensitivity for this calculation. Recall that the sensitivity, S=0.0757 °C that we obtained based on an exponential fit between 25 °C and 66 °C overpredicts the viscosity till a temperature of 47 °C and underpredicts it beyond 47 °C. This then means that if this sensitivity is used in a model for this experiment, then for a given rpm we will overpredict the torque till 47 °C and underpredict it beyond 47 °C. Now, to avoid such an error in a calculation, for every run we used a sensitivity that corresponds to the temperature range between the ambient temperature and the maximum temperature for that run. To do this requires us to first assume a maximum temperature so as to calculate the sensitivity. Once the maximum temperature is determined, then the sensitivity is recalculated for this new temperature range. The calculation is then repeated till the sensitivity that we use indeed corresponds to the temperature range that we determine. The reference viscosity is calculated at the ambient temperature for that run.

Figure 8.3 shows the plot of torque vs. rpm from an experiment with those from a theoretical prediction. This demonstrates that the backward bending base curve of torque vs. rpm could be obtained by setting the power as an input. The experiment and the theory agree reasonably well to suggest that it is indeed the base flow that we are seeing in this experiment and the flow is indeed stable at constant power input under the experimental conditions.

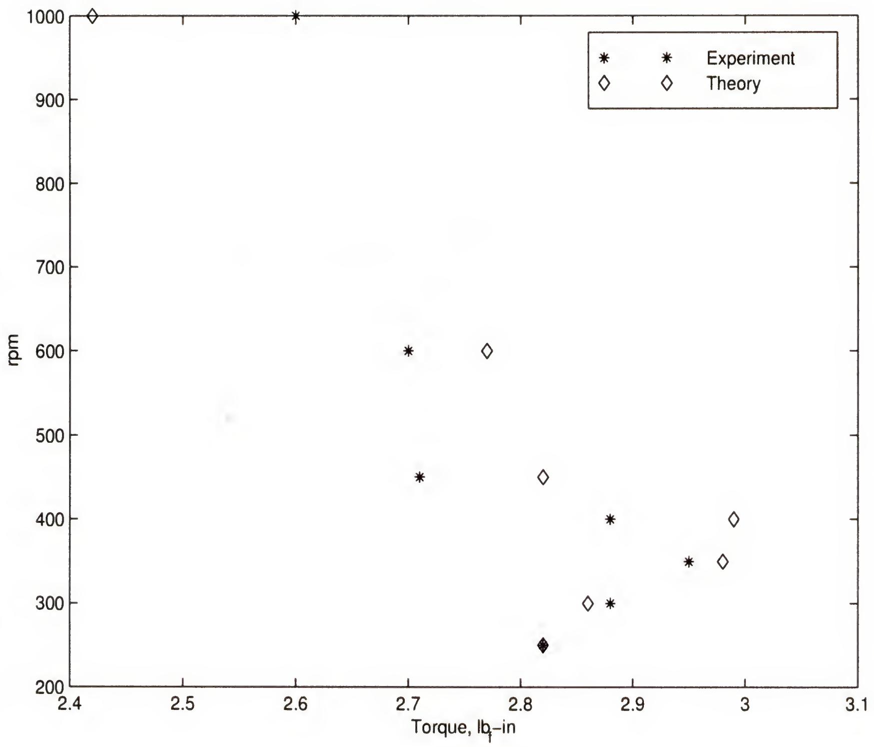

Figure 8.3: Comparison of the experimental base curve of torque vs. rpm with the theoretical predictions

8.1 Endnotes

In the main body of this chapter, we discussed how a suitable choice of a liquid and a wall are important in determining our objective of getting to the nose at a lower rpm. In this endnote, we will provide details about how we addressed certain other factors that are important in this experiment.

8.1.1 Check to see whether the Experimental Liquid is Newtonian

The model for our experiment assumes that the liquid is Newtonian. In other words, we assume that the liquid is just temperature thinning and not shear thinning. To check whether this is true, at least under the experimental conditions,[4] the shear viscosity of the liquid was experimentally determined at various temperatures. Figure 8.4 shows the shear viscosity plotted as a function of shear rate at various temperatures. We find that the shear viscosity remains almost invariant with respect to the shear rate. This ensures that the liquid is Newtonian under the experimental conditions.

8.1.2 The choice of a Radius Ratio

In the main body of this chapter, we declared that the radius ratio chosen for this experiment is 0.75. To see why this choice was made, first observe that for a constant viscosity liquid in circular Couette flow, for a given rotational speed and a given outer radius, r_2, the torque, $\tau_0 \propto \frac{\eta^2}{1-\eta^2}$ where η is the radius ratio. Now, this dependence of the torque on the radius ratio is interesting: it tells us that as the radius ratio approaches one, the torque shoots up drastically. Not only that, the rate of change of torque with respect to the radius ratio, $\frac{\mathrm{d}\tau_0}{\mathrm{d}\eta} \propto \frac{1}{(1-\eta^2)^2}$ goes up even more drastically. Pretending that this behavior carries through even at variable viscosity,[5] it has an important consequence on an experimental design: A small machining error has a more significant effect on the torque at a higher radius ratio than at a lower

---

[4] The maximum expected rpm in our experiment 2000 rpm corresponds to a shear rate of $2000 \times 2\pi/60 \simeq 200$ 1/s.

[5] Our numerical calculations at variable viscosity indeed suggest such a trend

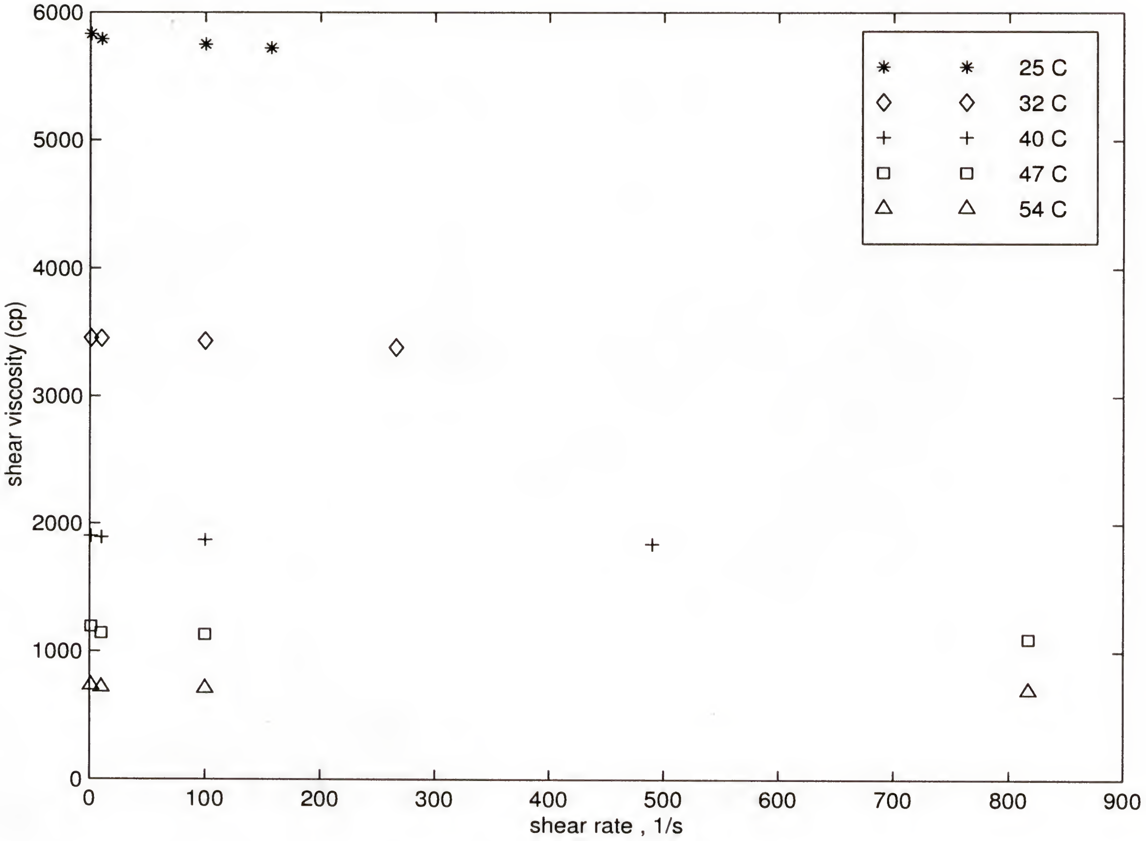

Figure 8.4: Shear viscosity vs. shear rate at various temperatures.

radius ratio. For example, a 1% increase in the radius ratio increases the torque by about 3% at 0.75 radius ratio and by 11% at 0.95 radius ratio. In view of this, we avoided higher radius ratios in our experiments. We chose a radius ratio of 0.75.[6]

8.1.3 Other Design Improvements

In this endnote, we will discuss the other significant design modifications that we undertook to minimize any experimental error. In one of the modifications, we decreased the empty torque by employing precision bearings. To see why this may be important, observe that in our experiments, the torque due to the bearing friction has to be subtracted from the total torque to get the torque due to the fluid. This necessitates a so called "empty run " which is essentially a run without the fluid. For the fluid and the geometry used in our experiment, the calculated torque due to the fluid was the order of 3.00 lb_f-in whereas the empty torque was initially the order of 2.00 lb_f-in. As the empty torque was of the same order of magnitude as the fluid torque, we believed that it might obscure our measurements. Therefore, to minimize the errors, we replaced the bearings by precision bearings which reduced the empty torque by half, to about 1.00 lb_f-in.

Yet another improvement was the use of a split-house bearing. To see how it reduces error, observe that after an empty run is completed, the Couette cylinder has to be taken out and filled with the liquid. When the Couette cylinder is re-fitted, the belt tension (the tension of the belt running from the motor to the Couette setup) may not be same as the tension when the dry runs are taken. This might affect the torque measurement. To overcome this problem, a split-house for the bearings was designed. With this design, for the Couette cylinder to be removed, only the cap of the split-housing has to removed. This ensures that the belt tension stays constant both for the dry runs and for the runs with the fluid. Refer to figure 8.5 and figure 8.6 for an illustration of this design .

---

[6] Going to too low a radius ratio is also not advisable as in that case, the fluid torque gets too low and it can be obscured by the torque due to the bearings.

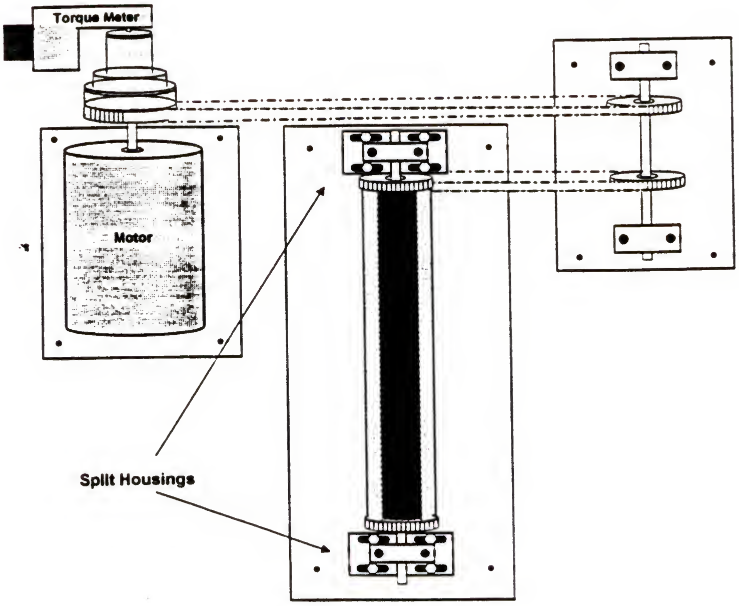

Figure 8.5: Couette Cylinder assembled in a split-house bearing

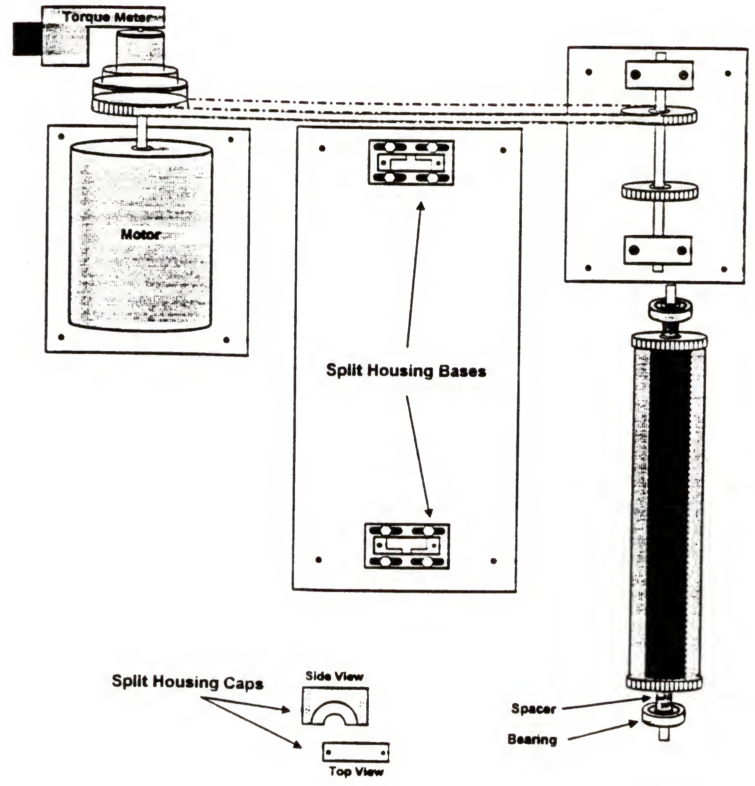

Figure 8.6: Couette Cylinder disassembled from a split-house bearing

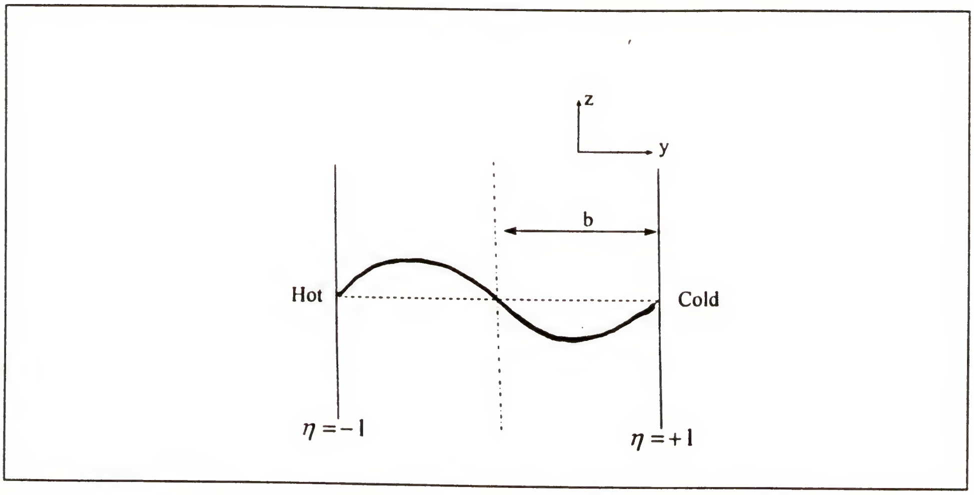

Figure 8.7: Illustration of a convective flow between a hot plate and a cold plate.

8.1.4 Effect of Convection

The experiment is run with an adiabatic inner cylinder and an outer cylinder which transfers heat to the surrounding. So, there is a radial temperature gradient with the core being hot and the outer cylinder cold. This temperature gradient induces a flow and if this flow is significant, the assumption that the flow is unidirectional is not valid. To test whether the flow due to convection effects is significant, we consider a model problem wherein a fluid is placed between two vertical walls, one hot and the other cold. Refer to figure 8.7. We assume the temperature gradient is just in the 'y' direction and solve for the momentum equation by assuming viscous forces balance the buoyancy forces. The solution is :

$$v_z = \frac{\rho\beta g b^2 \Delta T}{(\eta^3 - \eta)12\mu}$$

The values of physical properties and geometry that are relevant to our experiment are substituted in this equation to get an estimate of the flow due to convection. The density, ρ, at room temperature for S-2000 is 900 kg $/m^3$. The temperature coefficient of expansion β, is $10^{-4}/$ °C. We choose a gap width, b= 10 mm which is of the same order of magnitude as used in the experiment. Using the temperature gradient for the highest rpm run, we choose ΔT = 25 °C. A viscosity of $\mu = 0.5$ kg/m

Table 8.4: The details of the calculation that generated the base curve.

rpm	$T_{\text{amb.}}$	Range for S	S	$\mu(T_{\text{amb.}})$, c.p	$T_{\max}$	Torque, lb_f-in Theo.	 Expt.
250	26.0	25.0-32.0	0.085	5190	30.8	2.82	2.82
300	27.0	25.0-37.8	0.083	4790	32.1	2.86	2.88
350	27.0	25.0-37.8	0.083	4790	33.6	2.98	2.95
400	27.5	25.0-37.8	0.083	4597	34.9	2.99	2.88
450	29.1	25.0-37.8	0.083	4028	35.5	2.82	2.71
600	30.0	25.0-40.0	0.083	3740	38.9	2.77	2.70
1000	33.2	32.0-47.0	0.077	2846	45.6	2.42	2.60

s, which is at the highest temperature in the experiment is chosen. The chosen point in the gap is $\eta = -0.5$. Substituting these values in the equation, we obtained for the velocity $v_z = 1.4 \times 10^{-4}$m/s. We compared this velocity with the linear velocity corresponding to 200 rpm, the lowest rpm we encountered in our experiment. The corresponding linear velocity, at the outer cylinder is 0.5 m/s. Thus, we see from this calculation that the effects of convection are not significant in this experiment.

8.1.5 Details of the calculation of the Base Curve

In the main body of this chapter, we presented the results of the calculation of the base curve of the torque vs. the rpm. In this endnote, we will present the details of the calculation which generated the base curve.

Table 8.4 presents the details such as the temperature range at which the sensitivity was calculated for each run and the calculated sensitivity for that temperature range. In addition, the calculated maximum temperature for each run is also given. The wall viscosity was based at the ambient temperature. For example, for an rpm of 250, the wall viscosity was calculated at 26°C using the formula, $\mu_{26} = \mu_{25} \times e^{-0.085\times(26-25)}$ and at an rpm of 1000, the wall viscosity was calculated at 33.2°C using the formula $\mu_{33.2} = \mu_{32} \times e^{-0.077\times(33.2-32)}$.

Table 8.5: The effect of a change in the thermal conductivity on the calculated base curve

rpm	Theo.Torque, $\mathrm{lb_f - in}$ at			Expt. Torque, $\mathrm{lb_f - in}$
	$k = 0.22$	$k = 0.242$	$k = 0.198$	
250	2.82	2.85	2.77	2.82
300	2.86	2.90	2.81	2.88
350	2.98	3.03	2.93	2.95
400	2.99	3.04	2.92	2.88
450	2.82	2.87	2.75	2.71
600	2.77	2.83	2.70	2.70
1000	2.42	2.48	2.34	2.60

8.1.6 Sensitivity of the Base Curve to a change in the Physical Properties

The measurement of physical properties typically involve an error. In this endnote we will see how an error in the measurement of the physical properties affects the calculated base curve. The properties in question are the viscosity and the thermal conductivity of the liquid. As an example, we will consider how a 10% change in these properties affect the base curve.

First let us consider a change in the thermal conductivity of the liquid. A decrease in thermal conductivity would imply that for a given rpm, the temperature in the gap must be higher and consequently the viscosity must be lower. Hence the torque must be lower. Similarly, for an increase in thermal conductivity, the torque must be higher for a given rpm. In our calculations earlier, we used a value of $k = 0.22 \mathrm{J/s\ m^\circ C}$. Table 8.5 shows how much the calculated torque changes as the thermal conductivity of the liquid is changed by 10% holding the rpm fixed.[7]

Next, we will see how a change in viscosity affects the calculation of the base curve. If the viscosity increases, the torque increases for a given rpm. On the other

---

[7] Note that the Biot number, $\mathrm{Bi} = \frac{\mathrm{k_w r_2}}{\mathrm{k \Delta_w}}$ also changes as the thermal conductivity is changed. For a 10% increase in the thermal conductivity from 0.22 to 0.242, the Biot number decreases by 10% from 6.19 to 5.63. Similarly, for a 10% decrease in the thermal conductivity from 0.22 to 0.198, the Biot number increases by 10% from 6.19 to 6.81. This fact was incorporated in this calculation.

Table 8.6: The effect of a change in the viscosity on the calculated base curve

rpm	Theo.Torque, $\text{lb}_\text{f} - \text{in}$ with			Expt. Torque, $\text{lb}_\text{f} - \text{in}$
	Measured viscosity	10 % higher	10 % lower	
250	2.82	3.00	2.61	2.82
300	2.86	3.04	2.67	2.88
350	2.98	3.16	2.80	2.95
400	2.99	3.16	2.81	2.88
450	2.82	2.97	2.65	2.71
600	2.77	2.90	2.63	2.70
1000	2.42	2.52	2.31	2.60

hand, if the viscosity decreases, the torque decreases for a given rpm. Table 8.6 reports the torque value for a 10% change in the viscosity from its measured value.[8]

8.1.7 The Effect of Eccentricity of the cylinders on the calculated Torque

The calculation of the torque assumes the cylinders are perfectly concentric. One might inquire how much the torque changes if the cylinders are slightly eccentric. It turns out that one can predict that a slight eccentricity, ϵ, where ϵ is the normalized distance between the centers of the two cylinders, may affect the torque only at order ϵ^2 or at higher even powers. To see this, first realize that the torque due to eccentric cylinders can be written as a Taylor series expansion of the torque due to concentric cylinders. Now, realize that physically, for a given eccentricity, ϵ, no matter what the azimuthal orientation is, the torque must be the same as the system does not differentiate between the infinite possible azimuthal orientations for a given ϵ. This then means that there must be no contribution to the torque at order ϵ, or for that matter, any odd powers of ϵ. Thus a 1% eccentricity can affect the torque at best by 0.01%.

---

[8] In this calculation, we have assumed that the change in viscosity is uniformly 10% for all temperatures. Therefore, the sensitivity in this calculation remains the same as before.

CHAPTER 9
CONCLUSIONS

The main aim of this thesis was to answer the following questions about the Couette flow of a temperature-thinning liquid: (i) Can we understand the stability of this flow under various imposed conditions? (ii) What is the input variable when an experiment is run to obtain this flow? In this concluding chapter, we will present the important results that helped us to answer these questions. Alongside this, we will also present some other interesting results which were obtained on the way to answering these central questions.

To understand the stability of the flow required us to first understand the base state about which perturbations are made. In doing this, we inquired when a nose ought to occur in the base curve and specifically its dependence on the fluidity-temperature relationship. And to analyze this, we introduced an eigenvalue problem which is the homogeneous part of the equation that defines the rate of change of temperature in the gap as a function of the shear stress. We defined a nose on the base curve as a point at which the leading eigenvalue from this problem is equal to the wall stress. This definition was motivated by a calculation for linear fluidity, which is straightforward. For this case, we found out from our calculations that the fundamental eigenvalue, $\pi/2$, is equal to the wall stress at the nose. We then showed that this definition should carry over to general fluidity-temperature relationships. Further, we obtained an equation that defines how the eigenvalues change with a change in the wall stress. This equation turned out to be dependent, as one would expect, on the fluidity-temperature relationship. We first looked at fluidities that increase with an increase in temperature. For these fluidities, we found out, based on this equation, that a nose arises if $f_0'' \geq 0$ where f_0'' is the second derivative of fluidity with respect to temperature. Thus we concluded that linear fluidity should lie at the edge of base curves that bend backward. Lastly, we also studied fluidities that decrease with an increase in temperature. We were able to prove that for these fluidity types, a nose does not arise at all. An interesting result on the shape of the base curve was obtained for a fluidity that decreases exponentially with temperature. In this case, we found out that there is an upper bound on the wall speed and all values of wall shear stress between zero to infinity are contained within this upper bound.

Now, in a Couette flow experiment, one can visualize setting either the wall stress or the wall speed as an input, at least on paper. This led us to ask whether the stability behaviour in Couette flow depends on what we set as an input. In thinking about this, we had a picture argument that explained why perturbations at constant wall stress linger longer than perturbations at constant wall speed. This argument was based on the decay of velocity disturbances alone and it was based on the observation that at constant wall speed, there is a momentum sink on both the boundaries while at constant wall stress, only one boundary has a momentum sink and the other boundary is adiabatic to momentum. Therefore a perturbation lingers longer at constant wall stress as compared to constant wall speed. To check the prediction from this simplified picture that ignores temperature disturbances, we carried out a stability calculation under these two conditions. The calculation not only told us that perturbations linger longer at constant wall stress as compared to constant wall speed but also told us that the upper branch actually goes unstable at constant wall stress whereas it is stable at constant wall speed.

The stability results that we obtained above is independent of the Prandtl number[1], i.e., constant wall stress is always more unstable than constant wall speed and the upper branch is always unstable at constant wall stress- no matter what the Prandtl number is. This was interesting and this led us to inquire about the role of Prandtl number in the stability. Now, by definition, Prandtl number is the ratio of momentum diffusivity to thermal diffusivity. Hence, one would presume that in this flow where the thermal and mechanical disturbances are coupled, that at low Prandtl numbers, the mechanical disturbances must dominate and at high Prandtl numbers, the thermal disturbances must dominate. With this presumption, we performed a calculation for the rate of change of eigenvalues with respect to Prandtl number. We learned that at low Prandtl numbers, the eigenvalues are independent of Prandtl number and at high Prandtl numbers, the eigenvalues varied inversely with respect to the Prandtl number. This was good to know as it agreed with what we expected. This however raised the question: Can one declare what is a high Prandtl number limit and what is a low Prandtl number limit it a priori? To answer this question, we realized that it is the minimum viscosity of the fluid in the gap that determines the rate of decay of mechanical disturbances, and hence we corrected our definition of Prandtl number by multiplying it by the minimum viscosity of the liquid in the gap. Based on the modification of Prandtl number, we discovered that the rate of decay of perturbations roughly follow a pattern: when the modified Prandtl number is less than one then the decay is mechanically dominated in the sense that a change in Prandtl number does not change the eigenvalues. On the other hand, if the modified Prandtl number is greater than one, the decay is thermally dominated in the sense that the change in Prandtl number changes the eigenvalues significantly. Based on this observation, we concluded that Prandtl number, when defined based on the minimum viscosity, is a good guide to decide what is the controlling mode for the decay of disturbances. Lastly, we tried to see whether we could mathematically prove our intuitive notion that a low Prandtl number corresponds to a purely mechanical problem and a high Prandtl number corresponds to a purely thermal problem. To do this, we came up with a new scaling law that used a velocity scale that is based on the specific heat. We applied the Pr = 0 and Pr = ∞ limit on the scaled equations that arise out of this scaling. At Pr $\to$ 0, the result was in tune with what we expected: we recovered the purely mechanical problem. At the other limit, Pr $\to \infty$, we learned that when we impose constant wall stress boundary conditions, the perturbed temperature equations look identical to the perturbed temperature equations in the thermal ignition problem. However, the perturbed velocity does not become equal to zero even in this limit. Thus we did not recover the purely thermal problem in the limit Pr $\to \infty$.

---

[1] excluding the case of Pr = 0 in which case there is no upper branch, anyway.

The realization that power is the input variable and the wall speed and the wall stress are both output variables was another important result. To see why this seemingly straightforward observation was elusive initially, our initial view point about this experiment may be worth mentioning once more. We initially thought that one can run an experiment in Couette flow holding the speed on the moving plate to be fixed or the shear stress on the moving plate to be fixed. In other words, we believed that either the wall speed or the wall shear stress could be an input variable. However, the shape of the base curve threw some doubts on this view: For example, in a wall speed vs. wall stress curve that is double-valued, setting a wall stress as an input would lead to this question: "if we input a wall stress, which of the two wall speeds will be the output?" To resolve these questions, we performed a stability calculation. We expected the stability results to tell us whether either variable had a priority. And they did. The result was this: The entire base curve is stable at constant wall speed and the upper branch is unstable at constant wall stress. This made us conclude that in this flow that wall speed is the input variable and the wall stress is an output variable. This then was our view to begin with. We wanted to run an experiment to verify this view point. The objective of an experiment was this: Setting the wall speed, we wanted to see whether we could trace the base curve.

This would then prove that the wall speed is the input. And then, setting the wall stress at a point on the upper branch, we wanted to see experimentally whether the flow jumps to the lower branch. This would then prove that the wall stress is not an input variable, but only an output. There was a nagging difficulty, however, with this view. This appeared when we considered fluidities that decrease with an increase in temperature. In particular, when we considered the case of a fluidity that decreased exponentially with an increase in temperature, i.e., $f_0 = \mathrm{e}^{-\theta_0}$, we discovered that the wall speed vs. wall stress curve in this case has an upper bound on the wall speed. For this case, we cannot set *all* values of wall speed as an input. Our choice is constrained by the upper bound on the wall speed. So, we asked ourselves "Will we change our opinion on what an input variable is based on this?" Indeed if we do, the conclusion would then be that the choice of an input variable and an output variable hinge on the fluidity-temperature relationship. And this is an unacceptable conclusion as one cannot imagine the fluid dictating what ought to be an input. In trying to resolve this difficulty, we began thinking about how experiments are really run to obtain this flow. We eventually learned that the power to shear the fluid is indeed the input in the sense that to obtain a wall speed or a wall shear stress we actually put in power. Both the wall speed and the wall stress, which we initially considered to be input variables, are in fact, output variables. Further, a stability calculation at constant power told us that the entire base curve is stable at constant power. Thus we concluded that the entire base curve could be obtained setting the power as an input. And this view point would not create any difficulty if the fluidity-temperature relationship is changed!

Now in a real experiment, the power is not directly sent into the fluid but to a plate that shears the fluid. Therefore, we had to later generalize the stability calculation at constant power by incorporating the finite mass of the plate. This calculation told us that as the mass of the plate approaches infinity, the dynamics of the flow approaches that of the constant wall speed conditions. This result was in fact verified by performing a Taylor-Couette instability experiment. The onset of centrifugal instability as the inner cylinder is rotated and the outer cylinder is held fixed was observed in an experiment for a given fluid and for a known geometry. Then the expected onset of instability was calculated using linear stability theory imposing (1)constant wall speed boundary condition and (2) constant power condition on the rotating inner cylinder. We found out that the prediction from the theoretical calculations matched the experiments for the boundary conditions of constant wall speed even though we were performing the experiments at constant power. We reasoned that it is the large mass of the cylinder as compared to the fluid that makes the dynamics approach that of constant wall speed conditions.

Consequent to the realization that the power is the input variable in this flow, we asked whether we could still see the shear instability by controlling the power to hold the wall stress fixed. The answer turned to be negative based on a thought-experiment. In this, we first imposed a perturbation on the wall stress holding the power to the fluid fixed. A perturbation that increases the wall speed should therefore decrease the wall stress and vice-versa. As a response to the imposed perturbation, the power to the fluid was adjusted so as to bring the wall stress back to the set point. Then the flow was run at constant power till the wall stress starts to move once again away from the set point. Now, the short time response of the flow at constant power need not be identical to its long time response which is always towards its steady state. Based on this observation, we learned that the response of the flow for the above sequence of steps not only depends on the nature of the initial perturbation but also on the short time response of the flow at constant power. We considered four possible scenarios based on the different combinations of the initial perturbation and the short time behaviour at constant power. We found that in only one of these four possible scenarios does the flow go from the upper branch to the lower branch. And that too not in a way as we initially conjectured. We initially believed that when the wall stress is held constant on the upper branch, the flow *jumps* to the lower branch. That conclusion was based on treating the wall stress as an input. However, as the wall stress is reality an output and its dynamics is dictated by the fluid properties, we eventually concluded that even if the flow goes to the lower branch, it will not be an abrupt jump but a slow change.

In conclusion, in this thesis, the physics of the stability of Couette flow of a temperature-thinning fluids under various imposed restrictions has been explored, explained, analyzed and delineated. The input variable and the output variables in a Couette flow experiment have been identified: Such experiments are run with power being the input and torque and the rpm being the output.

REFERENCES

[1] Chandrasekhar S, Hydrodynamic and Hydromagnetic Stability, Dover Publications Inc., New York, 1961.

[2] Frank-Kamenetskii, D A, Diffusion and Heat Exchange in Chemical Kinetics, Princeton University Press, Princeton, New Jersey, 1955.

[3] Joseph D D, Variable viscosity effects on the flow and stability of flow in channels and pipes, *Physics of Fluids*, Vol 7, No 11, p1761, 1964.

[4] Davis S H, Kriegsmann G A, Laurence R L & Rosenblat S, Multiple solutions and hysteresis in steady parallel viscous flows, *Physics of Fluids*, Vol 26, No 5, p1177, 1983.

[5] Pearson J R A, Shah Y T & Vieira E S A, Stability of non-isothermal flows in Channels. I: Temperature-dependent Newtonian fluid without heat generation, *Chemical Engineering Science*, Vol 28, p2079, 1973.

[6] Shah Y T, Pearson J R A, Stability of non-isothermal flows in Channels. II: Temperature-dependent Power-law fluid without heat generation, *Chemical Engineering Science*, Vol 29, p737, 1974.

[7] Shah Y T, Pearson J R A, Stability of non-isothermal flows in Channels-III: Temperature-dependent Power-law fluid with heat generation, *Chemical Engineering Science*, Vol 29, p1485, 1974.

[8] Kearsley E A, Solutions of the equation $\Psi_{xx} + \frac{1}{x}\Psi_x + Kx^n e^{\Psi} = 0$, Journal of Research of the National Bureau of Standards-B, Mathematics and Mathematical Physics, Vol 67B, No 4, p245, 1963.

[9] Sukanek P C, Problems in flow of fluids with viscous dissipation, Ph D thesis, University of Massachusetts, Amherst, 1972.

[10] Drazin P G and Reid W H, Hydrodynamic Stability, Cambridge University Press, New York, 1981.

[11] Chao-Sheng Yueh and Cheng-I Weng, Linear Stability analysis of Plane Couette flow with viscous heating, *Physics of Fluids*, Vol 8, No 7, p1802, 1996.

BIOGRAPHICAL SKETCH

The author was born in Chennai, a metropolitan city in South India. He obtained his undergraduate degree from Anna University, Chennai in 1992 and later his master's degree from the Indian Institute of Technology, Kanpur in 1994. After a one year stint as a Design Engineer at Larsen and Toubro, a multinational company in India, he came to Gainseville in 1995 to pursue his graduate studies.

I certify that I have read this study and that in my opinion it conforms to acceptable standards of scholarly presentation and is fully adequate, in scope and quality, as a dissertation for the degree of Doctor of Philosophy.

Ranganathan Narayan

Ranganathan Narayanan, Chairman
Professor of Chemical Engineering

I certify that I have read this study and that in my opinion it conforms to acceptable standards of scholarly presentation and is fully adequate, in scope and quality, as a dissertation for the degree of Doctor of Philosophy.

Lewis E. Johns

Lewis E. Johns, Cochairman
Professor of Chemical Engineering

I certify that I have read this study and that in my opinion it conforms to acceptable standards of scholarly presentation and is fully adequate, in scope and quality, as a dissertation for the degree of Doctor of Philosophy.

Chang Won Park

Chang Won Park
Associate Professor of Chemical Engineering

I certify that I have read this study and that in my opinion it conforms to acceptable standards of scholarly presentation and is fully adequate, in scope and quality, as a dissertation for the degree of Doctor of Philosophy.

Raj Rajagopalan

Raj Rajagopalan
Professor of Chemical Engineering

I certify that I have read this study and that in my opinion it conforms to acceptable standards of scholarly presentation and is fully adequate, in scope and quality, as a dissertation for the degree of Doctor of Philosophy.

Robert T. DeHoff

Robert T. DeHoff
Professor of Materials Science and
Engineering

I certify that I have read this study and that in my opinion it conforms to acceptable standards of scholarly presentation and is fully adequate, in scope and quality, as a dissertation for the degree of Doctor of Philosophy.

Peter C Sukanek

Peter C. Sukanek
Professor of Chemical Engineering
University of Mississippi

This dissertation was submitted to the Graduate Faculty of the College of Engineering and to the Graduate School and was accepted as partial fulfillment of the requirements for the degree of Doctor of Philosophy.

May 2000

M. J. Ohanian
Dean, College of Engineering

Winfred M. Phillips
Dean, Graduate School